The Dissertation Committee for Karishma Surendra Kaushik Certifies that this is the approved version of the following dissertation:

Overcoming antibiotic resistance in microbial populations: An interdisciplinary perspective

Committee:

Vernita Gordon, Supervisor

Marvin Whiteley

Jeffrey E Barrick

Bryan Davies

Edward Marcotte

Overcoming antibiotic resistance in microbial populations: An interdisciplinary perspective

by

Karishma Surendra Kaushik, B.M.B.S., M.D.

Dissertation

Presented to the Faculty of the Graduate School of

The University of Texas at Austin

in Partial Fulfillment

of the Requirements

for the Degree of

DOCTOR OF PHILOSOPHY

The University of Texas at Austin

August 2015

Dedication

I dedicate this work to my paternal grandfather, N. Srinivasan (1925–2011), who ignited in me a torch of accomplishment and achievement. It is through his ardent support, blessings, and best wishes, that I have realized my goals.

Acknowledgements

I thank my advisor, Prof. Vernita Gordon, and members of the Gordon lab, past and present. To Vernita, thank you for being an incredible mentor and guide. To my laboratory colleagues, thank you for your scientific input and companionship. I specifically acknowledge Nalin Ratnayeke, Parag Katira, Ashley Kessel, and Jake Stolhandske for their scientific collaboration. I thank my laboratory friends Dr. Jaime Hutchison, Orrin Shindell, Chris Rodesney, Qiuxian Cai, Megan Davis-Fields, and Kristin Kovach for their camaraderie.

I am grateful to my parents, Surendra and Dr. Vineeta Kaushik, for their love and guidance. I also acknowledge my parents-in-law Mr. V. Balasubramanian and Dr. B. Balasubramanian, and extended family, for their encouragement. To my husband Kaushik, thank you for your incredible support and motivation. I could never have done this without you. To my son Abhay, thank you for the perspective and joy you bring into my life. I also acknowledge Mrs. Sunitha Adhikari, Abhay's nanny, for her dedication to my family. It is because she took her work seriously, that I could take my work seriously.

Finally, I thank all my previous teachers and mentors, from school to present, especially Mrs. Lira D'Mello, Col (Dr) A. L. Sharma, and Brig (Dr). Ketoki Kapila. Thank you for bringing out the best in me.

Overcoming antibiotic resistance in microbial populations: An interdisciplinary perspective

Karishma Surendra Kaushik, Ph.D.

The University of Texas at Austin, 2015

Supervisor: Vernita Gordon

Antibiotic resistance is a major public health problem. The increase in antibiotic-resistant bacteria and decline in the approval of newer antibiotics has prompted the need for novel therapeutic approaches. In the environment and in the human body, microbes are exposed to varying spatial landscapes. Further, bacteria assemble into multicellular assemblies called biofilms, which possess intricate spatial structure. Inherent to this spatial structure, microbial communities also possess population structure, characterized by cell density, spatial organization, and different cell types. This dissertation has three main goals: i) to study the effect of microbial population structure on the survival of antibiotic resistant mutants, using *P. aeruginosa*, an opportunistic human pathogen as a model organism, ii) to evaluate the therapeutic potential of using bicarbonate to enhance the efficacy of aminoglycoside antibiotics, first-line agents for *P. aeruginosa* infections, and develop an improved method of analysis of drug interactions iii) to develop a low-cost, hands-on, educational module to characterize antimicrobial compounds using an interdisciplinary, biophysical approach.

Table of Contents

List of Tables

List of Figures

Chapter 1: Introduction

1.1 A BRIEF OVERVIEW OF THE MAIN TOPICS

The following chapter will review two main topics discussed in this dissertation. The first part of the chapter will provide an overview of the structure of microbial communities, including its effect on function and key microbial processes. This is followed by a detailed account of our model organism and the opportunistic human pathogen *Pseudomonas aeruginosa*. The second part of the chapter will review the importance and need for interdisciplinary research experience as part of science education, and introduce the hands-on, interdisciplinary educational module we have developed and executed as a science outreach tool.

1.2 PHYSICAL AND SPATIAL STRUCTURE IN MICROBIAL COMMUNITIES

1.2.1 Microbial communities possess spatial structure

Much of our current understanding of microbiology derives from laboratory-based studies of pure, well-mixed cultures. Such reductionist studies have contributed greatly to our understanding of microbes. However, it is increasingly being recognized that in a majority of environments, microbes exist as interacting, spatially-structured communities [1].

1.2.1.1 Spatial structure in environmental microbial communities

In these real-world landscapes, microbial populations experience differing environmental conditions within areas that would be classified as single habitats [2]. Biotic and abiotic factors such as cell density, nutrient availability and toxic metabolites, vary substantially over space. This results in a heterogeneous environment, where physical and spatial structure exists over different length scale [3]. The existence of spatial structure in the environment has been shown to have profound effects on a range of biological phenomena [4, 5]. In aquatic environments inhabited by phytoplankton, energy inputs of thermal, mechanical, gravitational, chemical and even radioactive origins are found. The spatial and temporal heterogeneity of energy inputs leads to the formation of spatial discontinuities, or interfaces between two environments, in homogeneous zones [3, 6]. In the soil, these heterogeneities and discontinuities are the result of physical, geochemical and biological processes [7]. The spatial structuring of the physical environment induces similar heterogeneities of biological organisms, generating diversity in communities of biological populations. As shown in Figure 1.1, a spatially complex soil system shows an assemblage of microbes with different morphologies (round spores versus string-like mycelia) [8]. Similarly, Figure 1.2, depicts the spatial structure of microbial communities in granular sludge. In this sludge structure, bacteria from the first layer ferment sucrose to short-chain fatty acids such as propionic acid, acetic acid, and butyric acid. The

second layer of the sludge comprises of methanogens, which covert these fatty acids to methane [9].

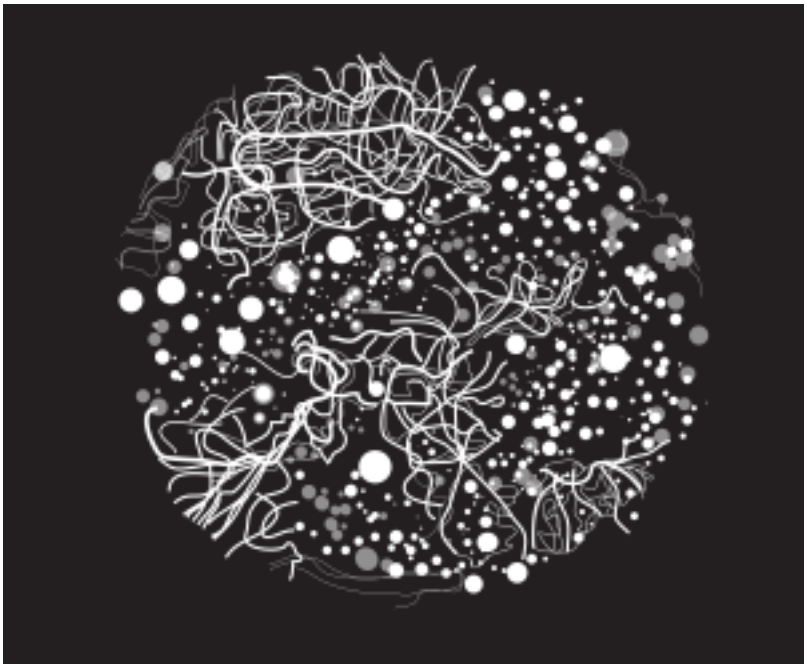

Figure 1.1 Illustration of a spatially complex soil arrangement brings out the diversity and complexity of the system.

This image depicts an assortment of microbes with different morphologies, for example, round spore-forming microbes versus string-like mycelia.
Credit: Sakurako Gibo from California College of the Arts. Image obtained from [8].

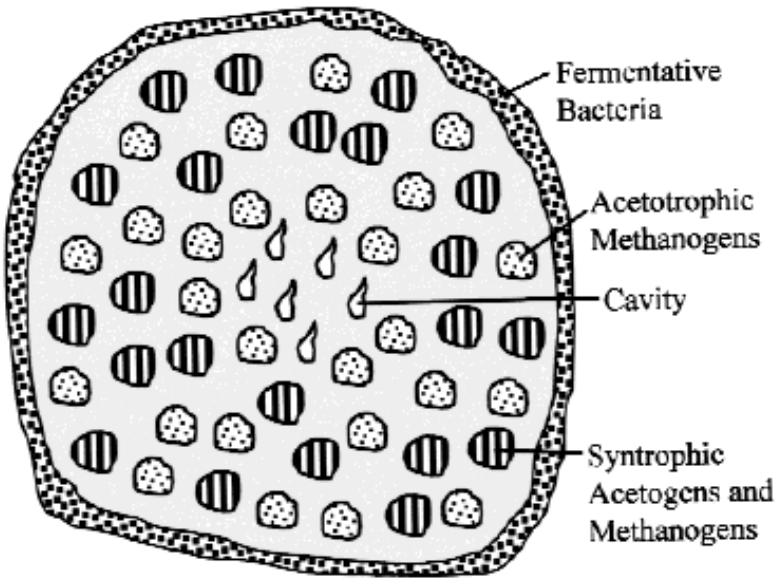

Figure 1.2 Schematic drawing showing the spatial structure of granular sludge from a bioreactor.

The sludge is seen to consist of three layers: an outer layer containing mainly bacteria, a second layer composed of microcolonies of methanogens, and a central core consisting of cavities, inorganic materials and methanogenic microcolonies. Figure from [9].

1.2.1.2 Spatial structure in human microbial communities

In the human body, microbial communities inhabit matrices with intricate spatial structure [10]. For example, microbes encounter spatial structure between different patient groups, within different organ systems in a single host, as well as within different tissues within a single organ. As shown in Figure 1.3, infecting strains of a bacterium (*Pseudomonas aeruginosa)* genetically adapt to produce a chronic sinus infection, following which adapted strains migrate to the lungs where they produce chronic lung infection. In this process, the infecting strain encounters different spatially-structured environments in the sinuses and lungs [10]. Another example of spatial structure is observed in dental plaque - a complex organization of microbial communities found in the human mouth (Figures 1.4 and 1.5). Oral bacteria in plaque exist as coordinated, spatially organized and fully metabolically integrated microbial community [11] . Structural analysis of dental plaque revealed that this community is dominated by species of *Streptococcus, Prevotella, Actinomyces, and Veillonella.* Further, cells of the genera *Prevotella* and *Actinomyces* showed the most interspecies interactions, suggesting a role for this association in maintaining the structure and/or function of the biofilm matrix [12]. It is also known that a wide-range of factors such as oxygen and nutrient availability, toxic metabolic products, and biomolecules influence the composition and spatial organization of dental plaque, leading to a general hypothesis for the structure of dental plaque [13].

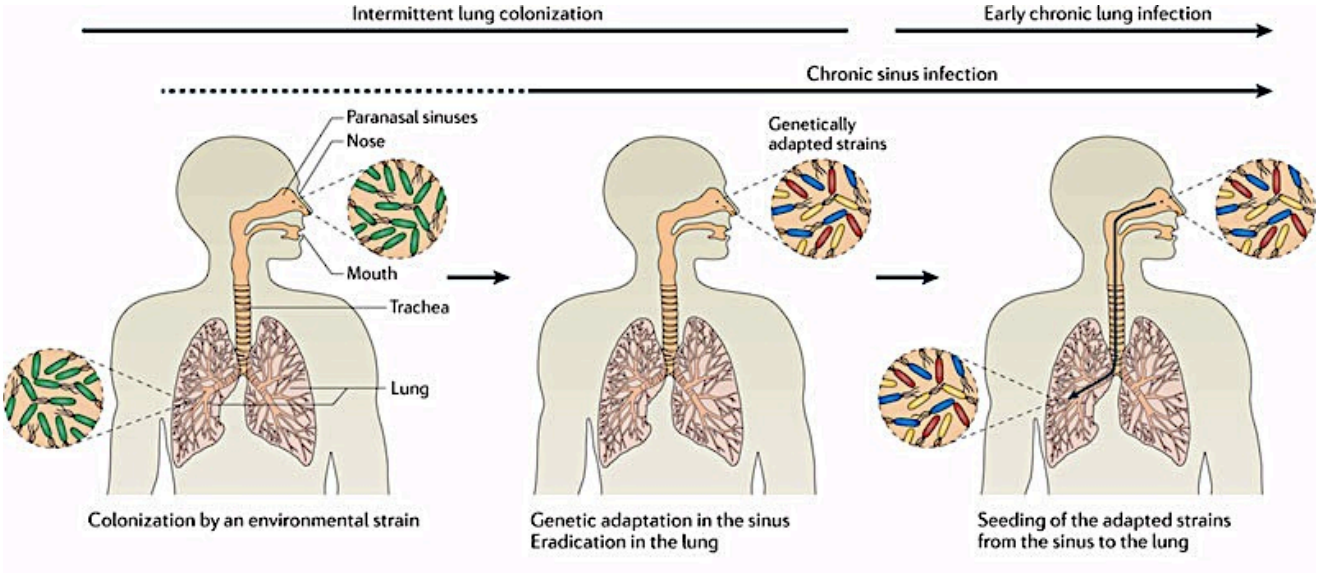

Figure 1.3 Typical course of *P. aeruginosa* infection in the Cystic Fibrosis airway, in which it encounters different spatial-structures.

The bacterium *Pseudomonas aeruginosa* most often invades the airway of patients with cystic fibrosis from the environment. Colonization can occur both in the paranasal sinuses and in the lungs. Compared to in the lungs, the immune response and antibiotic-mediated stress in the sinuses are less severe, providing a protected niche for bacterial colonization. During waves of antibiotic treatment and host immune responses, *P. aeruginosa* can be eradicated from the lungs. Subsequently, the lungs can be recolonized by the same *P. aeruginosa* genotype, which has survived the immune and antibiotic attacks in the sinuses. Figure from [10].

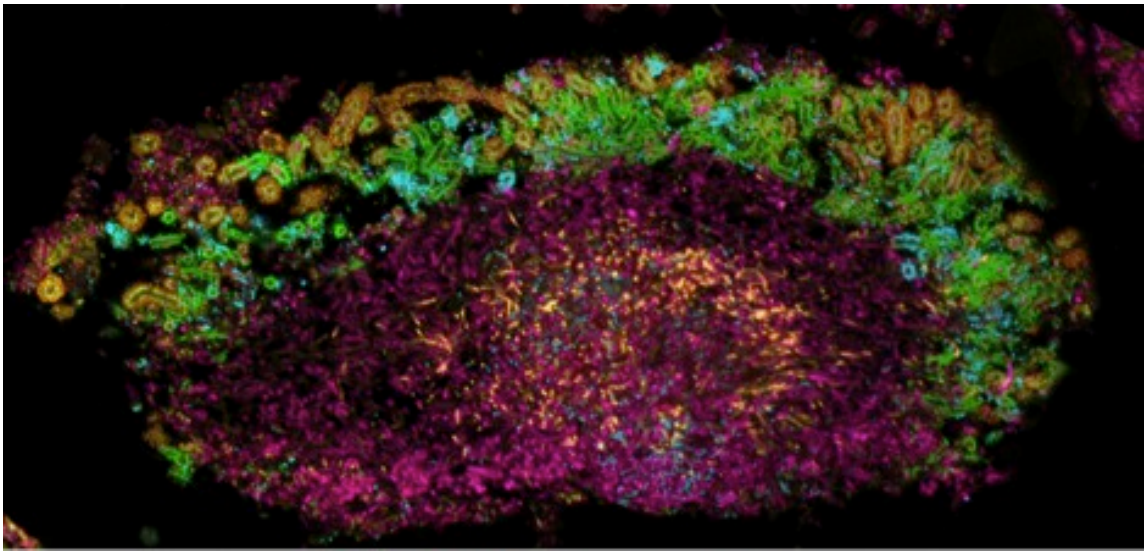

Figure 1.4 Interactions of bacterial cells in human dental plaque.

Dental plaque was hybridized with fluorescent probes targeting 15 groups (genera or families) of oral bacteria. Each small dot or rod is a single bacterial cell. Bacteria hybridizing to 6 different probes are seen in this image: *Pasteurellaceae* (dark orange), *Streptococcus* (yellow), *Actinomyces* (magenta), *Porphyromonas* (green), *Neisseriaceae* (blue), and *Fusobacterium* (peach). Several kinds of corncob structures, in which dot-like cells surround a central filament, can be seen in the upper part of the image, including multilayer corncobs in which the filament is surrounded by Streptococcus (inner ring) and *Pasteurellaceae* (outer ring), as well as single-layer corncobs composed of *Porphyromonas* and of *Neisseriaceae.*
Photo credit: Blair Rossetti. Image from [11].

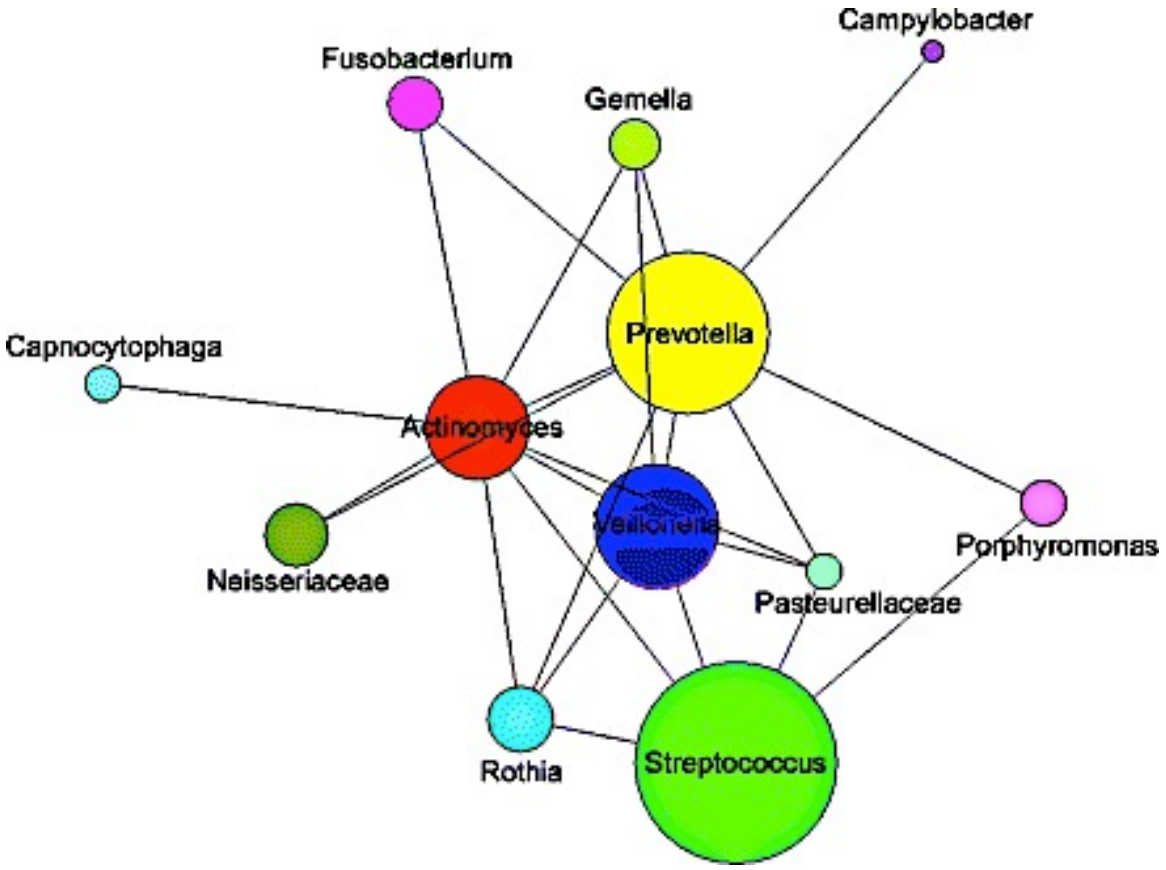

Figure 1.5 Spatial analysis of human dental plaque.

The area of the circle represents the relative abundance of each taxon. Lines connecting the two taxa indicate that cells of the lower-abundance taxon of any pair were observed to associate with cells of the higher-abundance taxon more frequently than would be expected from random associations. Figure from [12].

Microbes are also known to self-assemble into highly organized, naturally occurring communities known as biofilms [14, 15]. The structure of these microbial communities ranges from thin layers of scattered single cells to thick structures of macroscopic dimensions. Biofilms consist of a matrix of microcolonies, extracellular polymeric substance (EPS), and channels, which shape and determine the inherent spatial structure of these ordered communities (Figure 1.6). In addition to these fundamental elements, a number of additional factors contribute to the heterogeneity and spatial structure of biofilms (Table 1.1).

Table 1.1 Summary of factors influencing biofilm formation
Adapted from [16].

Genotypic factors	Specific genotype of the microbial populations Expression of genes encoding surface properties Expression of signaling systems Organism growth dynamics
Physicochemical factors	Substratum composition Temperature, pH, pressure, oxygen, radiation
Mechanical processes	Shear due to laminar and turbulent flow conditions
Stochastic processes	Initial colonization, attachment, detachment Changes in biotic and abiotic factors
Deterministic phenomena	Specific interactions between organisms, competition, cooperation

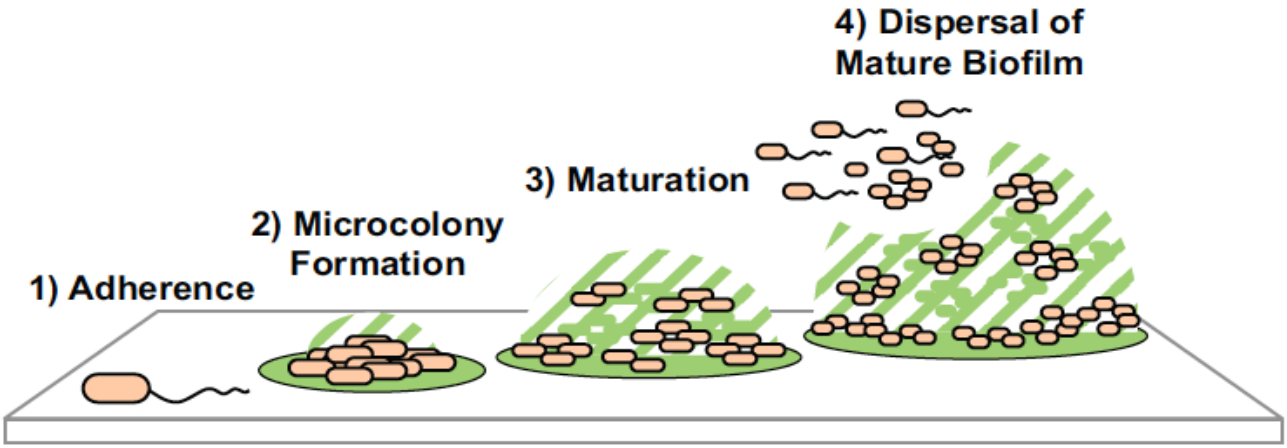

Figure 1.6 Different phases of biofilm formation *in vitro*.

1) Initial attachment of a cell to a surface is the starting point for biofilm formation. Bacteria attach to the surface using surface structures such as pili and flagellum, and start to produce extracellular polymeric matrix (EPS) 2) Within 24 hours, microcolony formation occurs over several rounds of cell division. Increased expression of EPS strengthens the association of the cells to the surface. 3) Over the next 24 – 72 hours, continued growth leads to the formation of the mature biofilm structure. The microcolony acquires a heterogenous landscape of water channels and mushrooms towers with distinct subpopulations of cells resulting from nutrient, oxygen, and signaling gradients. 4) In the late stage of a biofilm, external and internal cues lead to detachment of cells from the outer surface of the biofilm colony, leading to dispersal of the biofilm. Figure from [17].

Therefore, spatial structure is an integral component of microbial communities both in the environment and in the human host. However, the influence of physical and spatial structure on the pathogenesis and virulence of microbial populations is poorly understood.

1.2.2 Spatial structure and antibiotic resistance

As discussed previously, in the natural world, microbial populations are often dispersed over a heterogeneous spatial environment [3]. When bacteria are inoculated into this habitat, this ecological landscape provides bacterial communities with a distinct array of niches, in which populations can coexist. This results in a collection of interacting populations inhabiting a spatial landscape. This spatial landscape has been shown to have implications on microbial evolution and adaptation in spatially-structured systems [18].

1.2.2.1 Source-Sink Systems

Source-sink systems are the most commonly studied type of spatial structure in ecology [19]. A species' habitat is defined as a 'source' if it possesses a fundamental set of environmental conditions that permits a population to persist and where the growth rate exceeds the death rate. Any habitat outside this fundamental niche where the death rate exceeds the growth rate and which cannot be sustained without immigration from a source is called a 'sink'. To populate the sink habitat, bacterial populations have to migrate into the

sink and acquire mutations that enable them to reproduce there [20]. Growth in the sink population indicates that the new environment has been incorporated into the fundamental niche of the organism and the new habitat now changes from a ‘sink’ to a ‘source’. Widely studied in ecology, habitat conservation and animal behavior, source-sink systems are also known to have implications in the evolution of antibiotic resistance in microbial pathogens [21, 22].

1.2.2.2 Source-Sink Systems in relation to antibiotic resistance

In community and clinical settings, source-sink systems can result from the transmission of pathogens between healthy individuals, livestock and inanimate reservoirs (sources) and patients on antibiotic therapy (sinks) [23]. In a single individual on antibiotic therapy, drug levels vary between different organ systems, creating sources and sinks within a single host [24]. In patients with cystic fibrosis, antibiotic levels are lower in upper airway sites such as the paranasal sinuses as compared to the lungs. Sinuses serve as protective niches for bacterial colonization, after which adapted strains with increased fitness can migrate and establish chronic infection in the lower airway [10]. In a single organ system exposed to antimicrobial agents, differences in drug uptake between healthy and damaged tissue can introduce source-sink dynamics. In cystic fibrosis, heterogeneous antibiotic distribution in the lung is reminiscent of a source-sink like system, where regions with minimal drug concentrations could serve as sources from which bacteria could migrate to higher drug

concentrations or sinks [25]. Further, microbes self-assemble into biofilm structures, where several factors such as thickness, viscosity, density, nutrient availability, polymeric matrix and dead cells result in uneven antibiotic distribution; imposing source-sink dynamics on inhabiting populations [26].

1.2.2.3 Recent physics-based, source-sink models of antibiotic resistance

Recent, physics-based models have analyzed the dynamics of bacterial adaptation to vastly different source-sink environments [27, 28, 29]. In the simplest model of source-sink dynamics, an environment consists of two distinct habitats - one in which bacterial populations are well-adapted (the 'source') and one in which they are unable to reproduce (the 'sink') [29]. In this model, bacterial populations assume one of two possible genotypes, wild-type or mutant, and adaptation consists of two parts, arrival of a viable mutant into the sink and establishment of a population. In the predominant scenario, mutants arising in the sink are the result of a neutral mutation in the source, which by chance migrated into the sink. Such a mutant can be successful even if it does not have a competitive advantage in the source; it is sufficient if the mutation allows it to colonize the sink. This environment assumes no spatial gradient between the source and the sink and a spatially uniform drug concentration in the sink. However, in clinical situations, this binary source-sink scenario is unlikely to exist and drug concentrations are actually seen to vary in space [30]. Furthermore, evolving microbial populations often contain multiple, coexistent lineages

following different mutational pathways and competing for resources until one gains a new, better mutation allowing it to dominate [31]. This has been examined in other physics-based models, which analyze the effect of spatial gradient on the development of antibiotic resistance [28, 29]. In these models, an array of spatially-connected, increasingly disadvantageous sink microcosms result in a series of successive mutations and a genetic pathway to antibiotic resistance. Antibiotic-resistant mutants arise in the sink as a consequence of selection pressure, resulting in waves of increasingly better-adapted mutants invading the sink environment in a step-wise manner. Experimental evolution has a rich history in studying basic evolutionary processes as well as applied topics such as the evolution of antibiotic resistance [32]. Previous experimental studies on evolutionary adaptation using P. aeruginosa have employed spatially-uniform antibiotic concentrations [23, 33]. However, this scenario appears highly improbable in real-world contexts. Recent experimental work with *E. coli* indicates that the evolution of antibiotic resistance is greatly accelerated in spatial gradients, a mode of adaptation impossible in uniform environments [34].

1.2.3 Population structure in microbial communities

A major component of spatial structure in microbial communities is the consortium of cohabiting, interacting microbial species. For pathogenic microbes, the interaction of these communities with the human host is of high biomedical significance. Population dynamics in mixed microbial communities depend on

external selection pressures such as environmental conditions and intrinsic selection pressures such as strain competition and kin selection [35]. This heterogeneity confers population structure on microbial communities, which varies over spatial and temporal scales [36]. The existence of this population structure is likely to impact interactions between coexisting microbial populations, such as the evolution of antagonistic relationships and altruistic behaviors [37]. While a single cell can exert only a minimal influence on its surroundings, strength via numbers (cell density) and privileged location in space (spatial organization) can significantly amplify the impact of microbial populations. While the influence of spatial structure on antibiotic resistance has been addressed, the impact of this microbial population structure remains to be elucidated.

Microbial population structure can be defined in terms of the cell density, spatial organization, and cell types in the microbial community.

1.2.3.1 Cell density as a type of population structure

Density-dependent processes are widely known in microbial populations and cell density constitutes a type of population structure [38]. Positive density-dependence describes a situation where the population growth or gain rate is facilitated by increased population density levels [39]. An example is the inoculum effect on antibiotic efficacy; the rate of antibiotic killing declines at higher densities of bacterial populations [40]. Bacterial cellular components such

as membrane lipids, extracellular DNA and periplasmic glucans are known to sequester antibiotic molecules, lowering the effective antibiotic concentration [41] [42]. Negative density-dependence describes a situation in which population growth or gain rate is curtailed by crowding, predation and competition [43]. An example of this is density-dependent contact inhibition, seen in stationary phase populations of *E. coli*, where an evolved mutant inhibits its ancestral strain [44].

1.2.3.2 Spatial organization as a type of population structure

Microbial behaviors are increasingly being recognized as 'multicellular', resulting as a consequence of intercellular interactions [45, 46]. Spatial localization of cell groups is known to influence microbial relationships resulting in stable bacterial communities, programmed pattern formations and the evolution of 'cheater' populations [47, 48, 49]. New insights into antibiotic resistance suggest a role for spatial organization in a population-based resistance mechanism. For example, highly resistant mutants are seen to improve the survival of neighboring less-resistant strains, allowing mixed-populations to resist antibiotic concentrations beyond that achievable by a population in isolation. The mechanism was related to the production of the signaling molecule indole, which upregulated drug efflux pumps and oxidative stress protection [50]. It was recently demonstrated using 3D printing of microbial populations that a localized shell of *P. aeruginosa* afforded substantial protection to an encapsulated core of *Staphylococcus aureus* against ampicillin [51]. The

mechanism is related to the production of the enzyme β-lactamase by *P. aeruginosa* that degraded ampicillin, thereby protecting *S. aureus* [51]. Thus, spatial organization at very small scales affects antibiotic susceptibility (Figure 1.7).

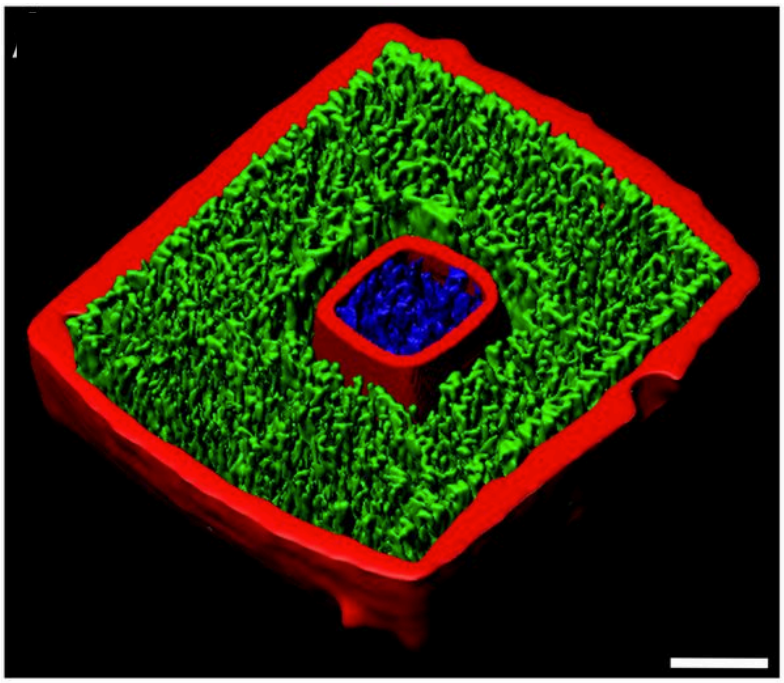

Figure 1.7 Spatial organization in a microbial community impacts the development of antibiotic resistance.

Cut-section of a 3D printed microcolony revealing a nested *S. aureus* community (blue) surrounded by *P. aeruginosa* [51]. Confined microcolonies of *S. aureus* display resistance to ampicillin via the action of β – lactamase produced by cocultured *P. aeruginosa*. Figure from [51].

1.2.3.3 Cell types as a component of population structure

As seen in the case of spatial organization, species of *P. aeruginosa* alters the antibiotic susceptibility of the population as a whole [51]. In the above example, a susceptible strain of *S. aureus* is protected from ampicillin by its close proximity with *P. aeruginosa.* Production of the enzyme β-lactamase by *P. aeruginosa* destroys ampicillin, rendering the population resistant.

In recent work from our laboratory, optical trapping and stamping were used to create artificial structures of *P. aeruginosa* and *S. aureus*, to probe interspecies interactions [52]. In coculture with *P. aeruginosa*, *S. aureus* counts are observed to decline after an initial rise, which does not happen in *S. aureus* monoculture. Further, we observe *S. aureus* grows more poorly in the proximity of *P. aeruginosa* [52]. We attribute these effects to antagonism by *P. aeruginosa.* These findings are consistent with observations that *P. aeruginosa* increases the expression of virulence factors that lyse *S. aureus,* upon sensing of peptidoglycan from this Gram-positive species [53, 54]. This demonstrates that cell type is an important component of population structure, affecting microbial interactions (Figure 1.8).

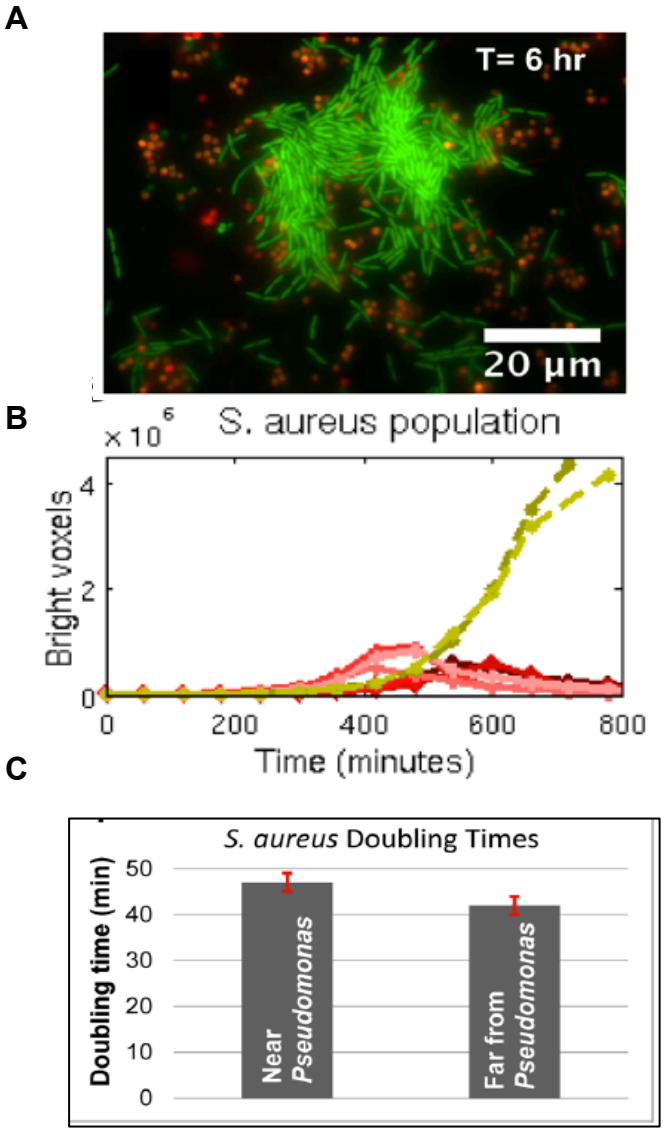

Figure 1.8 Interspecies interactions, resulting from different cell types, influence the structure of the microbial population.

(A) Optical trapping was used to create artificial structures of *P. aeruginosa* and *S. aureus.* **(B)** Proximity to *P. aeruginosa* delays the growth of *S. aureus* (solid red lines), whereas *S. aureus* in monoculture grows unaffected (dashed yellow lines). **(C)** Doubling time of *S. aureus* in coculture also demonstrates that it grows more slowly in the immediate presence of *P. aeruginosa.* Figure from [52].

Hutchison J, Rodesney C, Kaushik K, Le HH, Hurwitz DA, Irie Y, Gordon VD. 2014.Single-cell control of initial spatial structure in biofilm development using laser trapping. *Langmuir.* **30,** 4522-4530. (doi: 10.1021/la500128y). Reference [52].

1.2.4 *P. aeruginosa* as a model organism to study physical and spatial structure

P. aeruginosa is a Gram-negative, rod-shaped bacterium that is ubiquitous in the environment, living in the soil, and in water, and on plant and animal tissues [55]. In the hospital, *P. aeruginosa* can be isolated from a variety of sources, including respiratory therapy equipment, antiseptics, soap, sinks, mops, medicines, and physiotherapy and hydrotherapy pools [56]. Community reservoirs of this organism include swimming pools, whirlpools, hot tubs, contact lens solution, home humidifiers, and vegetables [57].

1.2.4.1 Clinical relevance of P. aeruginosa

In recent years, *P. aeruginosa* has emerged as a major opportunistic human pathogen. An estimated 51,000 healthcare-associated *P. aeruginosa* infections occur in the United States each year, and cost billions of dollars of healthcare costs annually [58]. A leading nosocomial (or hospital-associated) pathogen, *Pseudomonas aeruginosa* is responsible for ~10% of all hospital-acquired infections [59]. In immunocompromised hosts such as those with severe burn wounds, HIV/AIDS, and cancer, *P. aeruginosa* infections often result in severe and life-threatening bacteremia and sepsis [60]. It is also a significant cause of pneumonia in Cystic Fibrosis patients and ventilator-associated individuals, urinary tract infections in catheterized patients, post-surgical wound infections, and ocular infections in contact-lens wearers [60]. Limited

susceptibility to antimicrobial agents and the high frequency of emergence of drug resistance further contribute to severe adverse outcomes [61].

1.2.4.2 P. aeruginosa biofilm assemblies

P. aeruginosa is well-known to self-assemble into multicellular, spatial structures called biofilms. As described previously, biofilms are complex organizations of bacterial microcolonies embedded in a matrix of extracellular polymeric substance (EPS), composed of a complex mixture of polysaccharides, extracellular DNA (eDNA), and proteins [15]. *P. aeruginosa* is known to form biofilms on a wide variety of biotic and abiotic surfaces including the Cystic Fibrosis lung, contact lenses, chronic wounds as well as industrial equipment and hospital niches [62]. In *P. aeruginosa,* biofilm formation is a multicellular process involving environmental signals and concerted regulatory networks, such as quorum sensing, a well-known bacterial cell-cell communication system [63]. Therefore, in biofilms, *P. aeruginosa* populations display properties that are physiologically-distinct from their free-living, planktonic counterparts [14].

P. aeruginosa biofilms possess inherent spatial structure which is shown to be dependent on several factors such as their polymicrobial nature, the spatial distribution of cells, signaling state of the cells, the availability and transport of nutrients, and diffusion of oxygen [64]. For example, *P. aeruginosa* biofilm formation is dependent on the carbon source used to support growth. A flat *P.*

aeruginosa biofilm is seen to form when citrate, benzoate, or casamino acids are used as a carbon source, and a heterogenous *P. aeruginosa* biofilm with mushroom-shaped multicellular structures is formed when glucose was used as the carbon source [65].

It is thus not surprising that *P. aeruginosa* is a model organism for biofilm research. Given its propensity to form spatially-structured biofilms, the recalcitrant nature of these sessile communities, and their contribution to chronic and persistent infections, studying the spatial structure of *P. aeruginosa* could open novel strategies that target or harness the effects of spatial structure as a therapeutic approach.

1.2.4.3 Population structure in P. aeruginosa infections

Following primary infection, for example in the cystic fibrosis lung, *P. aeruginosa* diverges into a population of multiple, coexisting variants, derived from the single, ancestral strain [66]. Genetically diverse mutants, particularly those resistant to multiple antimicrobial agents result in a heterogeneous population [67]. A similar scenario occurs in biofilm assemblies, where multiple cell groups with different physiological states (including antibiotic susceptibility) are seen to coexist [68]. This coexistence of heterogeneous P. aeruginosa lineages in the cystic fibrosis lung underscores the importance of population structure in intra-strain interactions. Determining the impact of population

structure on antibiotic resistance in *P. aeruginosa* will allow for novel therapeutic options that account for the effects of population structure.

1.2.4.4 P. aeruginosa is a well-developed model organism

In addition to the above features, *P. aeruginosa* is a well-developed model organism [69]. The laboratory strains PA14 and PAO1 have fully sequenced and annotated genomes [70] [71]. The tractability of the *P. aeruginosa* genome to genetic manipulations has resulted in a library of transposon-insertion mutants [71], which are available for use upon request. In addition, a vast amount of data is available on the metabolic networks of this organism, including detailed information on metabolic substrates, enzymatic steps, and end-products [72].

All the above considerations make *P. aeruginosa* a well-suited model organism to study the effects of physical and spatial structure on microbial populations.

1.2.5 Infections caused by *P. aeruginosa*

An opportunistic human pathogen, *P. aeruginosa* causes a range of infections in the human host from dermatitis to life-threatening septicemia. This section discusses specific infections that are directly relevant to this work.

1.2.5.1 Infections in Cystic Fibrosis

Cystic fibrosis (CF) is the most common genetic disorder in the western world; and in the United States alone about 1000 new cases are diagnosed each year [73]. The disorder results from mutations in the Cystic Fibrosis Transmembrane Conductance Regulator (CFTR) gene, which encodes the CFTR membrane protein. These mutations possibly impact the synthesis, processing, and transport of the of the CFTR protein to the apical surface of cells. Absence of this protein in its correct cellular location results in a failure to secrete chloride and bicarbonate into and out of the cell. In the lungs, the CFTR protein is expressed in the submucosal glands and ciliated epithelial cells [74]. Normally, mucociliary transport is facilitated by hydration of airway surface liquid (ASL) that lines the respiratory tract. Absence or dysfunction of CFTR leads to a lack of chloride efflux and hyperabsorption of sodium ions, causing ASL dehydration, increased mucoviscosity and impaired mucociliary clearance Further, the absence of CFTR leads to defective secretion of bicarbonate in airway epithelial cells [75]. This has shown to result in decreased ASL pH and impaired function of innate antimicrobial factors. Restoration of ASL pH by aerosolization of sodium bicarbonate was seen to improve the activity of these antimicrobial factors [76]. Infact, in recent developments, aerosolized bicarbonate is being evaluated as a therapeutic strategy for CF lung disease. This would possibly enhance innate antimicrobial activity, as well as facilitate the unfolding of

mucins (via chelation of cations that hold highly-compacted mucins) and release of mucous, thereby increasing mucociliary clearance [77].

P. aeruginosa is a major pathogen in the CF lung. In these patients, infection with this opportunistic pathogen leads to causes chronic, persistent, life-threatening pulmonary infections, which are notoriously recalcitrant to antibiotic therapy [78]. Conversion to the mucoid phenotype and formation of biofilms and believed to be the two main mechanisms by which this organism gains such a strong foothold [79]. Notably, in the cystic fibrosis lung, spatial structure is imposed on *P. aeruginosa* by structural airway remodeling resulting in a heterogeneous distribution of nutrients and antibiotics [80].

1.2.5.2 Chronic wound infections

P. aeruginosa is well-known to cause biofilm-based chronic infections, and a number of studies have demonstrated that *P. aeruginosa* is frequently present in chronic wounds [72]. Evidence suggests that formation of biofilms in these wound sites is a key factor contributing to the increased severity and delayed healing observed in these infections [65]. This is of particular relevance to diabetic foot ulcers, pressure ulcers, and venous leg ulcers [72]. Chronic wound infections are often polymicrobial, and *S. aureus* is a common co-pathogen with *P. aeruginosa* in this setting [81]. Examination of the spatial organization of *S. aureus* and *P. aeruginosa* in chronic wounds using reveals a nonrandom

distribution of these species [81], with *P. aeruginosa* localizing to the deeper regions of the wound and *S. aureus* remaining closer to the wound surface (Figure 1.9). Such insights into the spatial organization and population structure of chronic wounds could help design effective management solutions.

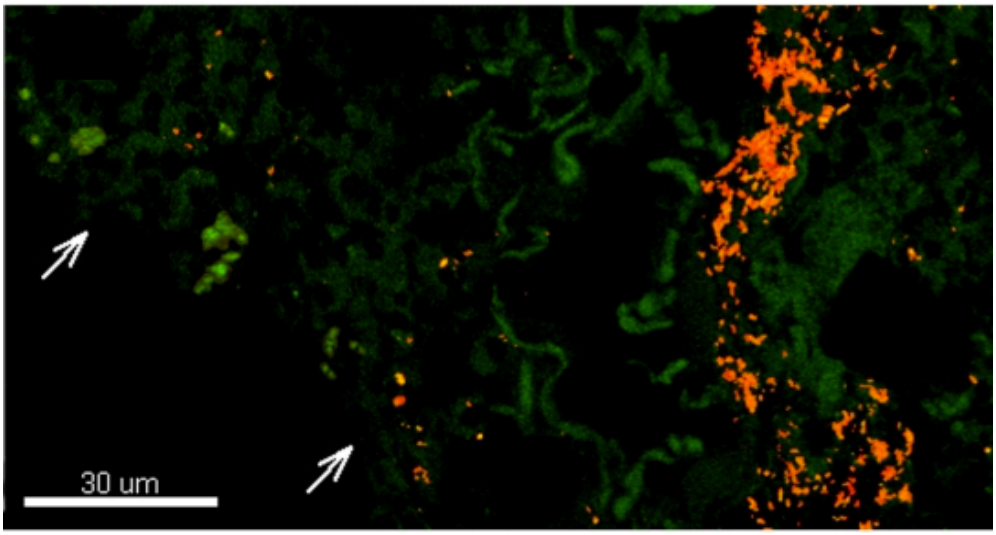

Figure 1.9 Nonrandom distribution of *P. aeruginosa* and *S. aureus* in chronic wounds.

The centers of mass of the *P.* aeruginosa aggregates were located at a distance of 50-60 μm from the wound surface, whereas the centers of mass of the *S. aureus* aggregates were located at a distance of 20-30 μm from the wound surface. This indicates the presence of spatial organization in polymicrobial infections in chronic wounds. Image from [81].

1.2.5.3 Acute (often planktonic) infections

While a great deal of research focuses on biofilm-associated chronic *P. aeruginosa* infections, opportunistic infections with this pathogen can also be acute in nature [82]. Examples of acute infections are typically skin and soft tissue infections such as acute (burn or post-surgical) wounds, dermatitis, cellulitis, and ocular infections such as conjunctivitis, keratitis (infection of the cornea) and endophthalmitis, although systemic infections such as acute pneumonia, urinary tract infections and bloodstream infections (sepsis) also fall into this category. Interestingly, burn wound infections with *P. aeruginosa* often deteriorate rapidly leading to systemic dissemination and septicemia [72].

1.2.6 Antibiotic resistance in *P. aeruginosa*

1.2.6.1 Rising trends in antibiotic resistance to antipseudomonal agents

Treatment of *P. aeruginosa* infections poses a serious challenge, and selection of appropriate antibiotics is essential to gaining a positive outcome [57]. Unfortunately, the increasing drug resistance of *P. aeruginosa* strains complicates this selection of appropriate antibiotic. Infections caused by drug-resistant *P. aeruginosa* are associated with significant increases in morbidity, mortality, need for surgical intervention, length of hospital stay and chronic care, and overall costs of treatment [61]. Even more problematic is the development of

resistance during the course of therapy, a complication which has been shown to double the length of hospitalization and overall cost of patient care [57]. *P. aeruginosa* can develop resistance to antibiotics either through the acquisition of resistance genes on mobile genetic elements (i.e., plasmids) or through mutational processes that alter the expression and/or function of chromosomally-encoded mechanisms [83]. Both strategies for developing drug resistance can severely limit the therapeutic options for treatment of serious infections. As shown in Figure 1.10, hospital and Intensive Care Unit (ICU) strains of *P. aeruginosa* show resistance to several antipseudomonal drugs, including aminoglycosides [57]. Though not inclusive of all published data on *P. aeruginosa* resistance, this summary highlights the fact that *P. aeruginosa* strains show resistance to multiple classes of antibiotics, which is definitely a huge concern.

Antibiotic	% of strains exhibiting resistance[a]							
	Hospital study, 2006 (n = 606) (211)	Hospital study, 2005 (n = 589) (212)	Hospital study, 2002 (n = 9,896) (54)	ICU study, 2002 (n = 951) (178)	ICU study, 2000–2002 (n ≥ 7,500) (95)	Hospital study, 2001 (n ≥ 2,157) (99)	ICU study, 2001 (n ≥ 543) (99)	Hospital study, 2000 (n = 882) (100)
β-Lactams								
Cefepime	6	5	9	25	12	8	10	9
Ceftazidime	13	10	13	19	17	9	9	13
Piperacillin-tazobactam	11	9	11	10	14	8	8	13
Aztreonam		12		32				
Imipenem	11	7	16	23	22	12	16	16
Meropenem	6	7			18	11	16	10
Fluoroquinolones								
Ciprofloxacin	21	22	35	32	33	26	25	25
Levofloxacin	22	22		34	32	27	25	27
Aminoglycosides								
Amikacin			5	10		4	3	
Tobramycin	8	10	12	16				
Gentamicin	12	12	16		22	15	15	14

Figure 1.10 Rates of antibacterial resistance among *P. aeruginosa* isolates from hospitals and ICUs after 2000.

P. aeruginosa exhibits resistance to all three main classes of antipseudomonal drugs. Figure from [57].

1.2.6.2 Multidrug-resistant (MDR) P. aeruginosa

Not only are rates of resistance to individual drugs or drug classes a concern, but the prevalence of multidrug-resistant strains (resistant to three or more drug classes) is an even more serious therapeutic challenge [84]. Multidrug-resistant (MDR) strains of *P. aeruginosa* have been designated as a 'serious' level threat by the CDC AR threat report [58]. As seen in Figure 1.11, of the total *P. aeruginosa* infections, ~13% are caused by multidrug-resistant strains, with roughly 400 deaths each year [57].

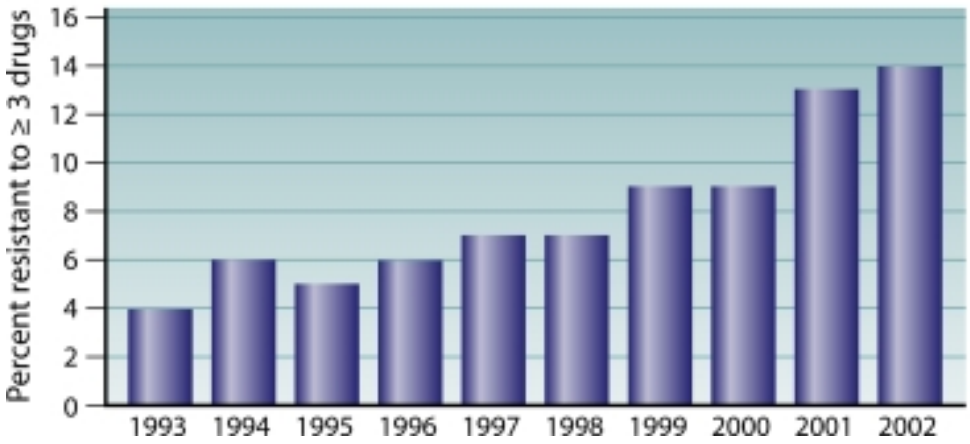

Figure 1.11 Increasing prevalence of multidrug resistance among *P. aeruginosa* isolates from ICU patients in the United States from 1993 – 2002. Figure from [57].

1.2.6.3 Aminoglycoside resistance in P. aeruginosa

Aminoglycosides are an important component of antipseudomonal therapy. The majorities of aminoglycosides are bactericidal and often act in synergy with other antimicrobials, properties that make them valuable as anti-infectives. Aminoglycosides are hydrophilic sugars that possess several amino and hydroxyl functionalities (Figure 1.12). The amine moieties are mostly protonated in biological situations; hence, these antibiotics can be considered polycationic species [85]. Since they are polycationic, they display a binding affinity for nucleic acids, which is the basis for their mechanism of inhibition. Aminoglycosides are known to bind to the 30S ribosome and inhibit protein synthesis [86]. Specific mechanisms include perturbation of peptide elongation, giving rise to inaccurate mRNA translation and truncated biosynthesis of proteins. Further, a subset of these aberrant proteins may get incorporated into the bacterial cell membrane leading to altered membrane permeability. However, before exerting their lethal effects, aminoglycosides have to traverse the bacterial cytoplasmic membrane. Previous work has shown that the transport of aminoglycosides is an energy-requiring process; depending on the electrical component of the proton motive force (PMF) [87].

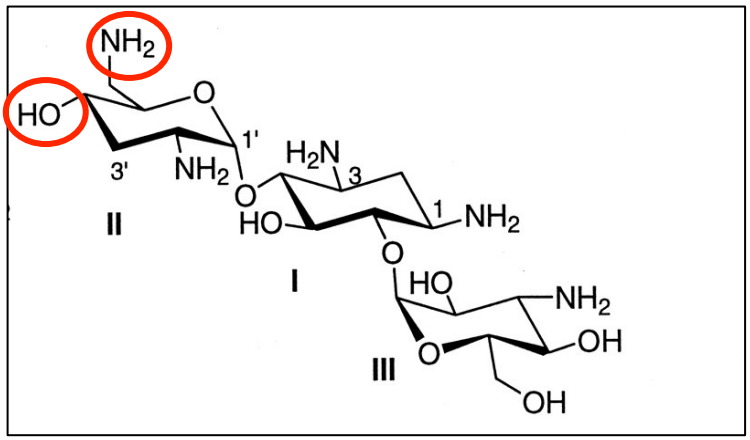

Figure 1.12 Structure of Tobramycin showing several amino and hydroxyl functionalities.

Examples of amine and hydroxyl groups are highlighted in red. Figure from [85].

Resistance to aminoglycosides is very common, and several possible mechanisms have been implicated [88]. Table 1.2 lists the summary of mechanisms known to mediate the resistance of *P. aeruginosa* strains to aminoglycosides.

Table 1.2 Summary of mechanisms mediating aminoglycoside resistance in *P. aeruginosa.* Adapted from [89].

Modifying enzymes	Modification by enzymes that phosphorylate, acetylate or adenylate aminoglycosides
Impermeability	Often most common resistance mechanism in CF isolates Reduced uptake due to decreased permeability
Adaptive resistance	Reduced level of aminoglycoside accumulation; disappears after removal of antibiotic
Efflux	MexXY efflux pump (RND family)
Outer membrane components	OprH-PhoP-PhoQ operon that modifies lipid A portion of LPS LPS component of the OM implicated in resistance (related to aminoglycoside binding prior to uptake)
Ribosomal changes	Reduced ribosomal affinity of the drug
Defects in electron transport	Decreased aminoglycoside uptake

1.2.6.4 Resistance in P. aeruginosa biofilms

Resistance to antimicrobial agents is an important feature of *P. aeruginosa* biofilm infections. It has been postulated that the biofilm exopolysaccharide component provides an effective barrier that restricts the penetration of antibiotics [88].

Differences in environmental conditions within the biofilm structure result in a non-uniform access to resources for the residing bacterial population. As a consequence, bacteria located in the periphery of the biofilm have better access to nutrients and oxygen than those located deeper in the community, resulting in differences in metabolic activity among the bacterial population [90], influencing their susceptibility to antibiotics.

P. aeruginosa cells in the biofilm state are also known to have distinct changes in physiology, gene expression, and protein regulation [64], resulting in a phenotype that is unique to these populations. Induction of this biofilm-specific phenotype could lead to the activation of mechanisms that are critical for the development of antibiotic resistance. Alternatively, it has been proposed that a small fraction of biofilm cells known as ‘persister’ variants is responsible for the high level of resistance in biofilms [89]. Based on these results it has been suggested that the most of the cells in a biofilm are as susceptible to antibiotics

as their planktonic counterparts and this persister subpopulation allows the population to survive.

Other mechanisms for resistance proposed are activation of a generalized stress response, and expression and overproduction of multidrug-resistant efflux pumps [88]. Therefore, resistance of biofilms to antibiotics is most likely multifactorial and the precise contribution of each of these mechanisms warrants further understanding (Figure 1.13).

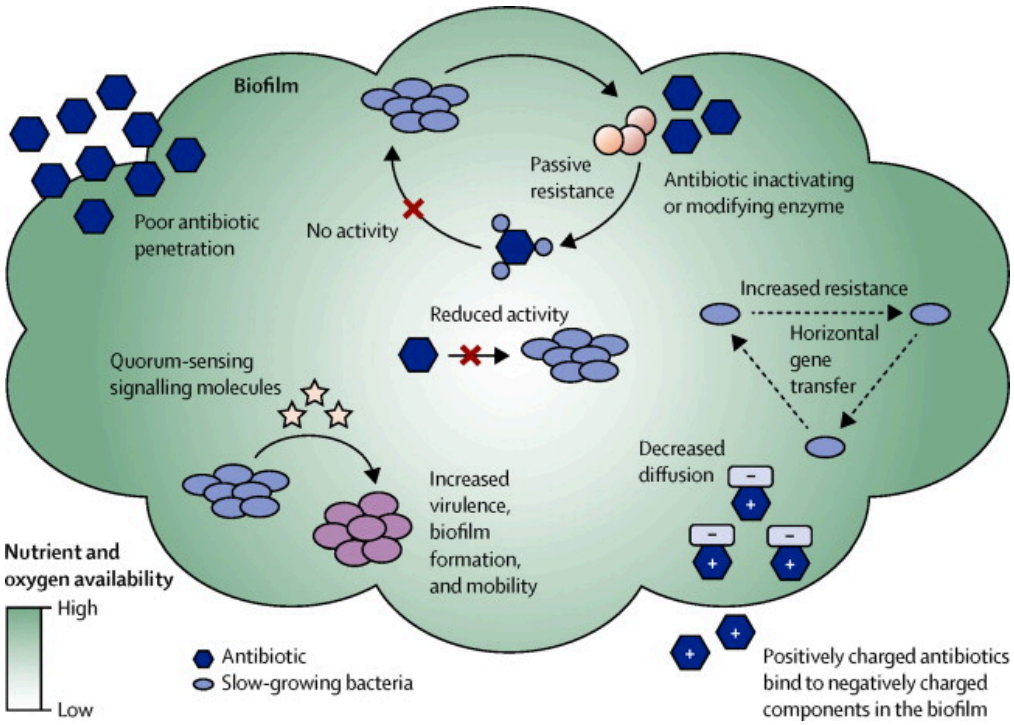

Figure 1.13 Mechanisms of biofilm antibiotic resistance.

Resistance to antimicrobial agents in biofilms is multi-factorial and mediated by different genotypic and phenotypic mechanisms. Figure from [91].

1.2.7 Need for novel therapeutic approaches to combat *P. aeruginosa* infections

Rising concern about the impact of antibiotic resistance in *P. aeruginosa* has prompted the search for novel strategies. Approaches include the use of quorum sensing (QS) inhibitors, iron chelators, and bacteriophages [91]. Antibiotic adjuvants, agents that act alongside a co-administered antibiotic, potentiating its action, are considered a possible future approach. This would not only delay the development of resistant strains, but also limit the dosage and toxicity of antibiotics (further details on toxicity and adverse effects specific to aminoglycoside antibiotics are provided in Chapter 3).

1.3 INTERDISCIPLINARY RESEARCH INITIATIVES

1.3.1 Importance of Interdisciplinary Research

Collaboration across disciplines has played a pivotal role in understanding and advancing science. However, formal education or training that extends across scientific disciplines is hard to obtain [92]. This is often due to the inherent challenges of interdisciplinary research such as attitudinal resistance, impediments to funding, scarcity of academic programs, and the perceived lack of career opportunities [93]. However, despite these barriers, the wide-ranging scope and benefits of interdisciplinary research have been recognized [94, 95]. Collaboration across disciplines fosters innovative thinking, widens a scientists' repertoire of techniques, offers greater insight into complex scientific problems than that achievable by a single discipline, and can open new fields for scientific research [96]. Therefore, it is important to promote interdisciplinary initiatives at all levels of teaching and research, including at science outreach and community education programs.

1.3.2 Need for Hands-on, Interdisciplinary training

Using the terms "interdisciplinary" and "hands-on", we searched previously published educational modules in the education series section of PLoS biology (as of 11-20-2015) and analyzed the top 10 articles found (Table 1.3). Based on our analysis, only 6 out of the 10 modules had a 'hands-on' training component,

4 out of the 10 modules demonstrated interdisciplinary science, and only 2 out of the 10 modules possessed both hands-on and interdisciplinary aspects. There is thus a need for science modules that are both hands-on and interdisciplinary, and that can be executed at a relatively low-cost to make them tractable for science outreach programs.

1.3.3 Focus of our interdisciplinary, hands-on, low-cost educational module

We have developed a hands-on, experimental module that uses an interdisciplinary approach, combining biology experiments and a physics-based analytical model, to address the problem of antibiotic resistance. This module was first implemented at the Hands-on Research in Complex Systems School held at The Abdus Salam International Centre for Theoretical Physics (ICTP), Trieste, Italy from 29th June – 11th July 2014. In our experience, this module was robust, reproducible, resource-efficient, and cost-effective. These serve as favorable features in taking this module to diverse settings such as undergraduate research manifestos, STEM camps, school programs, and laboratory training workshops. Given the paucity of structured training or education programs that integrate diverse scientific fields, this module can provide valuable, interdisciplinary, research experience in science outreach and education initiatives.

Table 1.3 Analysis of educational modules from PLoS Biology using the search terms “hands-on” and “interdisciplinary”. The top ten modules generated by the search were used for this analysis.

Module	Hands-on experiments?	Interdisciplinary?
A wee lesson in science (2004)	Yes	No
Biology by numbers – introducing quantitation into life science education (2005)	No	Yes
Ask a Biologist: Bringing science to the public (2010)	No	No
Creative Research Science experiences for high school students (2010)	Yes	No
It’s elementary: science buddies bring biology to life (2009)	Yes	Yes
Rethinking outreach: teaching the process of science through modeling (2009)	Yes	Yes
Breaking down the stereotypes in science by recruiting young scientists (2004)	Yes	No
Workshops without walls: broader access to science across the world (2011)	No	Yes
Discovery-based science education: functional genomic dissection in *Drosophila* by undergraduate researchers (2005)	Yes	No
“Deconstructing” scientific research: A practical and scalable pedagogical tool to provide evidence-based science instruction (2009)	No	No

1.4 DISSERTATION OBJECTIVES

The goal of this proposal is to understand approaches to overcome antibiotic resistance in microbial populations using an interdisciplinary perspective. We approach this by elucidating the effects of physical and spatial structure on microbial populations. This approach would not only provide additional insights into the structure and functions of microbial communities, but also open possibilities of harnessing these effects as novel treatment strategies. We address this by using insights from our work on microbial population structure to enhance the efficacy of antibiotics, and develop a method of analysis of drug interactions that goes extant traditional approaches. Further, we use insights from our work to develop a hands-on educational module that can provide valuable interdisciplinary research experience in science outreach initiatives.

This dissertation is comprised of five chapters. Chapter 1 is an overview of the physical and spatial structure of microbial communities, including a description of microbial population structure, inherent to these communities. This population structure is further discussed in the context of our model organism *Pseudomonas aeruginosa*, along with a description of this pathogen and associated infections. Chapter 2 describes the study of the effect of population structure (cell density, cell types, and spatial organization) on the survival of antibiotic resistant mutants of *P. aeruginosa*. We find that an alkaline, metabolic by-product of amino acid catabolism acts synergistically with the aminoglycoside

antibiotic tobramycin to enhance its efficacy against antibiotic-resistant mutants. Chapter 3 is an assessment of a novel therapeutic approach to combat *P. aeruginosa* infections using insights from our study on the effect of population structure on antibiotic resistance. Here, we evaluate the therapeutic efficacy of a combination of the antibiotic tobramycin and an alkaline compound sodium bicarbonate against planktonic and biofilm states of *P. aeruginosa.* Chapter 4 is a description of a low-cost, hands-on, educational module to study antimicrobial compounds using an interdisciplinary approach. This module uses a standard microbiology experiment called the disc-diffusion assay together with a diffusion-based analytical model to evaluate the efficacy of antimicrobial compounds and determine the physical characteristics of the active antimicrobial component. Chapter 5 is a discussion of the conclusions from my work on the impact of physical and spatial structure on microbial populations, and I present possible future directions that could be pursued beyond my work related to Chapters 2 - 4. Finally, I also present an account of specific advances made in the field as a consequence of my work.

Chapter 2: The spatial profiles and metabolic capabilities of microbial populations impact the growth of antibiotic-resistant mutants[a]

2.1 INTRODUCTION

Understanding how populations of antibiotic-susceptible bacteria give rise to resistant strains is essential to designing treatments that prevent or delay the development of antibiotic resistance [98]. Recent work has shown that heterogeneity in the spatial distribution of antibiotic in the environment can accelerate the evolution of genetically based antibiotic resistance [21, 28, 29, 34]. While these studies examine the impact of spatial structure in the microbial environment, the role of the spatial distribution of the microbial population itself remains to be further explored. In the context of microbes, spatial structure of the population includes cell density, population composition, and spatial organization of cell types. Most microbial communities consist of interacting, heterogeneous, multispecies populations [99, 100]. The per-strain spatial structure of microbial populations is a primary determinant of inter- and intra-species interactions. The simplest parameter characterizing spatial structure is the number density of a disordered population. To date, few studies have examined the effects of microbial density on the development of antibiotic resistance [40, 51, 101].

[a]This chapter was adapted from reference [102]. Kaushik KS, et al (2015). *J. Roy. Soc. Interface* (12): 20150018.

An exception is the case of bacterial biofilms, which are multicellular bacterial aggregates embedded in an extracellular matrix [15]. Typically, a bacterial infection begins with a low-density inoculum of planktonic cells, which may then develop into a chronic, high-density biofilm infection [15]. High cell density can promote phenotypic antibiotic resistance [40, 51]. However, the impact of a microbial population's spatial distribution on the development of genotypic antibiotic resistance remains to be explored. Unlike biofilm-based phenotypic antibiotic resistance, genetically based antibiotic resistance can play a role in planktonic cells as well as in biofilms and has the potential to be inherited and spread to descendent populations.

Here we show that at cell densities lower than those found in biofilms and therefore corresponding to those in many initial infections, increasing cell density can impair the survival of antibiotic-resistant mutants in the presence of aminoglycoside antibiotics. We term this negative impact "inhibition". The antibiotic-resistant mutants in this study are strains of *Pseudomonas aeruginosa*, a common nosocomial pathogen that affects burned, wounded, and ventilator-assisted patients, and also one of the leading proximate causes of death in patients with the genetic disorder Cystic Fibrosis (CF). We observe inhibition with two different aminoglycoside antibiotics: tobramycin, a front-line drug for treatment of *P. aeruginosa* infections, and gentamicin, used in the treatment of a wide range of Gram-negative bacterial infections [103, 104]. Furthermore, we find

that a wide range of microbial species can produce inhibition. Our results indicate that this is because the molecular agent of inhibition is a by-product of native bacterial metabolism and that the mechanism of inhibition involves an alkaline change in the pH of the environment.

We examine both heterogeneous and well-mixed systems, and find that inhibition can act over long ranges by diffusion. We describe heterogeneous systems with a model, which considers the diffusion of the inhibitory molecule from regions of high density to regions of low density, and estimate the molecular weight of the agent of inhibition. We additionally develop a stochastic model of inhibition in a well-mixed system, which considers microscopic variation in cell density. This model quantitatively describes our observations and offers an explanation of the apparently contradictory observation that high-density mutant colonies are capable of growth in the presence of antibiotics.

Our work indicates that microbial population structure might be a target for, or a tool in, novel therapeutic approaches to combat antibiotic resistance, and that the lifetime of current antibiotics might be extended with the use of natural products as synergistic agents.

2.2 MATERIALS AND METHODS

2.2.1 Bacterial strains and growth conditions

P. aeruginosa PA14 was used as the wild-type (WT) strain (gift from Marvin Whiteley, UT Austin). WT overnight cultures, grown in antibiotic-free media, were plated on tobramycin 8 μg/mL agar. Spontaneous antibiotic-resistant mutants grew colonies and were archived in 20-30% glycerol at -80°C. Upon subsequent plating, samples that showed mixed colony types were re-isolated.

To generate mutants in the presence of antibiotic, WT were passaged in twofold increasing tobramycin concentrations, starting at 0.3 μg/mL, for eight successive days. Samples were archived at -80°C daily.

Transposon-insertion mutants were obtained from the PA14 nonredundant transposon library [71]. *P. aeruginosa* strain PAO1, seventeen clinical *Pseudomonas* isolates [105], *Pseudomonas* sandgrass isolate, *P. fluorescens,* Methicillin-resistant *S. aureus* Mu50 [106], *E. coli* DH5α, *Burkholderia cepacia* and Δ*phz1/2* mutant [107] (gifts from Whiteley, UT Austin), *Serratia marcescens* (gift from Rasika Harshey, UT Austin) and *Saccharomyces cerevisiae* S288C (gift from Edward Marcotte, UT Austin)

All bacterial strains were grown in Luria-Bertani broth or on LB agar except where otherwise indicated (Miller). *Saccharomyces cerevisiae* was grown in Yeast-Peptone-Dextrose (YPD) broth or agar except where otherwise indicated [108]. Overnight cultures were shaken at 180 rpm for 16-18 hours at 37°C, except *P. fluorescens* and *B. cepacia* were grown at 30°C. When indicated, agar incorporated tobramycin (Indofine Chemical Company, NJ) or gentamicin (Fisher Scientific, NJ). Except when indicated otherwise, the concentrations used were 8 μg/mL.

2.2.2 Determination of Minimum Inhibitory Concentrations (MICs)

MICs to antibiotic tobramycin and gentamicin were measured using broth microdilution methods as recommended by CLSI [109].

2.2.3 Whole-Genome Sequencing

Except when stated otherwise, one spontaneous mutant strain was used for all experiments. This mutant strain was characterized using whole-genome sequencing. Sequences were deposited in the National Center for Biotechnology Information Short-Read Archive http://www.ncbi.nlm.nih.gov/sra (accession no. SRP042054). Three single-nucleotide polymorphisms (SNPs) unique to the antibiotic-resistant mutant strain were identified.

2.2.4 Experiments in spatially-mixed systems

10^6-10^{11} cells in 3 mL of 0.6% LB agar were overlaid on tobramycin-containing agar (4 μg/mL). Number of cells was found from optical density (OD_{600}) of the overnight cultures (Nanodrop 2000c, Thermo Scientific), using the conversion factor OD 1 is $0.8X10^9$ cells/mL. Plates were incubated at 37°C for 48 hours and colonies were counted (ImageJ v.1.47 [110]).

2.2.5 Disc diffusion assay for spatially-structured systems

To form uniform lawns of antibiotic-resistant mutants on the surface of antibiotic agar, we used an overlay agar technique. ~10^8 mutants, unless otherwise stated, were added to 3mL of 0.6% (soft) LB agar and overlaid on antibiotic-containing LB agar.

For deposition onto discs, overnight cultures (32 mL) were centrifuged to form a pellet (4000 rpm, 20 min), washed 3x by removing supernatant and adding sterile media, and resuspended in 100 μl of fresh, sterile LB broth. From this, 10 μl (~10^9-10^{10} bacteria, ~10^{11}-10^{12} yeast, unless otherwise stated) was deposited on sterile 7-mm diameter filter discs (Whatman) on the agar. We used the conversion factor OD 1 is $0.8X10^9$ cells/mL for bacteria and $3X10^7$ cells/mL for yeast. Plates were incubated at 37°C for 24-48 hours, after which the width of inhibition (X) was measured.

2.2.6 Creating structured agar plates

To create agar with spatially-structured composition, agar was poured and allowed to cool as usual. Then, cores of different diameters (7, 10 and 15-mm) were created with a sterile metal punch. Wells were filled with agar containing a different set of nutrients or antibiotic, and allowed to set. As soon as the cores set (within 10 min), filter discs were placed on the core and WT cells were deposited.

2.2.7 Using pH change to probe the nature of the released inhibitory factor

Bromthymol blue (BTB) was added to agar at a final concentration of 0.002%. 32 mL of overnight microbial cultures were deposited as above. Plates were incubated at 37°C and observed every hour for an alkaline or acidic change around the filter discs. Images were taken immediately after deposition (for nutrient-free BTB agar) or 2 hours after deposition (for LB-tobramycin BTB agar) or after overnight incubation (for antibiotic-resistant mutant lawns).

2.2.8 Testing the effect of different nutrient conditions of overnight growth media on inhibition

In LB and YPD, WT PA14*, S. aureus* and *E. coli* grew to a density of ~10^9 cells / mL. In YPD, *S. cerevisiae* grew to a density of ~10^8 cells / mL. *S. cerevisiae* grew poorly in LB medium, to a density of ~10^7 cells / mL. The pH of

the cell cultures and of filter-sterilized supernatant was measured using pH indicator strips (Cardinal Health, IL).

Overnight cultures were centrifuged (4000 rpm, 20 min), washed 3x, and resuspended in fresh, sterile LB or YPD broth (100 μL). ~10^9 cells were deposited on filter discs. Filter-sterilized supernatant from each culture condition and sterile, fresh LB and YPD broth were also deposited onto filter discs. Plates were incubated and pH change monitored as above.

2.2.9 Deposition of exogenous alkali compounds

10 μL of ammonium hydroxide (NH_4OH) (14.8M, 7.4M, 4.9M, 3.7M, 2.9M, 2.4M), sodium hydroxide (NaOH) (1M, 0.5M, 0.33M, 0.25M, 0.2M), sodium bicarbonate ($NaHCO_3$) (1M, 0.5M, 0.33M, 0.25M, 0.2M) and 1M ammonium chloride (NH_4Cl) were deposited on agar plates. Plates were incubated and pH change monitored as above. 10 μL of exogenous alkali compounds (2.1M NH_4OH, 0.5M NaOH and 0.5M $NaHCO_3$) were also deposited on decreasing dilutions (10^8 to 10^5 cells) antibiotic-resistant mutant lawns overlaid on antibiotic-free LB agar.

2.2.10 Detection of ammonia and/or amine emission

An ion-selective electrode (Orion 920A, Thermo Scientific) was used to detect ammonia or amine emission. LB-tobramycin agar filled 20 mL sterile,

narrow-necked glass vials almost filled to capacity. This reduced the headspace available between the upper meniscus of the agar and cap of the vial. Cells were deposited on the filter discs placed on the upper surface of the agar and the vials were immediately capped. The electrode was calibrated using 0.1, 0.5, 1, 2.5 and 5 mg/L concentrations of ammonium sulfate. While measuring ammonia levels for calibration and in the experiment vials, the electrode was held at a distance of 1 cm. above the upper surface of the media (gaseous phase). All measurements were conducted at 37°C.

2.2.11 Modeling diffusion of the IF in a spatially-structured system

The disc diffusion assay can be modeled using diffusion laws. In this system, a finite quantity of IF is released by cells at the disc and diffuses into a cylindrical agar volume with radius much larger than height. A system with this geometry has been solved with a non-closed form solution [111]. However, this solution has been shown numerically to be approximated by the solution of one-dimensional diffusion from a constant source [111]:

$$[IF] = \frac{[IF]_0}{4\pi Dt} \exp\left(-\frac{x^2}{4Dt}\right) \qquad (1)$$

where $[IF]$ is the concentration of IF as a function of distance from the disc x, time t, the initial concentration at the disc $[IF]_0$, and the diffusion coefficient D.

At the critical time T_c when zone size is set, the distance $x = X$ defines the region in which the concentration of IF exceeds the critical concentration $[IF]_c$. Assuming the amount of IF produced is proportional to the number of cells on the disc gives Equation (1). If the mutant overlay is pre-incubated for a set time h before the disc is placed, the zone size X is given by:

$$X^2 = 4D(T_c - h)\ln(N_0) + F(N_c, D, T_c)$$

where N_0 is the number of cells placed on the disc and N_c is the minimum number of cells on the disc required to produce a zone of inhibition. The diffusion coefficient of a molecule is inversely proportional to its radius. To first order, a molecule's volume and therefore its molecular weight MW scales as the cube of its radius. Thus for IF and a molecule A:

$$MW_{IF} = MW_A \left(\frac{D_A}{D_{IF}} \right)^3$$

2.2.12 Measurement of the critical incubation time T_c and the diffusion coefficient D of the IF

Increasing numbers of WT cells (10^7 to 10^{11} in 10 μL) were deposited on filter discs. A linear regression of (X^2) as a function of $\ln(N_0)$, where X is the zone size and N_0 is the number of cells placed on the disc, was performed using R v2.15.2 [97].

In parallel, to measure critical time T_c, antibiotic-resistant mutants were overlaid onto antibiotic agar and then pre-incubated. At set increments of pre-incubation time, WT cells (~10^{10}) were placed on filter discs. To estimate the time after which no zone of inhibition would be formed, a linear regression of X^2 as a function of pre-incubation time was used to find the X^2 = 0 intercept. This is T_c. Corresponding experiments were performed for tobramycin as a molecular weight calibrator.

2.2.13 Modeling the effect of small fluctuations in population density of antibiotic-resistant mutant survival in a spatially-mixed system

We model the probability of mutant survival P in spatially-mixed systems by $P = 1 - e^{-V_e \rho_0} \sum_{i=0}^{\Gamma V_e \rho_0^{\eta} - 1} \frac{\left(V_e \rho_0\right)^i}{i!}$, where ρ_0 is the average cell density, V_e is an effective volume in which cells reduce antibiotic quantities per cell, and Γ and η are lumped parameters. The function P is defined for densities in which $\Gamma V_e \rho_0^{\eta} - 1$ is a positive integer n, such that ρ_0 must be equal to $\left(\frac{n+1}{\Gamma V_e}\right)^{\frac{1}{\eta}}$. We linearly interpolate between values of ρ_0 which satisfy this condition to generate a continuous function $\tilde{P}$. Model parameters were estimated using a non-linear least squares regression of the colony counts in replicate 1, Figure 1B (R v2.15.2 [97]. R^2 was calculated as the ratio of explained variance to total variance.

2.2.14 Statistical Tests

Correlation statistics and Student *t* tests were done in Microsoft Excel.

2.3 RESULTS AND DISCUSSION

2.3.1 In a spatially-mixed system, increasing cell densities negatively impact the survival of antibiotic-resistant mutants

We grew *P. aeruginosa* PA14 cultures overnight and then plated portions of the resulting populations onto Luria-Bertani (LB) agar containing tobramycin at 4 μg/mL. This is approximately four times the minimum inhibitory concentration (MIC) for wild-type (WT) PA14 cells. The overnight cultures consisted of a mixture of WT PA14 cells and spontaneously-generated antibiotic-resistant mutants. We used each overnight culture to prepare multiple agar plates, varying the density of bacteria spread on the plate over four orders of magnitude. The number of antibiotic-resistant colonies that grow on antibiotic agar is the product of (1) the number of antibiotic-resistant mutants plated and (2) the probability that an antibiotic-resistant mutant will grow after plating. The first number, will linearly increase as more of each culture is plated.

However, we find that the number of antibiotic-resistant colonies that grow depends non-monotonically on the initial density of the plated population. These data show a maximum, or 'sweet spot', for the number of plated mutants that survive antibiotic exposure and grow into colonies (Figure 2.1A). The fraction of the plated culture that gives rise to mutant colonies, *aka* the "mutation frequency" [112], decreases monotonically with increasing cell density (Figure 2.1B). Therefore, the probability of a mutant growing into a colony must also decrease

with increasing cell density. Since there are orders of magnitude more WT than antibiotic-resistant mutant cells present in the initially-plated cultures, we postulate that WT cells are inhibiting the antibiotic-resistant mutants.

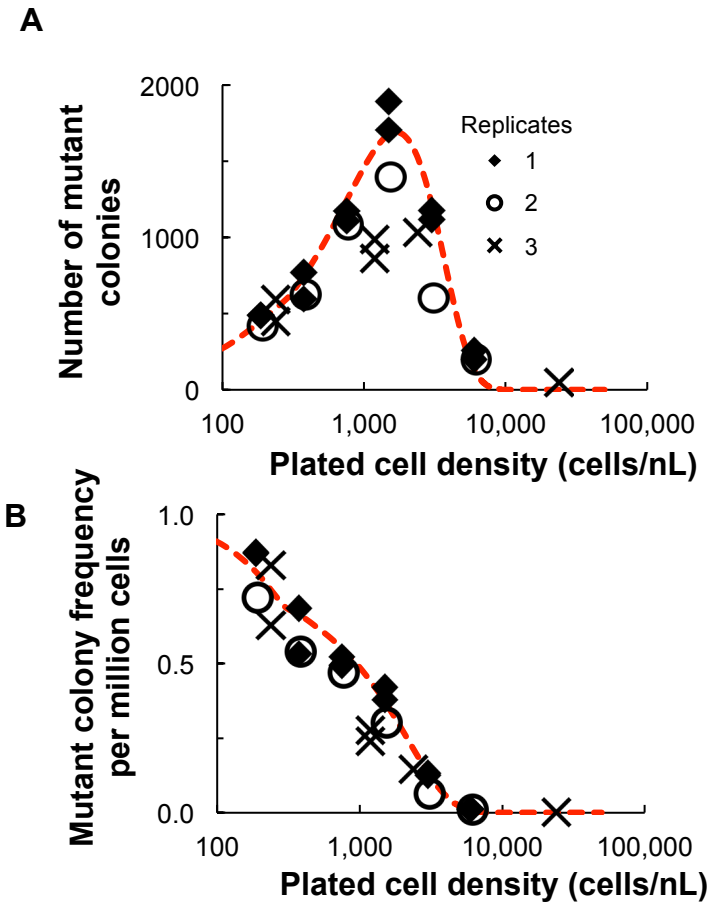

Figure 2.1 In a spatially-mixed system, high cell densities negatively impact the survival of antibiotic-resistant mutants in the presence of antibiotic.

Different cell densities from overnight PA14 cultures, containing WT cells and antibiotic-resistant mutants, were plated on LB-tobramycin 4 µg/mL agar. **(A)** The number of growing antibiotic-resistant mutant colonies varies non-monotonically with cell density. *N = 3*. **(B)** The fraction of the plated culture that grows into antibiotic-resistant colonies decreases monotonically with increasing cell density. *N = 3.* In **(A)** the red line shows our analytical model, derived using a Poisson distribution to describe random fluctuations in density that describes the number of surviving antibiotic-resistant mutants as a function of cell density. In **(B)** the red line shows the analytical model describing the frequency of mutant colonies as a function of cell density. R^2 = 0.78. Model parameters: V_e = 0.004, η = 1.164, Γ = 0.370 $nL^{\eta-1}$ and μ = 1.10×10^{-6}.

2.3.2 In a spatially-structured system, WT cells inhibit the growth of antibiotic-resistant mutants

For all further experiments we used the same spontaneously-generated mutant strain and tobramycin at 8 μg/mL, except when stated otherwise. To investigate the role of WT cells in inhibition, we overlaid antibiotic-resistant mutants onto LB-tobramycin agar, placed filter-paper discs onto this background, and deposited WT PA14 cells onto the filter discs. This system offers a simplified model to examine inhibition in populations exhibiting macroscopic heterogeneity in cell density, and is inspired by the disc diffusion assay often used to evaluate antibiotic susceptibility [113]. After growth of the antibiotic-resistant mutant lawn, we observed circular zones of inhibition surrounding the filter discs (Figure 2.2). Sterile LB broth produced no inhibition. From these experiments, we conclude that, in the presence of antibiotic, WT PA14 cells inhibit antibiotic-resistant mutants.

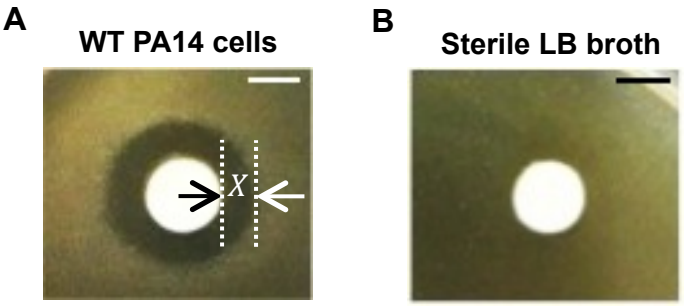

Figure 2.2 Inhibition is produced by WT PA14 cells, but not by sterile LB broth.

WT PA14 cells and sterile LB broth (control) were deposited on antibiotic-resistant mutant lawns on LB-tobramycin 8 µg/mL agar. **(A)** WT PA14 cells produce inhibition of antibiotic-resistant mutants. **(B)** Sterile LB broth does not produce inhibition. Scale bars are 5 mm.

2.3.3 Inhibition is not dependent on cell-to-cell contact or proximity

Other researchers have described contact- or proximity-dependent bacterial inhibition that depends on close positioning between cells [114-117]. In the disc diffusion assay, we considered the possibility that motile WT PA14 cells, initially deposited on the filter disc, could move out into the surrounding agar containing antibiotic-resistant mutants, thereby allowing contact- or proximity-mediated inhibition to take place. *P. aeruginosa* shows four types of motility: swimming, twitching, swarming and sliding [118]. The first three of these motility modes involves one or both of the motility appendages, flagellae or pili. To rule out the possibility of motility mediating cell-to-cell contact, we used *fliC*, *fliA,* and *pilT* mutants [71]. The *fliC* mutant is defective in the flagellin subunit protein, which polymerizes to form the bacterial flagellum [119]. The *fliA* mutant is defective for a sigma factor required for flagellin expression [120]. The *pilT* mutant is defective in type IV pilus retraction [121].

Swimming motility requires flagellar activity [122, 123]. The inhibition we observe with *fliC* and *fliA* mutants (*fliC* X = 5 mm, *fliA* X = 5 mm) is comparable to that of WT PA14 cells (X = 5 mm) (Figure 2.3). Further, at the 0.6% agar concentration used in the overlay agar, *P. aeruginosa* does not demonstrate swimming motility [124]. Therefore, we conclude that swimming motility does not play a role in inhibition.

At 0.5-1% agar concentrations, *P. aeruginosa* exhibits swarming or group-

mediated surface motility [122, 125]. Since swarming requires both flagella and type IV pili, *fliC* mutants show reduced or absent swarming [125]. Inhibition with *fliC* mutants is comparable to that of WT PA14 cells (*fliC* X = 5 mm, WT PA14 X = 5 mm) (Figure 2.3). Therefore, we conclude that swarming motility does not play a role in inhibition.

Twitching motility is a form of surface transclocation mediated by type IV pili [126] and *pilT* mutants are defective in twitching motility [121]. Inhibition seen with the *pilT* mutant (X = 5 mm) is comparable to that seen with WT PA14 cells (X = 5 mm) (Figure 2.3). Therefore, we conclude that twitching motility does not play a role in inhibition.

Finally, sliding motility is a type of surface translocation that is independent of both flagella and type IV pili. In fact, the presence of pili abolishes sliding motility, possibly by increasing interactions between the cell and the substrate [123]. WT PA14, *fliC* and *fliA* cells had intact type IV pili, hence sliding motility is not involved in inhibition.

Aggregated, these results indicate that bacterial motility is not involved in inhibition and therefore inhibition does not result from cell-to-cell contact or proximity.

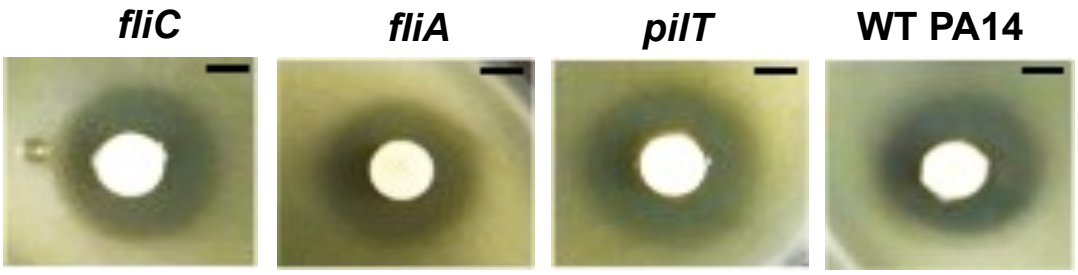

Figure 2.3 Impairing bacterial motility does not impact inhibition, which we therefore infer does not depend on cell-to-cell contact or proximity.

Motility-deficient mutants *fliC*, *fliA*, *pilT*, and WT PA14 cells were deposited on antibiotic-resistant mutant lawns on LB-tobramycin 8 µg/mL agar. No differences in inhibition zone sizes are observed between motility-deficient and WT cells (for *fliC* X = 5 mm; for *fliA* X = 5 mm; for *pilT* X = 5 mm; for WT PA14 X = 5 mm). Scale bars are 5 mm; *N = 3.*

2.3.4 Inhibition is not caused by nutrient depletion

It has long been recognized that plating an inoculum with high cell density will result in fewer colonies than expected [127, 128]. Depletion of nutrients has been proposed as a cause for this and nutrient availability has been shown to have wide-ranging effects on microbial communities [107, 129-131]. Therefore, we considered the possibility that the high density of WT PA14 cells on the filter disc locally depletes the agar gel of nutrients, and that this is the cause of the inhibition we observe.

To evaluate this possibility, we used a modified disc diffusion assay, in which WT PA14 cells were deposited on filter discs placed on LB-tobramycin 8 μg/mL agar cores containing single-strength nutrients (1X core), double-strength nutrients (2X core) and ten-times nutrient strength (10X core), surrounded by antibiotic-resistant mutants on LB-tobramycin 8 μg/mL agar. As a control, WT cells were deposited on filter discs directly on the antibiotic-resistant lawn (no core). If nutrient limitation mediated inhibition, we would expect to see decreasing zones of inhibition with increasing nutrient strength of the cores. However, no significant difference in inhibition is observed under the different conditions: For no core, X = 4 mm; for 1X core X = 4 mm; for 2X core X = 4 mm; for 10X core X = 4 mm (Figure 2.4A and B).

Furthermore, we created a nutrient sink in the form of a core containing

1.2% agar with tobramycin (8 μg/mL) but without nutrients (no WT cells were deposited). If nutrient availability played a role in inhibition, this nutrient sink would be expected to produce large zones of inhibition. However, no inhibition is observed around the nutrient-free core (X = 0 mm) (Figure 2.4B).

In the aggregate, these results indicate that inhibition does not result from nutrient depletion.

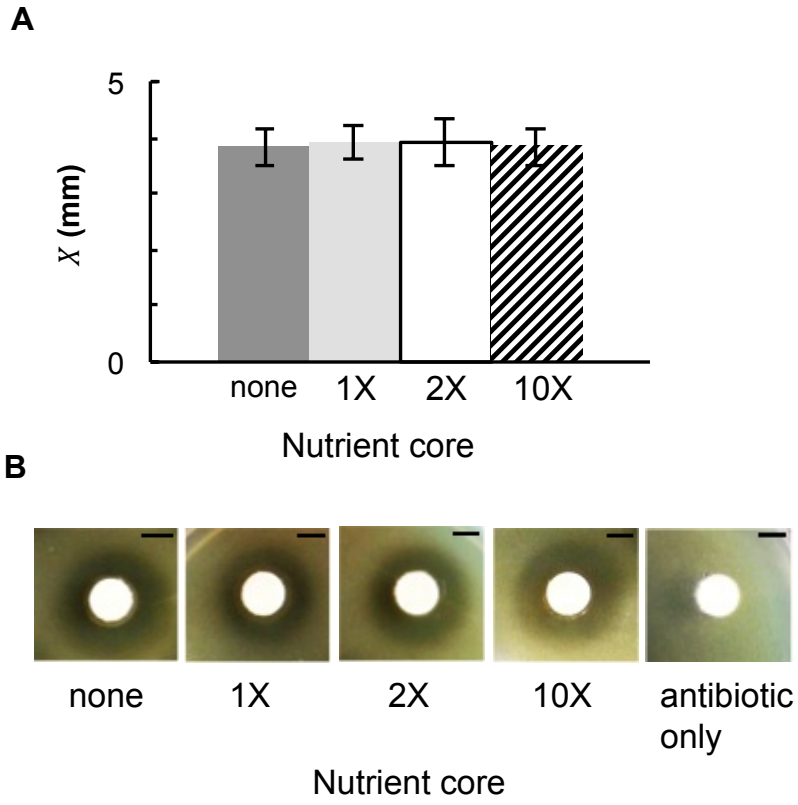

Figure 2.4 Inhibition is not due to nutrient depletion.

(A) WT PA14 cells were deposited directly on antibiotic-resistant mutants lawns (no core) on LB-tobramycin 8 μg/mL agar and on agar cores containing single-strength nutrients (1X core), double-strength nutrients (2X core), ten-times nutrient strength (10X core). Each core was surrounded by a lawn of antibiotic-resistant mutants on LB-tobramycin 8 μg/mL agar. No significant difference is observed in the sizes of inhibition zones produced with different nutrient cores. Error bars represent standard error of the mean; *N* = *3.* **(B)** Representative inhibition zones with WT cells deposited: (1) directly on filter discs (no core) (X = 4 mm); (2) on agar cores containing single-strength nutrients (X = 4 mm); (3) on double-strength nutrients (X = 4 mm); and (4) on ten-times nutrient strength (X = 4 mm). In [97], cores of agar with tobramycin (8 μg/mL) but without nutrients and WT cells, produce no inhibition (X = 0 mm). Scale bars are 5 mm.

2.3.5 Pyocins do not mediate inhibition

P. aeruginosa produces pyocins that exert lethal effects on similar or closely-related bacterial species [132]. Pyocin production is regulated by positive and negative regulatory genes, *prtN* and *prtR*, where the PrtR negative regulator represses the activator gene *prtN*. When stimuli inactivate the PrtR repressor, this leads to activation of *prtN* and production of pyocins [132]. To determine if inhibition is mediated by pyocins, we tested a *prtN* mutant [71] deficient for the production of all known *P. aeruginosa* pyocins. Pyocin-deficient *prtN* cells produce inhibition comparable to WT PA14 cells (for *prtN* X = 5 mm; for WT PA14 X = 5 mm) (Figure 2.5). From these results, we conclude that pyocins do not cause inhibition.

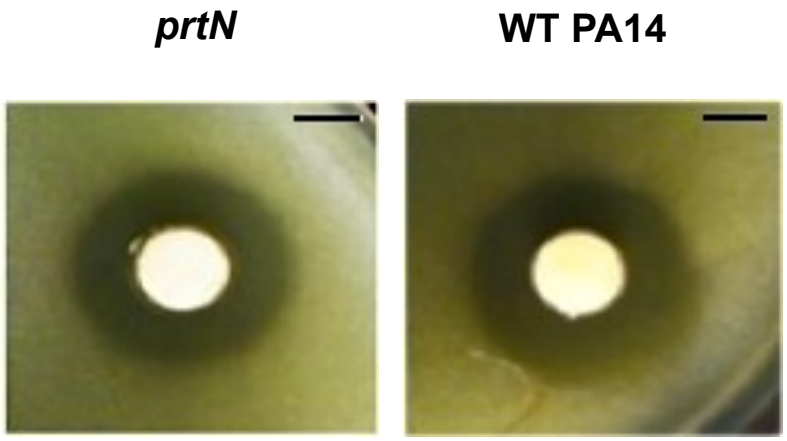

Figure 2.5 Pyocins do not mediate inhibition.

Pyocin-deficient *prtN* cells and WT PA14 cells were deposited on antibiotic-resistant mutant lawns on LB-tobramycin 8 µg/mL agar. No differences in inhibition zone sizes are observed between *prtN* mutant and WT cells (for *prtN* X = 5 mm; for WT PA14 X = 5 mm). Scale bars are 5 mm; *N = 3.*

2.3.6 Quorum sensing does not play a role in inhibition

Quorum sensing is the regulation of gene expression in response to population density [133]. *P. aeruginosa* has two hierarchically-connected quorum-sensing circuits, which regulate the production of acyl homoserine lactone (AHL) signaling molecules [134]. The Las and Rhl systems consists of transcriptional regulators, LasR and RhlR, and the AHL synthases LasI and RhlI. To determine if production of IF was influenced by quorum sensing, we tested *lasI*, *rhlI* and *rhlR* mutants. The *lasR* mutant is not available in the PA14 non-redundant transposon library [71]. We also tested the *Pseudomonas* strain PAO-JP2, which is a double *lasI-rhlI* mutant [135]. QS mutants produce inhibition comparable to WT PA14 cells (for *lasI* X = 5 mm; for *rhlI* X = 5 mm; for *rhlR* X = 5 mm; for PAO-JP2 X = 5 mm; for WT PA14 X = 5 mm) (Figure 2.6). From these results, we conclude that quorum sensing does not play a role in inhibition.

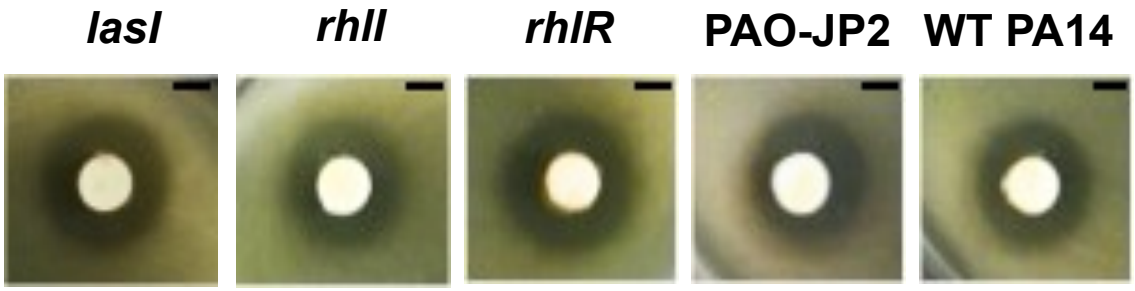

Figure 2.6 Quorum sensing (QS) does not play a role in inhibition.

QS-mutants *lasI*, *rhlI*, *rhlR*, *lasI-rhlI* double mutant PAO-JP2 and WT PA14 cells were deposited on antibiotic-resistant mutant lawns on LB-tobramycin 8 µg/mL agar. No differences in inhibition zone sizes are observed between QS-mutants and WT cells (for *lasI* X = 5 mm; for *rhlI* X = 5 mm; for *rhlR* X = 5 mm; for PAO-JP2 X = 5 mm; for WT PA14 X = 5 mm). Scale bars are 5 mm, *N = 3.*

2.3.7 Inhibition is not due to the production of Reactive Oxygen Species

Bacteria produce Reactive Oxygen Species (ROS) as a metabolic by-product, and it has been suggested that antibiotics exert their effect in part by inducing the production of ROS such as hydrogen peroxide (H_2O_2), superoxide (O_2^-) and hydroxyl radicals (OH^-) [136, 137].

To test the role of H_2O_2 in inhibition, we used catalase, which neutralizes the bactericidal effects of hydrogen peroxide by expediting its breakdown to water and oxygen [138, 139]. WT PA14 cells were deposited on antibiotic-resistant mutant lawns on LB-tobramycin 8 µg/mL agar with and without catalase (100 µg/mL). No significant difference in the inhibition caused by WT PA14 cells is observed between these two cases (Figure 2.7**)**. As a control to establish the efficacy of catalase against bactericidal effects of hydrogen peroxide, we deposited 10 µl of 30% hydrogen peroxide. This produces large bacteria-free regions on catalase-free agar (X = 9 mm) but only small bacteria-free regions on catalase-containing agar (X = 2 mm) (Figure 2.7**)**. From these experiments, we conclude that inhibition of antibiotic-resistant mutants by WT PA14 cells does not result from the production of hydrogen peroxide.

To further probe the role of ROS, we tested a phenazine-null mutant (Δ*phz1/2*), which is deleted in its two phenazine operons, *phzA1-G1* and *phzA2-G2* [140-142]. Phenazines are a distinct group of redox-active compounds,

known to exert toxic effects via the production of ROS [143-145]. Following their production, phenazines reduce molecular oxygen to hydrogen peroxide (H_2O_2) and superoxide (O_2^-); H_2O_2 can further react to produce highly reactive hydroxyl radicals (OH^-) [143-145]. The phenazine-null mutant (Δ*phz1/2*) is deficient for the production of H_2O_2 [143-145]. No significant difference in inhibition is observed with the Δ*phz1/2* mutant (X = 5 mm) as compared to WT PA14 (X = 5 mm) (Figure 2.7). These experiments indicate that inhibition is not mediated by ROS produced by phenazine-mediated reduction of molecular oxygen.

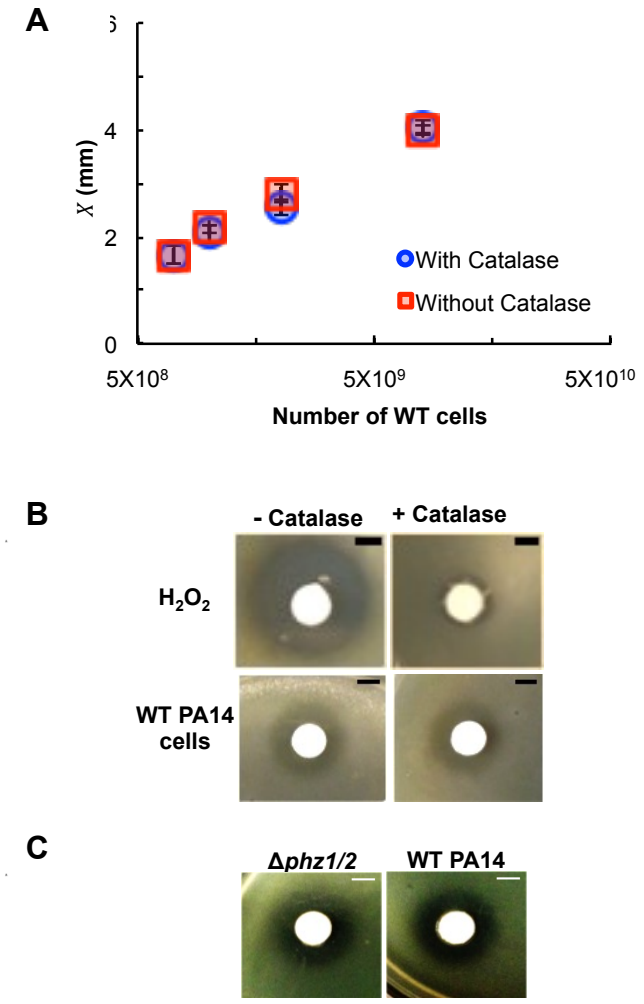

Figure 2.7 Inhibition is not due to ROS produced by phenazine-mediated reduction of molecular oxygen.

(A) Increasing numbers WT PA14 cells were deposited on antibiotic-resistant mutant lawns on LB-tobramycin agar with and without catalase (100 μg/mL). No significant differences in inhibition zone sizes under the two conditions are observed. Error bars represent standard error of the mean; *N = 3.* **(B)** Deposition of 10 μL of 30% hydrogen peroxide on LB-tobramycin agar produces a large bacteria-free region (X = 9 mm), which is smaller in the presence of catalase (X = 2 mm). No difference is observed in inhibition zones produced by WT cells on agar with and without catalase (X = 5 mm). **(C)** Phenazine-deficient (Δ*phz1/2*) and WT PA14 cells were deposited on antibiotic-resistant mutant lawns on LB-tobramycin agar. No differences in inhibition zone sizes are observed (Δ*phz1/2* X = 5 mm, WT PA14 X = 5 mm). Scale bars are 5 mm*, N = 3.*

2.3.8 Changes in the shape of inhibition zones are consistent with inhibition being caused by a diffusible factor

To probe the physical characteristics of the agent causing inhibition, we modified the geometry of the agar surrounding the filter disc using a trench or sterile glass barrier. Upon doing so, the shape of the inhibition zone changes in a way consistent with inhibition being caused by a diffusible factor that does not stick to glass (Figure 2.8). Many proteins stick to glass with some degree of permanence [146], so this suggests that the inhibitory factor is likely not protein in nature.

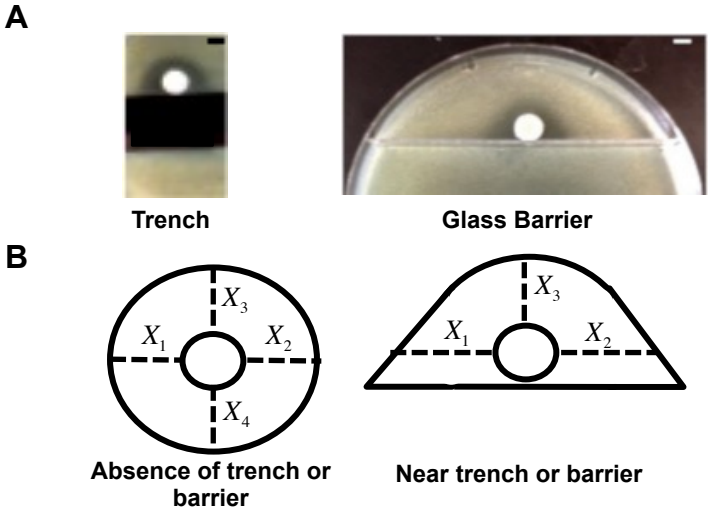

Figure 2.8 Modifications in the shape of the inhibition zones are consistent with inhibition being caused by a diffusible factor.

(A) WT PA14 cells were deposited near a trench and glass barrier on an antibiotic-resistant lawn overlaid on LB-tobramycin agar. In the absence of a trench or barrier, X = 4 mm (image not shown),

$$\frac{X_1 + X_2}{X_3 + X_4} = \frac{(4+4)}{(4+4)} = 1$$

Near a trench or barrier, inhibition zones show a departure from circularity:

Trench X = 5.5 mm, $\frac{(X_1 + X_2)/2}{X_3} = \frac{(5.5+5.5)/2}{4} = 1.4$

Glass barrier X = 7.5 mm, $\frac{(X_1 + X_2)/2}{X_3} = \frac{(7.5+7.5)/2}{4} = 1.9$

Scale bars are 5 mm.

(B) Schematic representation of measurements to quantify a departure from circularity following modification of the geometry of the inhibition zone by a trench or glass barrier, where X_1, X_2, X_3 and X_4 are as shown.

2.3.9 The inhibitory factor has a low molecular weight

We model the disc diffusion assay, informed by previous studies modeling antibiotic diffusion [147, 148].

Our model assumes:

1) The IF is released by WT cells to a concentration $[IF]_0$ at the disc;

2) The IF diffuses out of the disc with a constant diffusion coefficient D;

3) A threshold concentration of IF, $[IF]_{th}$, is required to inhibit mutant cells;

and 4) IF no longer causes inhibition after a critical time T_c of incubation.

Assumption (4) corresponds to an increase in the number of cells in the lawn that causes the per-cell concentration of IF to drop to sub-inhibitory levels [149]. This agrees with our finding that the size of the inhibition zone decreases with increasing initial lawn density (Figure 2.9). The width of the inhibition zone is the distance between the edge of the disc and the edge of the inhibition zone, X (Figure 2.9). Our model approximates X^2 as:

$$X^2 = 4DT_c \ln(N_0) + F(D, T_c, N_c) \qquad (2)$$

N_0 is the number of WT cells deposited on the disc, which we assume to be linearly proportional to the concentration of IF produced. F is a function independent of N_0. N_c is the minimal number of WT cells that produce measurable inhibition. The slope of X^2 as a function of $\ln(N_0)$ gives the diffusion coefficient D, if critical time T_c is known.

To vary N_0, we deposited increasing numbers of WT cells on antibiotic-resistant mutant lawns on tobramycin 4 μg/mL agar and measured X. On a semi-log plot, X^2 varies linearly with $\ln(N_0)$, as predicted by the model (Figure 2.9). To measure T_c, we pre-incubated the mutant lawn before depositing WT cells. *X* decreases with increasing pre-incubation times until *X*=0 (Figure 2.10). We measure T_c to be 110±30 minutes and N_c to be on the order of a million cells.

By fitting the model to the data in figure 2 we estimate the diffusion coefficient D of the IF to be 4.5±0.5x10^{-6} cm^2/s. To calibrate the relationship between *D* and the molecular weight of the IF, we performed the disc diffusion assay using varying concentrations of tobramycin (MW = 467.5 Da) deposited on filter discs on a WT lawn on antibiotic-free agar (Figure 2.11). Fitting these results gives a diffusion coefficient for tobramycin of 9.6±0.8x10^{-7} cm^2/s. Using the Stokes-Einstein relation, we estimate that the IF has a MW of the order of 10 Da, indicating it is a small molecule.

We also performed the above experiments using a tobramycin concentration of 8 μg/mL in the agar and find D of the IF is 2.5±0.4x10^{-6} cm^2/s, so the molecular weight of IF was again determined to be a few tens of Daltons (Figure 2.12). These results very nearly overlap with those taken at 4 μg/mL, and

suggest that the size of the IF is near the lower limit of what we can measure using this approach.

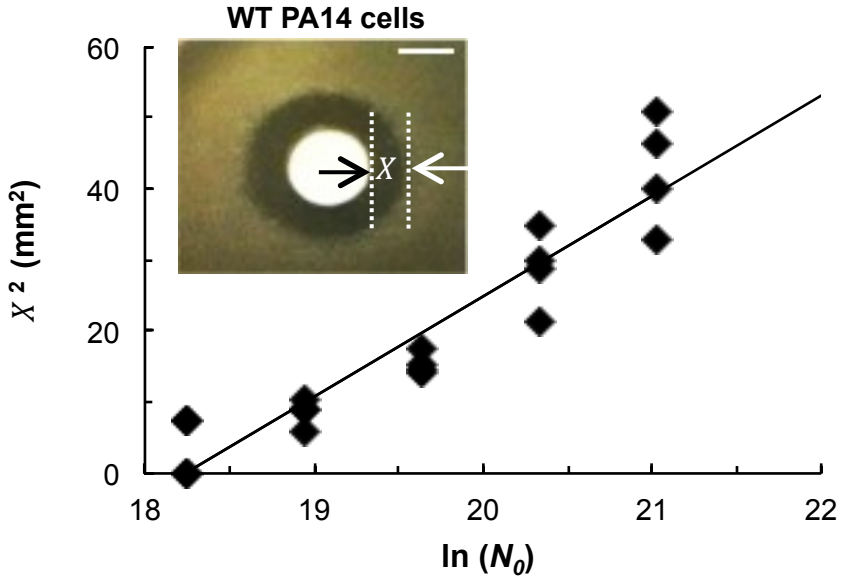

Figure 2.9 In a spatially-structured system, WT PA14 cells inhibit the growth of antibiotic-resistant mutants.

WT cells (~10^9-10^{10}) were deposited on antibiotic-resistant mutant lawns on LB-tobramycin 8 µg/mL agar. *Insert:* WT PA14 cells produce inhibition of antibiotic-resistant mutants (X = 4 mm). The width of inhibition X is measured from the edge of the filter disc to the edge of the inhibition zone. Scale bars are 5 mm. Increasing numbers of WT PA14 cells were deposited on antibiotic-resistant mutant lawns overlaid on LB-tobramycin 4 µg/mL agar. The square of the width of inhibition (X^2) varies linearly with the log of the number of WT cells deposited. R^2 = 0.87. N = 4.

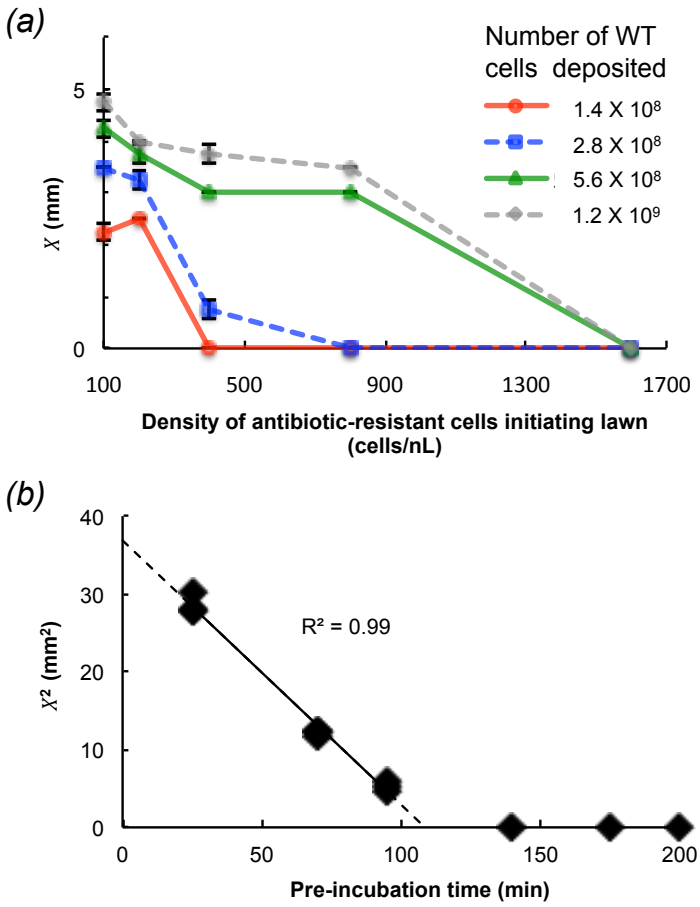

Figure 2.10 Determining the value of T_c

(A) Increasing numbers of WT PA14 cells were deposited on increasing densities of antibiotic-resistant lawns on LB-tobramycin 8 µg/mL agar. The size of the inhibition zone decreases as the lawn density increases, corresponding to the decrease in X seen with increasing pre-incubation time in **(A).** Error bars represent standard error of the mean; *N = 3.* Lines serve as a guide to the eye only. **(B)** Antibiotic-resistant mutants were overlaid on LB-tobramycin 4 µg/mL agar at time 0 min and incubated at 37°C. WT PA14 cells were deposited on filter discs at different time intervals after the lawn was overlaid. Squares of the width of inhibition (X^2) are plotted against corresponding pre-incubation times. From x-intercept of the fit obtained (R^2 = 0.99), the value of T_c is measured as 108±26 minutes. Error represents standard error of the mean; *N = 3.*

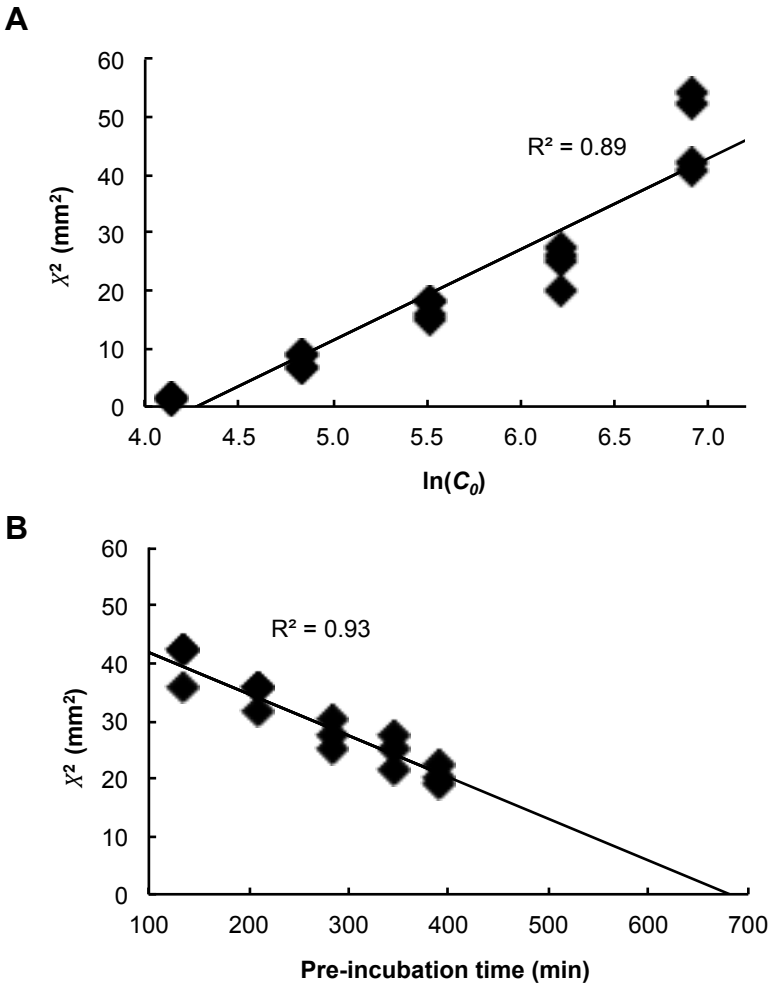

Figure 2.11 Modeling diffusion of tobramycin.

(A) Increasing concentrations of tobramycin were deposited on WT PA14 lawns overlaid on antibiotic-free LB agar. On a semi-log plot, the squares of the width of inhibition (X^2) vary linearly with concentration of tobramycin (C_0), consistent with the disc diffusion model (R^2 = 0.89). **(B)** To determine critical time T_c, WT PA14 cells were overlaid on antibiotic-free LB agar following which tobramycin was deposited at different time intervals. Squares of the width of inhibition (X^2) are plotted against corresponding pre-incubation times. From the x-intercept of the fit obtained (R^2 = 0.93), the value of T_c is measured as 680±50 minutes. Error represents standard error of the mean; *N = 4.*

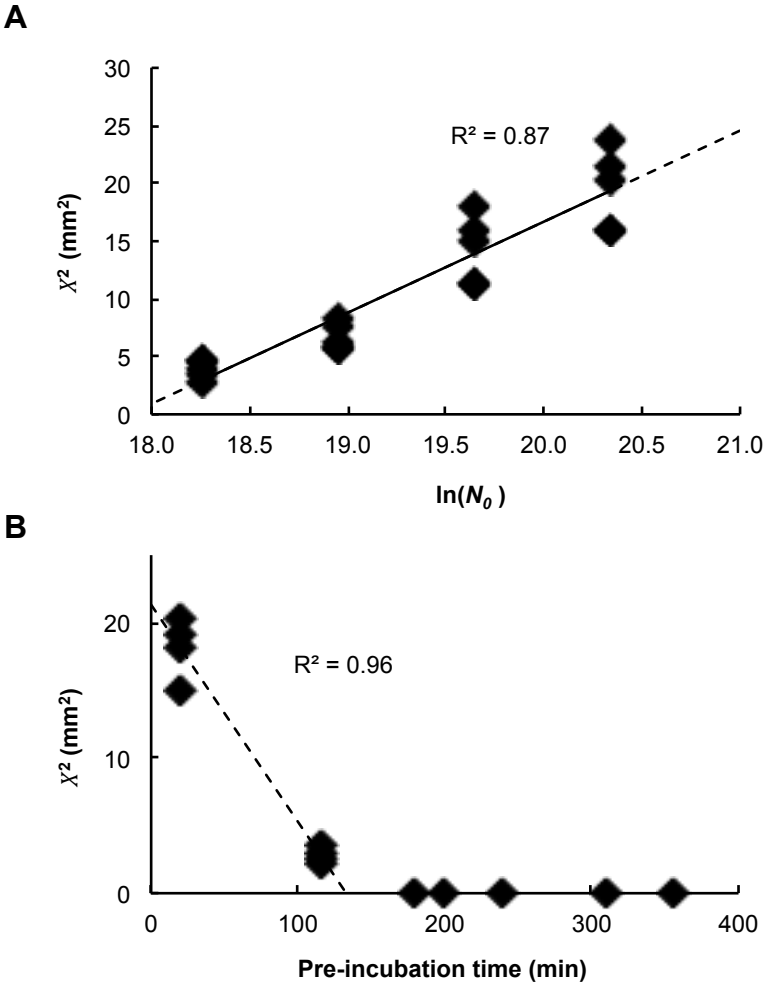

Figure 2.12 Modeling diffusion of the inhibitory factor on LB-tobramycin 8 µg/mL agar.

(A) WT PA14 cells were deposited on antibiotic-resistant lawns on LB-tobramycin 8 µg/mL agar. The squares of the width of inhibition (X^2) vary linearly with the number of WT cells deposited (N_0), consistent with the disc diffusion model (R^2 = 0.87). **(B)** To determine critical time T_c, antibiotic-resistant mutants were overlaid on LB-tobramycin 8 µg/mL agar following which WT PA14 cells were deposited at different time intervals. Squares of the width of inhibition (X^2) are plotted against pre-incubation times. From the x-intercept of the fit obtained (R^2 = 0.96), the value of T_c is measured as 130±10 minutes. Error represents standard error of the mean; *N = 4.*

2.3.10 The inhibitory factor is produced without antibiotic but causes inhibition only in the presence of antibiotic

When the agar does not contain antibiotic, inhibition does not occur (Figure 2.13). This could mean that antibiotic is required for production of the IF, the activity of the IF, or both. To dissect this, we developed a set of complementary experiments, in which the filter disc was centered on top of a cylindrical core of agar with different composition than that of the surrounding agar (Figure 2.14).

When the core does not contain antibiotic, tobramycin must diffuse into the core from the surrounding agar before reaching the WT cells deposited on the filter disc. This introduces a delay before WT cells are exposed to tobramycin which increases with increasing core diameter. Since the timescale for diffusive transport over a distance L scales as L^2/D, the core sizes we use correspond to delays in the range of tens of hours to reach the agar under the center of the disc and up to 13 hours to reach the agar under the edge of the disc. If exposure to tobramycin is required for IF production, this delay should act as a pre-incubation time and thereby decrease the size of the inhibition zones. To the contrary, we find no significant decrease in the size of the inhibition zones with increasing size of antibiotic-free cores (Figure 2.14). These results show that antibiotic is not required for the production of IF.

To evaluate whether antibiotic is required for the activity of IF, we made cores of LB-tobramycin agar in antibiotic-free LB agar. With this geometry, we find no inhibition even at low lawn densities (Figure 2.14). This confirms that antibiotic is required for the IF to cause inhibition.

Collectively, these results indicate that IF is likely a native product of WT PA14 cells that is produced without antibiotic but requires the presence of antibiotic to exert its inhibitory effect.

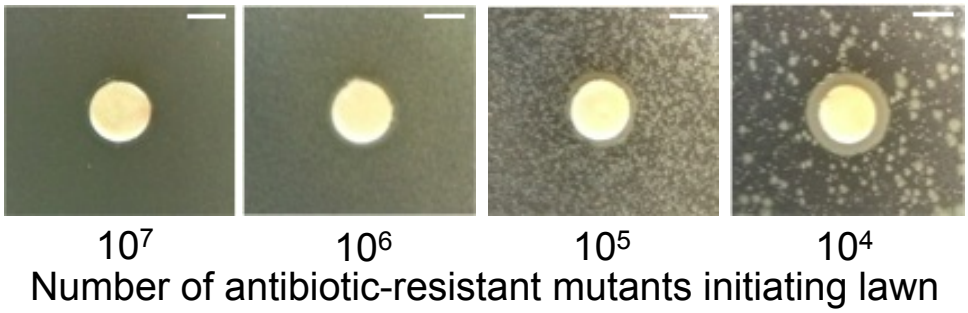

Figure 2.13 Inhibition does not happen in the absence of antibiotic.

WT PA14 cells were deposited on ten-fold decreasing densities of antibiotic-resistant mutant lawns (10^7 to 10^4 cells) on antibiotic-free LB agar. WT cells grow in the region of deposition but do not produce zones of inhibition. Scale bars are 5 mm.

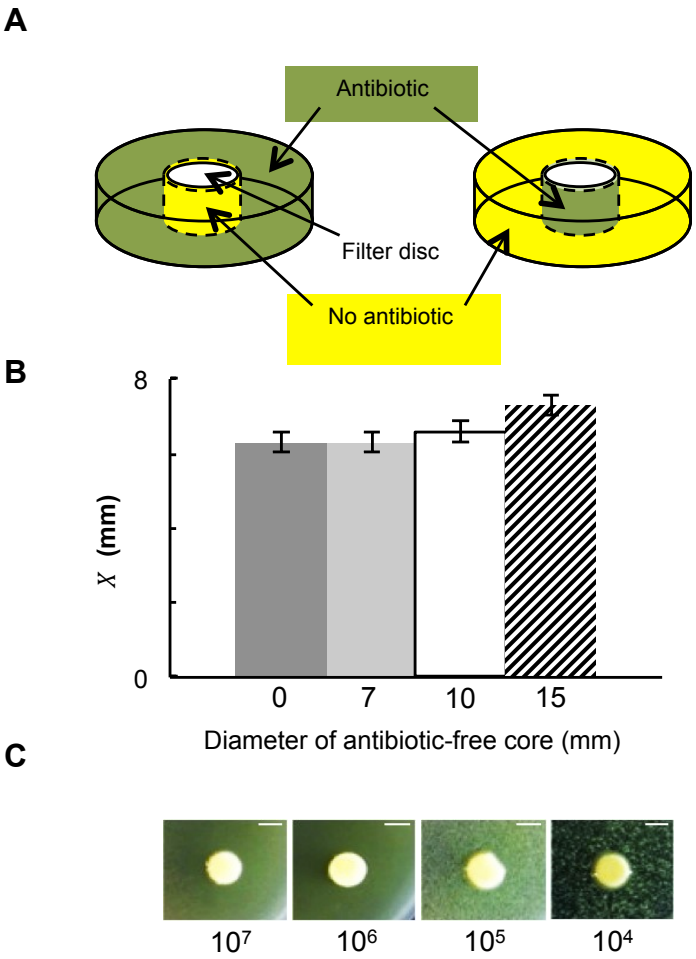

Figure 2.14 The inhibitory factor is produced without antibiotic but exerts its effect in the presence of antibiotic.

(A) A set of complementary experiments was used to determine the role of antibiotic in production and activity of the inhibitory factor. **(B)** Antibiotic is not required for production of the inhibitory factor. WT PA14 cells were deposited on agar cores (7, 10 and 15-mm diameters) containing antibiotic-free LB agar surrounded by antibiotic-resistant mutants on LB-tobramycin agar. Error bars represent standard error of the mean; *N = 3.* **(C)** Antibiotic is required for activity of the inhibitory factor. WT PA14 cells were deposited on agar cores containing LB-tobramycin agar surrounded by dilutions of antibiotic-resistant mutant lawns (10^7 to 10^4 cells) on antibiotic-free LB agar. Scale bars are 5 mm.

2.3.11 A wide range of bacterial species, and a second aminoglycoside antibiotic, produce inhibition

We find that antibiotic-resistant cells deposited on antibiotic-resistant mutant lawns also produce inhibition (Figure 2.15). This is true both for the mutants we generated and for PA14 strains that have a gentamicin resistance cassette (*aacC1*) inserted into their genome [71]. These data indicate that growing cells also inhibit antibiotic-resistant mutants, and that mutants can inhibit their clonal siblings.

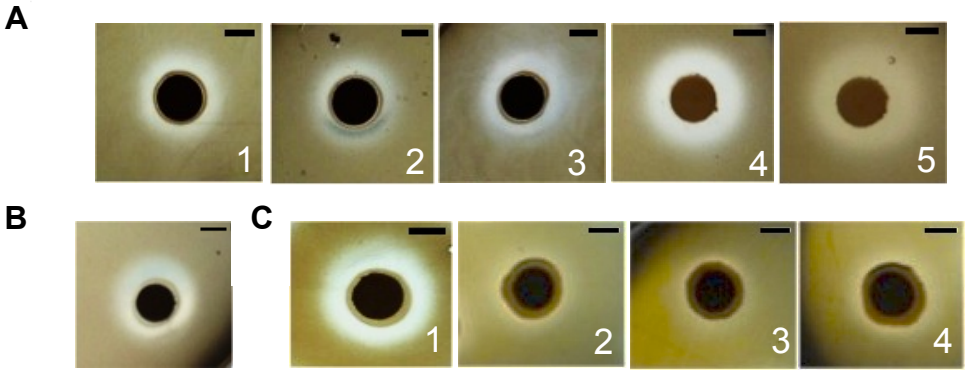

Figure 2.15 Different lines of antibiotic-resistant mutants are susceptible to inhibition, which can be produced with different antibiotics and growing cells.

(A) Five different antibiotic-resistant mutants show susceptibility to inhibition on LB-tobramycin. WT PA14 cells were deposited on lawns of five different antibiotic-resistant mutant strains, three spontaneously-generated in the absence of tobramycin (panels 1-3) and two evolved in the presence of tobramycin (panels 4, 5). The antibiotic-resistant strain in image 1 was used for all experiments in the paper except where otherwise indicated. **(B)** WT PA14 cells inhibit antibiotic-resistant mutants on LB-gentamicin agar (X = 4 mm). Gentamicin, like tobramycin, is an aminoglycoside. **(C)** Antibiotic-resistant, growing strains produce inhibition. (panel 1) Tobramycin- and (panels 2-4) Gentamicin-resistant strains were deposited on filter discs on antibiotic-resistant lawns on LB-tobramycin or gentamicin agar, respectively. Deposited strains grow on antibiotic-containing agar and produce zones of inhibition (For the tobramycin-resistant strain, X = 5 mm; for the gentamicin-resistant strains, X = 3 mm). In panel 1, the strain used was the spontaneously-generated antibiotic-resistant mutant used throughout the paper. Images were taken with an illumination source beneath the agar to improve visibility of the inhibition zones.

To determine whether IF is produced by organisms other than *P. aeruginosa* strain WT PA14, we evaluated a set of Gram-negative and Gram-positive bacteria as well as one strain of yeast. These organisms include known co-pathogens with *P. aeruginosa* as well as 17 clinical isolates of *P. aeruginosa* from Cystic Fibrosis patients [105]. All bacteria tested produce inhibition (Table 2.1, Figures 2.16-2.18). However, the yeast *Saccharomyces cerevisiae* fails to produce inhibition. In the absence of antibiotic in the agar, no inhibition is observed with the bacterial strains. This is consistent with the idea that the inhibitory factors in these cases are the same as that produced by WT PA14 cells. Our results suggest that, IF is produced by a wide range of bacterial species but not the yeast *S. cerevisiae*.

We tested five antibiotic-resistant mutant strains with different origins for susceptibility to inhibition. Three of these strains were spontaneously generated in antibiotic-free media and two evolved in the presence of increasing tobramycin concentrations. All show similar susceptibility to inhibition (Figure 2.15). Therefore, we infer that susceptibility to inhibition likely does not depend sensitively on the details of the mutation conferring antibiotic resistance.

The tobramycin-resistant mutants that we generated are also resistant to another aminoglycoside, gentamicin (MIC = 9.7 μg/mL). WT PA14 cells deposited on antibiotic-resistant mutant lawns on gentamicin agar also produce

inhibition. This result demonstrates that inhibition occurs in the presence of two different aminoglycoside antibiotics (Figure 2.15).

Table 2.1 Microbial species/strains that produce inhibition

Species/Strain	Additional Remarks
***Pseudomonas* strains**	
P. aeruginosa (WT PA14, WT PAO1)	Laboratory strains
Clinical *P. aeruginosa* strains (seventeen)	Cystic Fibrosis Isolates [105]
Sandgrass isolate	Uncharacterized environmental isolate
P. fluorescens	Environmental isolate
Other microbial species	
E. coli (DH5α, SM10)	Laboratory strains
S. aureus (Mu50) [106, 150]	Gram-positive, Methicillin-and Vancomycin-resistant clinical isolate, co-pathogen with *P. aeruginosa*
Serratia marcescens [151]	Gram-negative, nosocomial human pathogen
Burkholderia cepacia [152]	Gram-negative, nosocomial co-pathogen with *P. aeruginosa*

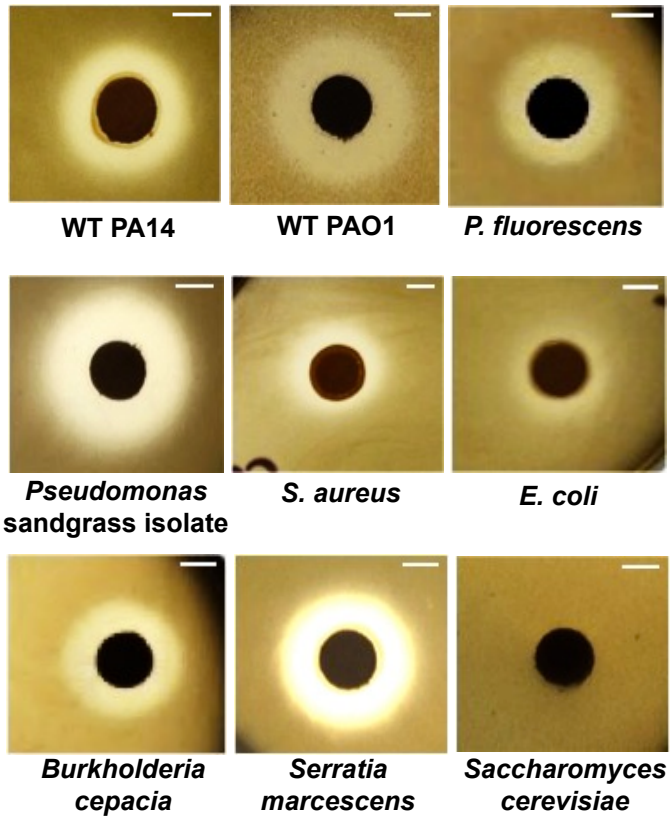

Figure 2.16 A broad range of bacterial species produce inhibition, but yeast does not.

P. aeruginosa WT PA14, *P. aeruginosa* PAO1, *P. fluorescens*, *Pseudomonas* sandgrass isolate, *S. aureus*, *E. coli*, *Burkholderia cepacia, Serratia marcescens* and *Saccharomyces cerevisiae* (~10^9-10^{10} cells for bacteria, ~10^{12} cells for yeast) were deposited on antibiotic-resistant mutant lawns overlaid on LB-tobramycin agar. All microbial species tested produce inhibition of antibiotic-resistant mutants except *Saccharomyces cerevisiae.* For *P. aeruginosa* WT PA14 X = 5 mm; for *P. aeruginosa* PAO1 X = 6 mm; for *P. fluorescens* X = 5 mm; for *Pseudomonas* sandgrass isolate X = 6 mm; for *S. aureus* X = 4 mm; for *E. coli* X = 3 mm; for *Burkholderia cepacia* X = 4 mm; for *Serratia marcescens* X = 5 mm; for *Saccharomyces cerevisiae* X = 0 mm. Scale bars are 5 mm; *N = 3.*

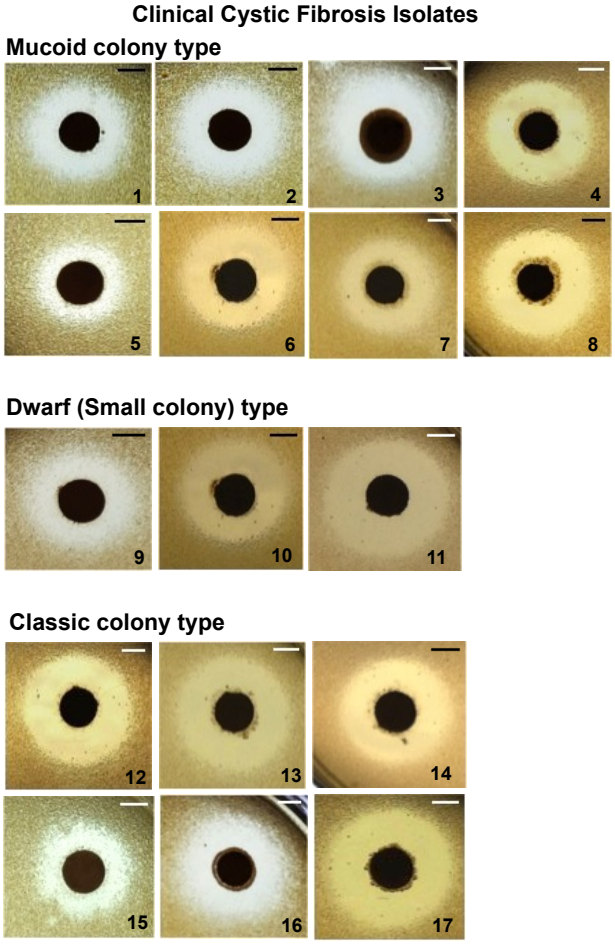

Figure 2.17 Clinical isolates of *Pseudomonas aeruginosa* from patients with Cystic Fibrosis produce inhibition.

For each isolate, ~10^9-10^{10} cells were deposited on antibiotic-resistant mutant lawns overlaid on LB-tobramycin agar. All strains tested (17/17) produce inhibition of antibiotic-resistant mutants Mucoid strains (1) for 0476M X = 5 mm; (2) for 4278M X = 5 mm; (3) for 5623M X = 6 mm; (4) for 2159M X = 6 mm; (5) for 5914M X = 4 mm; (6) for 3639M X = 6 mm; (7) for 4220M X = 6 mm; (8) for 5912M X = 7 mm; Dwarf strains (9) for 4219D X = 5 mm; (10) for 3488D X = 6 mm; (11) for 3640D X = 7 mm; Classic strains (12) for 4218C X = 5 mm; (13) for 1913C X = 7 mm; (14) for 0324C X = 7 mm; (15) for 3470C X = 6 mm; (16) for 2773C X = 7 mm; (17) for 5913C X = 5 mm. Scale bars are 5 mm; *N* = *3.*

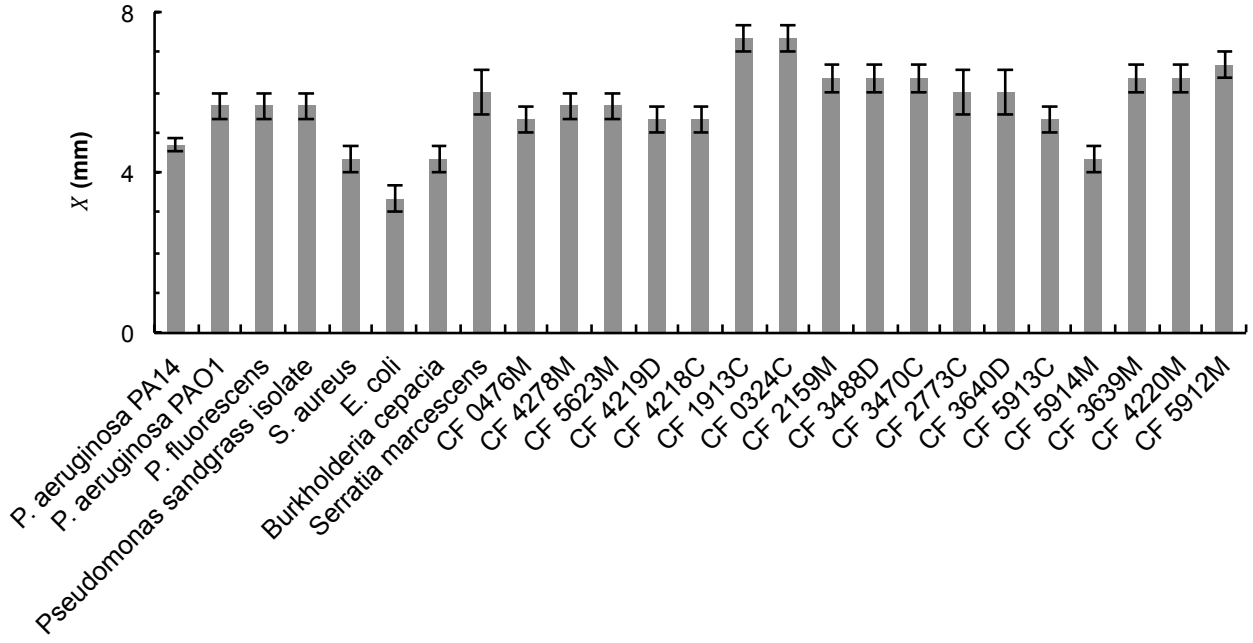

Figure 2.18 Quantitative representation of the width of the inhibition (X) produced by a wide range of bacterial species.

These include *S. aureus* and *B. cepacia*, co-pathogens with *P. aeruginosa* in infections of Cystic Fibrosis patients, and seventeen different clinical isolates of Pseudomonas from Cystic Fibrosis patients. Clinical Cystic Fibrosis isolates are labeled with “CF”. Error bars represent standard error of the mean; *N = 3.*

2.3.12 Inhibition is observed when bacterial cells are deposited on media devoid of nutrients

It is striking that antibiotic-susceptible WT PA14 cells produce inhibition even though the antibiotic agar contains an inhibitory concentration of antibiotic. This suggests that IF production may not depend on utilization of nutrients from the agar. To test this, WT PA14 cells were deposited on “cores” of nutrient-free, tobramycin-containing agar (Figure 2.19). To test for effects of diffusion from the surrounding LB agar into the cores, increasing core diameters were used. WT PA14 cells produce inhibition even when deposited on nutrient-free cores that is comparable to those seen with the “no core” and “LB-tobramycin core” controls (Figure 2.19). These data indicate that the production of IF does not depend on the utilization of nutrients in the agar plate.

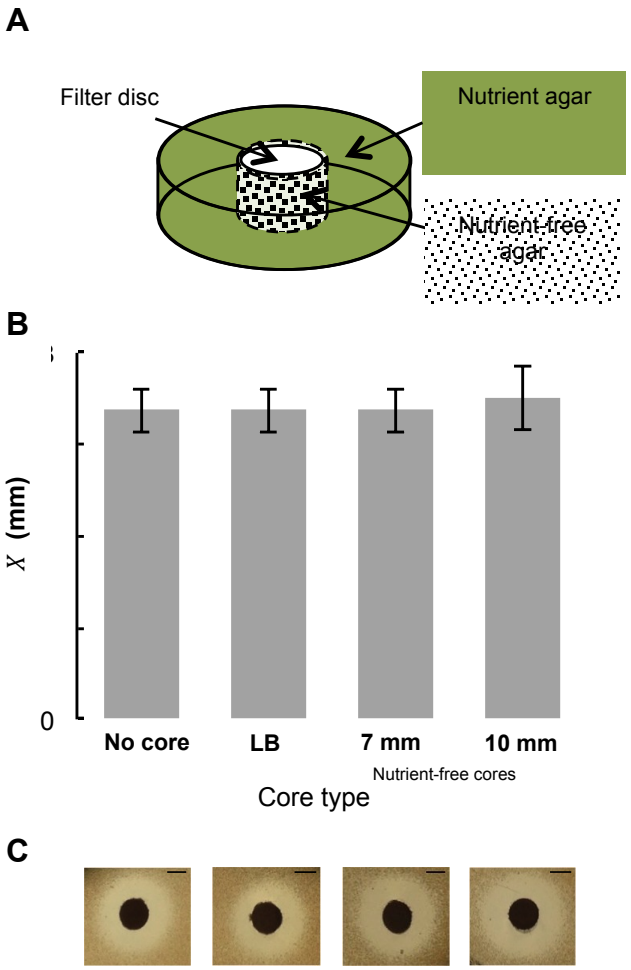

Figure 2.19 Utilization of nutrients in the agar plate is not necessary for production of the inhibitory factor.

(A) Cylindrical cores of nutrient-free tobramycin agar were created in LB-tobramycin agar. **(B)** WT PA14 cells were deposited on filter discs with no underlying core, on cores of LB-tobramycin agar, and on nutrient-free tobramycin agar cores with diameters of 7 mm and 10 mm. Each of these was surrounded by antibiotic-resistant mutants overlaid on LB-tobramycin agar. Error bars represent standard error of the mean; *N = 4.* **(C)** Representative images of inhibition with *P. aeruginosa* WT PA14 cells deposited directly on filter discs (X = 6 mm), on cores of LB-tobramycin agar (X = 6 mm), on 7-mm nutrient-free tobramycin cores (X = 6 mm) and on 10-mm nutrient-free tobramycin cores (X = 6 mm). Scale bars are 5 mm.

2.3.13 Alkaline metabolic products may play a role in inhibition

Since *S. cerevisiae* does not produce inhibition but all tested bacterial strains do, we infer that the nutritional substrate for microbial growth may be linked to the production of IF. All bacterial strains were grown in LB medium [153] but *S. cerevisiae* was grown in Yeast-Peptone-Dextrose (YPD) medium. In LB medium, amino acids are the only significant source of carbon and bacteria grow by catabolism, which produces alkaline by-products [153, 154]; overnight culture pH~8. In contrast, *S. cerevisiae* grows in YPD medium using the sugar dextrose as a source of carbon [155]. Yeast's fermentation of sugar produces acidic by-products [155]; overnight culture pH~6. To evaluate the relationship between pH and inhibition, we used agar plates that incorporated the pH indicator bromthymol blue (BTB). BTB has a pH range of 6-7.6, which permits detection of slight perturbations from neutral pH.

WT PA14 cells, WT PAO1 cells, *S. aureus*, *E. coli*, *Serratia marcescens*, *Burkholderia* cepacia, *Pseudomonas* sandgrass isolate, *Pseudomonas* PAO-JP2, *Pseudomonas Δphz1/2* and *S. cerevisiae* were deposited on nutrient-free tobramycin agar and nutrient-containing LB-tobramycin agar containing BTB. To quantify changes in color, images were split into red-green-blue (RGB) channels and the red intensity profiles were analyzed (Figure 2.20). We define intensity ratio as the intensity 2mm from the disc edge divided by the intensity at a

distance > 8mm from the disc edge. With no color change, the intensity ratio is expected to be ~1.

When deposited on nutrient-containing BTB agar, bacteria produce an alkaline change, with an intensity ratio < 1 (Figure 2.21, 2.22, 2.23). Yeast produces a slightly acidic change or no change, with an intensity ratio ≥ 1. The width of inhibition X and the width of the alkaline color change X_c are correlated (Figure 2.22). These results agree with the idea that inhibition is caused by the alkaline bacterial by-products. Alkaline change on nutrient-free agar (Figure 2.24) is consistent with our finding that inhibition does not result from utilization of nutrients from the agar plate. Rather, metabolic by-products from cells in the overnight cultures continue to be released following deposition on the agar.

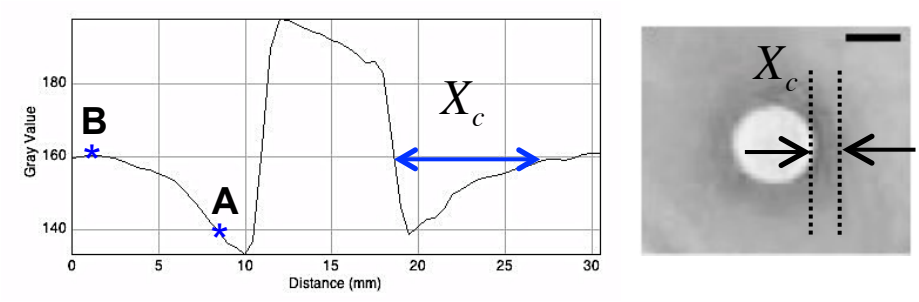

$$\text{Intensity ratio} = \frac{\text{Gray value at point A}}{\text{Gray value at point B}}$$

Figure 2.20 Representative measurements of intensity ratio and width of alkaline change (X_c).

Using intensity plot profiles generated in ImageJ v.1.47, intensity ratios were calculated as the gray value at a fixed distance of 2 mm from the edge of the disc (A, in the region with color change) divided by the gray value at a distance of more than 8 mm for microbial cells, more than 10 mm for NaOH, $NaHCO_3$ and NH_4Cl, sterile media and supernatant, and more than 40 mm for NH_4OH from edge of the disc (B, in a region with no color change). To measure the width of alkaline change (X_c), the distance from the edge of the disc to the edge of the alkaline change was measured. For each replicate, X_c represents the average of four measurements made along two perpendicular axes. Scale bars are 5 mm.

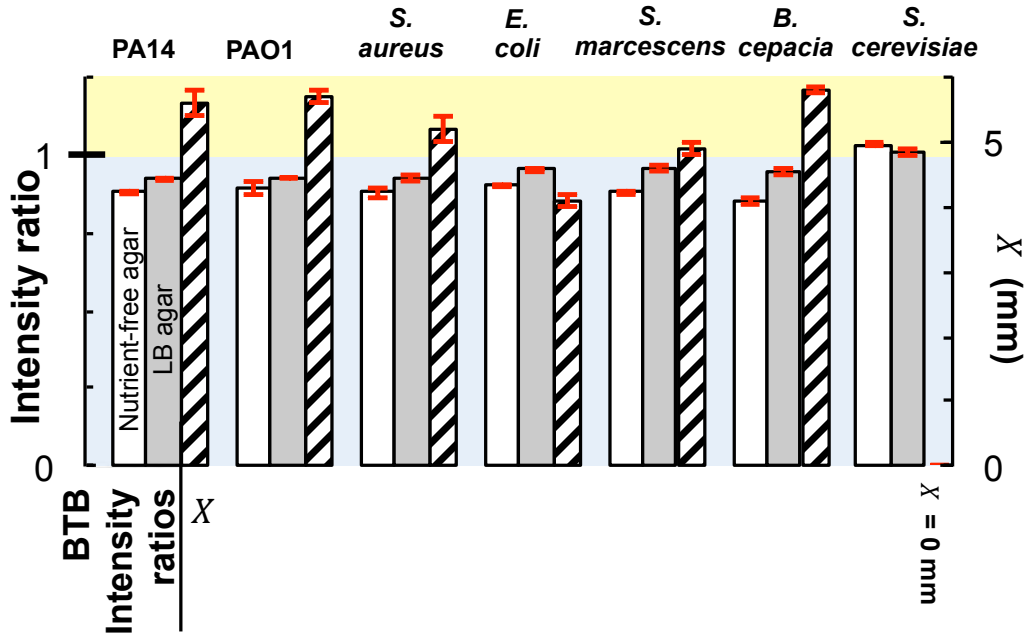

Figure 2.21 Alkaline metabolic by-products from a wide range of bacterial species likely mediates inhibition.

Different microbial strains were deposited on nutrient-free tobramycin BTB agar, on nutrient-containing LB-tobramycin BTB agar, and on antibiotic-resistant mutant lawns overlaid on LB-tobramycin agar. Images were taken immediately after deposition (for nutrient-free BTB agar), two hours after deposition (for nutrient-containing LB BTB agar) or after overnight incubation (for antibiotic-resistant lawns on LB-tobramycin 8 μg/mL agar). The width of inhibition (X) is shown as hatched bars. All bacterial strains produce inhibition of antibiotic-resistant mutant lawns, however the yeast strain fails to produce inhibition. Error bars (in red) represent standard error of the mean; *N = 3*.

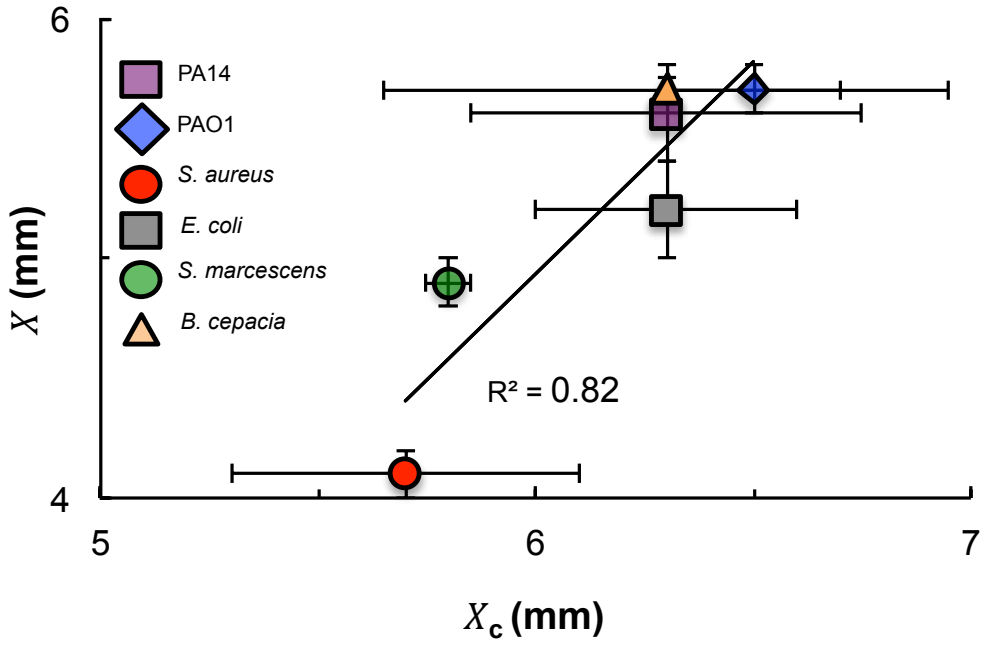

Figure 2.22 Alkaline metabolic by-products from a wide range of bacterial species correlate with inhibition.

For different inhibiting strains, when the width of alkaline change (X_c) is plotted as a function of the width of inhibition (X), a correlation is observed (R^2 = 0.82 from a linear fit, Pearson's correlation coefficient *r* = 0.9). Intensity profiles were used to measure the width of alkaline color change (X_c), representing the distance from the edge of the disc to the edge of the alkaline color change. For each replicate, X_c and X represent the average of four measurements made along two perpendicular axes. Error bars represent standard error of the mean; *N* = 2.

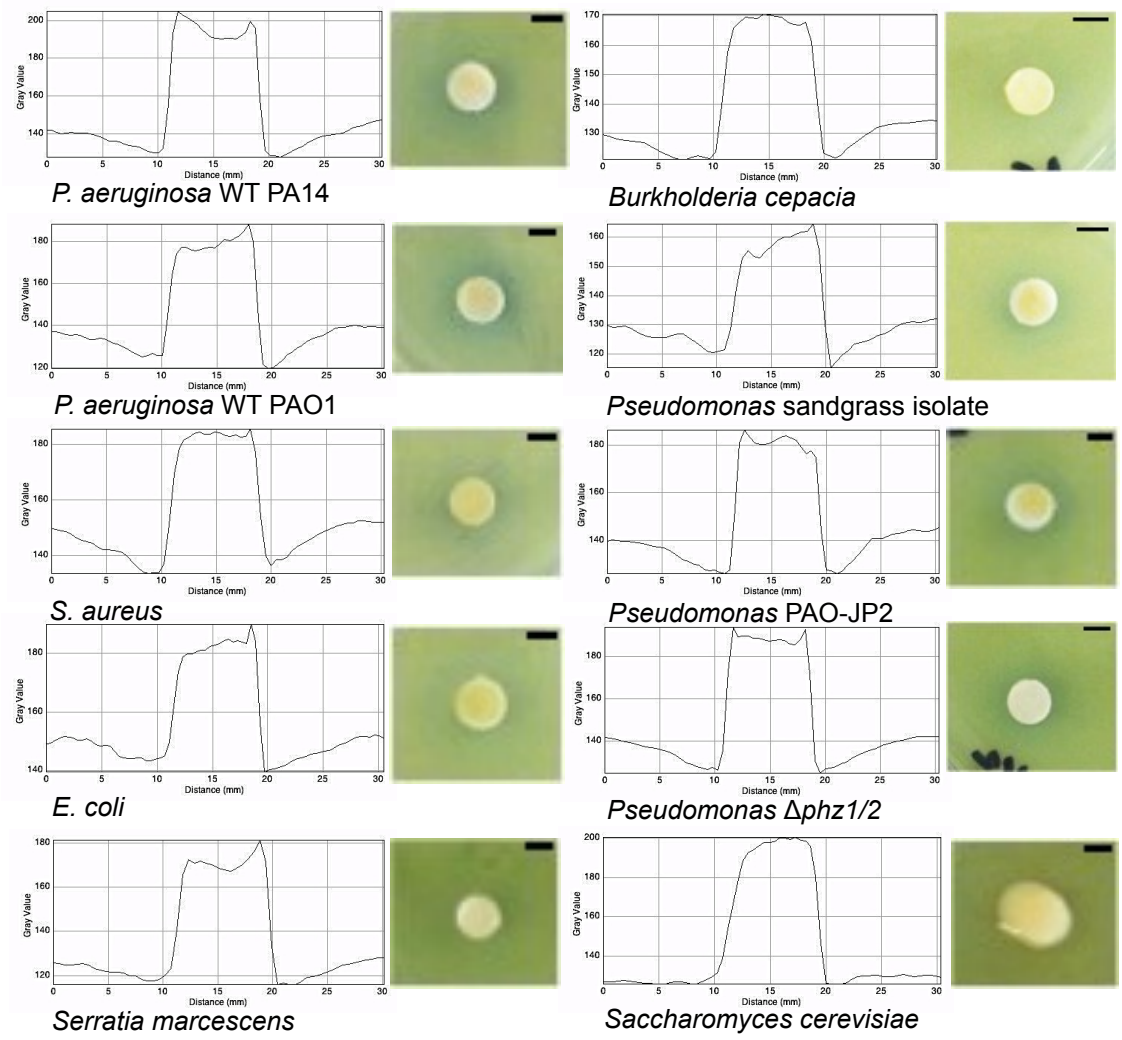

Figure 2.23 Representative intensity profiles and images on nutrient-containing LB-tobramycin BTB agar.

Bacterial strains and *S. cerevisiae* were deposited (~10^9-10^{10} cells for bacteria, ~10^{12} cells for yeast) on LB-tobramycin BTB agar. Images were analyzed using ImageJ v.1.47. The width of alkaline change (X_c) was measured as the distance from the edge of the disc to the edge of the alkaline change. Scale bars are 5 mm.

Nutrient-free BTB agar with 8 µg/mL tobramycin

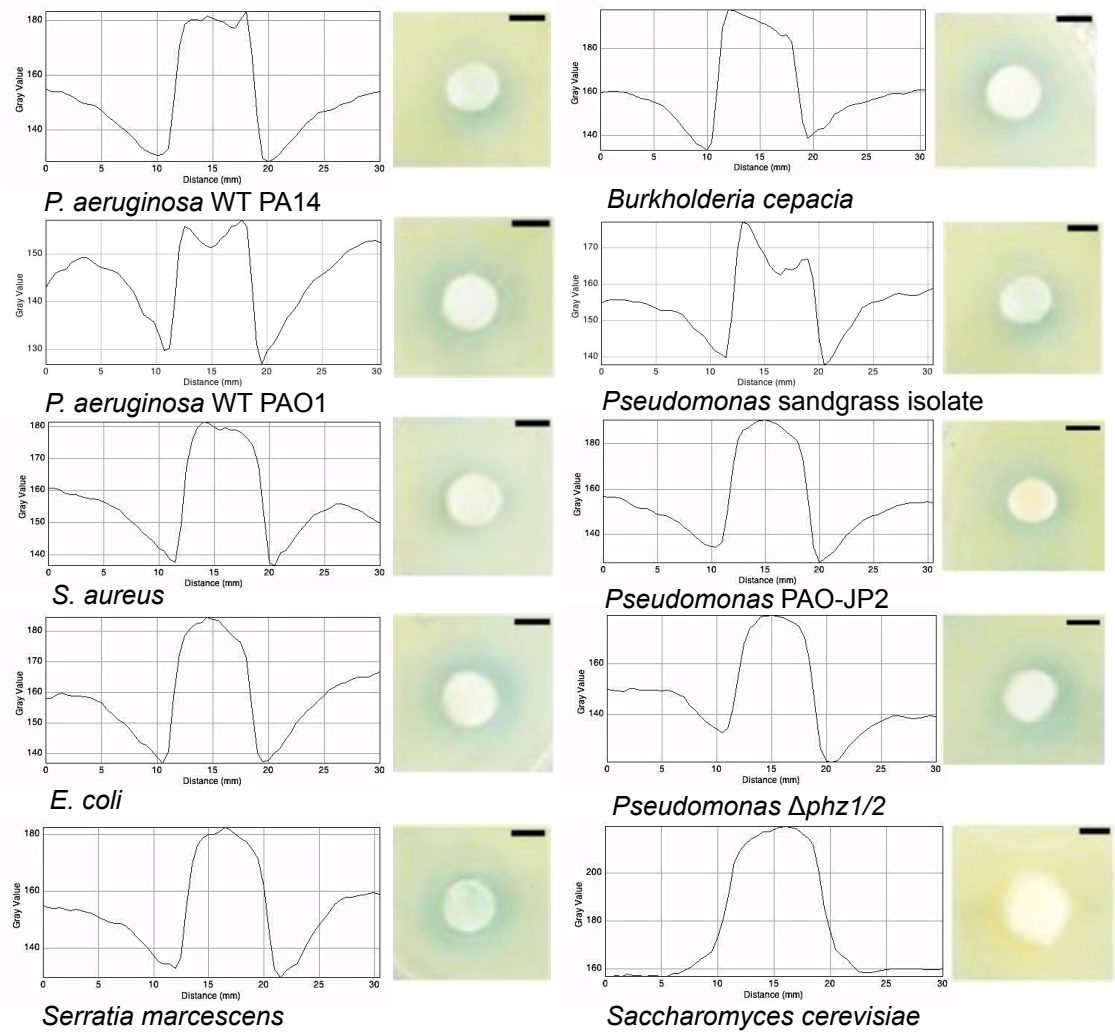

Figure 2.24 Representative intensity profiles and images on nutrient-free tobramycin BTB agar.

Bacterial strains and *S. cerevisiae* were deposited (~10^9-10^{10} cells for bacteria, ~10^{12} cells for yeast) on nutrient-free tobramycin BTB agar. Images were analyzed using ImageJ v.1.47. The width of alkaline change (X_c) was measured as the distance from the edge of the disc to the edge of the alkaline change. Scale bars are 5 mm.

2.3.14 The mechanism of inhibition is related to the alkaline pH change

To investigate a causative link between alkalinity and inhibition, we test exogenous alkaline solutions and find they produce both an alkaline change on BTB agar and inhibition of antibiotic-resistant mutants (Figure 2.25, 2.26, 2.27). We vary the concentration deposited and use linear regression to determine the relationship between concentration and X. From these, we extrapolate that deposition of 10 µL of 2.04M NH_4OH, 1M NaOH, or 1M $NaHCO_3$ produces inhibition of antibiotic-resistant mutants comparable to that seen with WT PA14 cells (Figures 2.28, 2.29, 2.30, 2.31). On antibiotic-free LB agar, zones of inhibition are either absent (with NH_4OH and $NaHCO_3$) or markedly reduced (with NaOH) (Figure 2.32). Collectively, these results indicate that alkaline compounds can recreate the characteristics we have found for the IF.

Other researchers have shown that alkalinity significantly enhances the bactericidal activity of aminoglycosides [156, 157]. At least two possible mechanisms have been suggested: (1) enhanced active uptake of aminoglycosides [87, 156-158]; (2) more aminoglycosides in their nonionized, more-bactericidal form [156]. Thus, we infer that the IF inhibits mutants by increasing pH.

We modify Equation 2 to use a threshold pH rather than a threshold IF concentration as the determinant of cell survival, thus:

$$X^2 = 4DT_c \ln\left(N_0\right) + F\left(D, T_c, pH_c, k_0, \alpha, \beta\right)$$

where pH_c is the pH above which cells die, k_0 is the IF production by one cell, and α and β are constants which account for the acid-base properties of the IF (electronic supplemental material). The N_0-dependent portion of this function is unchanged from Equation 2. Therefore, pH-mediated inhibition does not change our MW measurements. Further, this model predicts a linear relationship between X^2 and the squared size of alkaline color change (X_c^2), consistent with Figure 2.22.

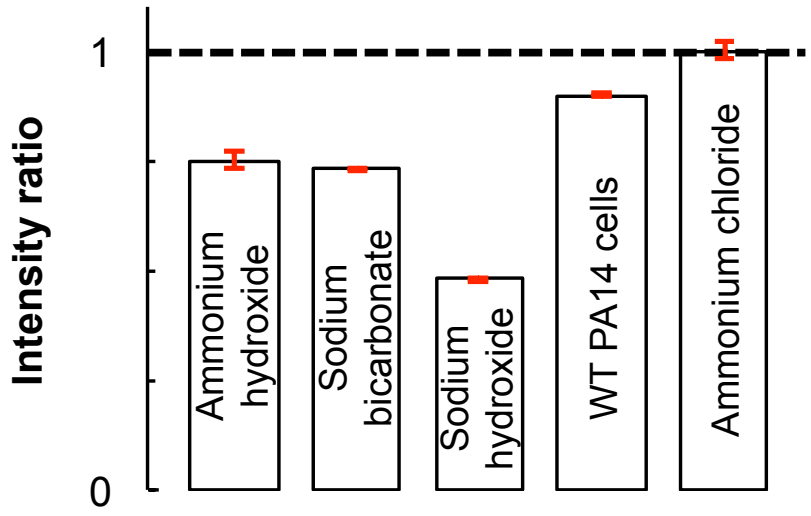

Figure 2.25 Exogenous alkaline solutions can recapitulate the phenomenon of inhibition.

10 µL of exogenous compounds - 2.4M ammonium hydroxide (NH_4OH), 1M sodium bicarbonate ($NaHCO_3$), 1M sodium hydroxide (NaOH), WT PA14 cells, and 1M ammonium chloride (NH_4Cl) - were deposited on LB-tobramycin BTB agar and on antibiotic-resistant mutant lawns on LB-tobramycin agar. Images were taken 2 hours after deposition (for LB-tobramycin BTB agar) or after overnight incubation (for LB-tobramycin agar with antibiotic-resistant mutant lawns). BTB color intensity ratios were determined as for figure 3, with the baseline gray value measured at a distance of more than 10 mm for NaOH, $NaHCO_3$ and NH_4Cl and WT PA14 cells, and more than 40 mm for NH_4OH. Intensity ratios less than 1 indicate an alkaline change, as produced by ammonium hydroxide, sodium hydroxide, sodium bicarbonate and WT PA14 cells. Ammonium chloride produces an intensity ratio ~1. Error bars (in red) represent standard error of the mean; *N = 2.*

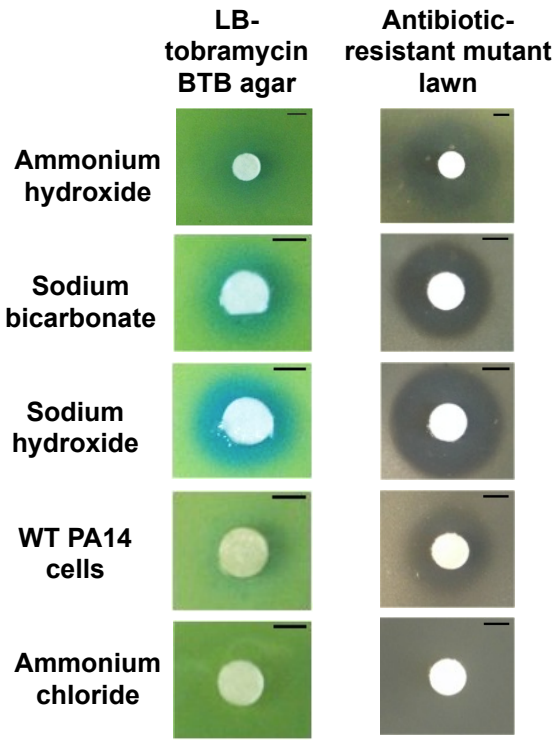

Figure 2.26 Representative images showing BTB color change and presence or absence of inhibition with exogenous alkalis.

2.4M ammonium hydroxide (NH_4OH)(X = 10 mm, X_c = 15 mm), 1M sodium bicarbonate ($NaHCO_3$) (X = 5 mm, X_c = 5.5 mm), 1M sodium hydroxide (NaOH) (X = 5 mm, X_c = 7.5 mm), WT PA14 cells (X = 5 mm, X_c = 6 mm) and 1M ammonium chloride (NH_4Cl) (X = 0 mm, X_c = 0 mm). Scale bars are 5 mm.

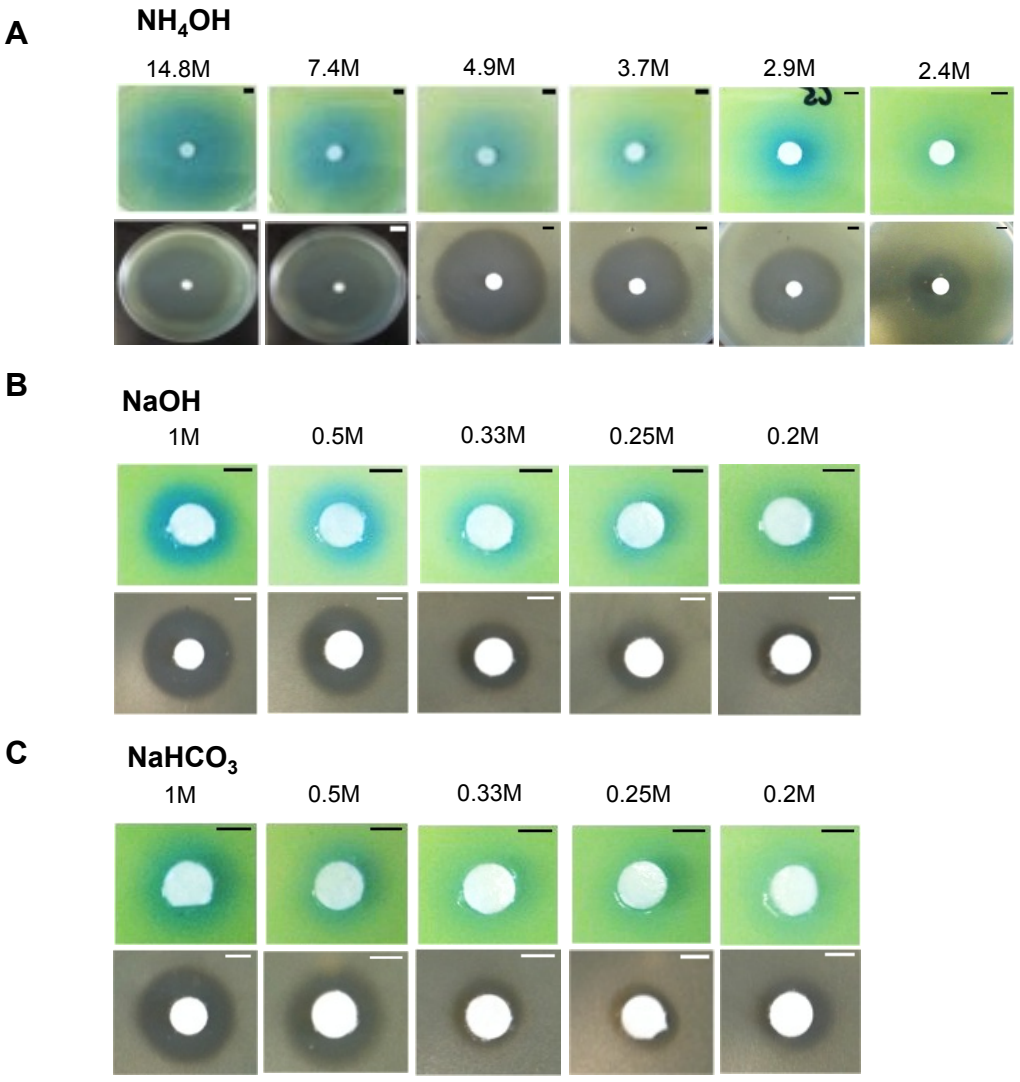

Figure 2.27 Alkaline change and inhibition produced by exogenous alkaline compounds.

Decreasing molar concentrations of exogenous alkaline compounds **(A)** ammonium hydroxide (NH_4OH), **(B)** sodium hydroxide (NaOH) and **(C)** sodium bicarbonate ($NaHCO_3$) were deposited on LB-tobramycin BTB agar and on antibiotic-resistance lawns on LB-tobramycin agar. Images were taken two hours after deposition (for LB-tobramycin BTB agar) and after overnight incubation (for LB-tobramycin agar with the antibiotic-resistant lawns). Exogenous compounds produce an alkaline change of the surrounding agar and inhibit antibiotic-resistant mutants in their region of deposition. Scale bars are 5 mm.

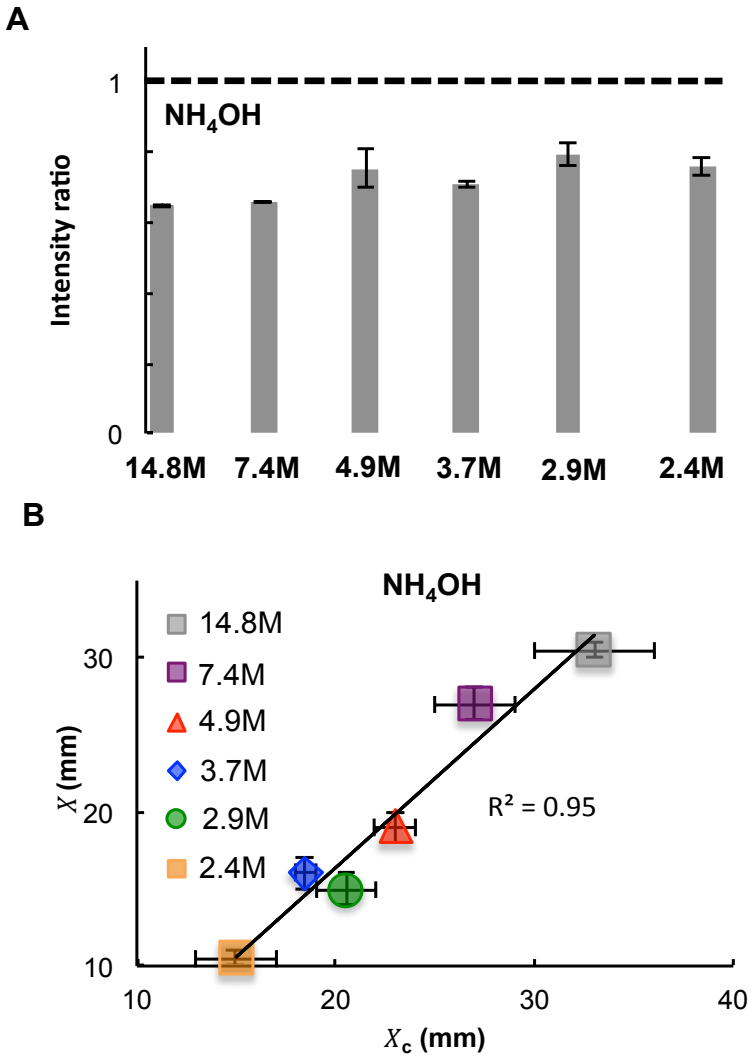

Figure 2.28 Alkaline change produced by ammonium hydroxide correlates with inhibition.

Decreasing concentrations of ammonium hydroxide (NH_4OH) was deposited on LB-tobramycin BTB agar and on antibiotic-resistant lawns overlaid on LB-tobramycin agar. Images were analyzed using ImageJ v.1.47. **(A)** Intensity ratios were calculated as the gray value at a fixed distance of 2 mm from the edge of the disc (in the region with color change) divided by the gray value at a distance of more than of more than more than 40 mm. **(B)** The width of alkaline change (X_c) was measured as the distance from the edge of the disc to the edge of the alkaline change. Error bars represent standard error of the mean; *N* = 2.

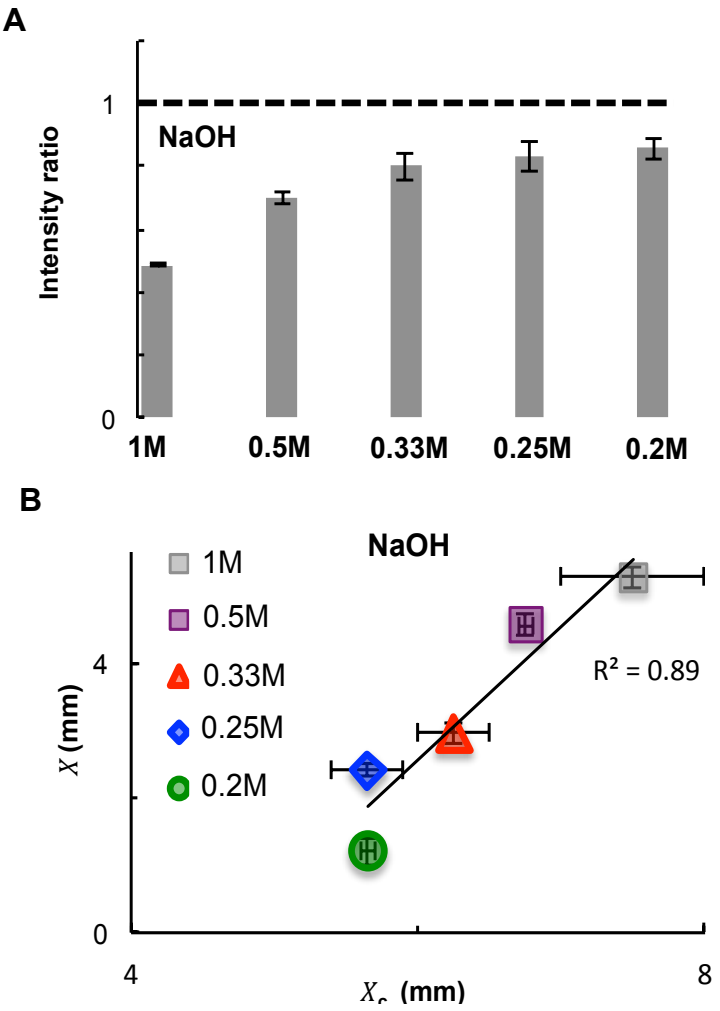

Figure 2.29 Alkaline change produced by sodium hydroxide correlates with inhibition.

Decreasing concentrations of sodium hydroxide (NaOH) was deposited on LB-tobramycin BTB agar and on antibiotic-resistant lawns overlaid on LB-tobramycin agar. Images were analyzed using ImageJ v.1.47. **(A)** Intensity ratios were calculated as the gray value at a fixed distance of 2 mm from the edge of the disc (in the region with color change) divided by the gray value at a distance of more than of more than more than 10 mm. **(B)** The width of alkaline change (X_c) was measured as the distance from the edge of the disc to the edge of the alkaline change. Error bars represent standard error of the mean; *N* = 2.

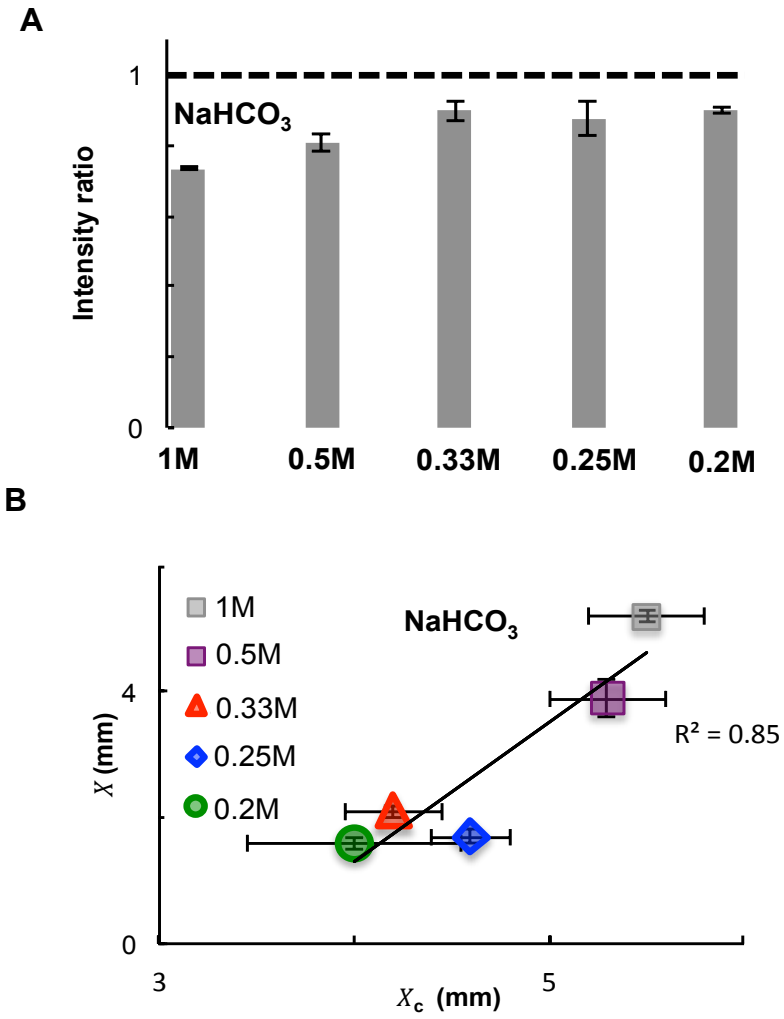

Figure 2.30 Alkaline change produced by sodium bicarbonate correlates with inhibition.

Decreasing concentrations of sodium bicarbonate ($NaHCO_3$) was deposited on LB-tobramycin BTB agar and on antibiotic-resistant lawns overlaid on LB-tobramycin agar. Images were analyzed using ImageJ v.1.47. **(A)** Intensity ratios were calculated as the gray value at a fixed distance of 2 mm from the edge of the disc (in the region with color change) divided by the gray value at a distance of more than of more than more than 10 mm. **(B)** The width of alkaline change (X_c) was measured as the distance from the edge of the disc to the edge of the alkaline change. Error bars represent standard error of the mean; *N* = 2.

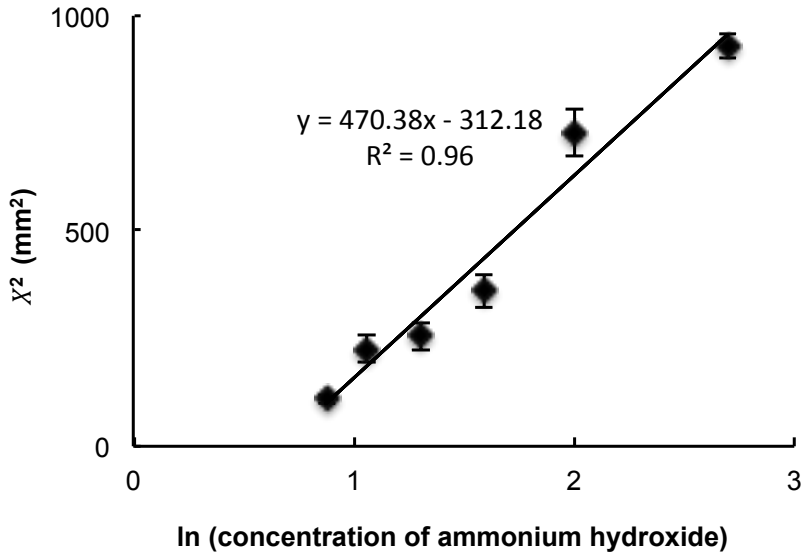

Figure 2.31 Determining the molar concentration of ammonium hydroxide that produces inhibition comparable to WT PA14 cells.

On a semi-log plot, squares of the width of inhibition (X^2) vary linearly with increasing concentrations of deposited ammonium hydroxide (NH_4OH), consistent with the disc diffusion model (R^2 = 0.96). Concentrations of ammonium hydroxide represent increasing concentrations normalized to a concentration of 1M. From the x-intercept of the fit obtained, it was determined that 2.04M of ammonium hydroxide produce a width of inhibition (X = 5 mm) comparable to that produced by WT PA14 cells (~10^{10} cells). Error bars represent standard error of the mean; *N* = 2.

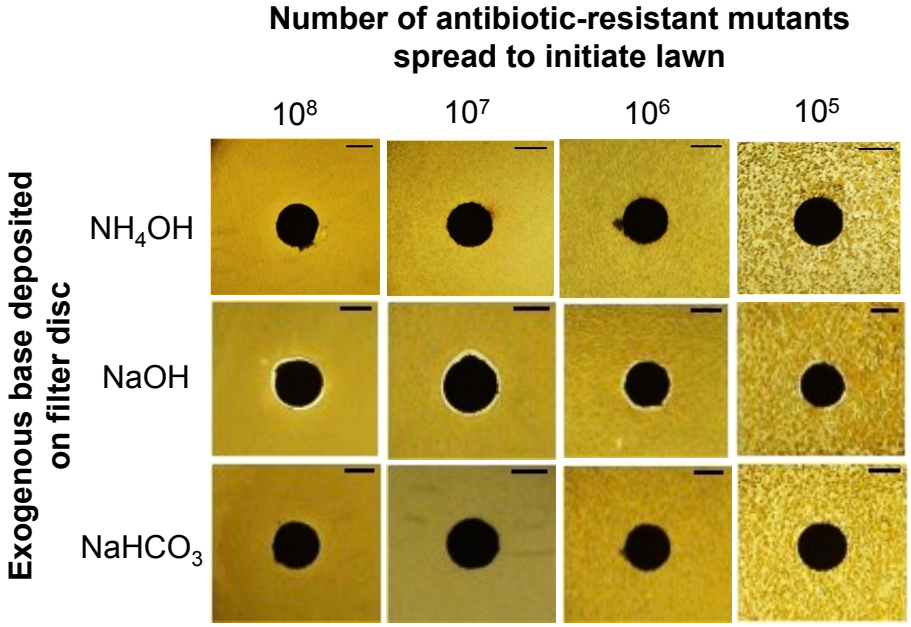

Figure 2.32 On antibiotic-free agar, exogenous alkaline compounds produce little or no inhibition.

Ten microliters of the alkaline compound, ammonium hydroxide (2.1M), sodium hydroxide (0.5M) or sodium bicarbonate (0.5M), were deposited on lawns initiated by overlaying decreasing numbers of antibiotic-resistant mutants on antibiotic-free LB agar. Inhibition observed is either absent (for NH_4OH and $NaHCO_3$) or markedly reduced (for NaOH), compared to the inhibition produced by exogenous alkaline compounds on LB-tobramycin agar. Scale bars are 5 mm.

2.3.15 Biogenic bases are plausible candidates for the inhibitory factor

The biogenic bases ammonia and amines are widespread by-products of bacterial catabolism of amino acids [153, 154, 159]. Ammonia has a MW of 17 Da, consistent with that of the IF. Microbially-produced ammonia and amines can mediate long-range intercellular interactions and influence antibiotic resistance [160-165]. Gaseous ammonia, from bacterial supernatant, and trimethylamine can decrease resistance to the aminoglycoside antibiotics kanamycin and spectinomycin [164, 165].

We used an ion-selective electrode to measure ammonia and amine emission when bacteria and yeast were deposited onto filter discs on LB-tobramycin agar. WT PA14 produce an emission nearly 5x that of *S. cerevisiae* (Figure 2.33). In the disc diffusion assay, deposition of 1M ammonium chloride (NH_4Cl) produces a slightly acidic change and no inhibition (Figure 2.26). Thus, we find a correlation between alkaline change and inhibition, but no inhibitory effect by the ammonia molecule itself when the pH is acidic. Therefore, we attribute inhibition to an alkaline pH change that is mediated, in part or in whole, by biogenic ammonia and/or low-molecular-weight amines.

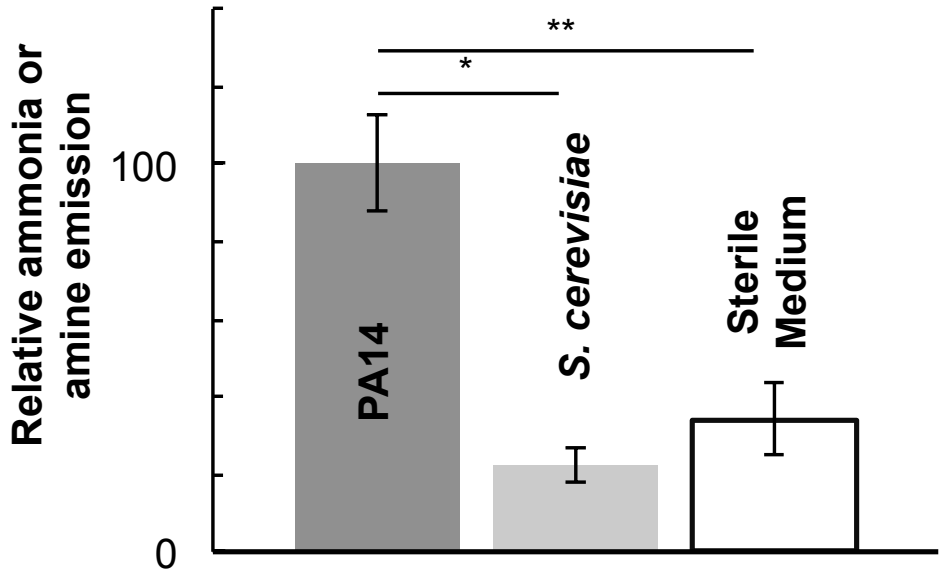

Figure 2.33 Production of ammonia or amines is associated with inhibition.

Using an ion-selective electrode, ammonia or amine emission was measured following deposition of WT PA14 and *S. cerevisiae* cells on filter discs on LB-tobramycin agar in vials. Emission levels are normalized to the PA14 average. Significantly higher levels of ammonia or amine emission are detected following deposition of WT PA14 cells than following deposition of *S. cerevisiae*. Error bars represent standard error of the mean; $N = 3$. * $P < 0.005$ by two-tailed Student *t* test. ** $P < 0.02$ by two-tailed Student *t* test.

2.3.16 Nutrient conditions provide a "switch" to control inhibition

Microbes capable of utilizing either amino acids or sugars as carbon sources should switch between producing inhibition and not producing inhibition depending on the carbon source available. *S. aureus* and *E. coli*, which can either catabolize amino acids or ferment glucose, *P. aeruginosa*, which is incapable of fermentation, and *S. cerevisiae*, which ferments glucose. We grew each organism in two culture media – LB, which contains almost entirely amino acids as a carbon source, and YPD, which likewise contains copious amino acids but is also supplemented with the sugar dextrose. The pH of overnight cultures grown in LB was alkaline (pH=9) for all bacterial strains and neutral (pH=7) for the yeast strain. *S. cerevisiae* grew poorly in LB broth, so we pool cells from multiple cultures so that approximately the same number of cells were deposited onto filter discs in all cases. The pH of overnight cultures grown in YPD was alkaline (pH=8) for WT PA14, and acidic for *S. aureus*, *E. coli*, and *S. cerevisiae* (pH=4, 4, and 5, respectively).

WT PA14, *S. aureus* and *E. coli* cultures grown in LB produce an alkaline color change and inhibit antibiotic-resistant mutants (Figure 2.34, 2.35, 2.36, 2.37). *S. cerevisiae* produces neither a pH color change nor inhibition. When grown in YPD, WT PA14 cells produce an alkaline change and inhibition. However, *S. aureus*, *E. coli* and *S. cerevisiae* grown in YPD produce an acidic change and no inhibition (Figure 2.34, 2.35). Culture supernatants and sterile LB

and YPD media produce no pH color change on nutrient-containing media and produce no inhibition (Figures 2.38, 2.39, 2.40, 2.41, 2.42).

From this we conclude that microbial metabolism and the nutrient environment can provide a switch to control inhibition.

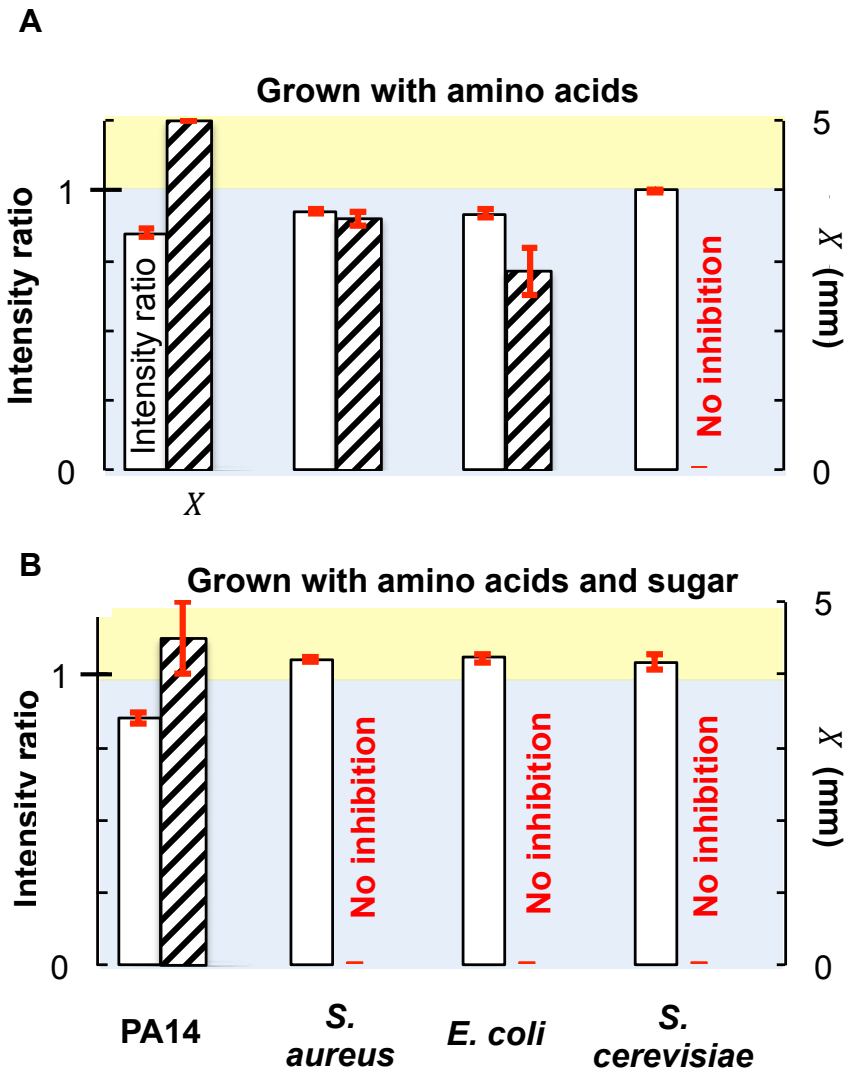

Figure 2.34 The carbon source used for growth can switch inhibition on or off.

WT PA14, *S. aureus*, *E. coli*, and *S. cerevisiae* were each grown in **(A)** LB medium, for which amino acids are the major carbon sources, and **(B)** YPD medium, which contains both amino acids and sugar. Following growth, cultures were deposited onto LB-tobramycin BTB agar and onto antibiotic-resistant mutant lawns on LB-tobramycin agar. **(A)** When grown on amino acids, the first three organisms produce both a BTB intensity ratio <1 and inhibition. The yeast *S. cerevisiae* produces no change in pH and no inhibition. **(B)** When grown in the presence of sugars, *S. aureus*, *E. coli*, and *S. cerevisiae* ferment sugars and thereby produce an acidic change and no inhibition. WT PA14 catabolizes amino acids, causing an alkaline change and inhibition.

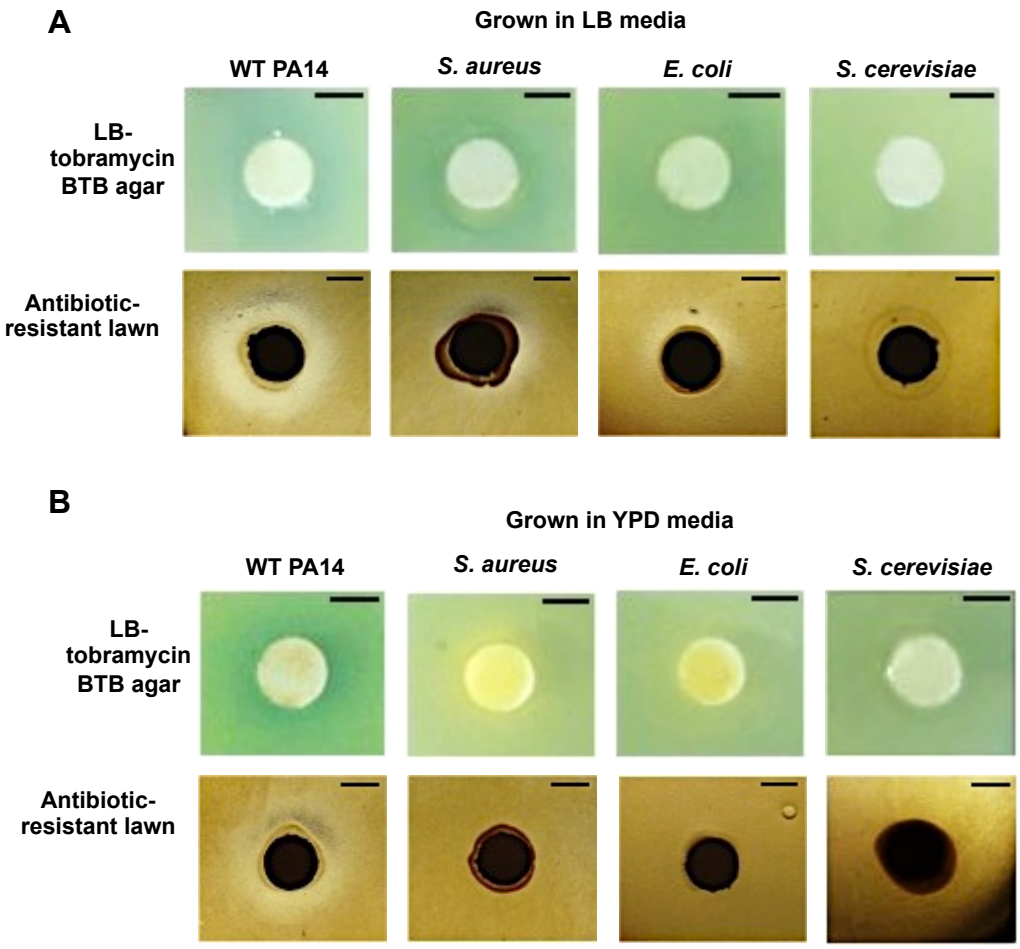

Figure 2.35 Representative images of color change and presence or absence of inhibition with microbial strains grown in LB and YPD media.

(A) For overnight cultures grown in LB medium, WT PA14, *S. aureus* and *E. coli* produce an alkaline change and produce inhibition of antibiotic-resistant mutants. *S. cerevisiae* does not produce a color change and fails to produce inhibition. **(B)** For overnight cultures grown in YPD medium, WT PA14 produces an alkaline change, and produces inhibition. *S. aureus*, *E. coli* and *S. cerevisiae* produce an acidic change and fail to produce inhibition. Scale bars are 5 mm.

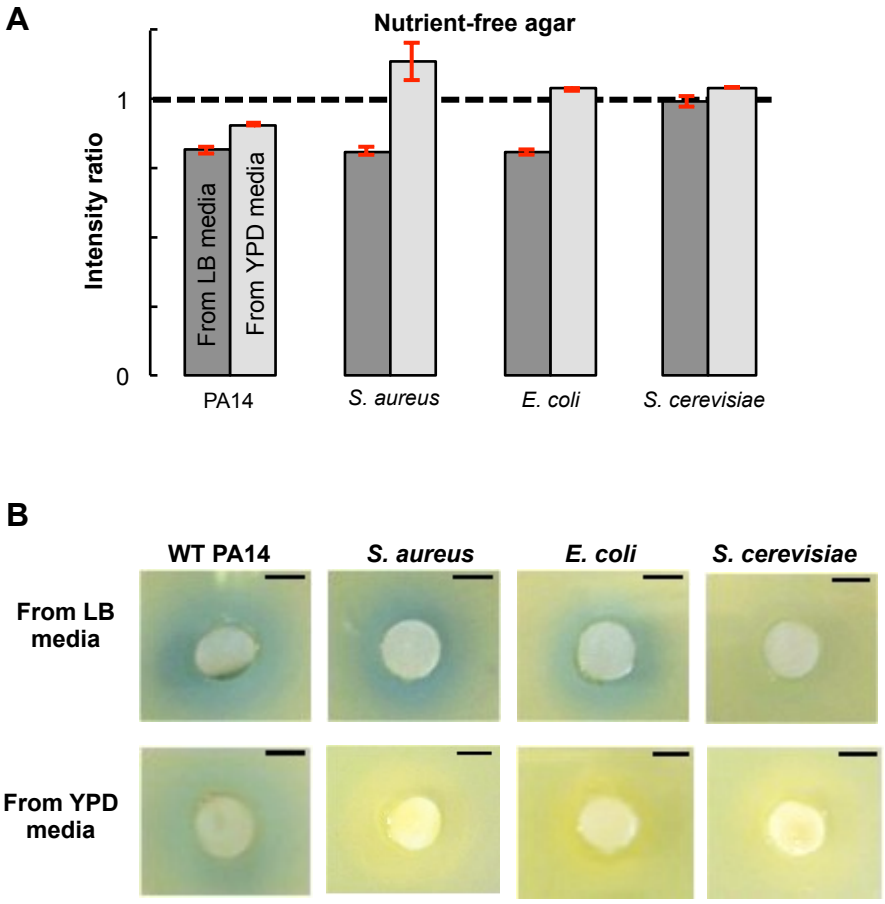

Figure 2.36 On nutrient-free tobramycin 8 µg/mL BTB agar, cell cultures produce a pH color change corresponding to that of seen on nutrient-containing LB-tobramycin 8 µg/mL BTB agar.

(A) For cultures grown in LB media, WT PA14, *S. aureus* and *E. coli* produce an alkaline change, indicated by an intensity ratio <1. *S. cerevisiae* does not produce a color change (intensity ratio ~1). For cultures grown in YPD media, WT PA14 produces an alkaline change, whereas *S. aureus*, *E. coli* and *S. cerevisiae* produce an acidic change (intensity ratio >1). Error bars represent standard error of the mean; *N = 2.* **(B)** Representative images of pH color change following deposition of cell cultures grown in LB and YPD media on nutrient-free tobramycin 8 µg/mL BTB agar. Scale bars are 5 mm.

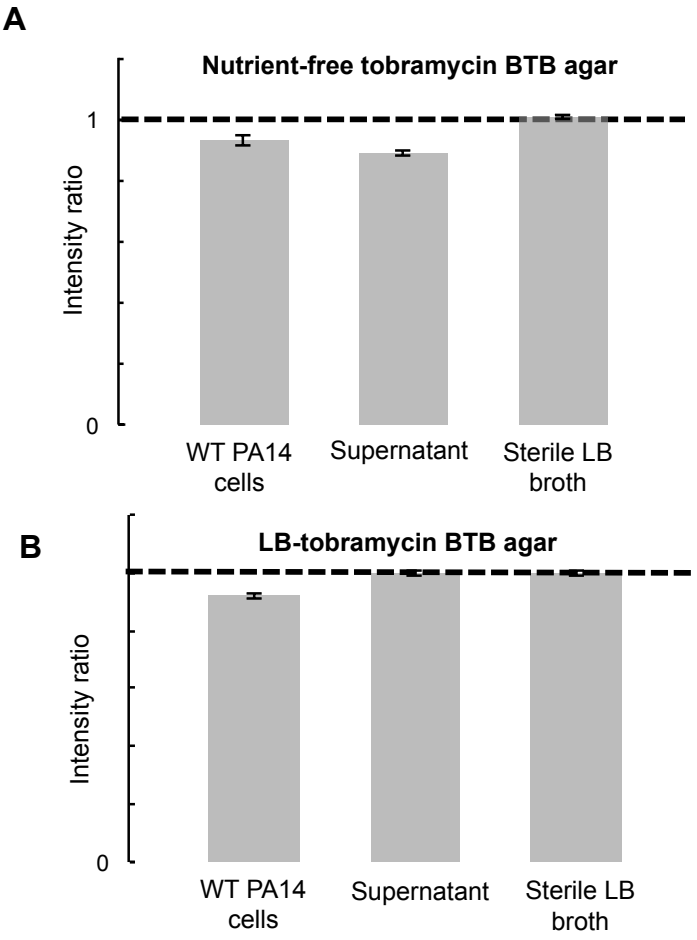

Figure 2.37 Production of an alkaline change on LB-tobramycin agar is associated with inhibition.

P. aeruginosa WT PA14 cells, filter-sterilized supernatant from WT PA14 cultures grown in LB broth, and sterile LB broth were deposited on nutrient-free tobramycin BTB agar, LB-tobramycin BTB agar and on antibiotic-resistant mutant lawns overlaid on LB-tobramycin agar. **(A)** On nutrient-free tobramycin BTB agar, WT PA14 cells and supernatant produce an intensity ratio < 1, indicating an alkaline change. Sterile LB broth produces no color change, as indicated by an intensity ratio ~1. Error bars represent standard error of the mean; *N = 3.* **(B)** On nutrient-containing LB-tobramycin BTB agar, WT PA14 cells produce an alkaline change, indicated by an intensity ratio < 1. Supernatant and sterile LB broth do not produce a color change, as indicated by an intensity ratio ~1. Error bars represent standard error of the mean; *N = 3.*

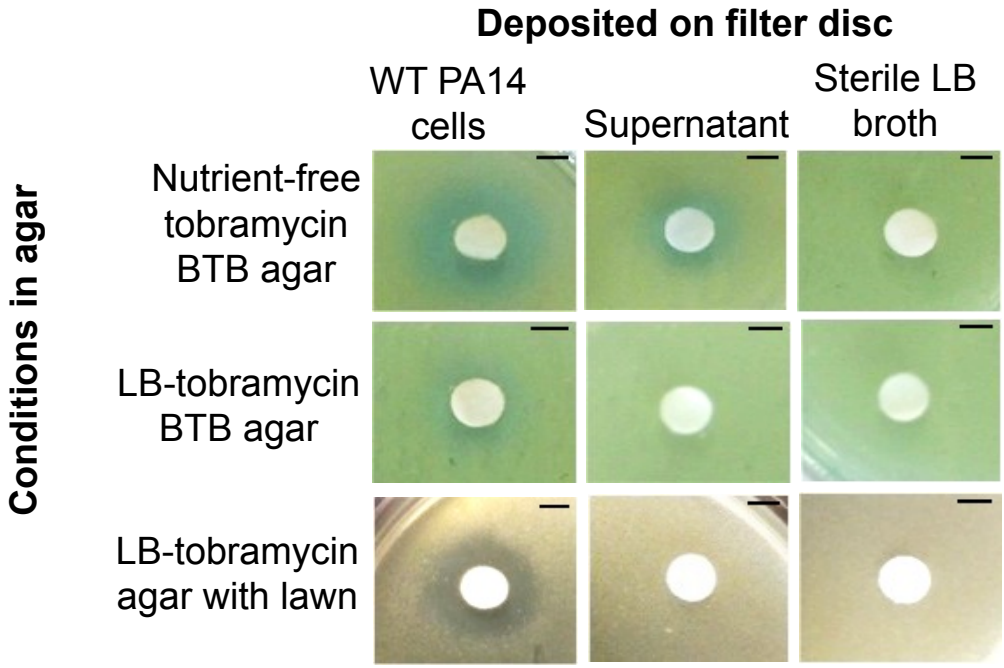

Figure 2.38 Representative images showing that production of an alkaline change on LB-tobramycin agar is associated with inhibition.

WT PA14 cells produce an alkaline change on nutrient-free tobramycin BTB agar (X_c = 9 mm) and LB-tobramycin BTB agar (X_c = 6 mm) and produce inhibition of antibiotic-resistant mutants (X = 5 mm). Supernatant produces an alkaline change on nutrient-free tobramycin BTB agar (X_c = 6 mm), but fails to produce both an alkaline change on LB-tobramycin BTB agar (X_c = 0) and inhibition of antibiotic-resistant mutants (X = 0 mm). Deposition of sterile, fresh LB broth does not produce an alkaline change (X_c = 0 mm) or inhibition (X = 0 mm). Scale bars are 5 mm; *N = 3.*

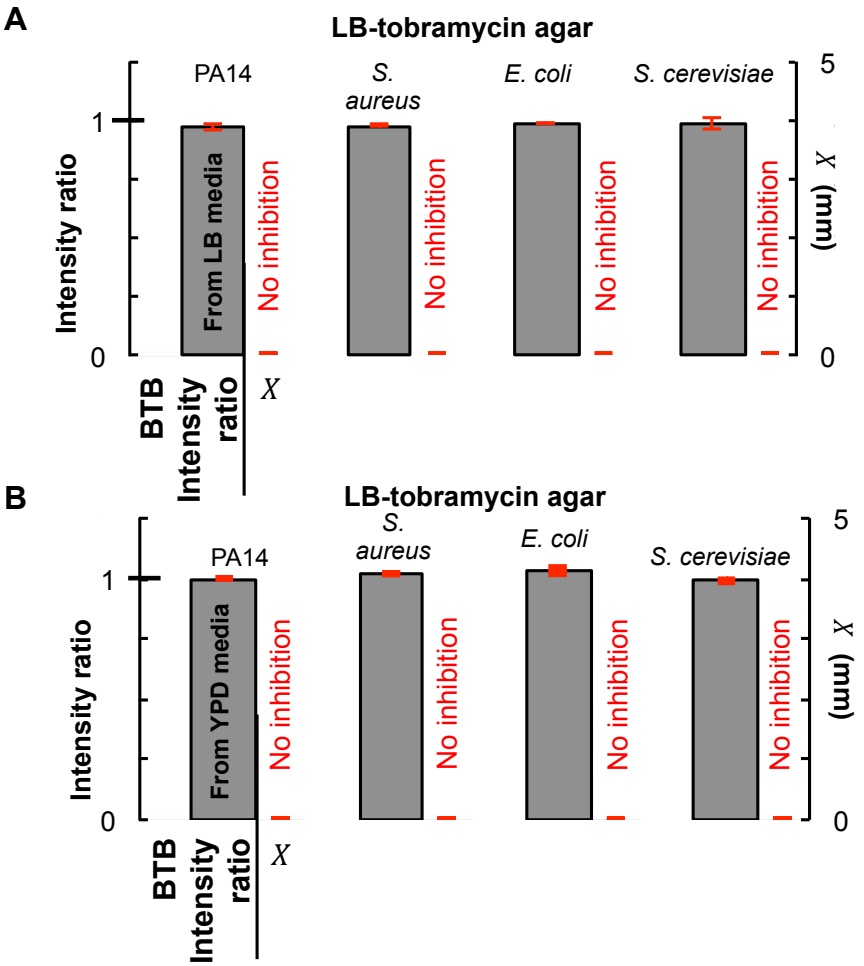

Figure 2.39 Supernatant from cultures grown in LB and YPD media on LB-tobramycin BTB agar and on antibiotic-resistant mutant lawns overlaid on LB-tobramycin agar.

Supernatant from overnight cultures from LB and YPD media was deposited on LB-tobramycin BTB agar and on antibiotic-resistant mutant lawns overlaid on LB-tobramycin agar. **(A and B)** On nutrient-containing LB-tobramycin BTB agar or antibiotic-resistant mutants, supernatant from WT PA14, *S. aureus*, *E. coli* and *S. cerevisiae* grown in LB and YPD media fail to produce a pH color change and inhibition (X = 0 mm). Error bars represent standard error of the mean; *N = 3.*

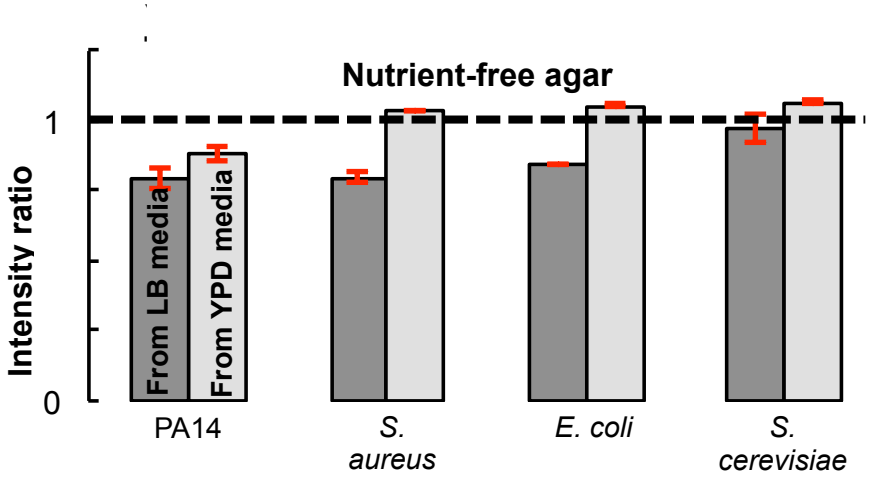

Figure 2.40 Supernatant from cultures grown in LB and YPD media nutrient-free tobramycin BTB agar.

On nutrient-free tobramycin BTB agar, supernatant produces a pH color change corresponding to that seen after deposition of cell cultures. Supernatant from WT PA14, *S. aureus* and *E. coli* cultures grown in LB produce an alkaline change,. Supernatant from *S. cerevisiae* cultures in LB produce no color change. As expected, *S. cerevisiae* grew poorly in LB medium. For cultures grown in YPD medium, WT PA14 supernatant produces an alkaline change, whereas for *S. aureus*, *E. coli* and *S. cerevisiae* supernatant produces an acidic change. Error bars represent standard error of the mean; *N = 2.*

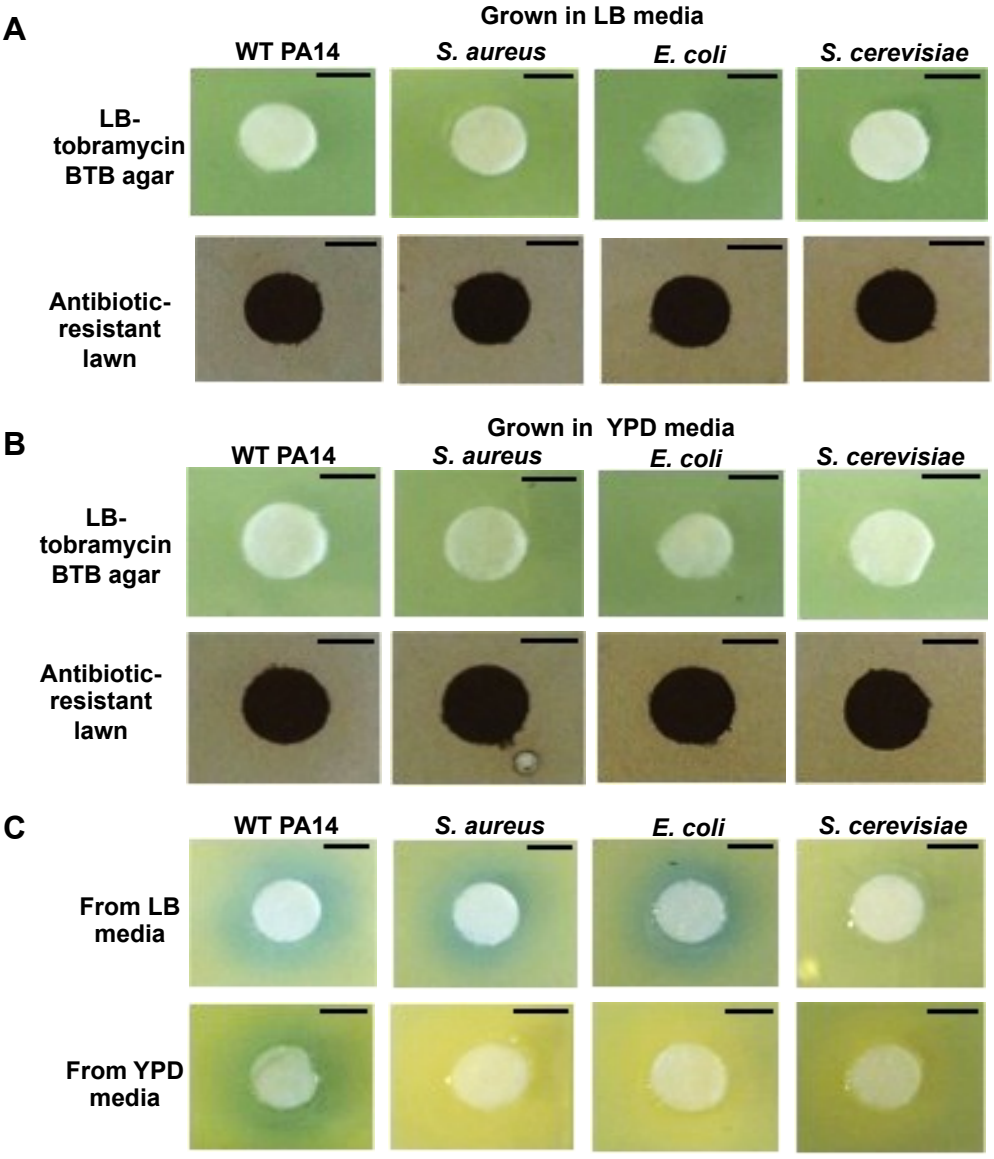

Figure 2.41 Deposition of supernatant from overnight cultures grown in LB and YPD media.

(A and B) Representative images of absence of pH color change and inhibition following deposition of supernatant from LB and YPD cell cultures on LB-tobramycin 8 µg/mL BTB agar and antibiotic-resistant mutant lawns. Scale bars are 5 mm. **(C)** Representative images of pH color change following deposition of supernatant from LB and YPD cell cultures on nutrient-free tobramycin 8 µg/mL BTB agar. Scale bars are 5 mm.

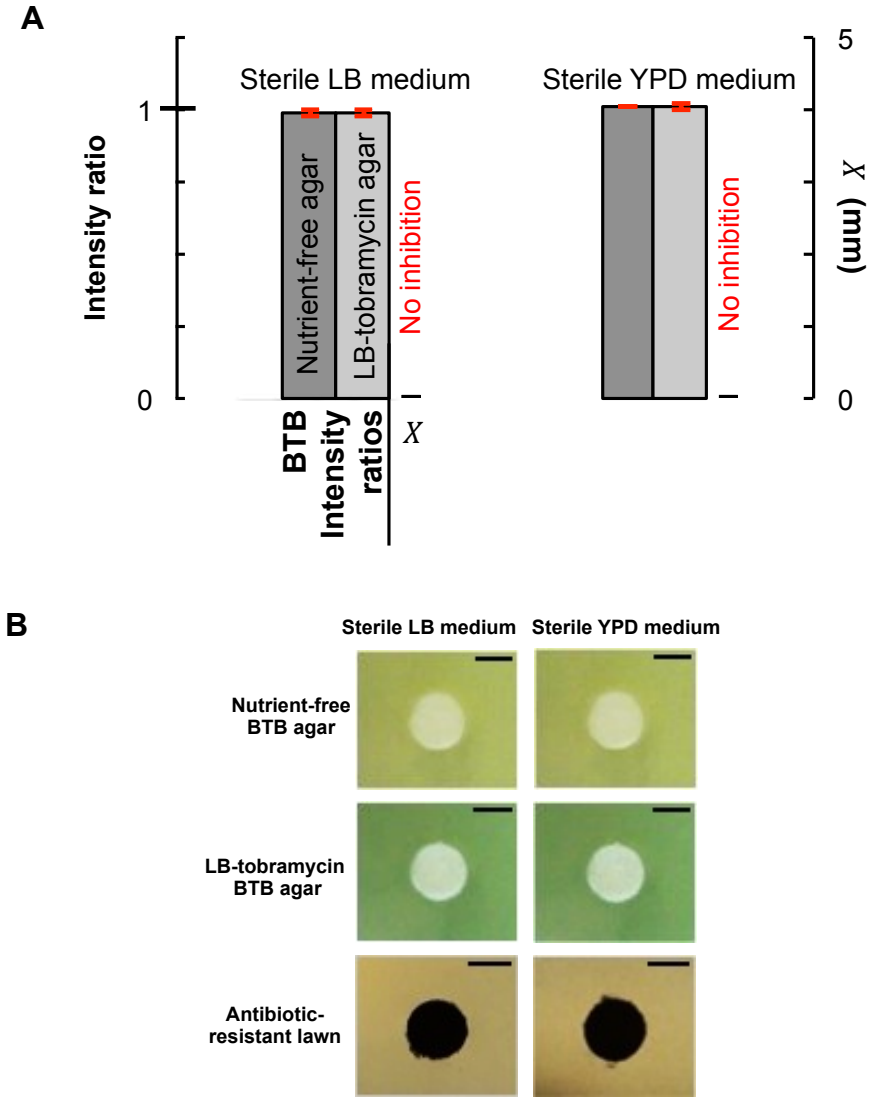

Figure 2.42 Deposition of sterile liquid media fails to produce a pH color change and inhibition,

Sterile LB and YPD media were deposited on nutrient-free tobramycin 8 µg/mL BTB agar, LB-tobramycin 8 µg/mL BTB agar and on antibiotic-resistant mutant lawns on LB-tobramycin 8 µg/mL agar. **(A)** On BTB agar, deposition of sterile LB or YPD media fails to produce an alkaline or acidic change, as indicated by an intensity ratio ~1, and fails to produce inhibition of antibiotic-resistant mutants. Error bars represent standard error of the mean; *N* = *2.* **(B)** Representative images of absence of pH color change and inhibition with sterile LB or YPD media. Scale bars are 5 mm.

2.3.17 Spatial fluctuations in population density influence the survival of antibiotic-resistant mutants in spatially-mixed populations

In the spatially-mixed system, mutant survival probability approaches zero with increasing cell density. Similarly, in disc diffusion assays, inhibition zone size increases with increasing density of deposited cells. Therefore, it seems paradoxical that mutant cells are able to grow into high-density colonies on the plate without inhibiting themselves. To resolve this paradox, we examine the effect of spatial fluctuations in initial population density on the survival of resistant mutants.

It is often found that the molar amount of an inhibitory substance *per cell* is a more accurate determinant of cell survival during exposure than the concentration, and therefore higher-density populations of bacteria can survive higher concentrations of antibiotics than lower-density populations [166]. In a well-mixed, homogeneous system with a constant antibiotic concentration $[AB]$, increasing cell density decreases the moles of antibiotic per cell, $\{AB\}$, thereby enhancing the resistance of cells to a given $[AB]$. However, we have postulated that the IF released by cells modulates antibiotic resistance by changing pH. Moreover, physically realistic spatial distributions of cells will have random fluctuations in cell density. Together, these two observations may lead to non-trivial probabilities of cell survival as a function of the average cell density.

We assume a uniform $[AB]$ throughout the plate. $\{AB\}$ in a small effective volume V_e containing N cells is thus $\frac{[AB]V_e}{N}$. If $\{AB\}$ is less than a critical value $\{AB\}_{th}$, mutant cells in V_e will grow. Since the number of WT cells is much greater than the number of antibiotic-resistant mutants and the volumes in question are small, we assume that no more than one mutant will be in V_e and that it will survive if $N_{WT}+1>\frac{[AB]V_e}{\{AB\}_{th}}$, where N_{WT} is the number of WT in V_e.

We model random deposition of bacteria as a Poisson process. The Poisson cumulative distribution function gives the probability that the number of WT in V_e will be greater than N_{WT} as $P=1-e^{-V_e\rho_{WT}}\sum_{i=0}^{N_{WT}}\frac{(V_e\rho_{WT})^i}{i!}$. ρ_{WT} is the average density of WT on the plate. Since $\rho_{WT}\approx\rho_0$, where ρ_0 is the total cell density on the plate, we approximate $P=1-e^{-V_e\rho_0}\sum_{i=0}^{N_{WT}}\frac{(V_e\rho_0)^i}{i!}$.

Previous studies at constant cell density have found an approximately exponential relationship between the MIC to aminoglycoside antibiotics and the pH [166]. We assume a similar exponential form for $\{AB\}_{th}=A\times10^{-b\times pH}+\{AB\}_{min}$, where A and b are scaling constants, and $\{AB\}_{min}$ is the minimum value of $\{AB\}_{th}$. We approximate the pH resulting from the release of IF as $pH=\alpha+\beta\log_{10}[IF]$, where α and β are constants describing the acid-base

properties of the IF, and $[IF]$ is the concentration of IF on the plate (electronic supplementary material). Assuming $\{AB\}_{min}$ is small compared to $\{AB\}_{th}$, the condition for mutant survival can be approximated as $N > \frac{[AB][IF]^{b\beta} V_e}{A \times 10^{-\alpha b}}$. If $[IF] = k_0 \rho_0$, where k_0 is a production constant and ρ_0 is the initial cell density, the probability of mutant survival becomes

$$P = 1 - e^{-V_e \rho_0} \sum_{i=0}^{\Gamma V_e \rho_0^{\eta} - 1} \frac{(V_e \rho_0)^i}{i!} \qquad (3)$$

where $\Gamma = \frac{[AB] k_0^{b\beta}}{A \times 10^{-\alpha b}}$ and $\eta = b\beta$. Γ is a lumped parameter which accounts for the alkalinity of the IF and a strain's production of IF and degree of antibiotic resistance; η accounts for the sensitivity of the antibiotic resistance to changes in pH; V_e accounts for the spatial extent over which surrounding cells can lower the $\{AB\}$ to which a mutant is exposed. P is discrete with respect to ρ_0, and a continuous function $\tilde{P}$ can be approximated from it using linear interpolation.

The function $\tilde{P}$ gives the fraction of plated antibiotic-resistant mutants that will grow to form colonies and as a function of the initial density of cells. The fraction of the plated culture that grows into antibiotic-resistant colonies, M, is thus described by $M = \mu \tilde{P}^{\theta}$ where μ is the true proportion of mutants in the

population. Similarly, the number of colonies formed, C, is given by $C = \mu\rho_0 V_{tot} P^{\eta}$, where V_{tot} is the total volume of the plated cell suspension.

We fit this model to our experimental data. A wide range of values of Γ, V_e, η and μ result in trends consistent with our measurements in Figure 2.1 (Figure 2.43). We can estimate physically reasonable values of V_e by examining how an individual cell might impact its surrounding antibiotic concentration. By modeling a cell as an antibiotic sink, we estimate the lowest reasonable V_e value to be 0.004 nL, corresponding to 1000 times the volume of a cell, or a sphere of radius 10 μm (electronic supplementary material). With a V_e of 0.004 nL, values of η ranging from 0.90 to 2.5, Γ ranging from $8\text{x}10^{-6}$ to 4 $\text{nL}^{\eta-1}$ and μ ranging from $4\text{x}10^{-7}$ to $4\text{x}10^{-6}$, produce reasonable fits to our data, and the least squares fit has an η of 1.186, Γ of 0.307 $\text{nL}^{\eta-1}$ and μ of $1.02\text{x}10^{-6}$ (R^2= 0.92) (Figure 2.1). Additionally, V_e of 0.04, 0.4 and 4 nL, produce similar trends and fits (Figure 2.43 and 2.44). Overall, the wide range of parameters values that produce reasonable fits reflects a robustness of this model to changes in specific values, and indicates that fine-tuning of the parameters is not necessary to match the trends, which we observe.

Guided by this model, we postulate that antibiotic-resistant mutants are able to grow into high-density colonies on antibiotic-containing agar because they are shielded from antibiotics by their WT neighbors. A mutant will grow into a

colony if it is in a region with high local cell density that reduces the $\{AB\}$ to which it is exposed below a threshold value. However, as the average cell density deposited on the plate increases, the resulting increase in $[IF]$ on the plate lowers this threshold value by causing an increase in pH, so there is a net decrease in mutant survival probability with increasing average density. This interpretation implies that small initial fluctuations in density will be magnified as they control the subsequent growth of bacteria.

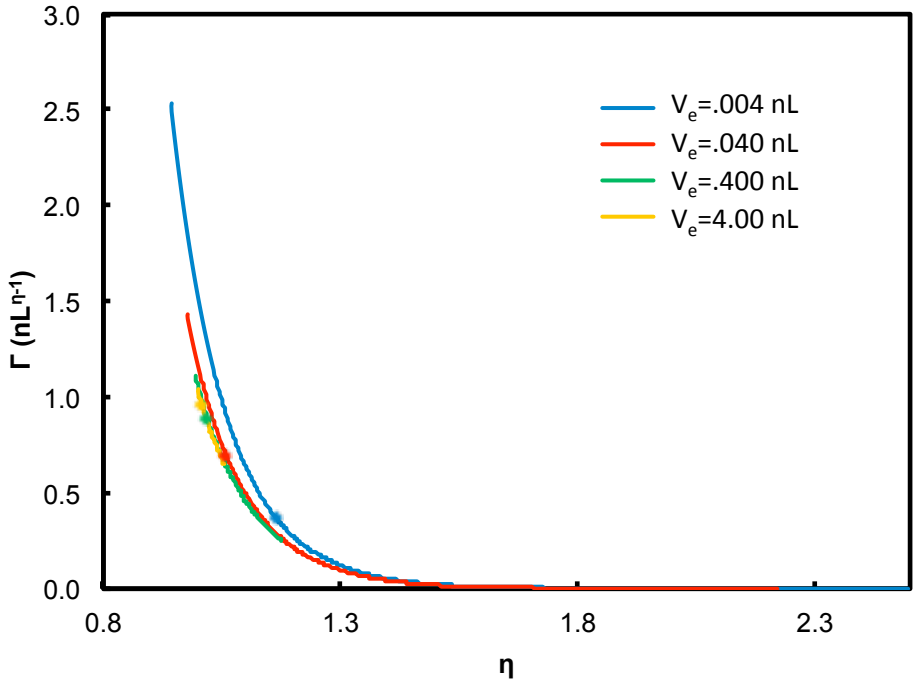

Figure 2.43 A wide range of mixed-system model parameters produce reasonable fits to observations.

Parameter estimates of Γ and μ, as well as the sum of squared residuals (SSR), were calculated for the least squares fit to colony counts in Replicate 1 of Figure 2.1 for set values of V_e and η. A SSR of 1.0×10^6 was estimated to be the threshold for reasonable fits, and fits with a SSR greater than this are excluded. Plotted are the least squares Γ estimated as a function of the set values of η for V_e of 0.004, 0.04, 0.4 and 4. Diamond points (♦) represent the fit values of Γ and η with minimum SSR.

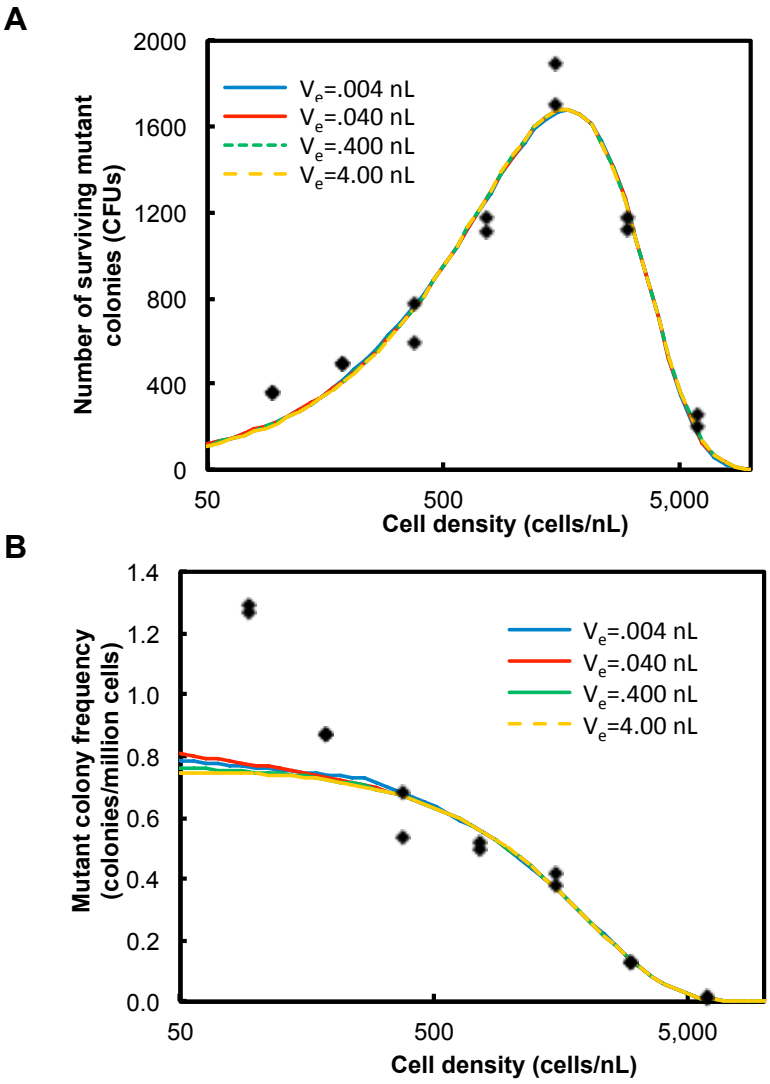

Figure 2.44 Fits of the mixed-system model describe our observations of inhibition well.

Least squares regression was performed on colony count data from Replicate 1 of Figure 2.1 for given values of V_e. The resulting fit parameters were 1) V_e = 0.004, η = 1.164, Γ = 0.370, μ = 1.10x10^{-6}; 2) V_e = 0.04, η = 1.059, Γ = 0.697, μ = 1.21x10^{-6}; 3) V_e = 0.4, η = 1.019, Γ = 0.888, μ = 1.26x10^{-6}; 4) V_e = 4, η = 1.006, Γ = 0.962, μ = 1.27x10^{-6}. **(A)** Colony forming unit (CFU) counts fit. R^2=0.953 (V_e = 0.004), 0.955 (V_e = 0.04), 0.954 (V_e = 0.4), 0.954 (V_e = 4). **(B)** Mutant colony frequency (colonies/million cells) fit. R^2=0.778 (V_e = 0.004), 0.784 (V_e = 0.04), 0.766 (V_e = 0.4), 0.759 (V_e = 4).

2.3.18 Identification of possible mutations conferring aminoglycoside resistance

Table 2.2. Single-nucleotide polymorphisms (SNPs) in the antibiotic-resistant mutant strain generated and used in this study.

Genome position	Codon change	Amino acid change	Gene	Description
741,564	C**A**C→C**G**C	His→Arg	EF-Tu	Elongation factor Tu
3,559,401	**A**AG→**G**AG	Lys→Glu	*phzD*	Phenazine biosynthesis protein
3,615,974	**T**CC→**C**CC	Ser→Pro	*trkH*	Potassium uptake protein

We used one antibiotic-resistant mutant strain of PA14 for all our experiments except when specifically stated otherwise. This strain was generated by spontaneous mutation during overnight culture in antibiotic-free liquid media. To identify the possible mutation(s) conferring aminoglycoside resistance in this strain, we performed whole-genome sequencing (Illumina MiSeq v2) of the antibiotic-resistant mutant and WT PA14 ancestral strain. These sequences have been deposited in the National Center for Biotechnology Information Short-Read Archive http://www.ncbi.nlm.nih.gov/sra (accession no. SRP042054). Using the BRESEQ 0.19 pipeline, we identified three single-nucleotide polymorphisms (SNPs) unique to the antibiotic-resistant mutant strain (Table 2.2).

Elongation factor Tu (EF-Tu), a member of the GTPase superfamily of proteins, has a crucial role in the elongation phase of bacterial protein synthesis, in which it delivers aminoacylated tRNAs (aa-tRNAs) to the ribosome [167]. After delivering the correct aa-tRNA complex to the ribosome, EF-Tu is released, a process initiated by GTP hydrolysis. This mechanism is catalyzed by EF-Tu, but requires activation by the ribosome [167]. It has been shown that a highly conserved histidine residue (His-84 in *E. coli* and His-85 in *Thermus thermophilus*) in the switch II region of the EF-Tu factor is critical for this catalysis [168, 169]. The antibiotic-resistant strain that we sequenced had a histidine-to-arginine substitution at this residue (H85R) (Table 2.2). Aminoglycoside antibiotics inhibit bacterial protein synthesis by targeting the ribosome [86]. Mutations in the eukaryotic elongation factor 1 (EF-1), analogous to bacterial EF-Tu, and other bacterial elongation factors, such as EF-G, have been associated with aminoglycoside resistance [170-172], indicating the possibility that the EF-Tu mutation contributes to antibiotic resistance in this mutant strain.

TrkH is a hydrophobic, membrane protein and a constituent of the potassium uptake system, which mediates the symport of potassium and hydrogen ions [173]. Mutations in Trk system have been associated with altered aminoglycoside susceptibility [171, 174, 175], and in one study 64% of sequenced aminoglycoside-adapted populations had *trkH* mutations [171]. The amino acid residue affected by one of these mutations was close to the ion

channel, possible leading to increased proton influx and diminished membrane potential [171]. Aminoglycosides require the membrane potential component of the proton motive force (PMF) for active cellular uptake [87, 176] and adaptation to this class of antibiotics frequently proceeds through mutations that diminish the generation of PMF [171]. The antibiotic-resistant strain sequenced in our study had a serine to proline substitution at residue 226 (S226P) of TrkH (Table 2.2). This could possibly lead to increased proton influx, diminished membrane potential and PMF, and reduced aminoglycoside uptake.

The *phzD2* gene is part of the phenazine biosynthetic cluster, encoded by two redundant operons *phzA1-G1* and *phzA2-G2* [142]. The antibiotic-resistant strain in our study had a lysine to glutamic acid substitution at residue 28 (K28E) of PhzD (encoded by *phzD2*) (Table 2.2). To the best of our knowledge, there is no direct evidence of *phzD* mutations conferring aminoglycoside resistance, and the redundant nature of this gene, makes its role further likely.

It is thus plausible that acquisition of these mutations, alone or in combination, confer aminoglycoside resistance in the antibiotic-resistant mutant strain.

2.3.19 Disc-diffusion model to incorporate a threshold pH

Previous work by others has shown several cases in which the MIC of aminoglycoside antibiotics decreases exponentially with increasing pH [166]. Therefore, we modify the disc-diffusion model of our spatially-structured system to incorporate a threshold inhibitory pH instead of a threshold IF concentration. For an alkaline IF, the concentration of OH^- is approximately $\left[OH^-\right] \approx A \times [IF]^{\beta}$ where A and β are constants, and $[IF]$ is the concentration of IF in the media. Thus, $pH = \alpha + \beta \log_{10}[IF]$, where $\alpha = 14 + \log_{10} A$. Combining this with equation 1 from the main text gives:

$$pH = \alpha + \beta \log_{10} \left\{ \frac{[IF]_0}{4\pi Dt} \exp\left(-\frac{x^2}{4Dt} \right) \right\}$$

This can be rearranged to:

$$x^2 = 4Dt \ln[IF]_0 - 4Dt \ln(4\pi Dt) - \frac{4Dt \ln(10)}{\beta}(pH - \alpha)$$

If $[IF]_0 = k_0 N_0$ where k_0 is a production constant and N_0 is the number of cells on the disc, this becomes:

$$x^2 = 4Dt \ln(N_0) + 4Dt \ln\left(\frac{k_0}{4\pi Dt} \right) - \frac{4Dt \ln(10)}{\beta}(pH - \alpha)$$

This function gives the point in space x at which the pH is a given value. Assuming there is a critical pH, pH_c, over which cells die at the critical time, the edge of the zone X will be:

$$X^2 = 4DT_c \ln(N_0) + F(D, T_c, pH_c, k_0, \alpha)$$

The N_0-dependent portion of this function is of the same form as the one predicted in the model without a pH-mediated IF. As a result, pH-mediated inhibition does not change our measurements of molecular weight.

2.3.20 pH-mediated inhibition predicts linear relationship between squared sizes of indicator color change and inhibition zone

Cells that produce inhibition also cause a blue discoloration in agar containing the pH indicator bromthymol blue (BTB). Because the change in color of BTB occurs over a narrow range of pH (approximately 6-7.6), the boundary of the discolored region will correspond to a specific threshold pH of ~7.6, which we term $pH_{c,BTB}$. Similarly, if inhibition is mediated by a change in pH, then the boundary of the zone of inhibition will correspond to a specific threshold pH, $pH_{c,IF}$. Thus, the size of the inhibition zone, X_{IF}, is

$$X_{IF}{}^2 = 4Dt \ln(N_0) + 4Dt \ln\left(\frac{k_0}{4\pi Dt}\right) - \frac{4Dt \ln(10)}{\beta}\left(pH_{c,IF} - \alpha\right)$$

and at the critical time T_c the size of the zone of color change X_{BTB} is

$$X_{BTB}{}^2 = 4Dt \ln(N_0) + 4Dt \ln\left(\frac{k_0}{4\pi Dt}\right) - \frac{4Dt \ln(10)}{\beta}\left(pH_{c,BTB} - \alpha\right)$$

Thus:

$$X_{IF}{}^2 = X_{BTB}{}^2 - \frac{4DT_c \ln(10)}{\beta}\left(pH_{c,IF} - pH_{c,BTB}\right)$$

This model therefore predicts a linear relationship between $X_{IF}{}^2$ and $X_{BTB}{}^2$, when X_{BTB} is measured around the critical time. This is consistent with our observations (Figure 2.22). From these data, we can also infer that the threshold pH value for inhibition is higher than the threshold pH value for the BTB color change.

2.3.21 Inhibition in spatially-mixed populations

We measure the number of colonies formed, C, in a spatially-mixed population exposed to antibiotics. Our model predicts $C = \mu\rho_0 V_{tot} \tilde{P}$, where $\tilde{P}$ is the function gained by linearly interpolating

$$P = 1 - e^{-V_e\rho_0} \sum_{i=0}^{\Gamma V_e \rho_0^{\eta} - 1} \frac{\left(V_e\rho_0\right)^i}{i!}$$

ρ_0 is average cell density, V_e is an effective volume in which cells reduce antibiotic quantities per cell, μ is the proportion of mutants in the initial population, and Γ and η are lumped parameters. We fit this model to our observations of C using least squares regression. A wide range of values of values of Γ, V_e, η and μ result in trends consistent with our measurements in Figure 2.1. We can estimate physically reasonable values of V_e by examining how an individual cell might impact its surrounding environment. V_e is the effective volume within which cells reduce the moles of antibiotic per cell acting on a cell at the center of the volume. The distance at which a cell no longer

effects a noticeable reduction in antibiotic amounts at the center would be equal to the radius of a spherical V_e. To estimate this distance, we can model cells as antibiotic sinks. The diffusion of antibiotics can by described by Fick's Second Law, $\frac{d[AB]}{dt} = D\nabla^2[AB]$, where $[AB]$ is antibiotic concentration. Since the diffusion of antibiotics is fast relative to the length scale of a cell (tobramycin diffusion coefficient D = 96±8 μm^2/s), we can consider the steady state distribution of antibiotics around a single cell. Approximating a cell to be spherical, the steady state antibiotic distribution around a cell which completely absorbs antibiotics $[AB]$= 0 at the cell surface is described by $[AB] = [AB]_\infty\left(1-\frac{a}{r}\right)$, where $[AB]_\infty$ is the antibiotic concentration far from the cell, a is the radius of the cell and r is the distance from the center of the cell. The concentration 10 times the radius of the cell away will be 90% of $[AB]_\infty$. This corresponds to a volume 1000 times the volume of the cell, which we take to be a minimum value of V_e. Thus, with a cell volume of approximately 4x10^{-6} nL, we estimate reasonable values of V_e to be at least .004 nL.

Table 2.3 Minimum Inhibitory Concentration (in μg/mL) for strains used in this study.

Strains	Tobramycin	Gentamicin
P. aeruginosa WT PA14	1.2	1.2
P. aeruginosa WT PAO1	1.2	Not tested
Spontaneously-generated antibiotic-resistant mutants (three different strains)	9.7	9.7
Continuously evolved antibiotic-resistant mutants (two different strains)	9.7	Not tested
PA14 transposon mutants	1.2	2500
Δ*phz1/2*	1.2	Not tested
Clinical cystic fibrosis isolates 2773C, 1913C, 3488D	1.2	Not tested
Clinical cystic fibrosis isolates 3470C, 3639M, 4278M, 4218C, 0324C, 2159M, 4220M, 5912M	0.6	Not tested
Clinical cystic fibrosis isolates 4219D, 0476M	0.3	Not tested
Clinical cystic fibrosis isolate 3640D	0.07	Not tested
Clinical cystic fibrosis isolate 5913C	4.8	Not tested
Clinical cystic fibrosis isolate 5623M, 5914M	2.4	Not tested
Pseudomonas sandgrass isolate	9.7	Not tested
S. aureus Mu50	1250	Not tested
E. coli SM10, *E. coli* DH5α	2.4	Not tested
Burkholderia cepacia	2500	Not tested
Serratia marcescens	4.8	Not tested
Saccharomyces cerevisiae (done in YPD broth)	1250	Not tested

Table 2.4 Mutants from the PA14 non-redundant transposon library that were tested for inhibition.

Mutant	Gene function	Width of inhibition (X)
prtN	Pyocin transcriptional regulator	5 mm
fliA	Motility sigma factor FliA	5 mm
fliC	Flagellin subunit protein	5 mm
pilH	Type IV pilus response regulator	5 mm
pilT	Twitching motility protein	5 mm
lasI	Acylhomoserine lactone synthesis protein	5 mm
rhlI	Acylhomoserine lactone synthesis protein	5 mm
rhlR	Acylhomoserine lactone dependent transcriptional regulator	5 mm
phzA1	Phenazine biosynthesis protein	5 mm
phzA2	Phenazine biosynthesis protein	4 mm
phzB1	Phenazine biosynthesis protein	4 mm
phzB2	Phenazine biosynthesis protein	5 mm
phzC1	Phenazine biosynthesis protein	5 mm
phzE1	Phenazine biosynthesis protein	4 mm
phzF	Phenazine biosynthesis protein	4 mm
phzG1	Phenazine biosynthesis protein	5 mm
mucB	Negative regulator for alginate biosynthesis	6 mm

Table 2.4 (continued)

ndvB	Synthesis of periplasmic glucans	6 mm
rpoS	Sigma factor	5 mm
mdoG	Periplasmic glucan biosynthesis protein	4 mm
algQ	Alginate regulatory protein	6 mm
algU	Sigma factor AlgU	4 mm
alg44	Alginate biosynthesis protein	6 mm
pelG	Putative component of polysaccharide transporter family	6 mm
pqsE	Quinolone signal response protein	5 mm
PA5437	Putative transcriptional regulator, Putative transcriptional regulator, LysR family	5 mm
PA0625	Putative tail length determinator protein	5 mm
PA0633	Putative major tail protein V	5 mm
PA0624	Conserved hypothetical protein	5 mm
PA4754	Conserved hypothetical protein	5 mm
PA0615	Conserved hypothetical protein	5 mm
PA0017	Putative tRNA and rRNA cytosine-C5-methylases	5 mm
mutS	DNA mismatch repair protein	5 mm
mutY	Adenine glycosylase / DNA mismatch repair protein	4 mm
uvrD	DNA helicase II	5 mm

Table 2.4 (continued)

envZ	Two component sensor kinase	5 mm
mutM	DNA glycosylase / DNA mismatch repair protein	4 mm
mutT	DNA mismatch repair protein	5 mm
aspC	Aspartate transaminase	5 mm
aspA	Aspartate ammonia lyase	5 mm

2.4 CONCLUSIONS

We have found that bacteria, regardless of their antibiotic susceptibility, can inhibit the survival and growth of antibiotic-resistant mutants in the presence of aminoglycosides. An alkaline by-product of amino acid catabolism, possibly ammonia or amines, mediates this inhibition. Further, these alkaline by-products likely mediate this effect by an increase in pH, which enhances the bactericidal effect of aminoglycosides. We find that microbial population structure, including cell density, spatial distribution and interspecies interactions, can impact the growth of pre-existing antibiotic-resistant through this mechanism.

For a favorable mutation (*i.e.*, one that confers a fitness advantage in the environment), the probability of fixation in a population increases with decreasing population size, which is a measure of the number of competitors. Although our liquid cultures are grown without antibiotics, it is possible that the resistance-conferring mutation(s) conveys some other growth advantage in antibiotic-free liquid culture. In that case, the probability of the mutation fixing would depend on whether the mutation occurred early or late in culture growth. However, this possibility does not confound the results we present here because in Figure 2.1 the ratio of mutants to WT is the same within each experiment, since all the data points for each experiment are done for the same overnight culture suspension. Therefore, Figure 2.1 measures the probability that a pre-existing mutant will grow into a colony, not the fixation of the mutants in a population.

Our finding, that increasing bacterial density can increase antibiotic susceptibility, is superficially in contrast to previous observations that in compact bacterial populations, such as in biofilms, the susceptibility against antibiotics is in fact decreased. However, it should be noted that bacteria in biofilms are in a different phenotypic state than that of the bacteria we plated from suspension onto agar. Most notably, biofilms are structured by embedding extracellular polymers, which can provide protection against aminoglycoside antibiotics. The bacteria in biofilm interiors also have limited access to growth substrates, which results in slowed growth and altered metabolic pathways that can protect against antibiotics.

Thus, the structure and the phenotypic state of the bacterial population need to be considered when designing treatment strategies.

This can easily be seen in the case of Cystic Fibrosis (CF), which is a genetic condition that renders the lung unusually susceptible to infection by *P. aeruginosa* and other pathogens. The CF lung contains an abundance of free amino acids [177, 178]. In microbes sampled from CF lungs, the genes and pathways involved in amino acid catabolism are significantly upregulated [177]. In accordance, elevated ammonia levels have been found in CF sputum [177]. These observations would seem to suggest that the microbial population in the CF lung is well-poised to inhibit each other in the presence of aerosolized tobramycin, which is commonly used in the treatment of CF.

However, CF results from a genetic defect in the Cystic Fibrosis Transmembrane Receptor (CFTR), which causes decreased bicarbonate ion transport and acidification of CF airway fluids [76, 179]. This would prevent inhibition. Inhaled bicarbonate therapy is a possible remediation for this and is already being studied as a therapy for CF because it may help restore the innate antimicrobial activity of airway surface fluids as well as facilitate the thinning and clearing of airway mucus [76, 77]. Our results suggest a potential additional benefit for bicarbonate therapy in CF, where it could augment the activity of aminoglycosides and help curtail antibiotic resistance. Thus, optimizing therapeutic benefits of combining aminoglycosides with bicarbonate would require further work determining how the physiological environment of the host impacts microbial metabolism, pH changes, and pharmacokinetics of base and aminoglycoside in the lung. Moreover, while early infections of the CF lung are transient and associated with a planktonic bacterial phenotype, decades-long chronic infections are associated with a biofilm phenotype. Since biofilms have phenotypic resistance to aminoglycosides, full realization of the potential benefits of the work we present here would require determination of the degree to which pH-mediated inhibition is active against clinical biofilm infections.

More broadly, our findings indicate that manipulating the nutritional and metabolic environment of the CF lung, chronic wounds, or other sites of infection could potentially provide a set of management strategies that are complementary

to and synergistic with conventional antibacterial therapies. Developing approaches that limiting the availability of sugars, and/or using anti-fungal therapy, would promote amino acid catabolism and prevent microbe-caused acidification. Because the inhibition we characterize here results from highly-conserved bacterial metabolic pathways, evolutionary escape is likely to be difficult. In addition, because the IF is produced by bacteria and will therefore be localized to infection sites, approaches to treatment that exploit the structure of microbial populations may reduce system-wide high concentrations of antibiotics and resultant toxicity to patients. This approach could both help to curtail the rise of antibiotic-resistant strains and also extend the usage of currently available antibiotics.

We thank Andreas Matouschek for use of the spectrophotometer and ultracentrifuge, Mary Jo Kirisits for use of the ammonia-selective electrode, and Jeffrey Barrick and Daniel Deatheridge for guidance with the BRESEQ pipeline. We are grateful to Marvin Whiteley, Andy Ellington and Rasika Harshey for their experimental suggestions.

Chapter 3: A biophysical approach to novel antibiotic strategies: Evaluating the potential of tobramycin and bicarbonate in combination against *Pseudomonas aeruginosa*

3.1 INTRODUCTION

Rising trends in antibiotic resistance have prompted the search for newer therapeutic strategies [180]. This refers not only to the development of novel antimicrobial agents, but also underscores the importance of developing adjunct treatment approaches that can extend the lifetime of current antibiotics.

Pseudomonas aeruginosa is an important opportunistic human pathogen, and multi-drug resistant strains of *P. aeruginosa* are on the rise [55]. A major cause of hospital-acquired infections, *P. aeruginosa* affects burned, wounded, and ventilator-associated patients, causing both acute and chronic infections [55]. Acute *P. aeruginosa* infections, are usually associated with planktonic or free-floating cells, and burn wound infections, surgical-site wound infections, urinary tract infections, ocular infections, ear infections, meningitis, and sepsis [55]. Infections in burn wounds carry a heavy medical and economic burden and are associated with high mortality rates [72]. These infections often deteriorate rapidly leading to sepsis and death within few weeks. In surgical-site infections, *P. aeruginosa* often displays increased antibiotic resistance, which delays wound healing [83].

Chronic *P. aeruginosa* infections are commonly seen in patients with the genetic disorder Cystic Fibrosis [66]. In CF patients, infection with *P. aeruginosa* presents a multi-stage process. Early infection is mediated by planktonic cells, and is often transient and intermittent, with antimicrobial therapy initially eradicating the infection. Persistence in the respiratory tract leads to chronic infection, characterized by the formation of multicellular, aggregates of bacteria known as biofilms [15]. In this stage, *P. aeruginosa* is notoriously recalcitrant to antibiotic therapy [83]. In addition, *P. aeruginosa* biofilm formation plays a major role in the pathogenesis of chronic wound infections in patients with diabetic ulcers, venous ulcers, and pressure ulcers (bed sores) [181].

For *P. aeruginosa* infections, aminoglycosides, such as tobramycin, have been successfully used as therapy [103]. In CF patients, inhaled tobramycin is successfully used to eradicate *P. aeruginosa* infections [86]. However, maintaining clinical benefits often requires long-term therapy [182], which is often associated with toxic side effects [183]. Ototoxic side effects include dizziness, tinnitus, and leading to irreversible hearing loss. Damage inflicted on the kidneys (nephrotoxicity), though reversible, could lead to renal insufficiency, and is exacerbated with prolonged duration of therapy [183].

Alkaline pH has been shown to enhance the efficacy of aminoglycosides [156, 157]. Our previous work has demonstrated that native alkaline by-products of bacterial metabolism enhance the susceptibility of antibiotic-resistant mutants

of *P. aeruginosa* in the presence of tobramycin [102]. This effect was mediated by ammonia and or small amines, by-products of amino acid breakdown [102]. Further, we also demonstrated that exogenous alkaline compounds such as ammonium hydroxide, sodium hydroxide, and sodium bicarbonate could recapitulate this phenomenon. This indicates that the effect is likely mediated by the pH change produced by these agents in their region of deposition.

Bicarbonate has an important place in the pathology of Cystic Fibrosis (CF). In CF patients, a genetic defect in the Cystic Fibrosis Transmembrane Conductance Regulator (CFTR) is known to impair the regulation of chloride ion transport [184]. However, in addition to this role, CFTR is also shown to transport bicarbonate [185]. In CF patients, the absence of bicarbonate secretion is central to certain disease manifestations [186]. In a newborn CF pig model, defective bicarbonate secretion leads to acidified airway surface liquid (ASL) [76]. Reduced ASL pH inhibits the activity of innate antimicrobial factors, leading to reduced ability to eradicate *S. aureus* [76]. Further, aerosolizing bicarbonate into the CF lung increased *in vivo* bacterial killing. This indicates that increasing ASL pH might prevent initial infections in CF patients.

Another important feature in CF patients is impaired mucociliary transport and the presence of thick, sticky mucous, which promotes the growth of bacterial infections. It was recently proposed that bicarbonate plays a role in maintaining normal mucin unfolding and function [77]. Highly compacted mucins in

intracellular granules are held together by Ca^{2+} and H^{+} cations. Removal of these cations by bicarbonate is critical for mucin unfolding and expansion. A bicarbonate transport defect would result in defective bicarbonate secretion into the extracellular milieu, inability to remove the cations, and compacted, poorly soluble and transportable mucins.

As a consequence, inhaled bicarbonate therapy is being evaluated as a therapeutic approach in CF patients [77]. Given this and based on our previous work, we evaluate the potential of bicarbonate as an adjunctive therapy to enhance the efficacy of the aminoglycoside antibiotic, tobramycin, against *P. aeruginosa*. We find that the combination of bicarbonate and tobramycin shows a strong synergistic effect against planktonic *P. aeruginosa* cells. We observe this effect for a range of *P. aeruginosa* strains, including laboratory strains, spontaneously-generated antibiotic-resistant mutants, and clinical strains from patients with CF. For planktonic cells, this effect not only reduces the concentration of tobramycin required to kill *P. aeruginosa* cells but, for certain strains also enhances the rate of killing. However, this synergistic effect is not observed with biofilm cells of *P. aeruginosa*, rather the combination appears to have an antagonistic effect.

We present a method of analysis of drug interactions using analytical dose-response surfaces, which examines drug combinations in greater detail than traditional methods [187]. Of its many advantages, this dose-response

surface analysis allows us to more accurately estimate synergy regimes and make testable predictions of synergy combinations. Further, using predictions from Loewe additivity [188], we analyze the difference of the response surfaces from those predicted by additivity, resulting in a net outcome of the combination.

Our results indicate that the combination of tobramycin and bicarbonate has potential against planktonic infections with *P. aeruginosa.* This approach could enhance the efficacy of tobramycin, reduce the duration of therapy, and mitigate dosage-related toxicity and adverse effects. Further studies evaluating the *in vivo* effects of the combination would shed more light on this.

3.2 MATERIALS AND METHODS

3.2.1 Bacterial strains and growth conditions

Bacterial strains used include *P. aeruginosa* wild-type (WT) laboratory strains PA14 and PAO1 and clinical *Pseudomonas* isolates from patients with Cystic Fibrosis (gift from Marvin Whiteley, UT Austin). To generate spontaneous antibiotic-resistant mutants, WT overnight cultures, were grown in antibiotic-free media, and plated on tobramycin 8 μg/mL agar. Antibiotic-resistant mutants grew colonies and were archived in 20-30% glycerol at -80°C. Of the four independent antibiotic-resistant mutants (strain #1-4) used in this study, strain 1 was used for all experiments in Chapter 2 [102], except when stated otherwise.

All bacterial strains were grown in Luria-Bertani broth or on LB agar [91] except where otherwise indicated. Overnight cultures were shaken at 180 rpm for 16-18 hours at 37°C.

3.2.2 Antibiotics

Tobramycin (Indofine Chemical Company, NJ) and sodium bicarbonate (Fisher Scientific, NJ) were obtained as standard powders. A stock solution of 50 mg/mL tobramycin was stored at 4°C prior to use. The desired concentration of sodium bicarbonate solution was freshly prepared prior to use for each experiment.

3.2.3 Minimum Inhibitory Concentration determination for planktonic cells

MICs to tobramycin and bicarbonate were measured using broth microdilution methods as recommended by CLSI [109]. MICs were determined observing visual turbidity and measuring optical density (OD) at 600 nm. The lowest concentration that inhibited visual growth, which corresponded to ~90% inhibition of bacterial growth (MIC_{90}), was used for further analysis.

3.2.4 Checkerboard assay for synergy against planktonic cells

Standard checkerboard microdilution assays were used to test the combined antimicrobial activity of tobramycin and bicarbonate [189] against different *P. aeruginosa* strains. Briefly, an 8 X 8 array of serial two-fold dilutions of the two agents were mixed together in a flat-bottom, 96-well microtiter plate (polystyrene) such that each row (or column) contained a fixed amount of one agent and increasing amounts of the second agent. This resulted in a total of 64 different combinations. For each assay, the serial dilutions of each individual agent were also tested, and control wells containing untreated cells were also grown. Bacteria (~10^5 cells) were added to each well. Each strain was tested in duplicate. Plates were sealed with parafilm and incubated at 37°C under static conditions. After overnight incubation (16–18 hours), optical density was measured at 600 nm (OD_{600}). The fractional inhibitory concentration (FIC) was calculated for each well along the growth - no growth interface (corresponding to

~90% inhibition in the presence of the combination, with each agent below its own MIC). For agents A and B, the FIC of the combination is calculated as [190]

$$\Sigma \mathrm{FIC}_{\mathrm{A+B}} = \mathrm{FIC}_{\mathrm{A}} + \mathrm{FIC}_{\mathrm{B}}$$

$$\text{where } \mathrm{FIC}_{\mathrm{A}} = \frac{\mathrm{MIC}_{\mathrm{A+B}}}{\mathrm{MIC}_{\mathrm{A}}} \text{ and } \mathrm{FIC}_{\mathrm{B}} = \frac{\mathrm{MIC}_{\mathrm{A+B}}}{\mathrm{MIC}_{\mathrm{B}}}$$

An FIC index lower or higher than 1 indicates synergy and antagonism respectively. However, because of the two-fold drug dilution scheme and 1-dilution error of testing methods, we considered an ΣFIC value of ≤ 0.5 to indicate synergistic interactions; 0.5-1 to indicate an additive effect; > 1 to indicate antagonism [190].

The results of the checkerboard assays were represented graphically using isobolograms. The no-growth wells correspond to a ~90% inhibition. Combinations that fall along the line connecting the MIC values of the two agents (line of additivity) are additive interactions. If the combination is synergistic, the isobol will be overall concave-up. For combinations that are antagonistic, the isobol will be overall concave-down. Further, the magnitude of the overall average curvature indicates the degree of synergy or antagonism respectively.

3.2.5 Testing for synergy using LB media supplemented with serum

To simulate *in* vivo conditions, checkerboard assays were performed to test the combined effect of tobramycin and bicarbonate in LB media containing 25% bovine serum (Sigma).

3.2.6 Time-kill assays

To examine the rate of killing of the synergistic combination, time-kill assays were performed. Briefly, 96-well microtiter plates were set up using synergistic combinations (from the checkerboard assays), and concentrations of the individual agents alone. Bacteria (~10^5 cells) were added to each well. Plates were incubated at 37°C for 24 hours under static conditions. Colony-forming units per mL (CFU/mL) were enumerated at 0, 2, 4, 6, 8, and 24 hours. To count the number of colonies, serial dilutions of the bacterial suspension were plated on LB agar. Plates were incubated at 37°C overnight (16-18 hours) and CFUs were counted. Each combination or concentration at a given time-point was tested in triplicate.

3.2.7 Planktonic *in vitro* wound bed model

To examine the effects of the synergy on planktonic cells under more *in vivo* like conditions, we developed an *in vitro* planktonic infection wound model. For this model, two-layered LB agar plates were made by overlaying soft (0.6%) agar on standard LB agar (1.2%) plates. This resulted in a two-layered agar plate with soft agar lying on a base of standard LB agar. Using a sterile metal punch, 1-cm diameter cavities ("wound bed") were created in the top (soft) agar layer. In a separate plate, soft LB agar (83%), sheep blood (5%), bovine serum (10%) was mixed together and bacteria (~10^7 cells, 2%) were added to the mixture. The

mixture was poured and allowed to solidify. A metal punch was used to cut out 1-cm “wounds” from this layer. These “wounds” were then placed in the “wound bed” using a sterile metal forceps. Sterile filter paper pieces (2 X 2 cms) were soaked in test solutions (tobramycin, bicarbonate, combination, and sterile media) and placed on the “wounds”. Plates were incubated at 37°C for 24 hours. After treatment, to enumerate CFUs, the wounds were homogenized in 10 mL sterile LB media, serially diluted, and plated on LB agar. Plates were incubated at 37°C for 24 hours after which CFUs were enumerated.

3.2.8 Measurement of pH

To examine the pH effect, different concentrations of bicarbonate were added to sterile media (LB or LB with 5, 10, 25% serum), and the pH was measured using a pH meter (Thermo Scientific)**.** Instrument was calibrated using standard solutions of pH 4,7, and 10.

3.2.9 Testing the effect of the combination against pre-formed biofilms

Biofilms were grown in round-bottom, untreated, 96-well microtiter plates. Briefly, bacterial (~10^5 cells) were added to well of the microtiter plate in an 8 X 8 array to test different combinations of tobramycin and bicarbonate. In addition, wells to test serial dilutions of each agent, and control wells to grow untreated cells were also set up. Each strain was tested in duplicate. Plates were sealed

with parafilm and incubated at 37°C under static conditions for 18-24 hours (pvernight). The next day, wells were washed twice with sterile LB medium. Different combinations of tobramycin and bicarbonate (dissolved in LB medium) were added to the 8 X 8 array, such that each row (or column) contained a fixed amount of one agent and increasing amounts of the second agent. To obtain the Minimum Biofilm Inhibitory Concentration (MBIC), serial dilutions of each agent were also tested alone. The control wells were replaced with sterile LB medium without any antimicrobial agent. The plates were sealed with parafilm and incubated at 37°C static overnight (18-24 hours). The next day, the wells were washed with sterile LB medium twice and effect of the treatment on biofilm cells was assessed with the XTT assay and crystal violet staining [191, 192].

3.2.10 Crystal violet assay for biofilm mass

The crystal violet assay was performed as previously described [192]. Briefly, pre-formed biofilms (either treated or untreated) were washed twice with sterile LB medium. Cells were fixed at the bottom and sides of the wells by treating them with 100% methanol for 15 minutes. Following removal of methanol, 0.1% filter-sterilized crystal violet solution (Sigma) was added to the well and allowed to stain the biofilm for 30 minutes. Wells were washed in water and dye was solubilized using 100% ethanol. 200 µL of well contents were transferred to a new, clear, flat-bottom, 96 well plate and absorbance was read at 600 nm.

3.2.11 XTT assay for metabolic activity in biofilms

The XTT assay was performed as previously described [191]. Briefly, pre-formed biofilms (either treated or untreated) were washed twice with sterile LB medium. A solution of LB: XTT: Menadione (79:20:1) was prepared. XTT was dissolved to make a stock solution of 1 mg/mL. For Menadione, a 7 mg/mL stock solution was prepared in acetone, diluted 1:100 and then used. The solution of LB: XTT: Menadione was added to each well, and the plates were incubated at 37°C in the dark (sealed with aluminum foil) for 4 hours. 200 µL of well contents were transferred to a new, clear, flat-bottom, 96 well plate and absorbance was read at 492 nm.

3.2.12 Testing biofilm cells in the *in vitro* chronic wound infection model

Biofilms were grown in an *in vitro* model resembling the constituents of a chronic wound, with certain modifications [193]. Our collaborator Prof. Kendra Rumbaugh (Texas Tech University Health Sciences Center, Lubbock, Texas) developed this model and recently used it to study synergistic interactions between *P. aeruginosa* and *S. aureus* (well-known co-pathogens in chronic wounds). Known as the Lubbock Chronic Wound Infection model (LCWM), the constituents of this media include Bolton broth (45%), laked horse blood (5%), bovine plasma (49%), to which bacterial cells (2%) are added. Grown biofilms

were treated with combination of tobramycin and bicarbonate and assayed for XTT activity as previously described.

3.2.13 *Ex-vivo* chronic wound infection murine model

To test the effect of combined therapy with tobramycin and bicarbonate *in vivo,* we used a chronic wound infection mouse model [72]. Briefly, wounds on the backs of adult Swiss Webster mice were created, infected with *P. aeruginosa* PAO1, and allowed to become chronic. Three-day old infected wounds were harvested and cut into four parts. Each part was treated with tobramycin, bicarbonate, combination, or sterile medium for 4-6 hours. After *ex-vivo* treatment, the wound parts were homogenized, serially diluted, and plated on Pseudomonas Isolation agar (PIA). Plates were incubated at 37°C overnight (18-24 hours) and CFU/gram were enumerated.

3.2.14 Response-surface analysis

To examine these drug combinations in greater detail than traditional methods, we developed a method of response-surface analysis. Using second-order polynomial interpolation [194] of the checkerboard assays, we constructed analytical dose-response surfaces using Mathematica version 9.0. When rendered against appropriate MIC threshold planes, the resulting surface approximates the continuous set of drug combinations. While traditional

isobolograms are often useful to gain some insight into this regime, our calculated surface approximates the complex nature of nonlinear drug interactions with far greater resolution than allowed by the extant methods. Furthermore, we used the empirically observed MICs for both tobramycin and bicarbonate to calculate Loewe additivity. These predictions will be tested against further checkerboard assays in order determine validity of the fit, and whether the model can estimate where strong synergistic combinations may have been overlooked by logarithmic sampling. In addition to the clinical focus of MIC-based synergy surveys, we also developed a method of finding synergy for any combination of drug concentrations by studying the differences between the theoretical "Loewe Additivity response surface", and our empirical dose-response surfaces.

3.3 RESULTS AND DISCUSSION

3.3.1 Combination of tobramycin and bicarbonate produces synergy against planktonic cells of *P. aeruginosa*

Using checkerboard assays, combinations of bicarbonate and tobramycin were tested against planktonic cells of a wide-range of *P. aeruginosa* strains. These included laboratory strains PAO1 and PA14, four spontaneously-generated antibiotic-resistant mutants, and clinical strains from CF patients. Points along the growth-no growth interface were plotted using isobolograms. In

addition, the ΣFIC index for each well along the interface was determined. Addition of bicarbonate to tobramycin produces a strong synergistic effect for the strains tested (Figures 3.1-3.6). We observe a synergistic to additive effect for all strains tested. However, strain-to-strain variation is noted. Summary of the results for all strains tested is provided in Table 3.1. Further, in Figures 3.7 and 3.8, we show this synergistic effect for four select strains with addition of a fixed concentration of bicarbonate. As observed, addition of bicarbonate reduces the concentration of tobramycin required to kill the population of *P. aeruginosa* cells.

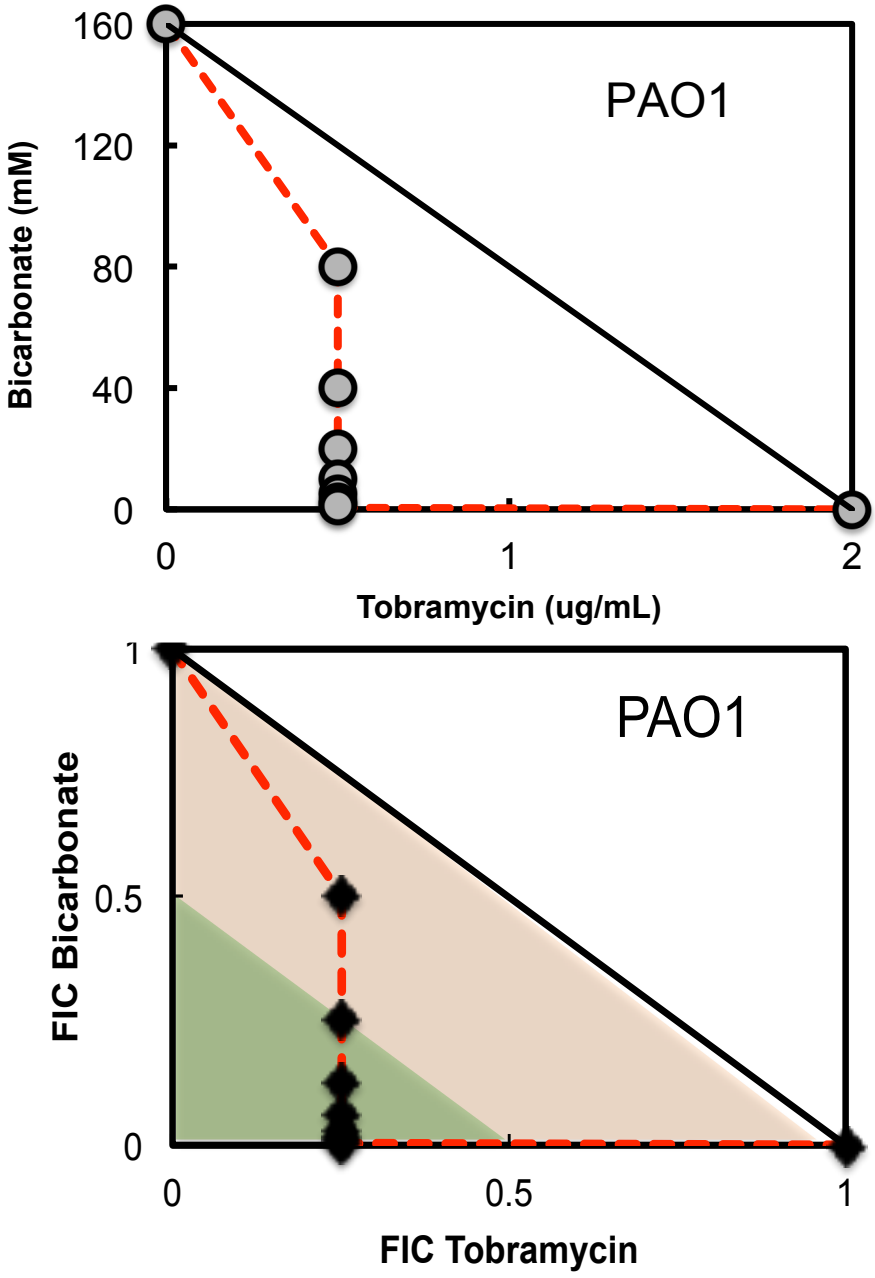

Figure 3.1 Isobologram analysis for planktonic cells of *P. aeruginosa* PAO1.

A strong synergistic-additive effect is observed for the combination of tobramycin and bicarbonate against PAO1 cells. Points along the isobologram represent the growth-no growth interface. The orange shaded area represents the additive region and the green shade area represents the synergistic region.

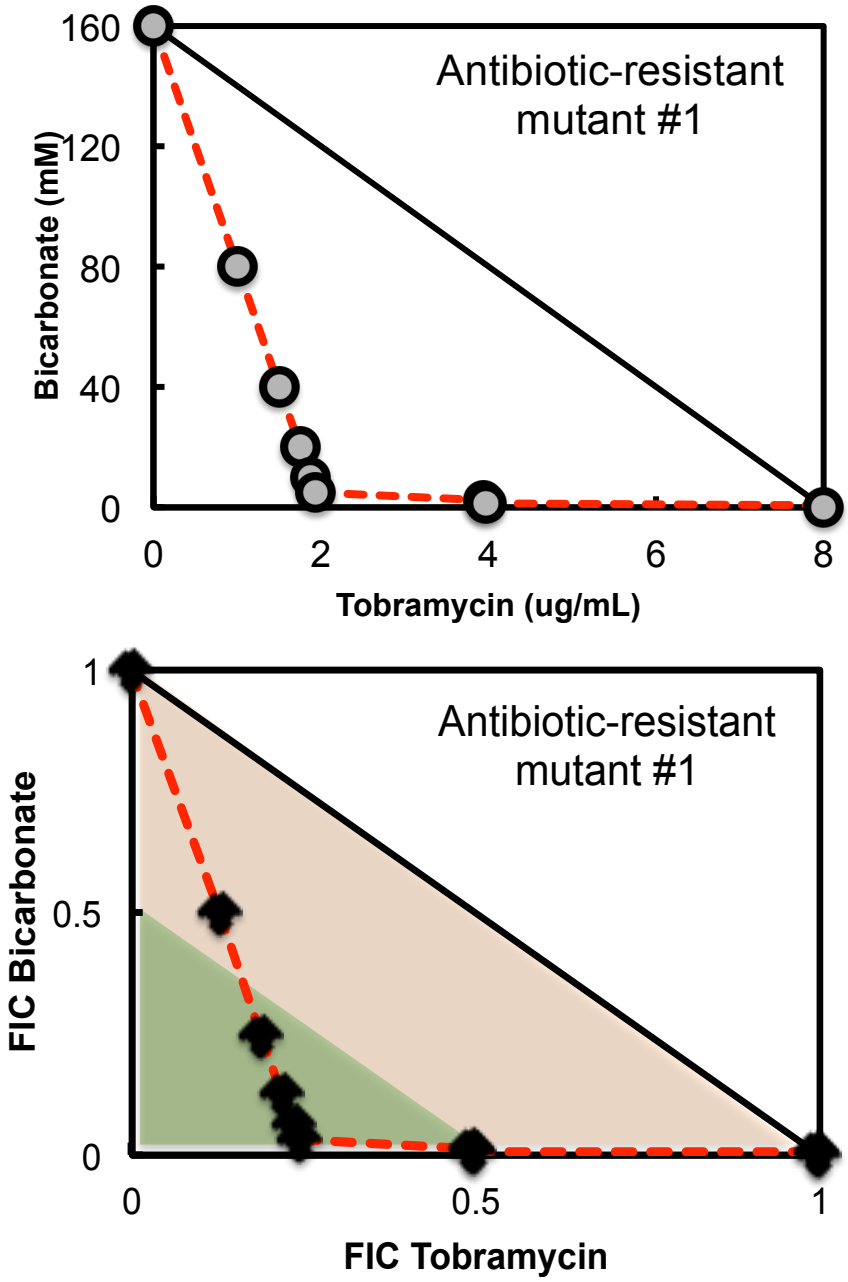

Figure 3.2 Isobologram analysis for planktonic cells of *P. aeruginosa* antibiotic-resistant mutant #1.

A strong synergistic-additive effect is observed for the combination of tobramycin and bicarbonate against the antibiotic-resistant mutant. Points along the isobologram represent the growth-no growth interface. The orange shaded area represents the additive region and the green shade area represents the synergistic region.

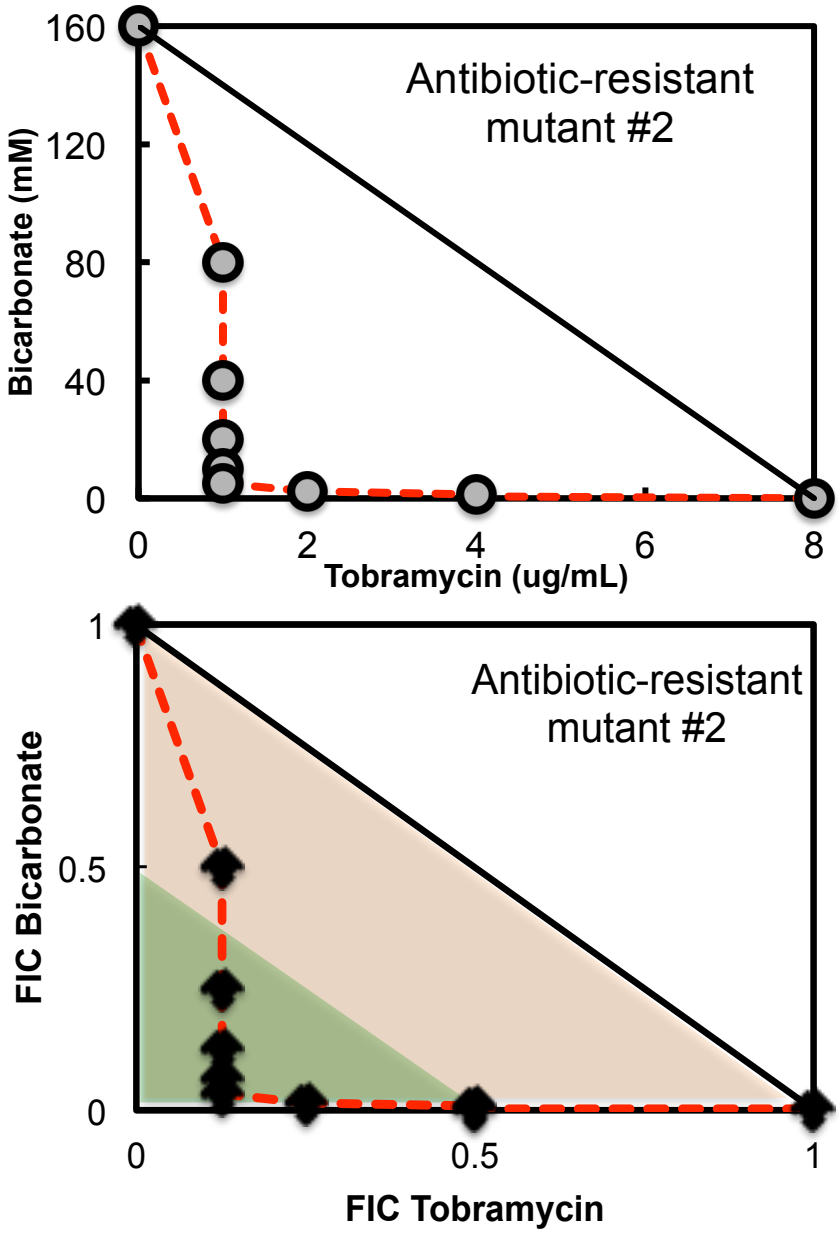

Figure 3.3 Isobologram analysis for planktonic cells of *P. aeruginosa* antibiotic-resistant mutant #2.

A strong synergistic-additive effect is observed for the combination of tobramycin and bicarbonate against the antibiotic-resistant mutant. Points along the isobologram represent the growth-no growth interface. The orange shaded area represents the additive region and the green shade area represents the synergistic region.

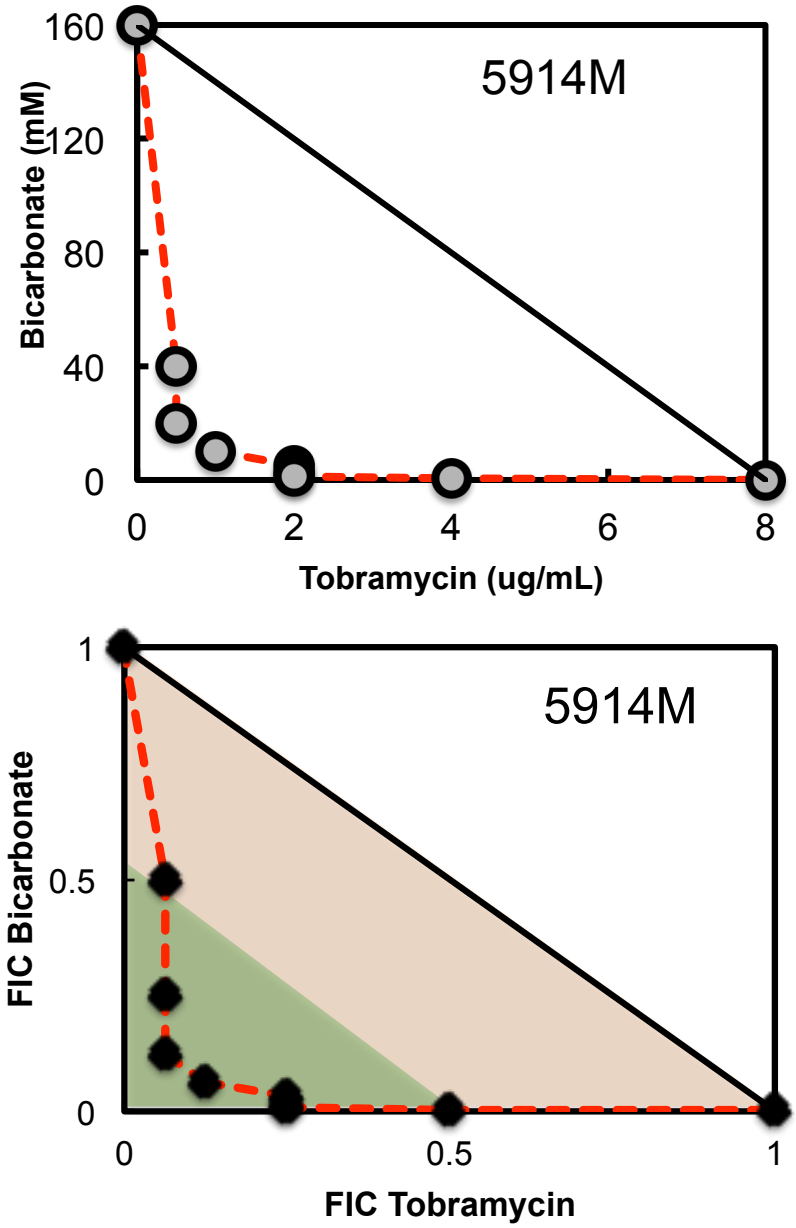

Figure 3.4 Isobologram analysis for planktonic cells of clinical *P. aeruginosa* strain 5914M.

A strong synergistic-additive effect is observed for the combination of tobramycin and bicarbonate against 5914M. Points along the isobologram represent the growth-no growth interface.The orange shaded area represents the additive region and the green shade area represents the synergistic region.

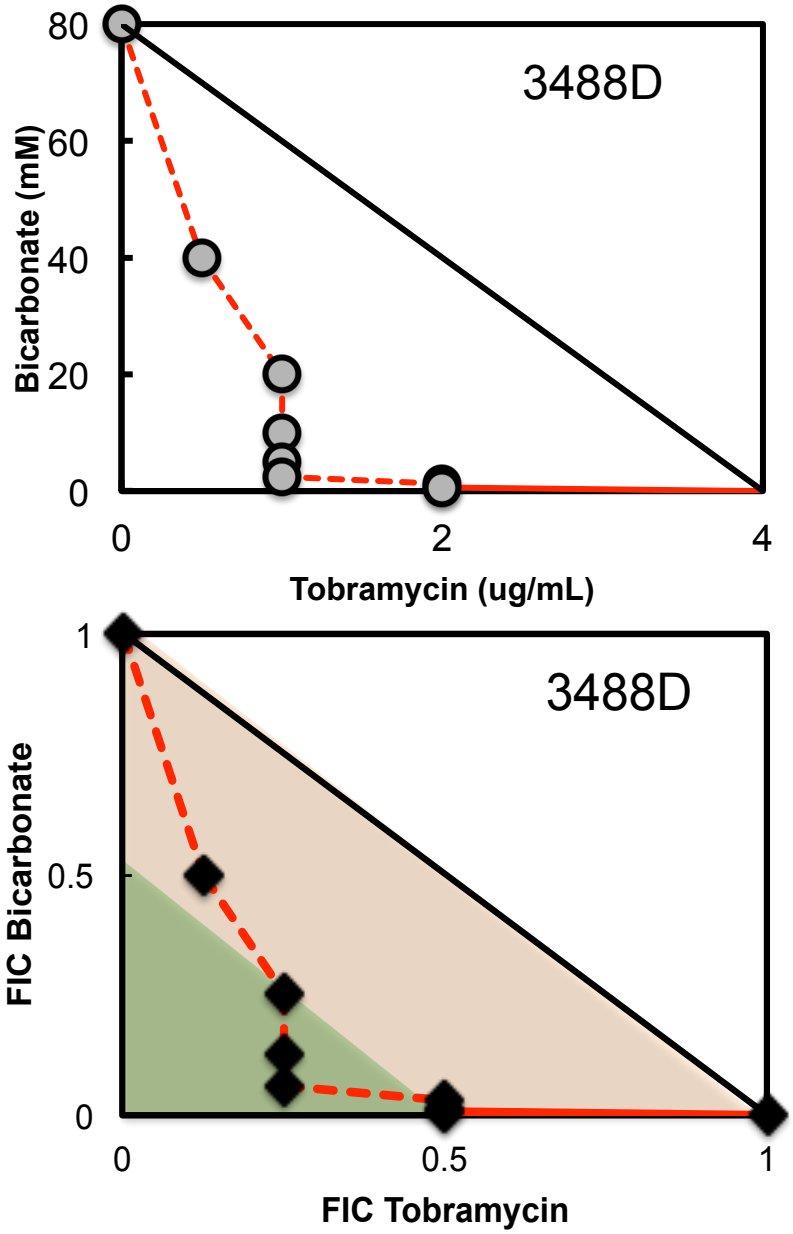

Figure 3.5 Isobologram analysis for planktonic cells of the clinical *P. aeruginosa* strain 3488D.

A strong synergistic-additive effect is observed for the combination of tobramycin and bicarbonate against 3488D. Points along the isobologram represent the growth-no growth interface. The orange shaded area represents the additive region and the green shade area represents the synergistic region.

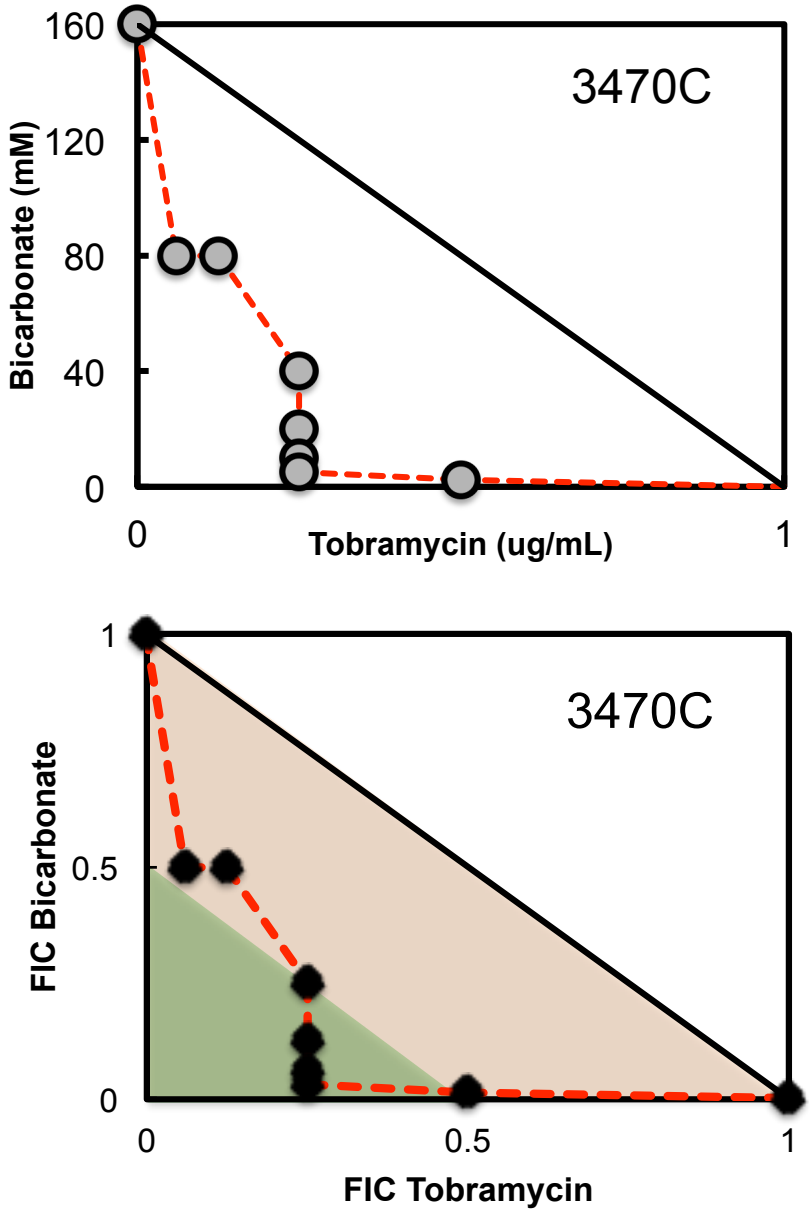

Figure 3.6 Isobologram analysis for planktonic cells of the clinical *P. aeruginosa* strain 3470C.

A strong synergistic-additive effect is observed for the combination of tobramycin and bicarbonate against 3470C. Points along the isobologram represent the growth-no growth interface. The orange shaded area represents the additive region and the green shade area represents the synergistic region.

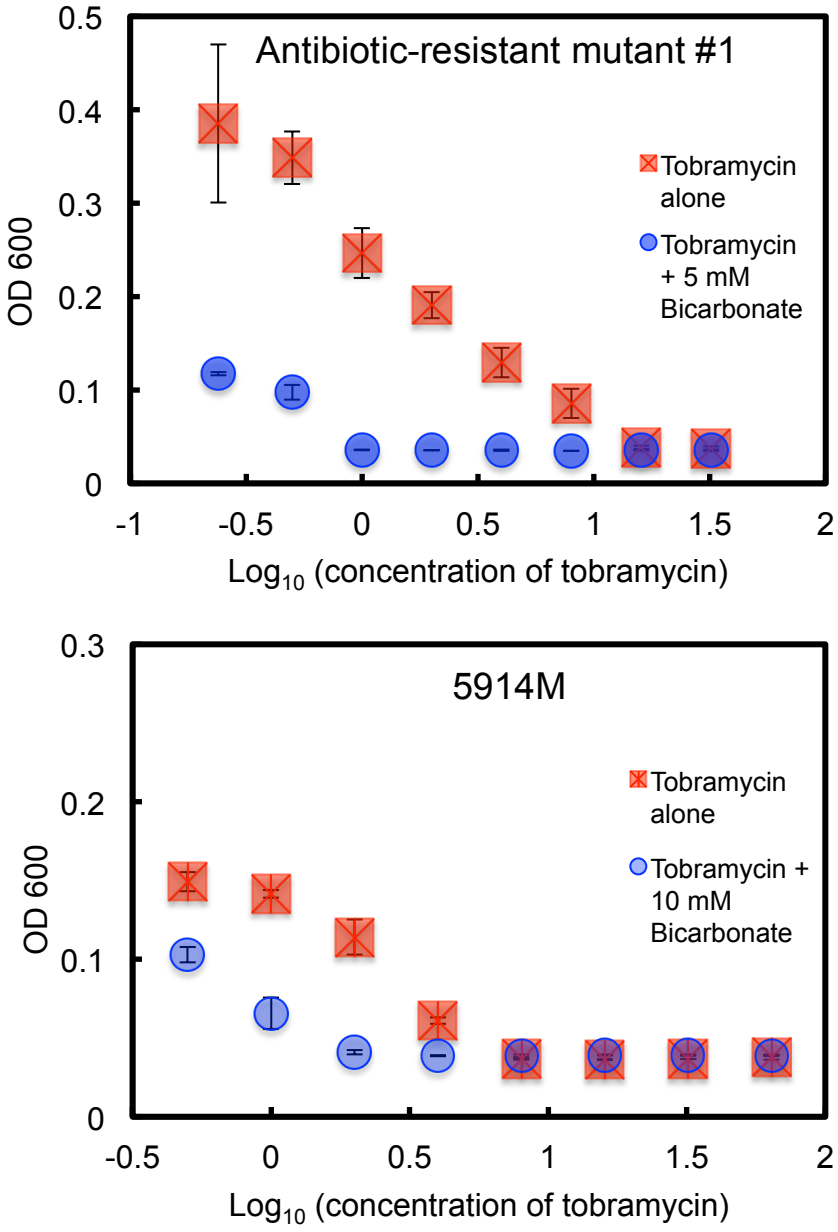

Figure 3.7 Synergy between bicarbonate and tobramycin in killing *P. aeruginosa* antibiotic-resistant mutant strain #1 and the clinical strain 5914M. Error bars represent SEM; *N = 3.* The concentrations here represent the lowest FIC in the checkerboard assay.

The combination of tobramycin and bicarbonate displays a strong synergy against antibiotic-resistant mutant strain #1 and the clinical strain 5914M.

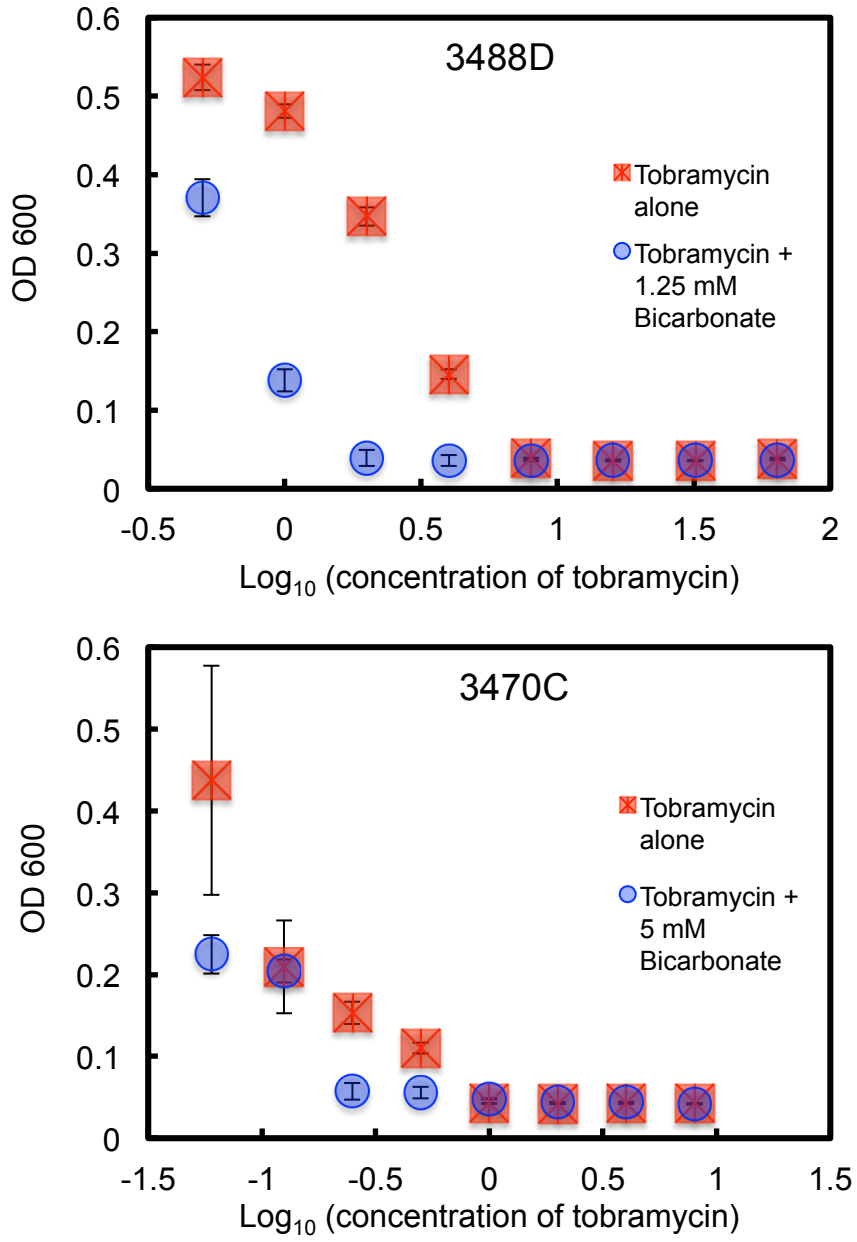

Figure 3.8 Synergy between bicarbonate and tobramycin in killing *P. aeruginosa* clinical strains 3488D and 3470C. Error bars represent SEM; *N* = *3*. The concentrations here represent the lowest FIC in the checkerboard assay.

The combination of tobramycin and bicarbonate displays a strong synergy against clinical strains 3488D and 3470C.

Table 3.1 Summary of the efficacy of the Tobramycin-Bicarbonate combination against planktonic cells of *P.aeruginosa*

Strains	MIC Tobramycin (µg/mL)	MIC Bicarbonate (mM)	ΣFIC index (average)	ΣFIC index (range)	Effect
PAO1	2	160	0.37	0.25 – 0.75	Synergistic/Additive
PA14	2	160	0.37	0.25 – 0.75	Synergistic/Additive
Antibiotic-resistant mutant #1	8	160	0.49	0.27 - 1	Synergistic/Additive
Antibiotic-resistant mutant #2	8	160	0.35	0.15 – 0.63	Synergistic/Additive
Antibiotic-resistant mutant #3	8	160	0.45	0.28 – 0.75	Synergistic/Additive
Antibiotic-resistant mutant #4	8	160	0.45	0.28 – 0.75	Synergistic/Additive
3639M	1	160	0.48	0.28 – 0.75	Synergistic/Additive
4278M	1	160	0.48	0.28 – 0.75	Synergistic/Additive
5623M	8	80	0.52	0.31 – 0.75	Synergistic/Additive
5914M	8	80	0.28	0.18 – 0.5	Synergistic/Additive
0476M	1	80	0.48	0.31 – 0.625	Synergistic/Additive
4220M	2	160	0.49	0.28 – 0.75	Synergistic/Additive
5913C	8	80	0.67	0.3 – 1	Synergistic/Additive
3470C	1	160	0.45	0.28 – 0.625	Synergistic/Additive
3488D	4	80	0.51	0.31 – 0.75	Synergistic/Additive
4219D	2	160	0.21	0.04-0.53	Synergistic/Additive
1913C	2	160	0.57	0.53-0.62	Additive

3.3.2 Time-kill assays

To confirm the synergistic effects observed and to examine the rate of killing with the synergistic combination, we performed time-kill assays for strains PAO1, D1R4, and the clinical strain 5913C. Combination of tobramycin and bicarbonate selected for the time-kill assays represented the concentrations that showed the maximum synergy (or lowest ΣFIC index) along the growth-no growth interface, where no growth is defined as MIC_{90}.

For PAO1, treatment with a combination of 0.25 μg/mL tobramycin and 5 mM bicarbonate eradicated the population by 4 hours; in contrast, each agent alone failed to kill the population (Figure 3.9 and 3.12). This confirmed the synergistic effect we observed for this combination against PAO1. Notably, this effect of the combination was comparable to that observed with 2 μg/mL tobramycin, the MIC_{90} for this strain. This indicates that the combination reduces the concentration of tobramycin needed to eradicate the population.

For the antibiotic-resistant strain #1, treatment with a combination of 1 μg/mL tobramycin and 5 mM bicarbonate killed the population by 6 hours, while each agent alone failed to kill the population (Figure 3.10 and 3.13). For this strain, treatment with the combination produced a faster rate of killing than that observed with 8 μg/mL tobramycin, the MIC_{90} for this strain. This is an additional

benefit to the reduction in the concentration of tobramycin needed to produce the effect.

For the clinical strain 5913C, killing with the synergistic combination of 1 µg/mL tobramycin and 5 mM bicarbonate expectedly produced killing. However, the combination showed effect only after 6 hours of treatment and complete killing was observed between 12-24 hours. At 8 hours, the killing curve for the combination lags behind that of 8 µg/mL tobramycin, the MIC_{90} for this strain (Figure 3.11 and 3.14). However, both treatments eradicate the population at the end of 24 hours, with the combination treatment affording a decrease in the concentration of tobramycin. These results reiterate that the effect of the combination tobramycin and bicarbonate shows notable strain-to-strain variation.

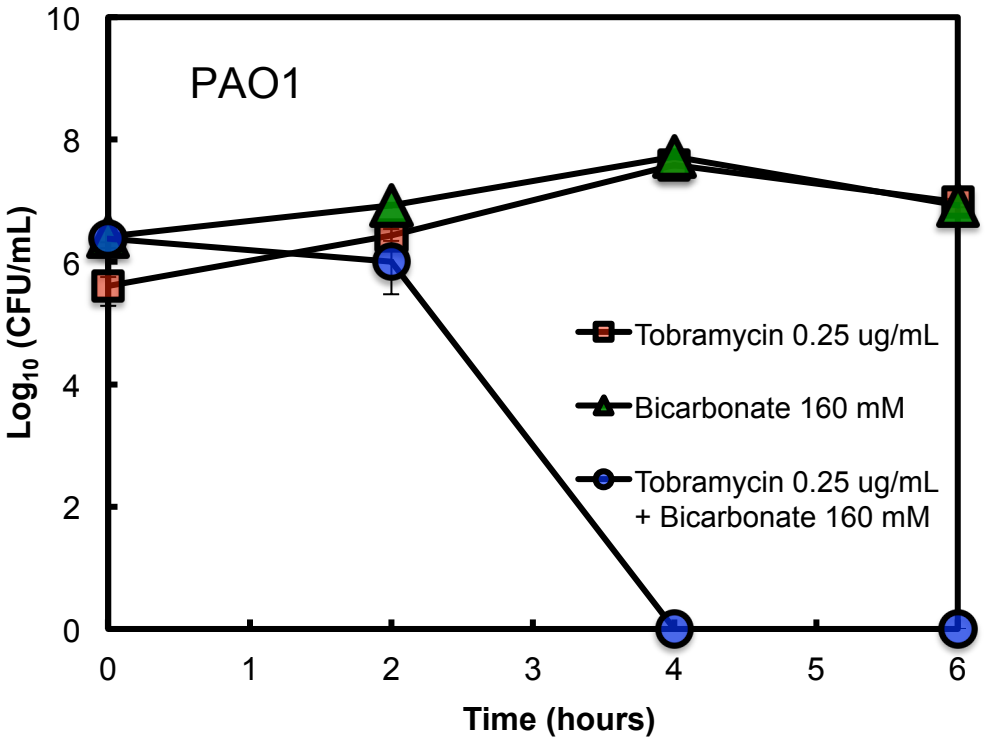

Figure 3.9 Time-kill assays demonstrating the synergy between bicarbonate and tobramycin against *P. aeruginosa* strain PAO1.

The combination of 0.25 µg/mL tobramycin and 5 mM bicarbonate displays a strong synergy against PAO1. Error bars represent SEM. *N = 3.*

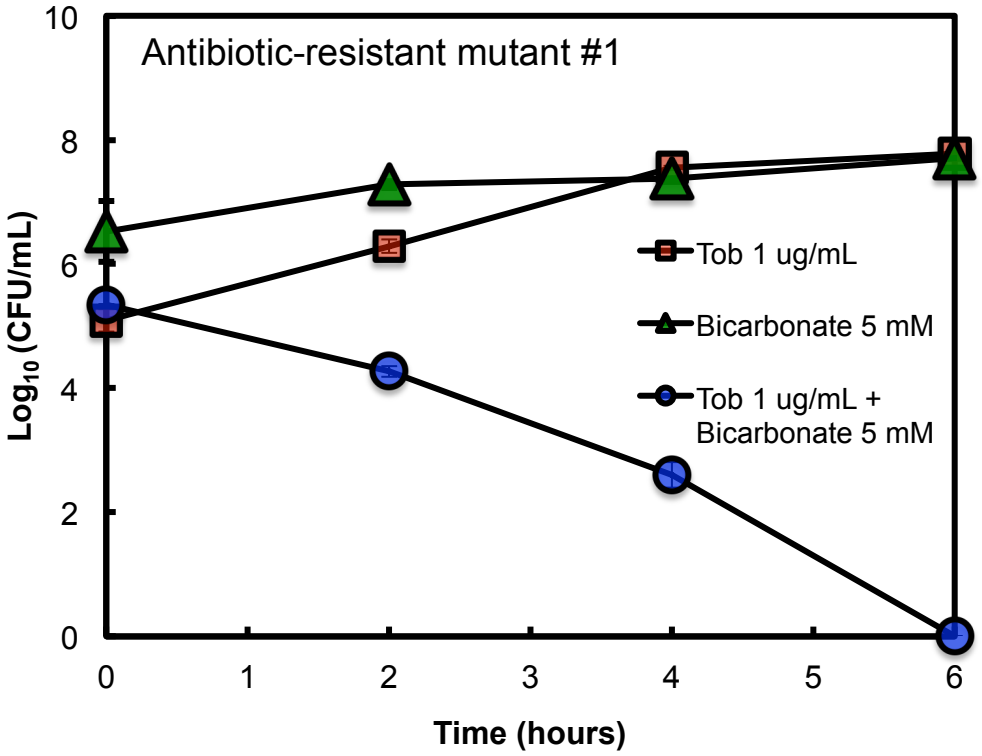

Figure 3.10 Time-kill assays demonstrating the synergy between bicarbonate and tobramycin against *P. aeruginosa* antibiotic-resistant mutant strain #1.

The combination of 1 μg/mL tobramycin and 5 mM bicarbonate displays a strong synergy against antibiotic-resistant mutant strain #1. Error bars represent SEM. *N = 3.*

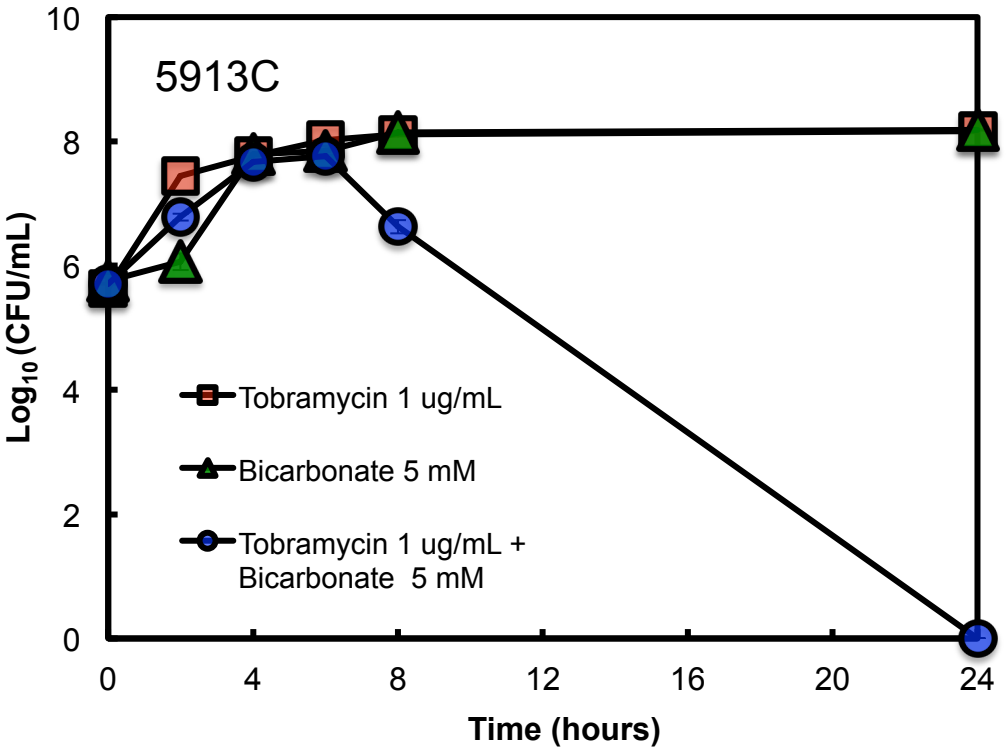

Figure 3.11 Time-kill assays demonstrating the synergy between bicarbonate and tobramycin against *P. aeruginosa* clinical strain 5913C.

The combination of 1 µg/mL tobramycin and 5 mM bicarbonate displays a strong synergy against 5913C. Error bars represent SEM. *N = 3.*

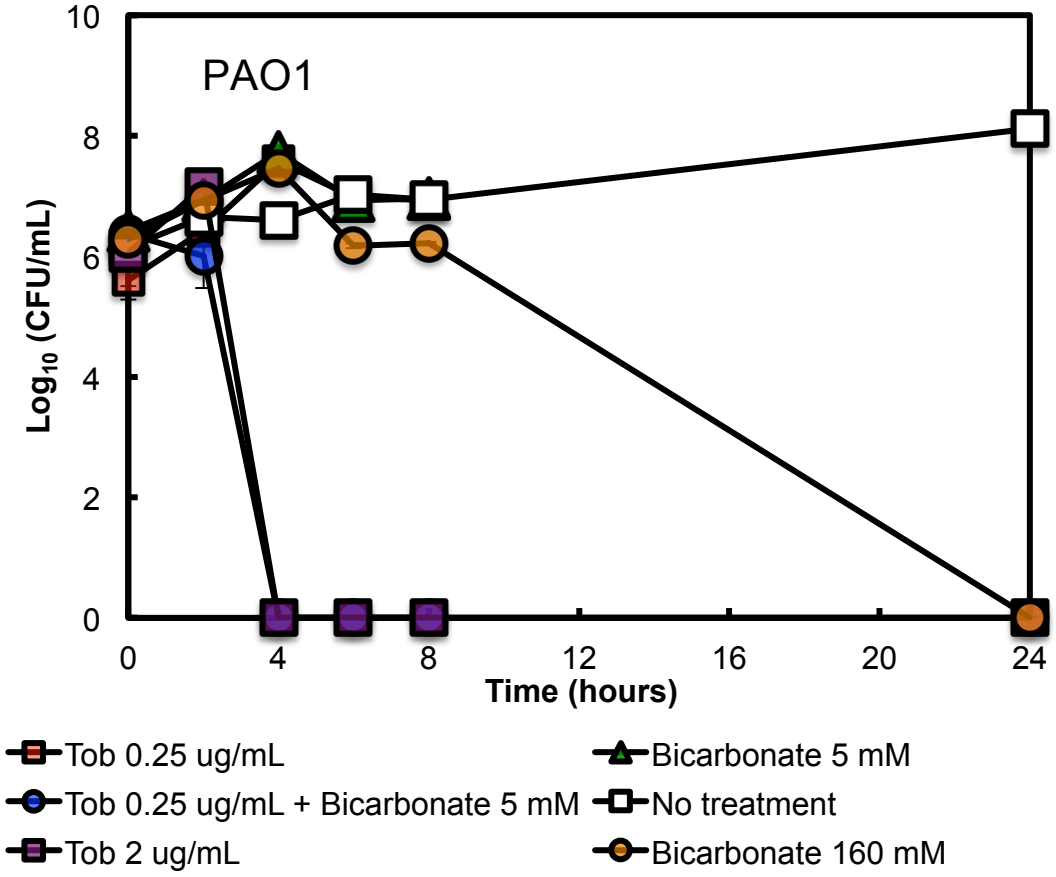

Figure 3.12 Time-kill assays demonstrating the comparison between the synergistic combination of bicarbonate and tobramycin and the MIC_{90} of 8 µg/mL against *P. aeruginosa* strain PAO1.

The combination of 0.25 µg/mL tobramycin and 5 mM bicarbonate displays a strong synergy against PAO1. Killing is achieved as early as 4 hours, which is comparable to that with observed with the MIC_{90} of 1 µg/mL. Error bars represent SEM. *N = 3.*

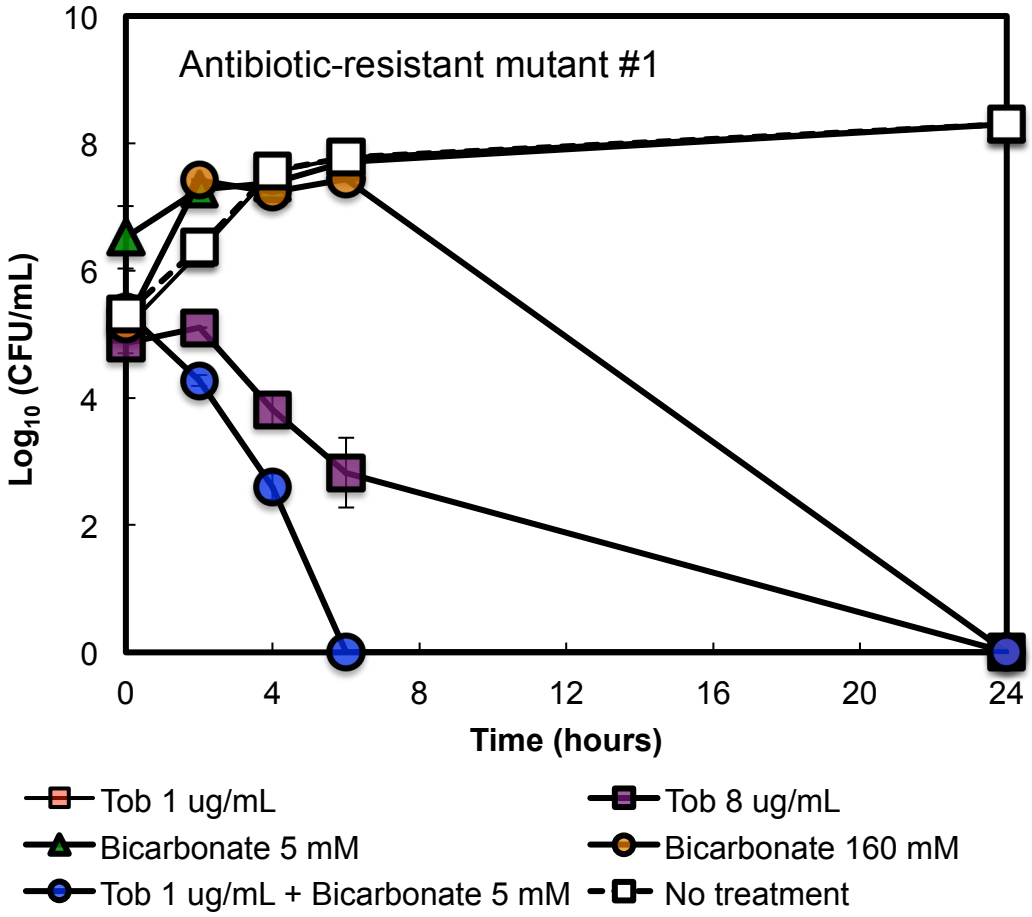

Figure 3.13 Time-kill assays demonstrating the comparison between the synergistic combination of bicarbonate and tobramycin and the MIC_{90} of 8 µg/mL against *P. aeruginosa* antibiotic-resistant mutant strain #1.

The combination of 1 µg/mL tobramycin and 5 mM bicarbonate displays a strong synergy against antibiotic-resistant mutant strain #1. As observed the synergistic combination not only reduces the concentration of tobramycin required to produce a killing effect, but also enhances the rate of killing in comparison to the MIC_{90} of 8 µg/mL. Error bars represent SEM. *N = 3.*

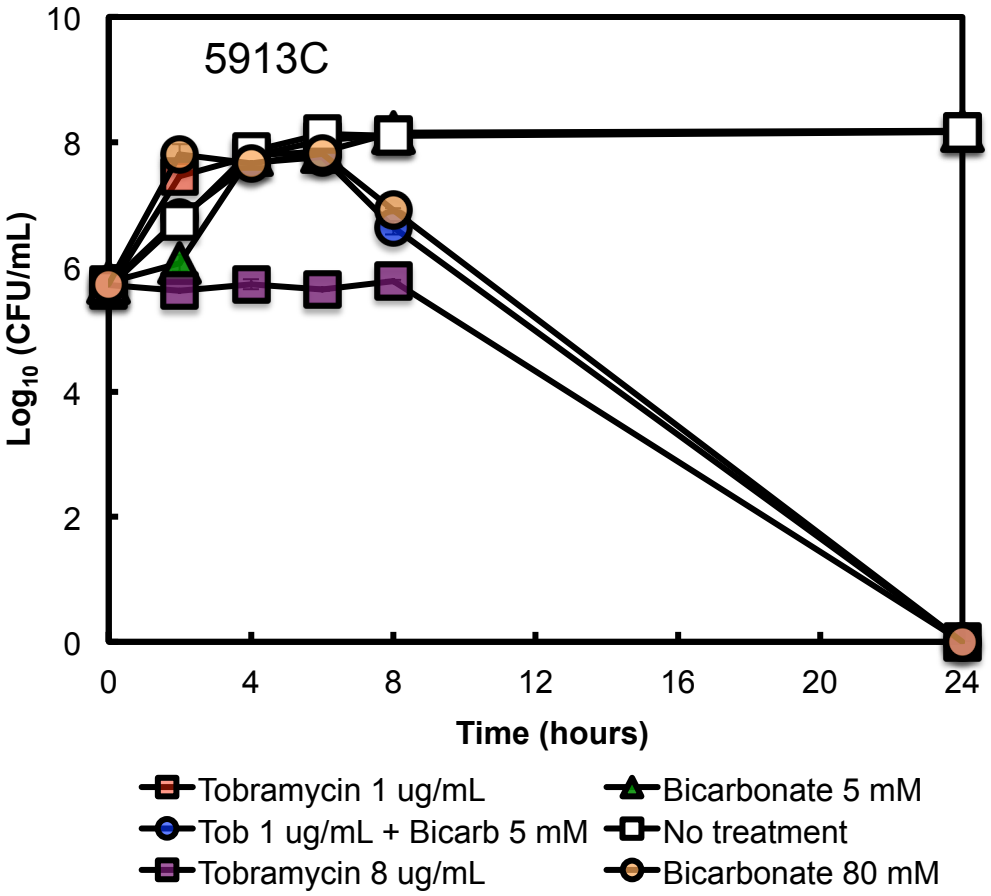

Figure 3.14 Time-kill assays demonstrating the comparison between the synergistic combination of bicarbonate and tobramycin and the MIC_{90} of 8 µg/mL against clinical *P. aeruginosa* strain 5913C.

The combination of 0.25 µg/mL tobramycin and 5 mM bicarbonate displays a strong synergy against 5913C. While the combination appears to exert its killing effect later than the MIC90, it reduces the concentration the tobramycin, and both achieve nearly comparable killing at 8 hours. Error bars represent SEM. *N = 3.*

3.3.3 Screen for biofilm formation by *P. aeruginosa* strains

The laboratory strain PAO1 and 17 clinical CF isolates (mucoid, dwarf, and classic phenotype) [105], were screened for biofilm formation using the microtiter dish biofilm assay and quantified using the crystal violet and XTT methods. Using the crystal violet assay, clinical strains 3639M, 4278M, 3470C, 1913C, 0476M, 4220M, 4219D, and laboratory strain PAO1 show robust biofilm formation (Figure 3.15A). Crystal violet is a basic dye that binds to negatively charged surface molecules. It thus stains the extracellular matrix, live and dead cells of the biofilm. To confirm the presence of metabolic activity (live cells), biofilm growth for different strains was quantified using the XTT assay. In live cells, XTT is reduced to a water-soluble formazan derivative that can be quantified colorimetrically [191]. Strains 3639M, 4278M, 3470C, 1913C, 0476M, 4220M, 4219D, and PAO1 which showed robust biofilm formation also demonstrated the presence of live, metabolically active cells (Figure 3.15B). Based on the results of this screen, three strains, PAO1, 4219D, and 3470C, were chosen for testing the effects of the tobramycin-bicarbonate combination on biofilms.

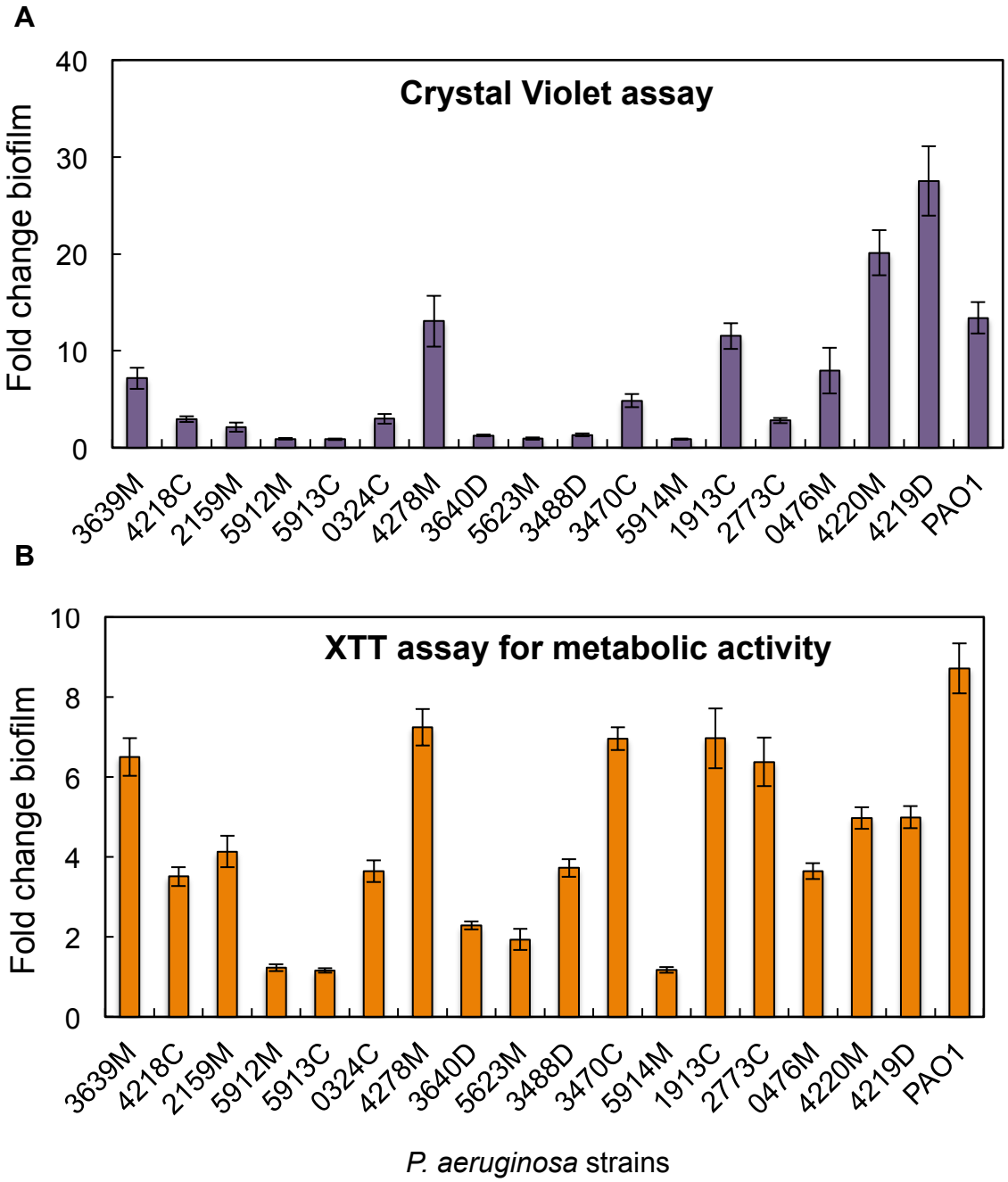

Figure 3.15 Screen for biofilm formation and metabolic activity of biofilm cells for different *P. aeruginosa* strains.

(A) Screen for biofilm formation by staining biomass with crystal violet assay and **(B)** XTT assay for metabolic activity in biofilm cells for different strains of *P. aeruginosa* strains.

3.3.4 Combination of tobramycin and bicarbonate fails to produce synergy in biofilm cells of *P. aeruginosa*

The effect of the tobramycin-bicarbonate combination was tested on biofilm cells of *P. aeruginosa* strains PAO1, 4219D, and 3470C. Biofilms were grown in microtiter dish wells, treated with each agent alone and in different combinations, and the effects were quantified using the XTT assay. For each agent alone, the Minimum Biofilm Inhibitory Concentration (MBIC) was determined. These results are summarized in Table 3.2. Based on our results, for the laboratory strain PAO1, and clinical strains 3470C and 4219D, the combination of tobramycin and bicarbonate produces an additive-antagonistic effect (Figures 3.16, 3.17 and 3.18). We thus observe that while bicarbonate enhances the effect of tobramycin against planktonic cells, this synergistic effect is reduced to an additive-antagonistic effect (for 3470C and 4219D). These results are summarized in Table 3.3. While we have not yet probed the cause for this loss of synergistic effect in biofilm cells, possible explanations include acidification of the biofilm environment [16] or limited diffusion into the interior of the biofilm [79]. We plan to do a preliminary test for the former by measuring the pH of biofilm supernatant.

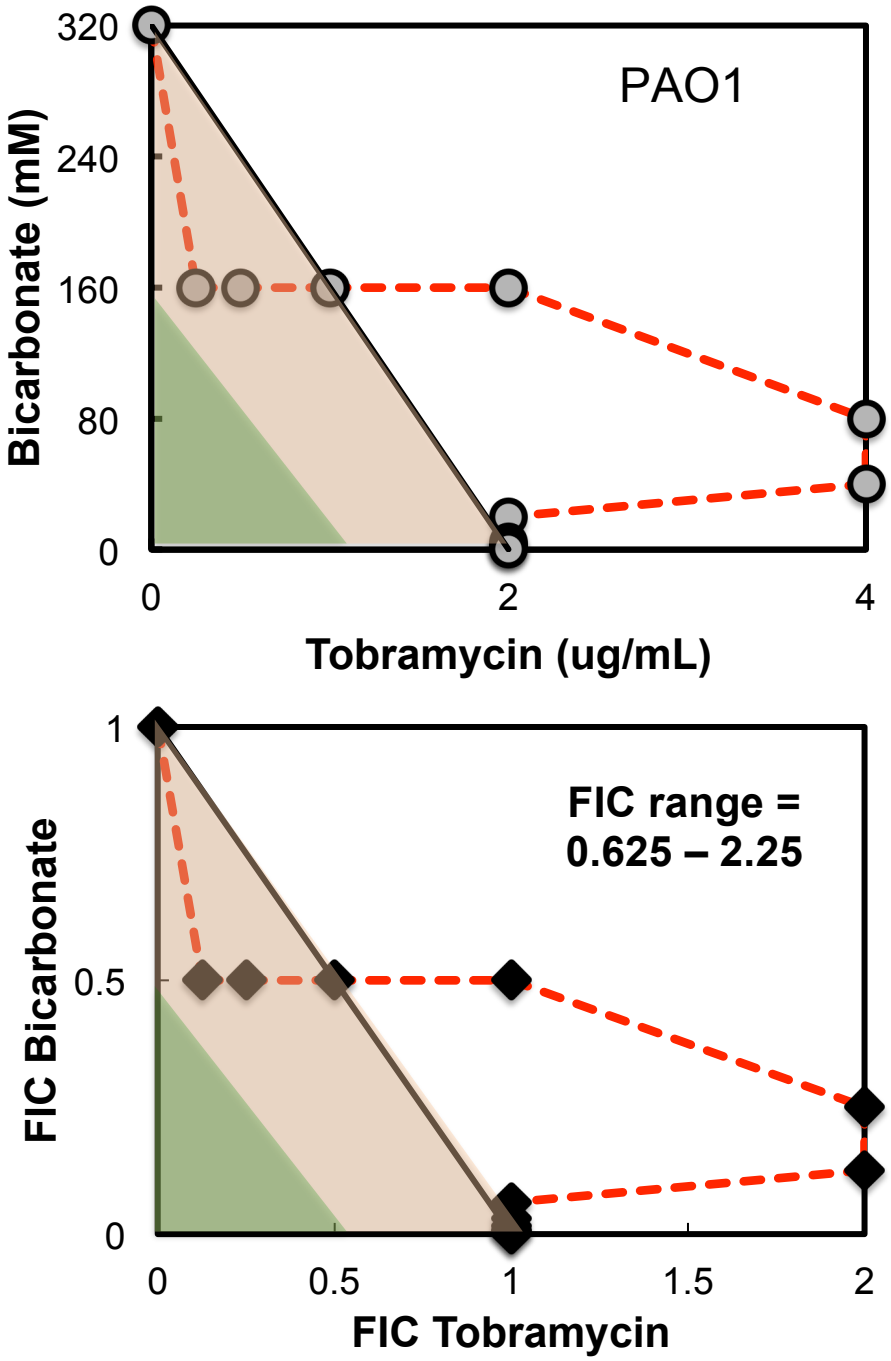

Figure 3.16 Isobologram analysis for biofilm cells of *P. aeruginosa* PAO1.

An additive-antagonistic effect is observed for the combination of tobramycin and bicarbonate against PAO1 cells, in contrast to the strong synergistic effect observed in Figure 3.1. Points along the isobologram represent the growth-no growth surface. The orange shaded area represents the additive region and the green shaded area represents the synergistic region.

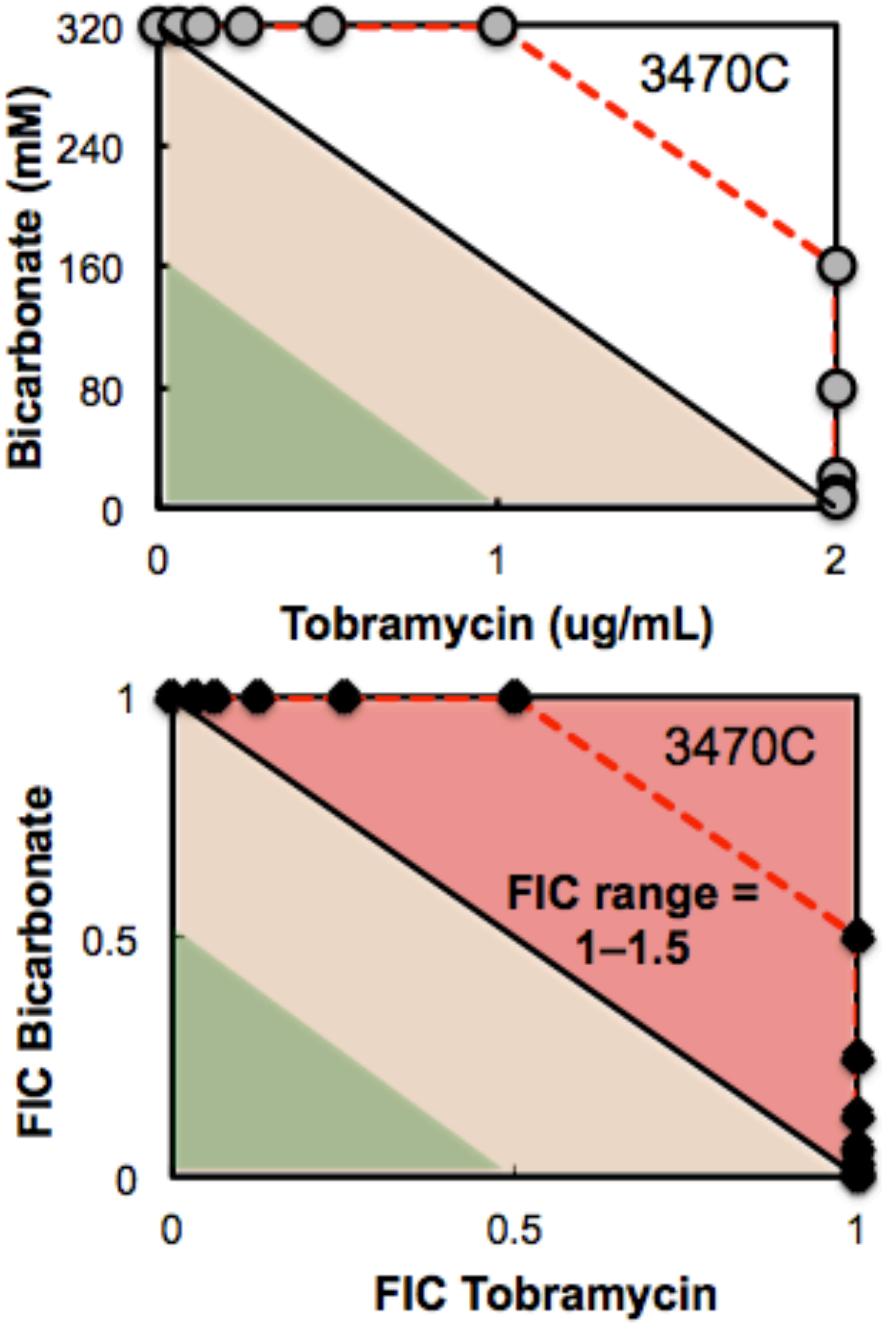

Figure 3.17 Isobologram analysis for biofilm cells of *P. aeruginosa* 3470C.

An additive-antagonistic effect is observed for tobramycin and bicarbonate against 3470C cells, in contrast to the strong synergistic effect observed in Figure 3.6. Points along the isobologram represent the growth-no growth surface. The orange shaded area represents the additive region, the green shaded area represents the synergistic region, and the red area is the antagonistic region.

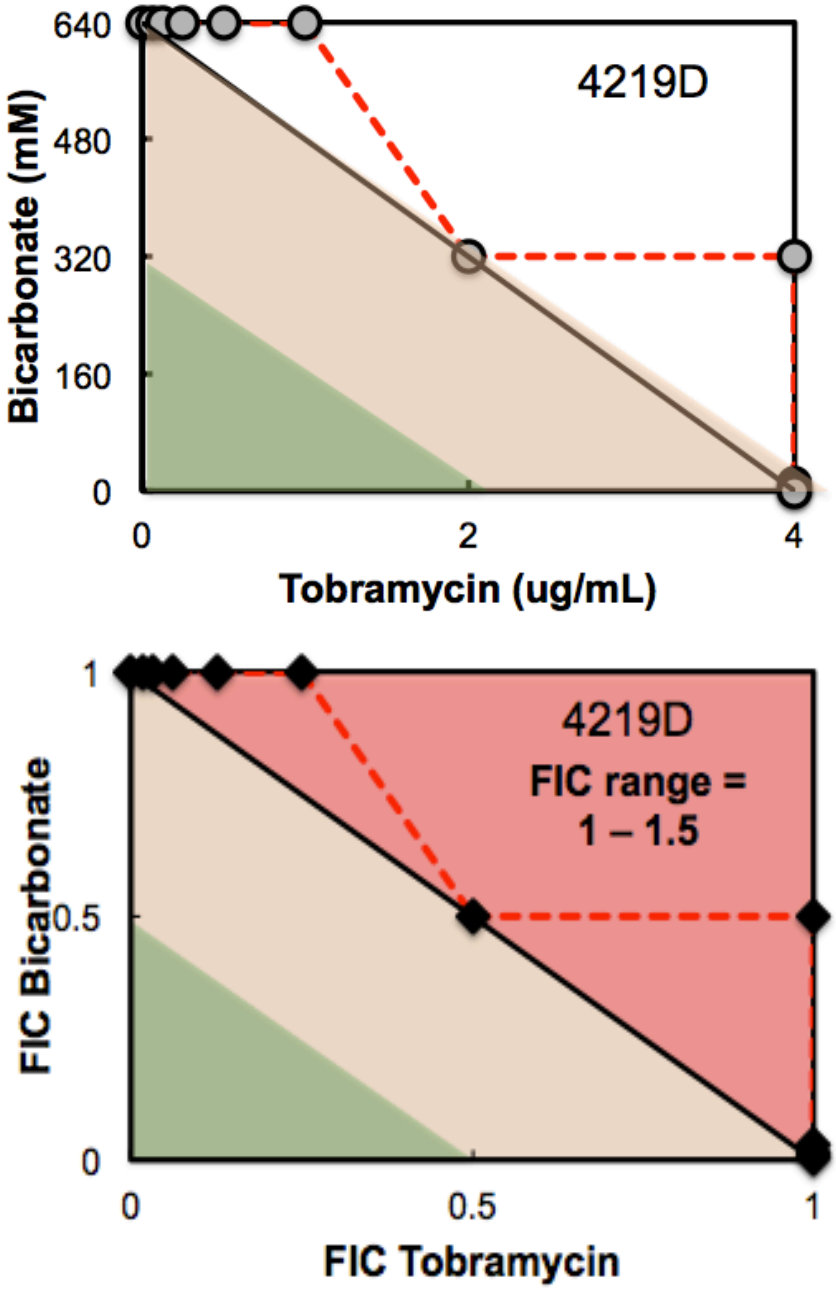

Figure 3.18 Isobologram analysis for biofilm cells of *P. aeruginosa* 4219D.

An additive-antagonistic effect is observed for the combination of tobramycin and bicarbonate against 4219D. The orange shaded area represents the additive region, the green shaded area represents the synergistic region, and the red area is the antagonistic

Table 3.2 Efficacy of the Tobramycin-Bicarbonate combination against biofilm cells of *P.aeruginosa*

Strains	*MBIC Tobramycin (µg/mL)	#MBIC Bicarbonate (mM)	ΣFIC index (average)	ΣFIC index (range)	Effect
PAO1	2	320	0.65	0.63 – 2.25	Additive Antagonistic
3470C	2	320	1.2	1 – 1.5	Additive Antagonistic
4219D	4	640	1.1	1 – 1.5	Additive Antagonistic

MIBC = Minimum Biofilm Inhibitory Concentration

* For strains PAO1 and 3470, a maximum of 80-fold reduction, and for strain 4219D, a maximum of 55-fold reduction was achievable at this concentration.
# For strains PAO1 and 3470, a maximum of 80-fold reduction, and for strain 4219D, a maximum of 60-fold reduction was achievable at this concentration.

3.3.5 Response-surface analysis

Isobolograms are a standard and widely used approach to examine drug interactions [187]. While they offer valuable insights, they do have limitations. Firstly, using traditional isobolograms we can only obtain estimates of synergy at points that have been biologically tested. Given that testing drug combinations is both labor-intensive and time-consuming, this imposes inherent limitations to the array of synergistic combinations we can estimate.

While testing drug combinations using serial dilutions the minimum inhibitory concentration (MIC) of each agent is determined as the lowest concentration that produces no growth, however the MIC value may lie anywhere between this no-growth concentration and last growth concentration. As expected, this results in a tendency to underestimate synergy, since all combinations in the intervening points will be considered additive.

Plotting isobolograms from the growth-no growth interface provides no information or context about the effect of other combinations over the rest of the dose-response surface.

Finally, traditional isolobologram analysis has limited predictive power to find untested synergistic combinations, and expanding the array of combinations would require additional biological testing.

To examine these drug combinations in greater detail than traditional methods, we developed a method of response-surface analysis. With data from the checkerboard assays, we constructed analytical dose-response surfaces using a second-order polynomial fit, given by

$$a(U_{Tobramycin})^2 + b(U_{Bicarbonate})^2 + 2c(U_{Tobramycin} * U_{Bicarbonate}) + d = 0$$

where U is the concentration of tobramycin or bicarbonate, a, b and c are undetermined coefficients used to fit parabolas between consecutive points, and d is the % change in inhibition. This dose-response surface interpolation provides additional insights into the effects of the combination of tobramycin and bicarbonate, as compared to standard isobolograms (Figures 3.19, 3.20 and 3.21 for planktonic PAO1 cells and 3.22 and 3.23 for biofilm PAO1 cells).

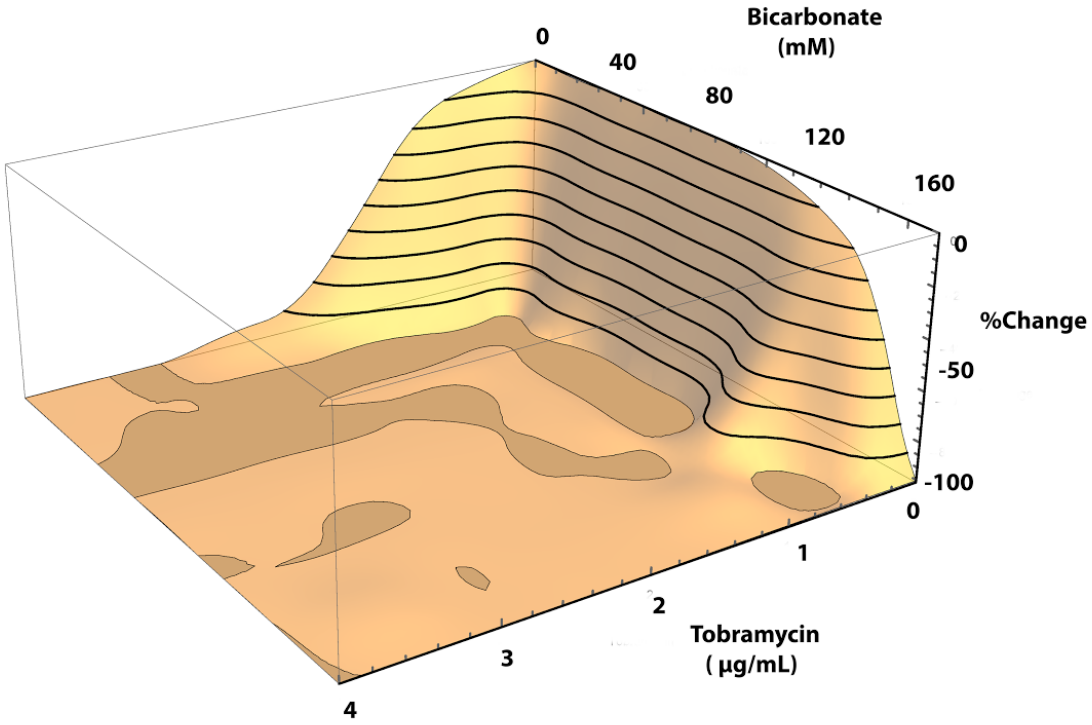

Figure 3.19 Dose-response surface for planktonic *P. aeruginosa* strain PAO1.

The dose-response surface (orange) shows the concentrations of tobramycin and bicarbonate along the X- and Y- axes, with the percent change in inhibition along the Z-axis. The MIC_{90} of tobramycin for planktonic cells of PAO1 Is circled in red. The response-surface interpolation shows a strong synergistic effect at sub-MIC concentrations for the combination of tobramycin and bicarbonate. Synergy is indicated by a convex upward curvature.

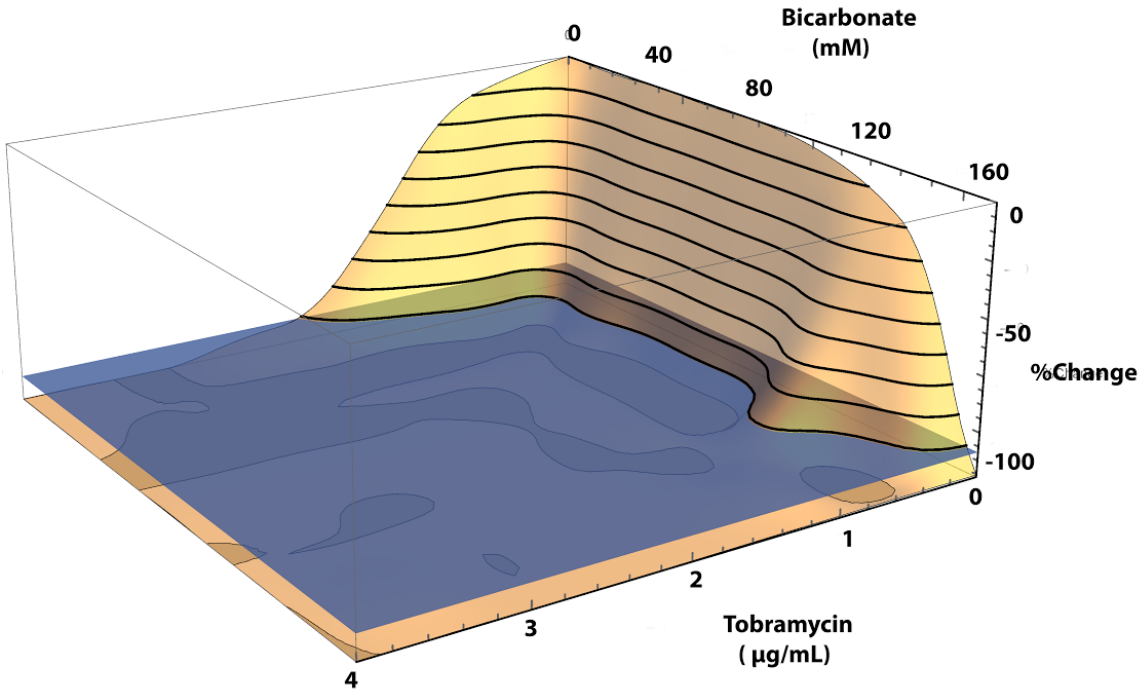

Figure 3.20 Dose-response surface for planktonic *P. aeruginosa* strain PAO1 showing an intersection at 90% reduction (MIC_{90} of the combination).

The dose-response surface (orange) shows the concentrations of tobramycin and bicarbonate along the X- and Y- axes, with the percent change in inhibition along the Z-axis. The grey plane intersecting the dose-response surface shows the 90% reduction. At the edge of the intersection is where the synergy achieves a 90% reduction (MIC_{90}). Other intersections along the response surface would show synergy combinations that achieve less than 90% reduction.

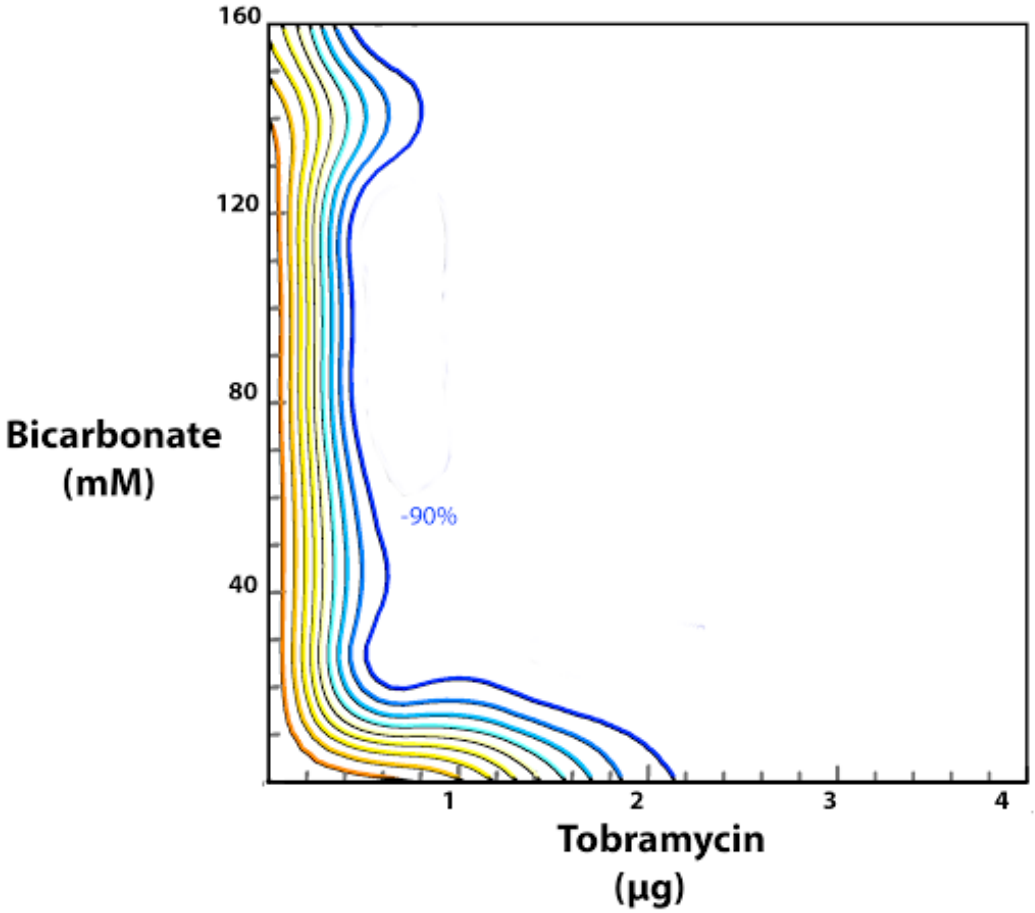

Figure 3.21 Response surface contour plots for planktonic *P. aeruginosa* strain PAO1.

The red line shows the upper bound for synergy for planktonic PAO1 as determined by the checkerboard assays. The MIC_{90} for tobramycin and bicarbonate is 2 µg/mL and 160 mM respectively from the checkerboard assays. As shown, the contour plot can accurately determine the MIC_{90} of tobramycin as ~2.1 µg/mL. The same would apply for bicarbonate (MIC_{90} not shown here). This allows all combinations under these values to be considered synergistic, expanding the synergistic regime.

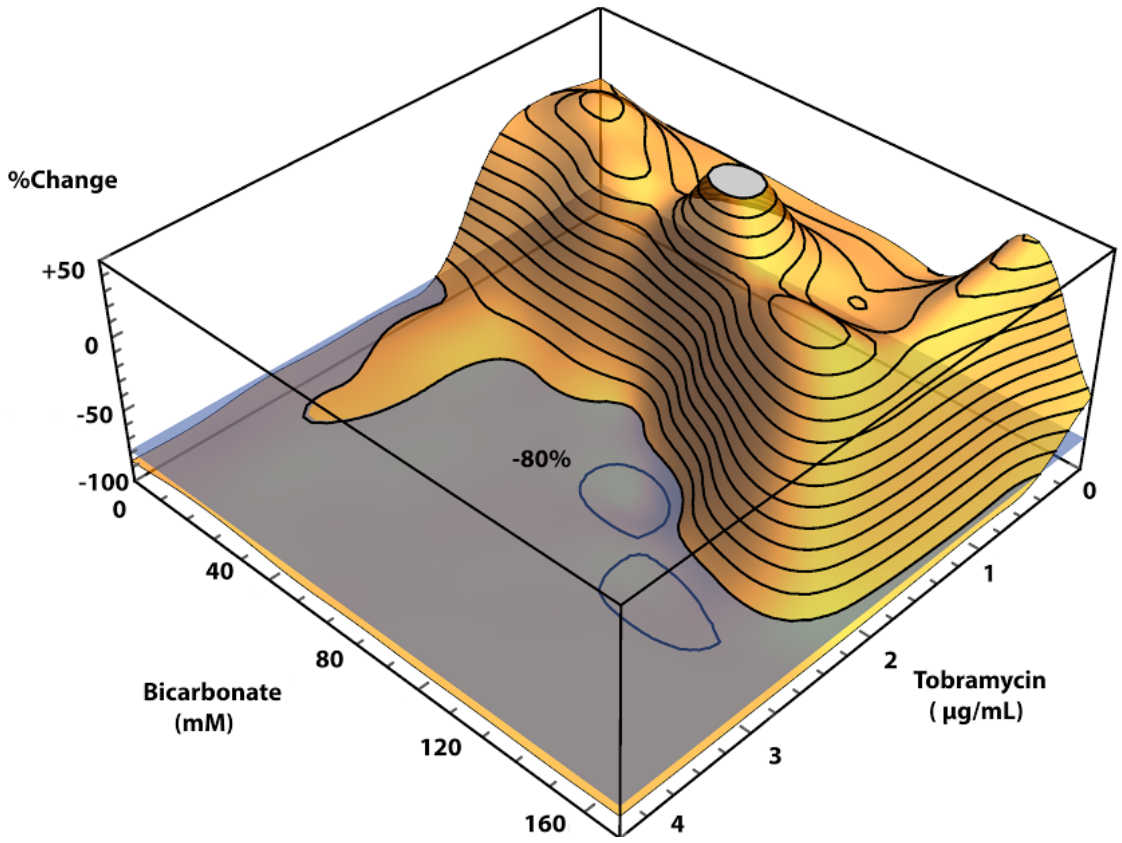

Figure 3.22 Dose-response surface and intersection plane at 90% reduction for biofilm cells of *P. aeruginosa* strain PAO1.

The dose-response surface (orange) shows the concentrations of tobramycin and bicarbonate along the X- and Y- axes, with the percent change in inhibition along the Z-axis. The grey plane intersecting the dose-response surface shows the 90% reduction. The MIC_{90} of tobramycin for biofilm cells of PAO1 is circled in red. The response-surface interpolation shows an antagonistic effect for the combination of tobramycin and bicarbonate. Antagonism is indicated by a convex downward curvature.

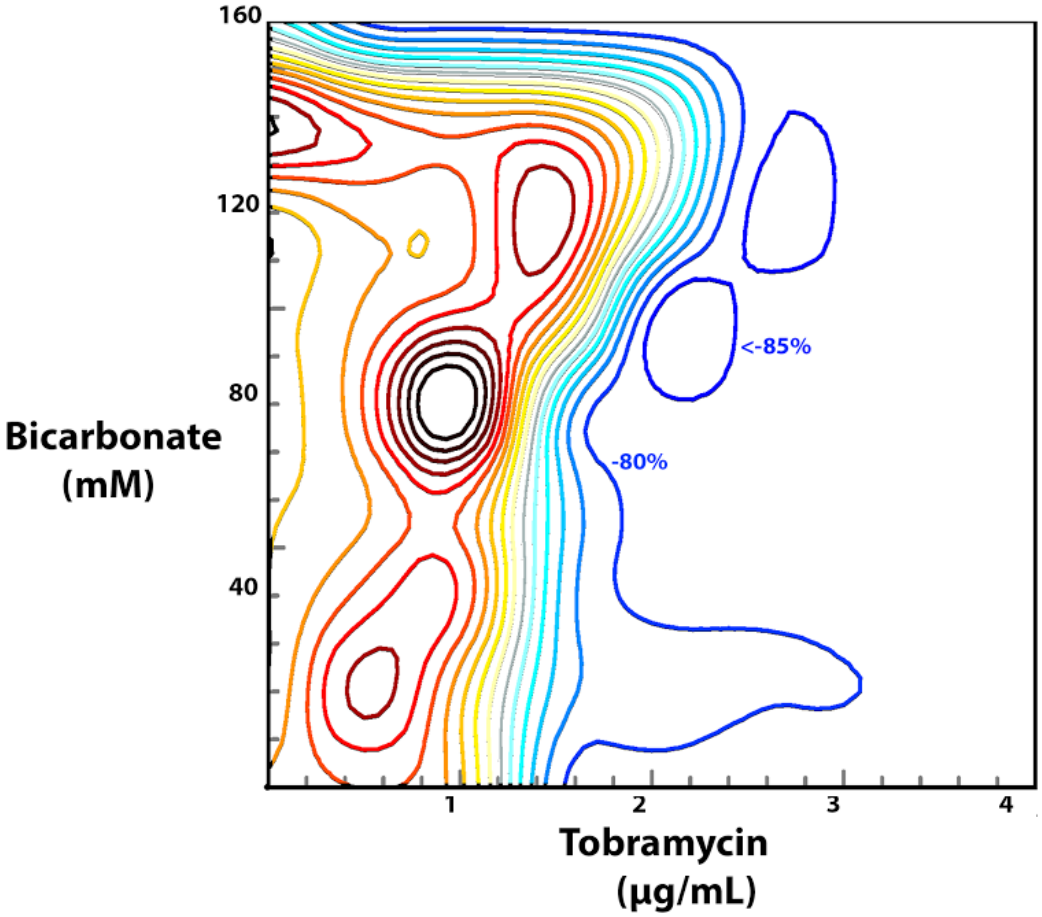

Figure 3.23 Response surface contour plots for biofilm cells of *P. aeruginosa* strain PAO1.

The red line shows the upper bound for synergy for planktonic PAO1 as determined by the checkerboard assays. The MIC_{90} for tobramycin and bicarbonate is 2 µg/mL and 320 mM respectively from the checkerboard assays. The contour plot determines the MIC90 for tobramycin as ~1.3 µg/mL. An antagonistic effect is observed with the combination of tobramycin and bicarbonate, in contrast to that seen with planktonic PAO1 cells.

3.3.6 Loewe additivity predicted surface analysis

Minimum inhibitory concentration values for tobramycin and bicarbonate were used to calculate the lines of Loewe additivity [188] and synergy for planktonic and biofilm cells of *P. aeruginosa* PAO1. Loewe additivity is a common reference model to define drug interactions [188]. According to this model, the combined effect of two drugs is predicted from the sum of the effects of the individual components.

This is done with the equation,

$$E = (E_{\max} - B) * \frac{(U / U_{50})^m}{[1 + (U / U_{50})^m]} + B$$

where E represents the calculated value (% change) for any point on the surface as predicted by additivity, $E_{\max}$ is the maximum effect attainable, B is zero effectiveness, U is the concentration of tobramycin or bicarbonate, U_{50} is the MIC_{50} for tobramycin or bicarbonate, and m is the slope of the linear regime of the sigmoidal curve.

Further, we plot the difference surface response between the additivity predicted surface and observed surface (from the checkerboard assays) to assess the net effect of the combination.

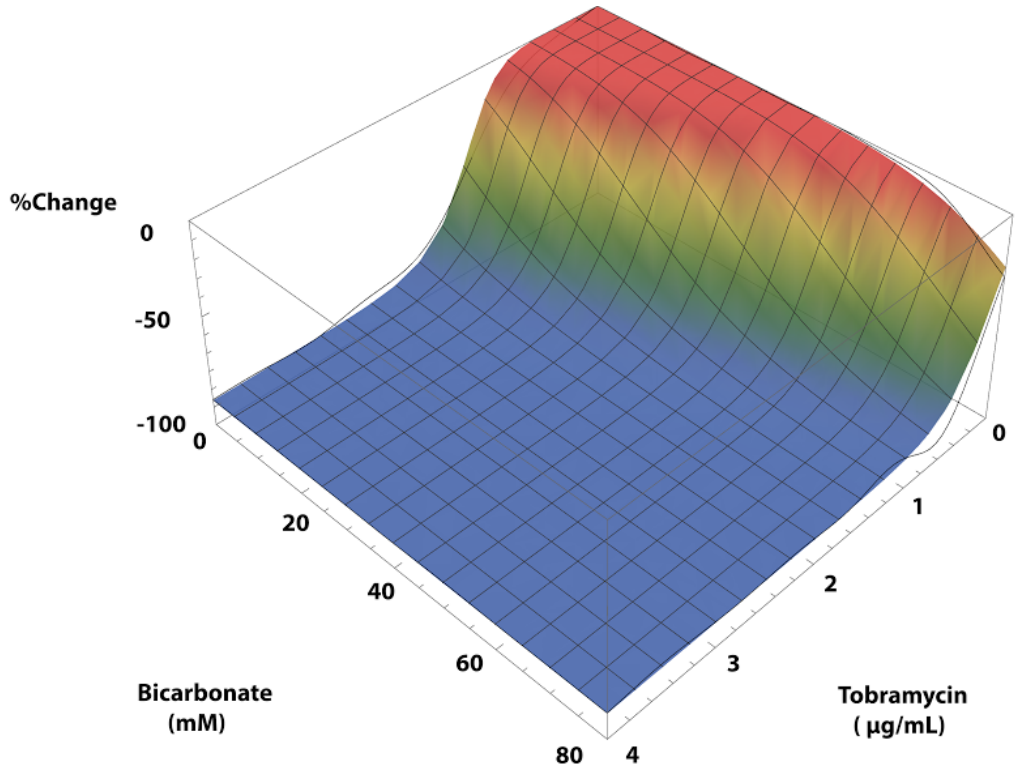

Figure 3.24 Loewe additivity predicted response surface for planktonic cells of *P. aeruginosa* strain PAO1.

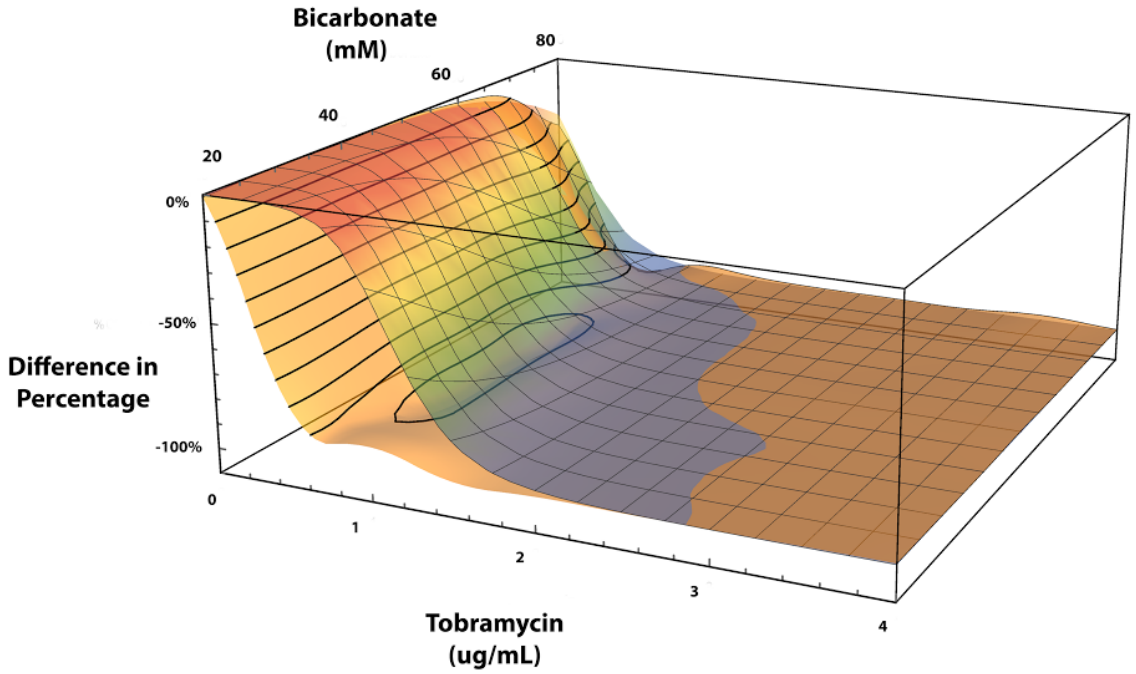

Figure 3.25 Loewe additivity predicted response surface (colored) and the observed surface (orange) based on checkerboard assay results for planktonic cells of *P. aeruginosa* strain PAO1.

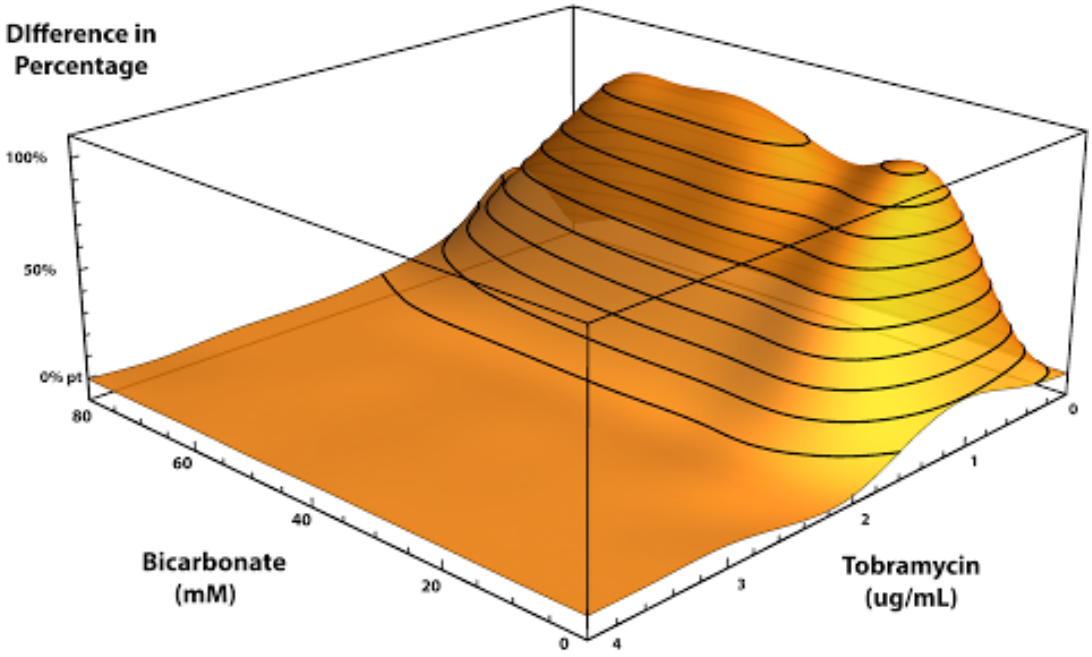

Figure 3.26 Total difference surface analysis (from the additivity predicted response surface and the observed surface) showing a strong synergistic effect for planktonic cells of *P. aeruginosa* strain PAO1. Synergy is indicated by a concave-downward curvature.

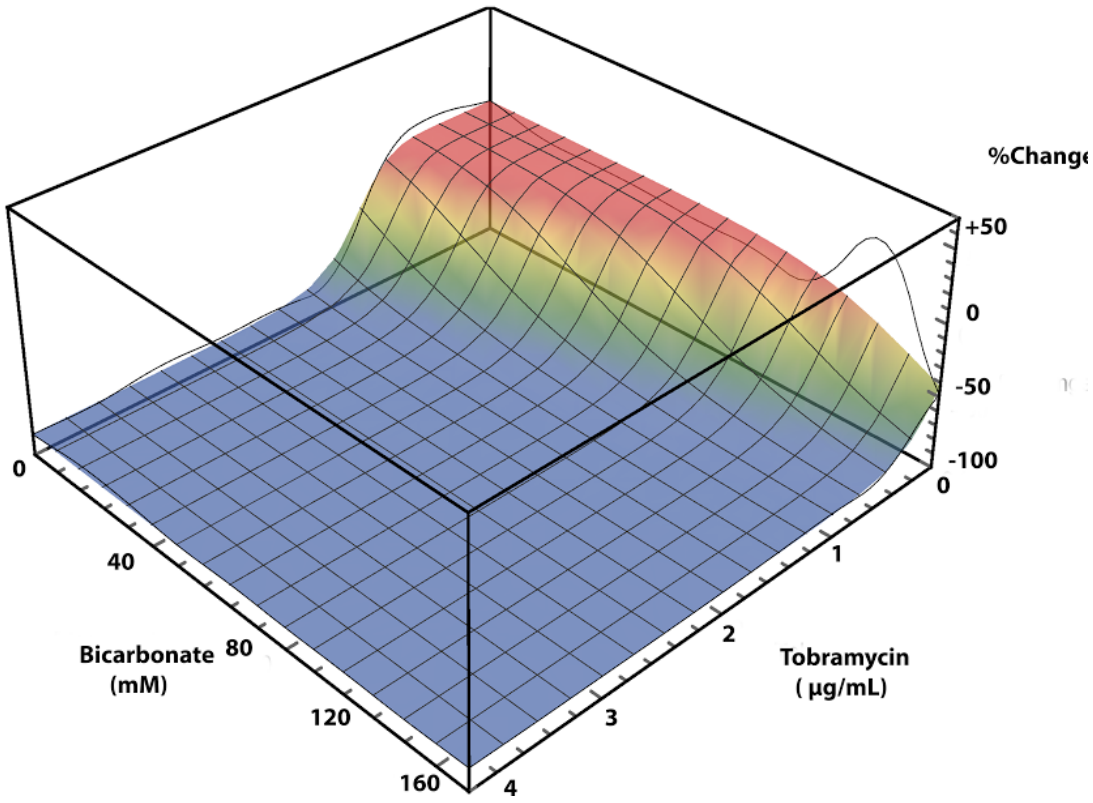

Figure 3.27 Loewe additivity predicted response surface for biofilm cells of *P. aeruginosa* strain PAO1.

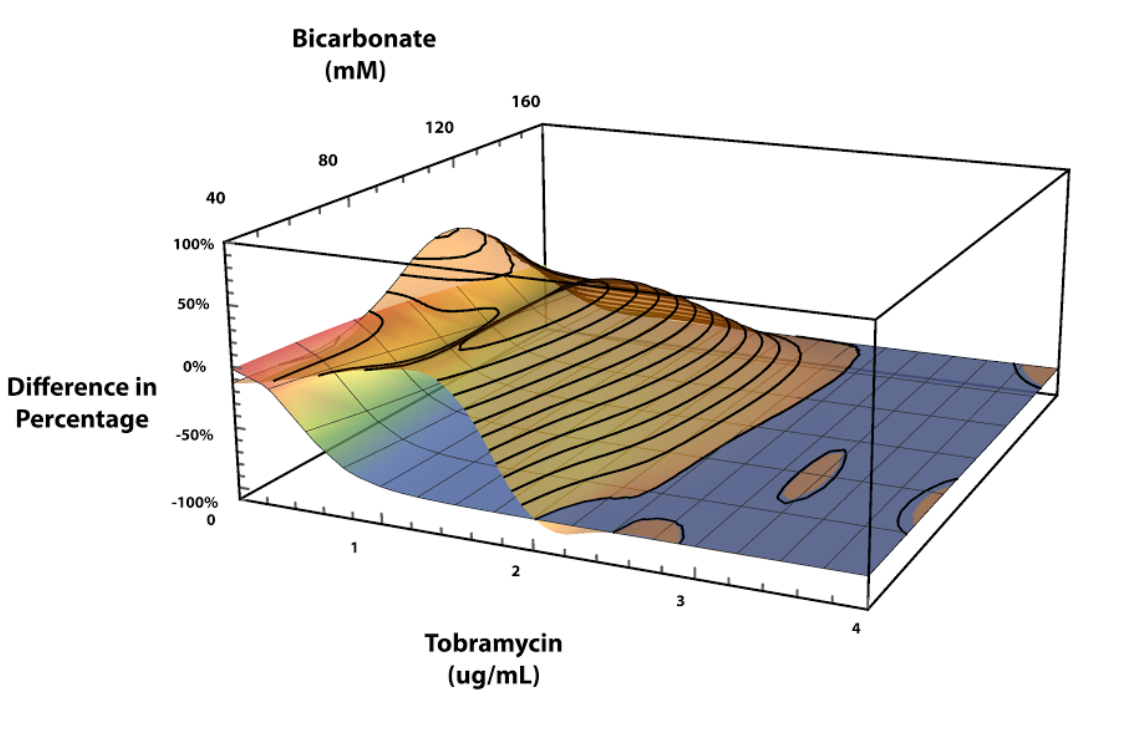

Figure 3.28 Loewe additivity predicted response surface (colored) and the observed surface (orange) based on checkerboard assay results for biofilm cells of *P. aeruginosa* strain PAO1.

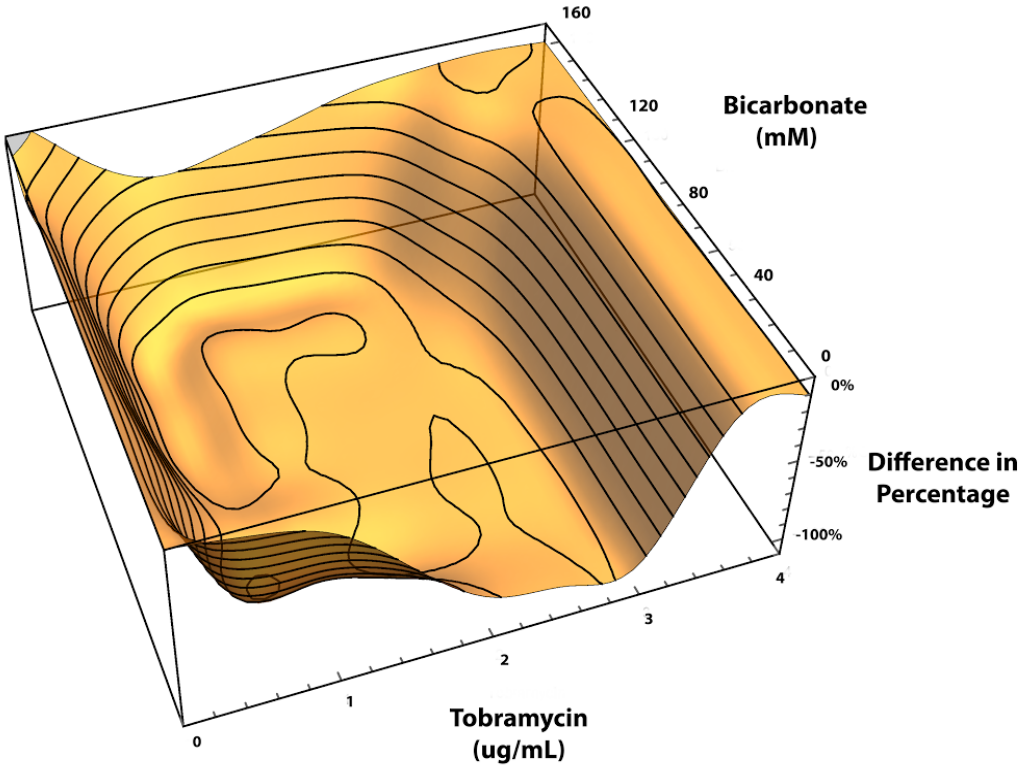

Figure 3.29 Total difference surface (from the additivity predicted response surface and the observed surface) showing a strong antagonistic effect for biofilm cells of *P. aeruginosa* strain PAO1. Antagonism is shown by concave-upward curvature.

3.3.7 Additional data demonstrating the synergistic effect of tobramycin and bicarbonate against planktonic *P. aeruginosa* cells

In addition to the strains demonstrated in Figures 3.1-3.6, we tested combinations of tobramycin and bicarbonate for synergy against several other *P. aeruginosa* strains. Isobolograms and FIC values for the different strains are shown in Figures 3.30-3.32.

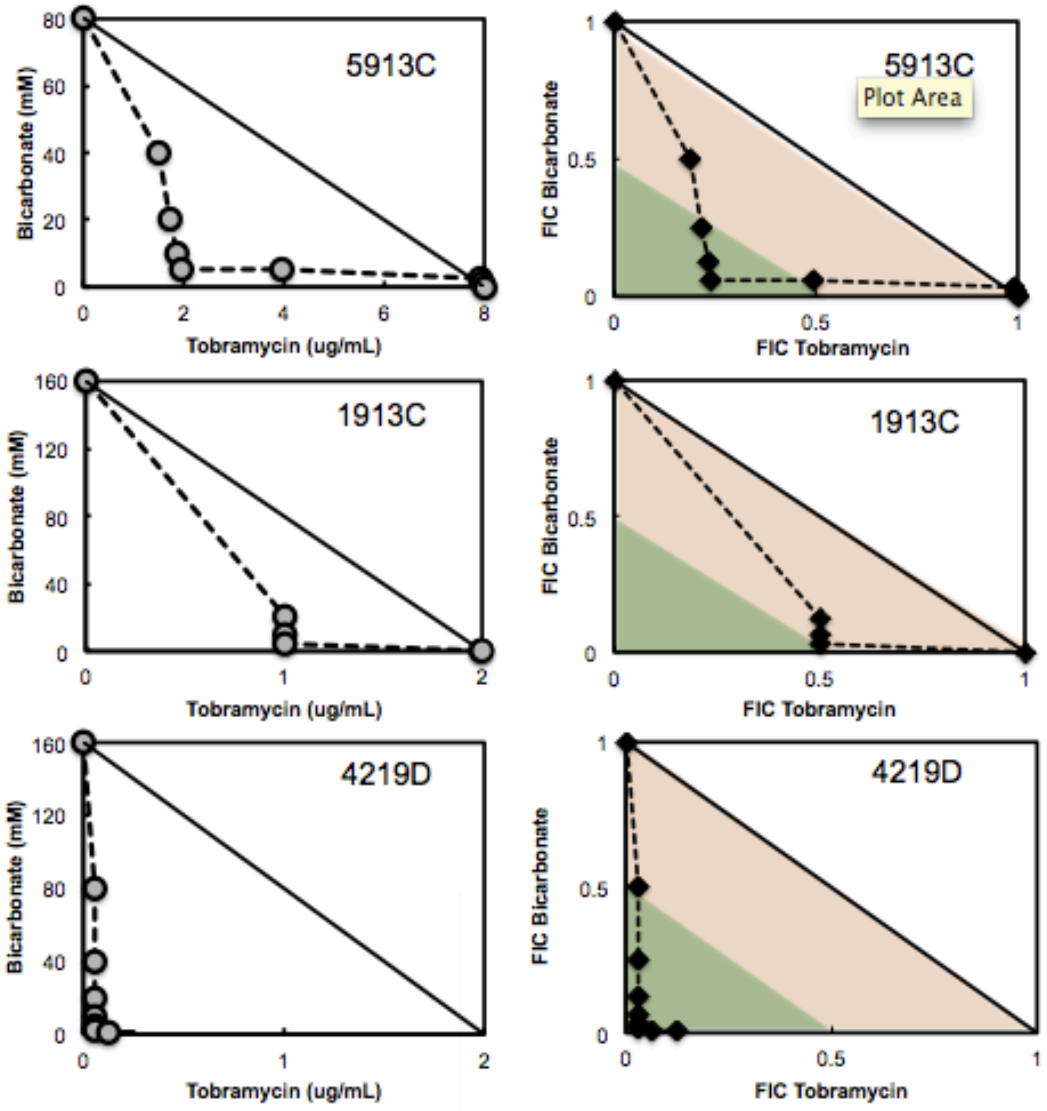

Figure 3.30 Isobologram analysis for planktonic cells of clinical *P. aeruginosa* strains 5913C, 1913C, and 4219D.

A synergistic-additive effect is observed for the combination of tobramycin and bicarbonate. Points along the isobologram represent the growth-no growth interface. The orange shaded area represents the additive region and the green shade area represents the synergistic region.

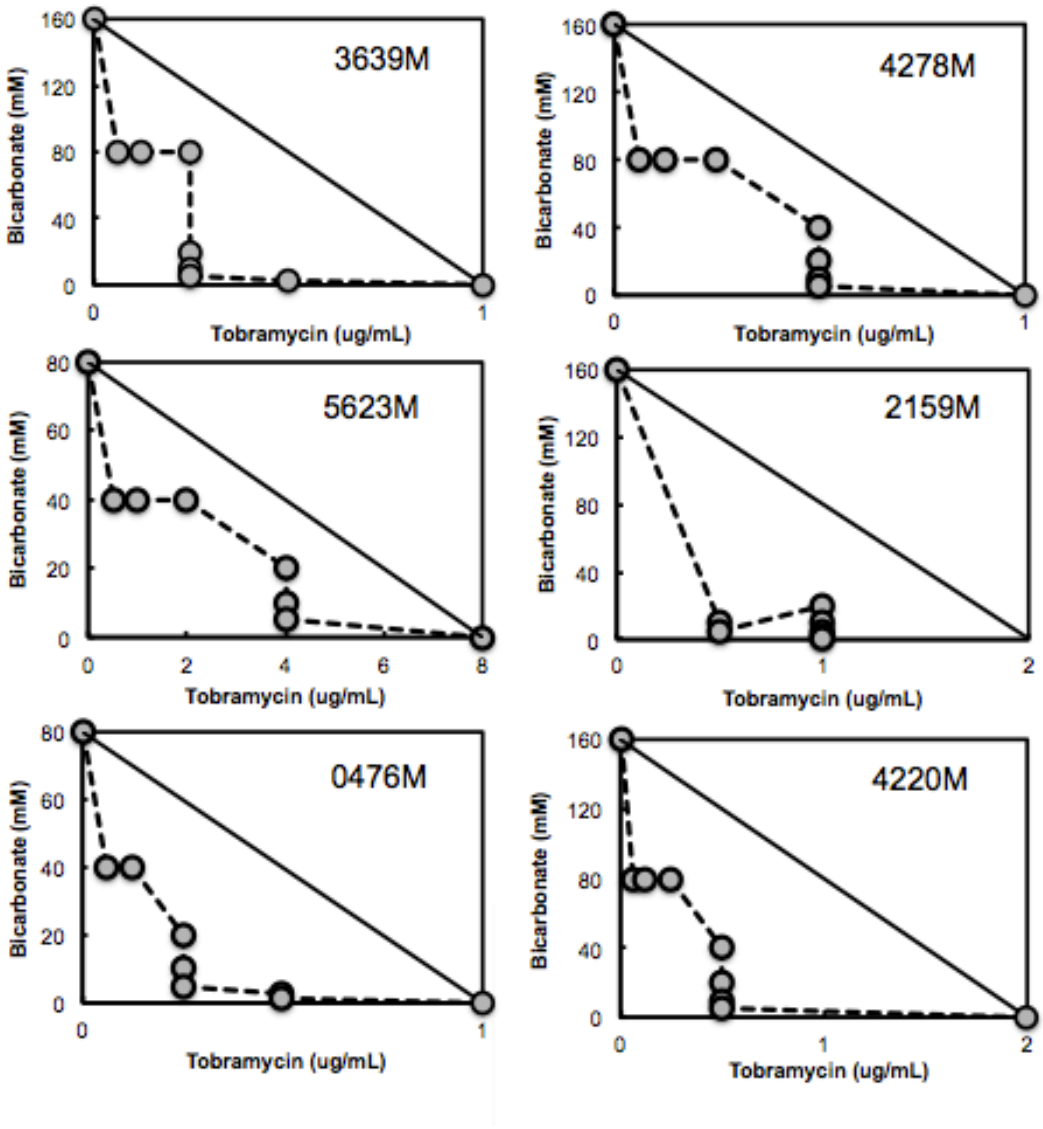

Figure 3.31 Isobologram analysis (based on MICs) for planktonic cells of clinical *P. aeruginosa* strains 3639M, 5623M, 0476M.

A synergistic-additive effect is observed for the combination of tobramycin and bicarbonate. Points along the isobologram represent the growth-no growth interface.

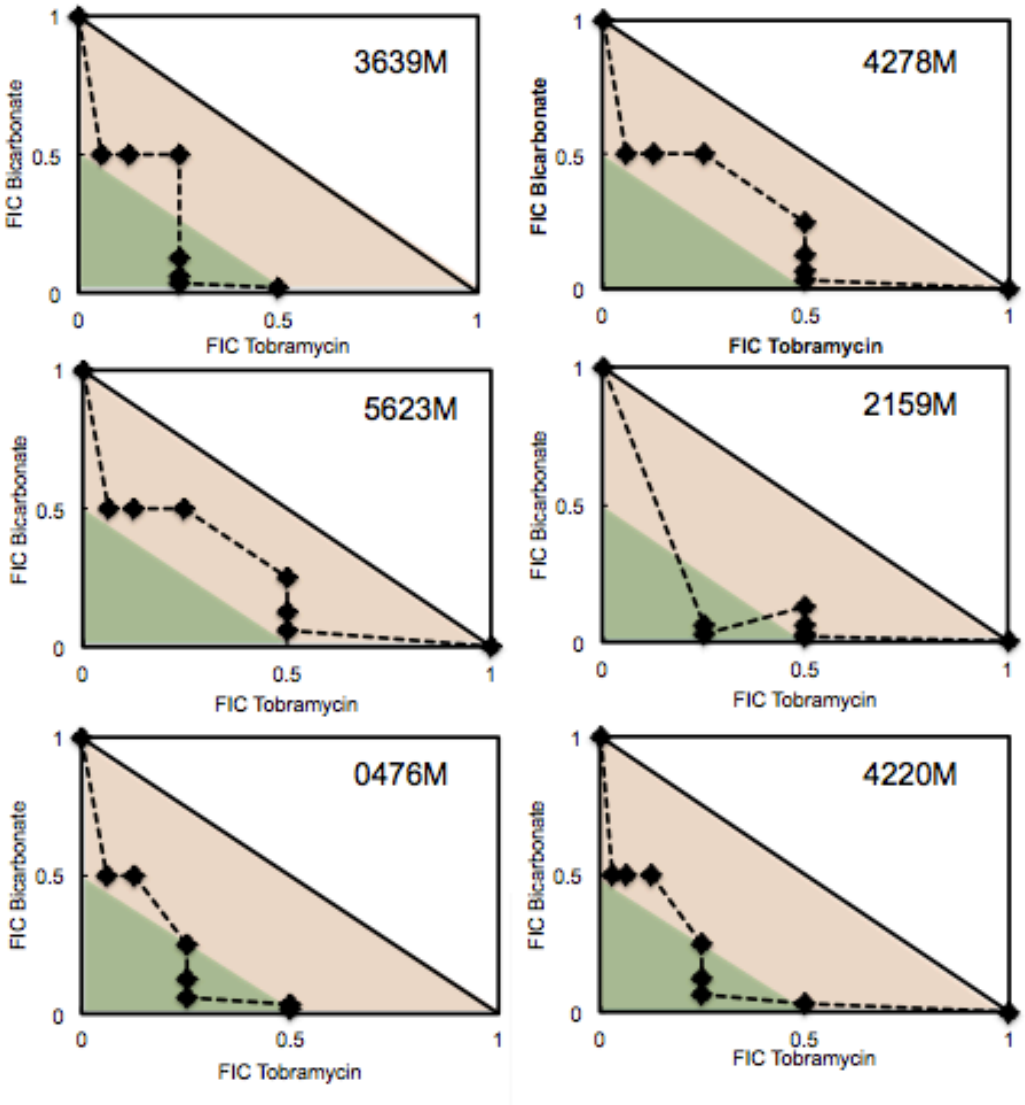

Figure 3.32 Isobologram analysis (based on FICs) for planktonic cells of clinical *P. aeruginosa* strains 3639M, 5623M, 0476M.

A synergistic-additive effect is observed for the combination of tobramycin and bicarbonate. Points along the isobologram represent the growth-no growth interface. The orange shaded area represents the additive region and the green shade area represents the synergistic region

3.3.8 The presence of serum reduces the synergistic effect for planktonic PAO1 cells

To examine the effect of serum on the synergistic effect observed with planktonic cells, PAO1 was tested in the presence of 25% serum (added to LB medium). As shown in Figure 3.33, the presence of serum reduced the synergistic effect, observed against PAO1 in LB medium alone (Figure 3.1), to an additive effect. The reduced effect in serum as compared to LB media could be due to the difference in the buffering capabilities of the two conditions, and we further examined this with pH measurements for different bicarbonate concentrations (Table 3.3). It is important to note that in the presence of 25% serum, bacterial growth was notably reduced in the untreated (control) cells, as compared to that seen with LB medium alone. This could possible be due to innate bactericidal factors present in the serum [195]. It is thus also possible that this lack of synergistic effect is due to some other effect of the serum. In the future, we plan to distinguish the buffering effect of the serum from some other possible effect by doing these assays in serum + bicarbonate, with the same pH range as in LB medium.

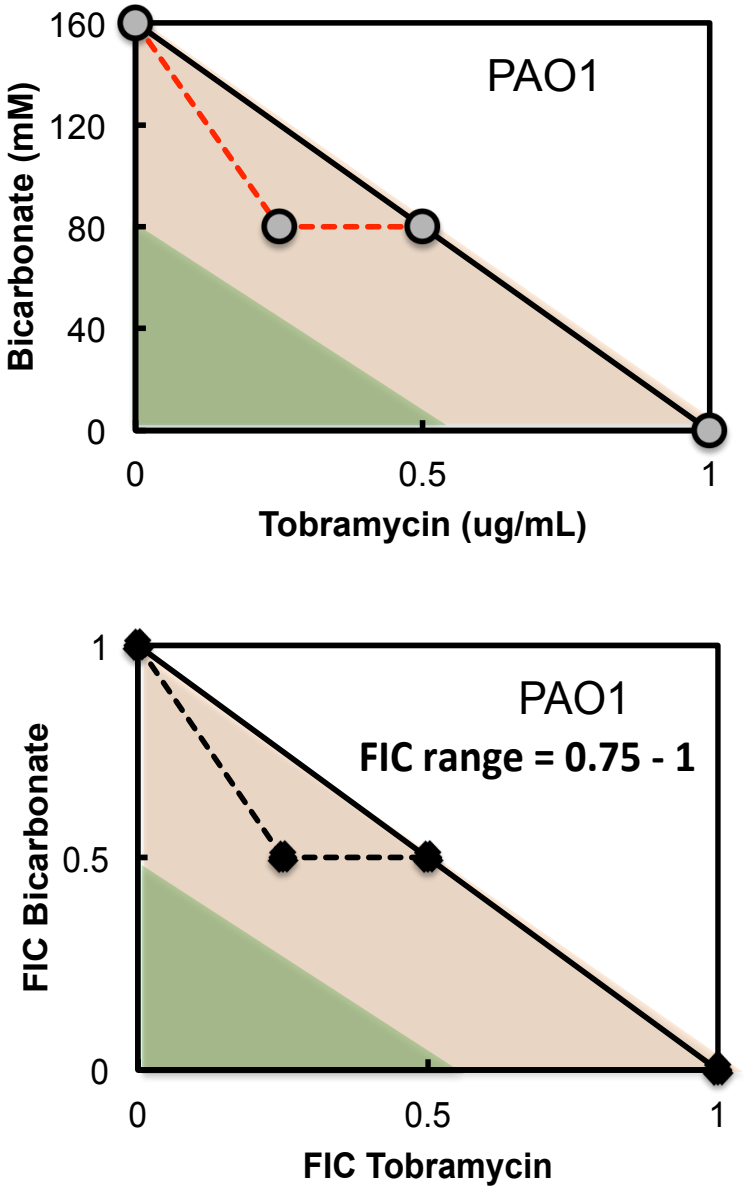

Figure 3.33 Isobologram analysis for planktonic cells of *P. aeruginosa* PAO1 in the presence of serum (25%).

An additive effect is observed for the combination of tobramycin and bicarbonate against PAO1, in the presence of serum. Points along the isobologram represent the growth-no growth surface. The orange shaded area represents the additive region and the green shade area represents the synergistic region.

Table 3.3 Corresponding pH values for different concentrations of bicarbonate added to LB media and LB media containing serum (5, 10, and 25%).

		Measured pH values (± SEM)		
Concentration of Bicarbonate (mM)	Luria-Bertani medium	Luria-Bertani medium with 5% serum	Luria-Bertani medium with 10% serum	Luria-Bertani medium with 25% serum
640	8.32 ± 0.02	7.83± 0.02	7.72 ± 0.03	7.66± 0.04
320	8.14 ± 0.01	7.77± 0.01	7.79 ± 0.01	7.72± 0.02
160	8.06 ± 0.02	7.68± 0.03	7.69 ± 0.02	7.64± 0.01
80	7.97 ± 0.03	7.55± 0.03	7.58 ± 0.03	7.65± 0.01
40	7.69 ± 0.01	7.43± 0.02	7.49 ± 0.01	7.51± 0.03
20	7.51 ± 0.01	7.26± 0.04	7.37 ± 0.02	7.38± 0.03
10	7.35 ± 0.02	7.18± 0.01	7.27 ± 0.03	7.32± 0.02
5	7.12 ± 0.07	7.15± 0.04	7.21 ± 0.01	7.25± 0.01
2.5	7.03 ± 0.03	Not tested	Not tested	Not tested
1.25	6.97 ± 0.03	Not tested	Not tested	Not tested
0.625	6.94 ± 0.03	Not tested	Not tested	Not tested
0	6.9 ± 0.08	7.07± 0.01	7.09 ± 0.02	7.11± 0.02

3.3.9 Combined treatment with tobramycin and bicarbonate demonstrates enhanced efficacy in an *in vitro* acute (planktonic) wound model

Using the *in vitro* wound model described above, “wounds” containing planktonic *P. aeruginosa* were treated with a combination of tobramycin and bicarbonate and each agent (tobramycin or bicarbonate) alone. In addition, an untreated wound (control) was also set up. Compared to the untreated control, the wound treated with the combination of tobramycin and bicarbonate showed a 2.5-fold decrease in colony counts. In comparison to the effects of tobramycin and bicarbonate alone, the combination treatment showed a 2-fold decrease. This finding is important as it indicates that the synergistic effect of this combination is observed in the presence of wound factors such as serum and blood.

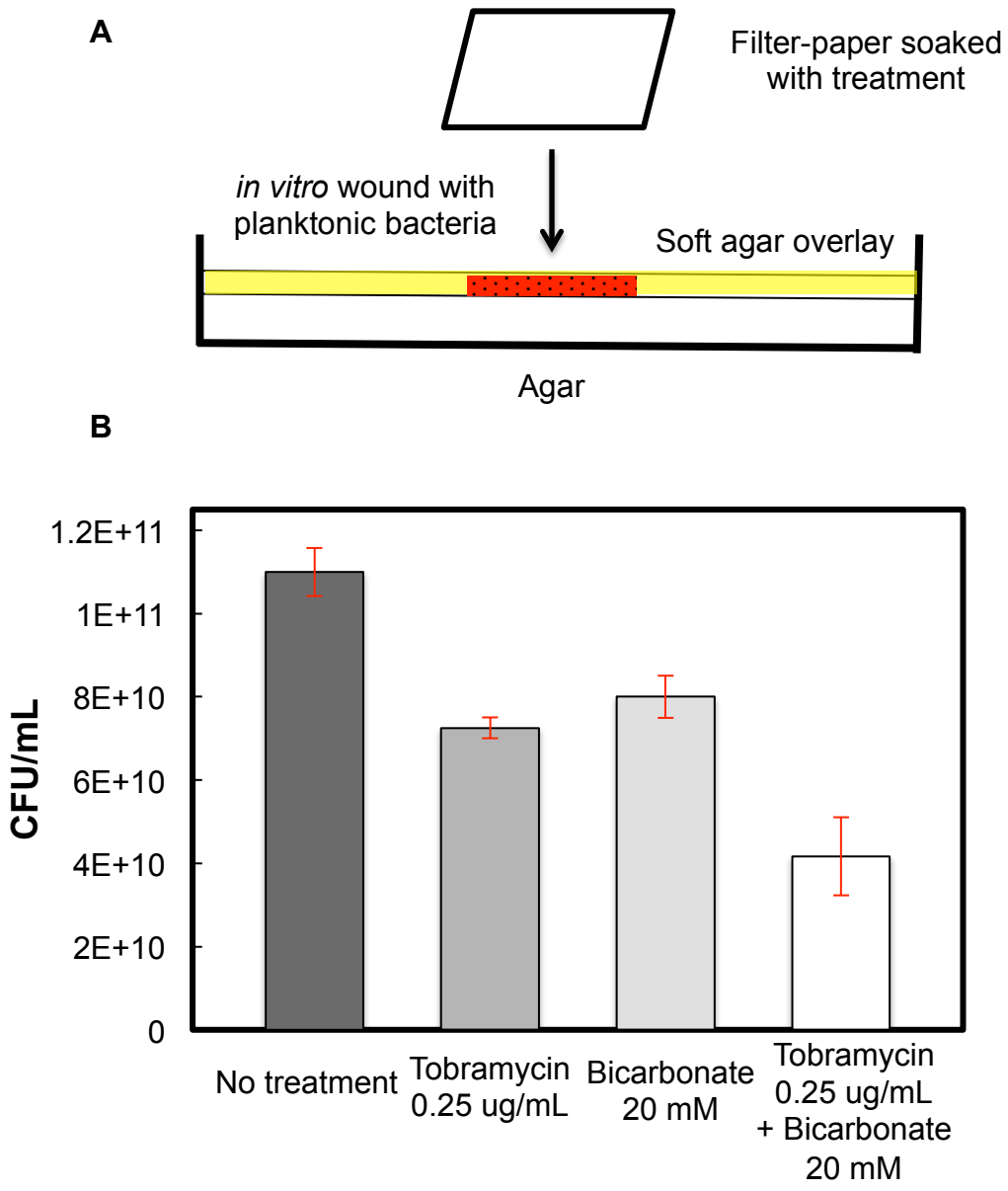

Figure 3.34 *In vitro* wound model demonstrates the efficacy of tobramycin and bicarbonate against planktonic *P. aeruginosa* PAO1 cells.

(A) An *in vitro* wound model, created with a 'wound' containing sheep blood, serum (10%), planktonic PAO1 cells, and LB agar, was placed in a 'bed' consisting of soft agar (0.6%), overlaid on LB agar (1.2%). Filter-paper dressings soaked with the treatments were applied to the 'wound'. **(B)** Estimation of CFU/mL after overnight incubation at 37°C reveals a two-fold decrease in colony counts for the combination treatment as compared to treatment with tobramycin or bicarbonate alone. Error bars represent SEM, N = 3.

3.3.10 Effect of addition of bicarbonate of the pH of media alone and media supplemented with serum

Based on previous work [102, 156, 157], an increase in pH, mediated by alkaline compounds, is believed to enhance the efficacy of aminoglycosides. To examine the effects increased pH produced by increasing concentrations of bicarbonate, we measured pH of LB media supplemented with the alkaline compounds. Further, to understand the additive, as opposed to synergistic effect, observed with media supplemented with serum, we measured pH of LB media with 10% serum. As expected, addition of bicarbonate increases the pH of LB media (Table 3.3). Addition of the same concentrations of bicarbonate increases the pH in LB media containing serum, however, the effect is less in comparison to LB media only (Table 3.3). This could explain the additive effect observed with planktonic PAO1 cells in media supplemented with serum.

3.3.11 Testing the effect of tobramycin and bicarbonate on biofilm cells using the Lubbock Chronic Wound Model (LCWM)

P. aeruginosa PAO1 biofilms were grown in an *in vitro* model resembling the constituents of a chronic wound. Known as the Lubbock Chronic Wound Infection model (LCWM), the constituents of this media include Bolton broth, laked horse blood, bovine plasma, to which bacterial cells are added [193]. Grown biofilms were treated with combination of tobramycin and bicarbonate and assayed for XTT activity. As seen with biofilm cells in LB media, we found that tobramycin and bicarbonate produced an additive effect for biofilm cells (Figure 3.35) in the LCWM (FIC range=0.5–1). These results reiterate that the strong synergistic effect observed with planktonic PAO1 cells, is reduced with biofilm cells.

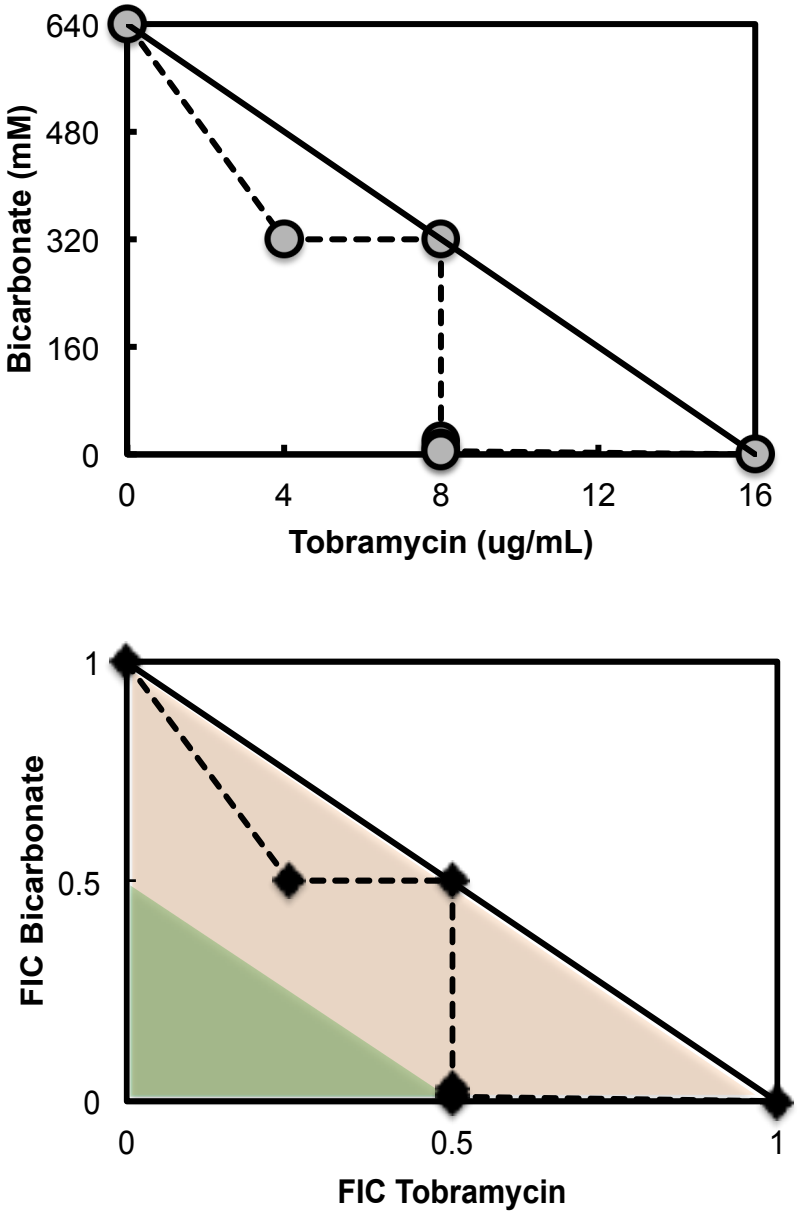

Figure 3.35 Isobologram analysis for biofilm cells of *P. aeruginosa* PAO1 in media with constituents resembling a chronic wound environment (Lubbock Chronic Wound Model).

An additive effect is observed for the combination of tobramycin and bicarbonate against PAO1 cells. Points along the isobologram represent the growth-no growth surface. The orange shaded area represents the additive region and the green shaded area represents the synergistic region.

3.3.12 *Ex-vivo* chronic wound (biofilm) mouse model of infection

To test the therapeutic potential of the tobramycin-bicarbonate combination, we used an *ex-vivo* chronic wound biofilm mouse model. This work was done in the laboratory of Dr. Kendra Rumbaugh at Texas Tech University Health Sciences Center, Lubbock, Texas. Our results (Figure 3.36) show that the combination of 2 μg/mL tobramycin and 160 mM bicarbonate fails to produce a synergistic effect in a chronic wound biofilm model infected with *P. aeruginosa* PAO1 cells. However, certain considerations relevant to these results need to be taken into account. This was the first time we tested this effect in a mouse model. Unexpectedly, 2 out of the 3 mice with chronic wounds died on the 2nd day of infection. While the exact cause for this is uncertain, this could be due to advanced age or physiological variation with a different batch of mice. As a result of this, we had only one replicate for the assay. Further, the concentration of tobramycin (2 μg/mL) and bicarbonate (160 mM) was based on our *in vitro* synergy assays. It is likely that this concentration needs to be adjusted for the *ex-vivo* testing. Finally, given that our *in vitro* biofilm assays failed to show a synergistic effect, it is also possible that this combination does not synergize against biofilm cells.

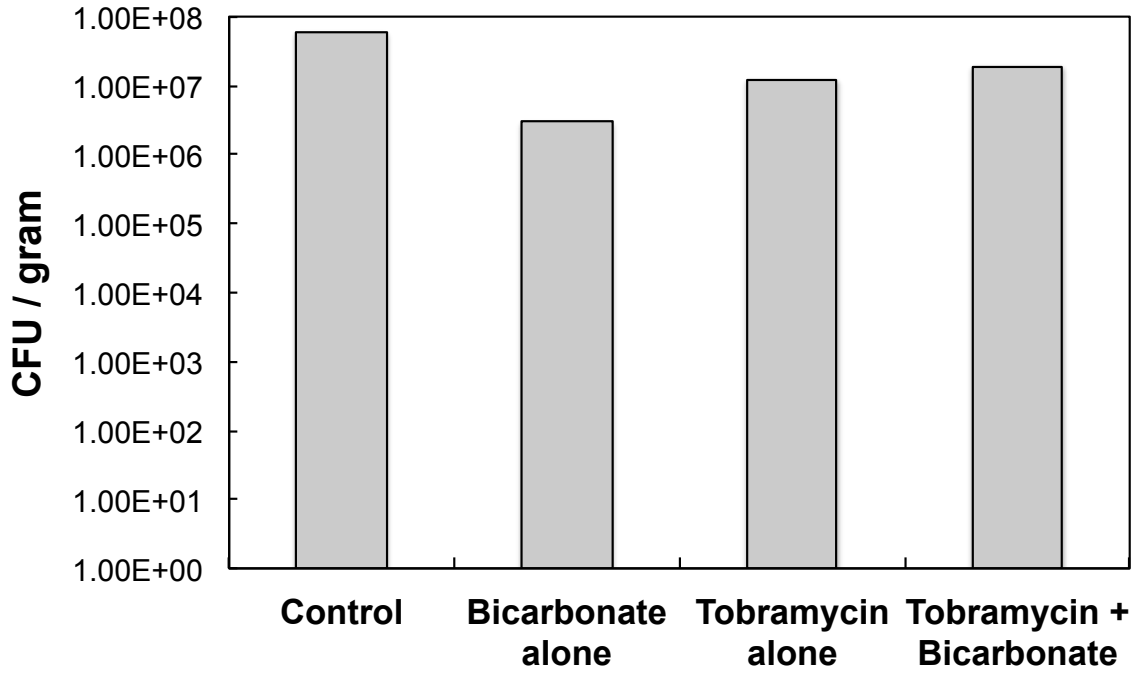

Figure 3.36 In an *ex-vivo* chronic biofilm wound infection model, the combination of tobramycin and bicarbonate fails to show a synergistic effect.

A chronic wound mouse model of biofilm infection was treated *ex-vivo* with 2 μg/mL tobramycin and 160 mM bicarbonate. The combination fails to produce a synergistic effect. Owing to the unexpected deaths of two mice, the assay was completed with only one replicate. The assay needs to be repeated with biological replicates to obtain statistically relevant result

3.4 CONCLUSIONS

Our results demonstrate that the combination of tobramycin and bicarbonate shows a strong synergistic effect against planktonic *P. aeruginosa* cells. As expected with a synergistic combination, addition of bicarbonate reduced the concentration of tobramycin needed to eradicate planktonic cells; it also significantly enhanced the rate of killing of cells in comparison to inhibitory concentrations of tobramycin alone. The combination of tobramycin and bicarbonate was at best additive against biofilm cells of *P. aeruginosa*, and was infact antagonistic in most combinations. Finally, we present an improved method for analyzing drug interactions using analytical dose-response surfaces, which allows us to more accurately estimate synergy regimes and make testable predictions of synergy combinations. This work opens the possibility of an additional role for bicarbonate therapy in CF patients, where it could augment the activity of tobramycin therapy against planktonic cells and early *P. aeruginosa* infections. This approach could also hold potential in the management of non-CF infections such as acute burn and post-surgical wounds, sepsis, urinary tract infections, and meningitis. These approaches could also hold promise in the management of acute wounds, but it is clear that more work needs to be done to fully understand the effects of local pH at wound infection sites [196].

We thank Dr. Hugh Smyth (UT Pharmacy) and Dr. Kendra Rumbaugh (Texas Tech University Health Sciences Center, Lubbock, Texas) for their scientific input.

Chapter 4: A low-cost, hands-on module to characterize antimicrobial compounds using an interdisciplinary, biophysical approach[b]

4.1 INTRODUCTION

Antibiotic resistance is a major public health problem worldwide [180]. The increased resistance to current antibiotics and steady decline in the development and approval of newer antibiotics motivate efforts to search for novel antimicrobial agents, especially from natural sources [198]. As part of a science outreach initiative, we have developed a "hands-on" experimental module to study and characterize antimicrobial compounds. This module was first implemented at the Hands-On Research in Complex Systems School held at The Abdus Salam International Centre for Theoretical Physics (ICTP), Trieste, Italy, July 2014 [199].

The Hands-On Research in Complex Systems School aims to introduce young scientists from developing countries to cutting-edge science in physical, chemical, and biological systems [199]. These two-week-long schools focus on using simple, low-cost, and reliable techniques to perform tabletop research in daily, three-hour-long laboratory sessions.

[b]This chapter was adapted from [197]. Kaushik KS, et al (2014). *PLoS Biol*. **13**(1): e1002044.

In these sessions, small groups of 4-6 participants work closely with two instructors, who conduct the same laboratory session each day with a different set of participants.

Typically, participants either have or are pursuing advanced degrees in a physical science or engineering field. More than half of the participants are theorists or simulators, not experimentalists. Instructors usually develop a hands-on module based on a research project being pursued in their lab and tailor it to the requirements of this science outreach initiative. Specifically, the module should last three hours, and cost $150 for 60 participants over 10 days.

The aim of the antibiotic resistance module is to introduce basic experimental microbiology concepts to an audience unfamiliar with biology, and to teach students to integrate physics-based quantitative analysis with biological data. Participants test the antimicrobial activity of different compounds to gain insights into the diffusive behavior, and thereby the physical size, of the active ingredient. The laboratory module is conducted over a three-hour time period, consisting of four main sections: overview of the scientific problem, introduction to experimental equipment and techniques, “hands-on” experiments, and application of experimental data to an analytical model.

Overview of the interdisciplinary hands-on module

A. Brief overview of the scientific problem
    * The problem of antibiotic resistance
    * Need to search for novel antimicrobial agents
    * Gaining insights into the active ingredient could help develop a therapeutic formulation
B. Introduction to experimental techniques to be used
    * Participants watch short video clips of the experimental techniques
    * The videos, created by us, included preparation of media, experimental design (disc diffusion assay), and analysis of results
C. Performing “hands-on” experiments
    * The assistant instructor demonstrates the experimental steps
    * Following this, each participant performs the experiment individually
    * Results from previous days’ experiments are read
D. Application of the experimental data to an analytical model
    * An analytical model is used to probe the physical characteristics of the active antimicrobial component
    * Participants watch video clips of additional experiments related to the analytical model
    * Data from biological experiments is used to determine the diffusion coefficient and molecular weight of the active ingredient

4.2 OVERVIEW OF THE SCIENTIFIC PROBLEM

Before the sessions, all participants received a handout describing the experimental module. In the first section, the instructor provided a brief overview of the global problem and challenges of antibiotic resistance and the imperative need to discover novel antimicrobial compounds. This opened a brief discussion on recent efforts towards exploring natural, biological, and indigenous resources as antimicrobial agents [198]. Importantly, this overview emphasized the key feature of our laboratory module, whereby an interdisciplinary approach could aid the discovery and identification of novel antimicrobial compounds, especially those from natural sources.

4.3 INTRODUCTION TO EXPERIMENTAL EQUIPMENT AND TECHINQUES

In the second section, participants were introduced to the experimental equipment and techniques used in the module. We used the disc diffusion assay to test the antimicrobial activity of different compounds [113] a technique used in clinical and research microbiology laboratories to study the bacterial and fungal strains' susceptibility to antibiotics. In the assay, compounds to be tested for antimicrobial activity are deposited on filter discs that have been placed on a lawn of bacterial cells. The perimeter at which the concentration of the compound falls below the inhibitory threshold defines the edge of the 'zone of inhibition' in which the lawn does not grow [147]. The size of this zone is set by the efficacy of

the antimicrobial compound against the bacterial strain on the lawn and the active ingredient's diffusion.

We created short video clips to help familiarize participants with the experimental tools and techniques. Before the hands-on experiment section, participants were introduced to the principles of sterilization, techniques for sterilization of media and equipment, differentiating sterile from non-sterile media, personal protective wear, precautions while working with a flame, levels of biosafety risk groups and biological containment, standard operating procedures for disposal of biological waste, and appropriate handling of biological waste spills. We reinforced these concepts at the end of the module, and emphasized the importance of close coordination with biological safety personnel.

4.4 HANDS-ON EXPERIMENTS

The hands-on sessions were conducted in improvised classrooms, so we used a risk group 1 (biosafety level 1) organism [200]. The bacterial strain, growth media, and antimicrobial compounds used are listed in Table 4.1. Briefly, we used *E. coli* DH5α, a commercial broth, and eucalyptus oil, ethanol, and hydrogen peroxide as antimicrobial compounds.

At the start of the hands-on section, the assistant instructor demonstrated the experimental steps of the assay, then each participant performed the assay.

The experimental scheme for the hands-on laboratory section is described in Figure 4.1. Three days before the sessions started, *E. coli* DH5α was streaked onto LB agar and allowed to grow at room temperature for 24-48 hours. A day prior to each session, overnight bacterial cultures were grown in 10 mL LB broth in plastic Falcon tubes (50 mL). Cultures were incubated under static conditions at room temperature for 16-18 hours. (The facilities available included neither a shaker nor incubator.) We inoculated overnight cultures for the first session, and participants inoculated cultures for all the other sessions. Since bacterial lawn growth and zones of inhibition would be visible only after overnight incubation, participants used experimental plates from the previous days' session to interpret the results of the assay.

Table 4.1 Bacterial strain, media conditions, and antimicrobial compounds

Bacterial strain	*E. coli* DH5α	Low-risk, non-pathogenic, laboratory strain Classified as a risk group 1 (biosafety level 1) organism [200].
Bacterial growth media	Luria-Bertani broth and agar	0.5% yeast extract, 1% tryptone, 1% sodium chloride, with 1.2% agar for plates.
Antimicrobial compounds	Eucalyptus oil, Ethanol, Hydrogen peroxide	Eucalyptus oil, a natural extract, is reported to have antimicrobial activity [201]. Ethanol and hydrogen peroxide are widely used for their antibacterial effects [202].

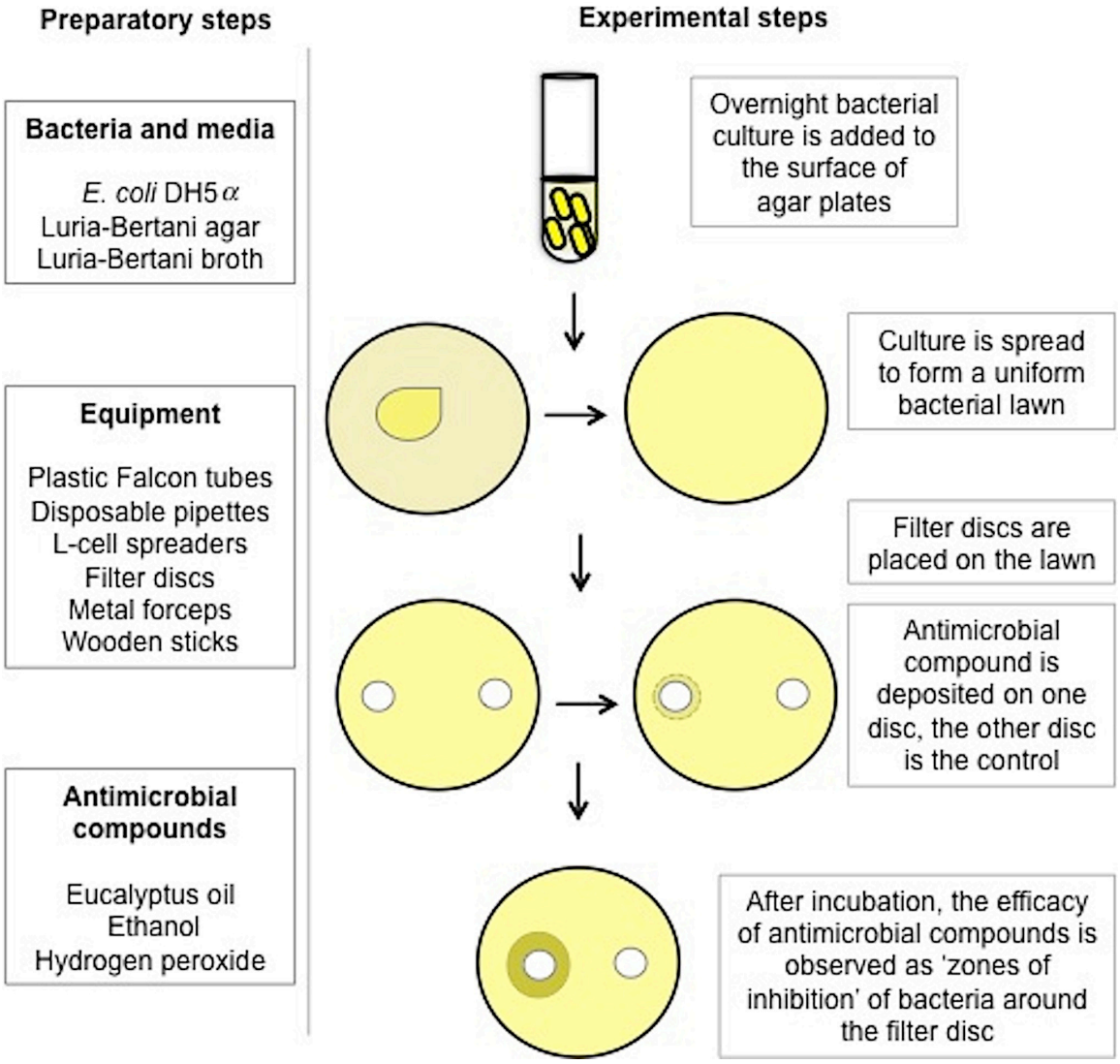

Figure 4.1 General scheme for the hands-on laboratory experiments.

Preparatory and experimental steps of the disc diffusion assay to test antimicrobial efficacy.

Participants noted the presence or absence of zones of inhibition caused by the test antimicrobial compounds and control and measured the width of the inhibition zone (X) as the distance from the edge of the disc to the edge of the zone (Figure 4.2). Temperatures of incubation, density of the bacterial lawn, bacterial strain used, and concentrations of the antimicrobial compound all influence the width of the inhibition zone. Differences in inhibition zone size allowed for comparison between the efficacies of different antimicrobial compounds and susceptibility profile of the bacterial strain. (Any open-access, image analysis software (such as ImageJ) could be used to measure the inhibition zones. Participants correctly determined that hydrogen peroxide was the most efficacious against the bacterial strain used, followed by ethanol, followed by eucalyptus oil.

At the end of each experimental session, we discussed biological safety and biohazard waste disposal, including how these practices could be implemented at their home institutions. Following each session, bacterial cultures and agar plates were collected in designated bags for biological waste (with the biohazard symbol), treated with 10% household bleach (5.25% sodium hypochlorite) for 30-60 minutes [203], followed by disposal in the sink or trash.

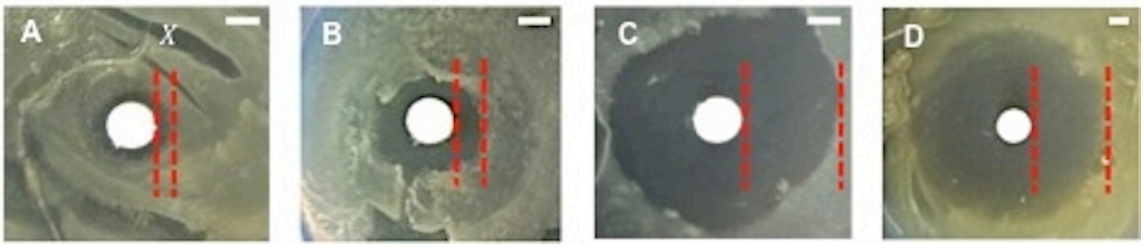

Figure 4.2 Representative zones of inhibition with different antimicrobial compounds.

Using the disc diffusion assay, representative zones of inhibition observed with **(A)** Eucalyptus oil (X = 2 mm), **(B)** 70% Ethanol (X = 5 mm), and **(C)** 3% Hydrogen Peroxide (X = 14 mm) on lawns of *E. coli*. Note that these are plates prepared by participants with no previous experimental biology experience. In **(D)** the zone of inhibition observed with the antibiotic tobramycin (10 μL of 50 mg/mL) is shown (X = 18 mm). Tobramycin was used as the molecular weight standard to calibrate the molecular weight of the test compound. Owing to budgetary constraints, participants could not be provided with antibiotics for testing purposes. This image is from the assay performed by the instructors to measure slope and critical time. For the analytical model, the width of inhibition (X) was measured as the distance from the edge of the disc to the edge of the zone. Scale bars are 5 mm.

4.5 APPLICATION OF EXPERIMENTAL DATA TO AN ANALYTICAL MODEL

An analytical model was employed to determine the physical characteristics of the active antimicrobial component as a way to prospect for novel antimicrobial agents, where insights into the active ingredient would aid the development of a therapeutic formulation. This model is based on the disc-diffusion assay [147], and assumes that the active ingredient has a constant diffusion coefficient D and that a threshold concentration of the active ingredient is required to inhibit bacterial cells. The number of cells in the lawn increases as the lawn incubates, which decreases the per-cell concentration of the active ingredient, which therefore no longer causes inhibition after a critical time T_c of incubation. The model describes the width of the inhibition zone (X) as

$$X^2 = 4DT_c \ln(C_0) + F(D, T_c, C_c) \qquad (1)$$

where C_0 is the concentration of the antimicrobial compound deposited on the filter disc. F is a function independent of C_0. C_c is the lowest concentration of the active ingredient required to cause measurable inhibition. The slope of X^2 as a function of $\ln(C_0)$ gives D, if T_c is known. We relate D to the molecular weight (MW) of the active ingredient using the Stokes-Einstein equation [204], thus:

$$MW_I = MW_A\left(\frac{D_A}{D_I}\right)^3 \qquad (2)$$

where A is the active ingredient and I is a known molecule that empirically calibrates the relationship between diffusion and molecular weight.

To measure the slope of X^2 as a function of $\ln(C_0)$ decreasing concentrations of the antimicrobial compound are deposited on bacterial lawns. After overnight incubation the width of inhibition (X) for each concentration is measured. Using linear regression, the slope of X^2 as a function of $\ln(C_0)$ is obtained (Figure 4.3A). To measure pre-incubation time, a given concentration of the antimicrobial compound is deposited on the bacterial lawn after different time intervals of incubation. After overnight incubation, the width of inhibition (X) for each time point is measured. Using linear regression, the time after which no inhibition is observed (X = 0 mm) is determined as the critical time of pre-incubation (Figure 4.3B). Since these experiments are essentially variations in the disc-diffusion assay, the hands-on session in the module would provide participants the requisite skills to perform these assays. For lack of time, participants used data we had taken in our research lab. Experiments were demonstrated using video clips and the participants were guided through each step in the assay. Data for hydrogen peroxide (test antimicrobial compound) and the known antibiotic tobramycin (MW = 467.5 Da) was provided to the participants (Figure 4.4A and B). Using a linear regression tool with which they were already familiar (such as MS Excel), participants determined the diffusion coefficient and molecular weight of the test antimicrobial compound. The handout also contained the solutions to the exercise.

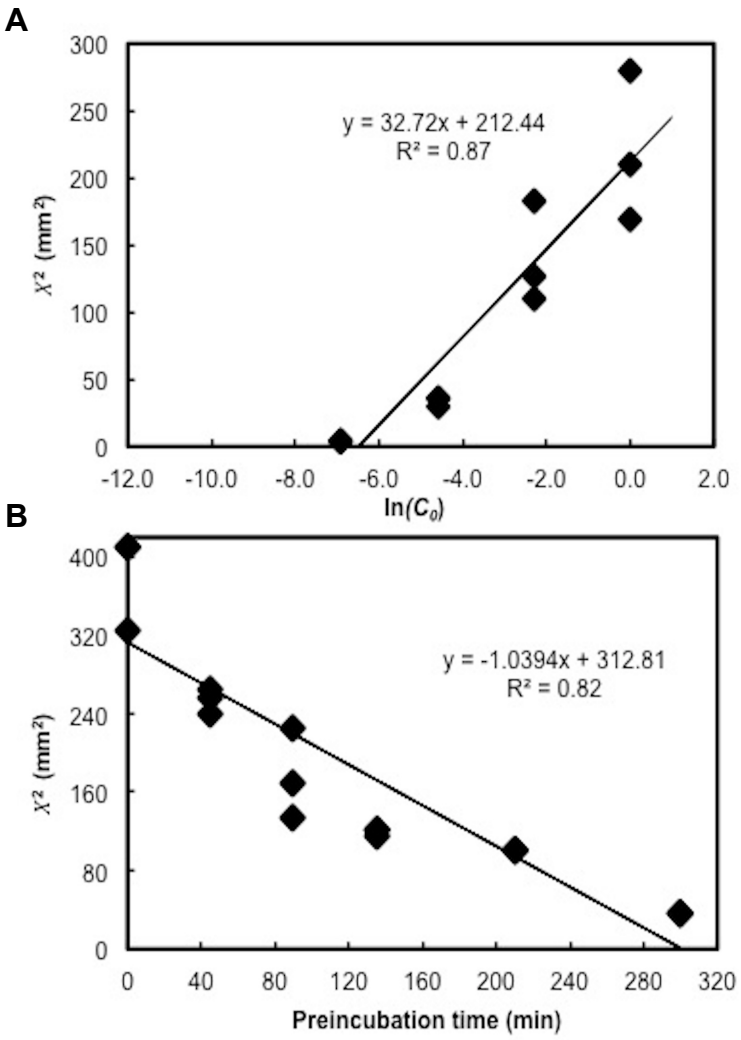

Figure 4.3 Measuring slope of X^2 as a function of $\ln(C_0)$ and critical time (T_c) of pre-incubation for hydrogen peroxide.

(A) To measure the slope of X^2 as a function of $\ln(C_0)$, decreasing concentrations of hydrogen peroxide are deposited and the width of inhibition (X) measured. Using linear regression, the slope of X^2 as a function of $\ln(C_0)$ is obtained. **(B)** To measure pre-incubation time, a given concentration of hydrogen peroxide (30%) is deposited on the bacterial lawn after different time intervals of incubation. After overnight incubation, the width of inhibition (X) for each time point is measured. Using linear regression, the time after which no inhibition is observed (X = 0 mm) is determined as the critical time (T_c) of pre-incubation.

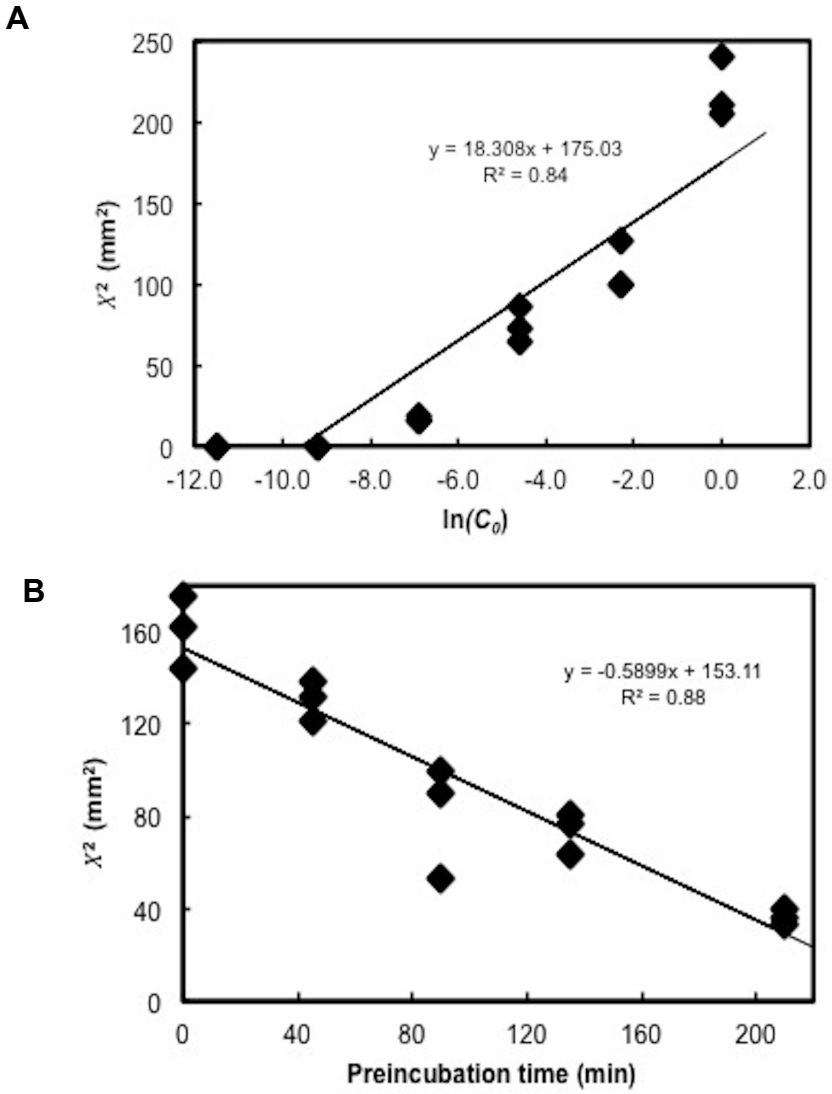

Figure 4.4 Measuring **(A)** Slope of X^2 as a function of $\ln(C_0)$ and **(B)** Pre-incubation time T_c for tobramycin.

4.6 MODULE HAND OUT FOR THE PARTICIPANTS

This handout was made available to participants before the hands-on session, using Google Drive. It contains more detailed information than we were able to go into during the three-hour laboratory session, as well as links to all videos.

4.6.1 Goal of this hands-on session

To assay the antimicrobial effects of compounds using the disc diffusion technique and apply an analytical model to determine the diffusion coefficient of the active antimicrobial component. The diffusion coefficient depends on size and is therefore a measure of the molecular weight of the active ingredient.

4.6.2 Preparation of equipment and bacterial growth media

4.6.2.1 Equipment to be procured from a commercial source

Pre-sterile petri dishes (alternatively, glass petri dishes may be cleaned and sterilized by autoclaving)

LB broth and agar (or individual components–tryptone, yeast extract and sodium chloride, and agar)

Pre-sterile 50 mL plastic falcon tubes

Pre-sterile plastic pipettes (3 mL, with 0.5 mL graduations) or automated pipettes with tips (1-10 μL, 10-100 μL). For the automated pipettes, tips can be bought pre-sterile or sterilized in the autoclave.

Pre-sterile L-cell spreaders (alternatively, a metal, reusable spreader can be used and sterilized by flaming with 70% ethanol)

Glassware for making and storing LB broth

Analytical balance (to weigh constituents of LB broth and agar)

4.6.2.2 Equipment to be sterilized prior to use

Filter discs (7 mm diameter, Whatman filter paper no. 1)

Wooden sticks (for inoculation of bacterial cultures)

Metal forceps

Pipette tips (if using automated pipettes)

Glass test tubes (if available, for inoculating bacterial broth cultures)

The above equipment was sterilized using an autoclave (121°C for 20 min at 15 psi) with a drying cycle. Alternatively, 70% ethanol and flame sterilization can be used.

Preparation of bacterial growth media

Luria-Bertani media is routinely used in microbiology laboratories to support bacterial growth. To prepare the liquid or broth form of this media, 10g tryptone,

5g yeast extract, 10g sodium chloride are dissolved in 500 mL distilled water, aliquoted into clean glass bottles and sterilized by autoclaving – *i.e*., by heating to 121°C for 20 min at 15 psi. To make LB agar, 6g of the solidifying agent agar is added to the above constituents before they are autoclaved. This gives an agar concentration of 1.2%. After sterilization by autoclaving, the molten LB agar is poured into pre-sterile petri dishes and allowed to set. Agar plates are then packed into plastic sleeves for storage at 4°C. It is preferable not to use plates more than 3-4 weeks old. Alternatively, instead of individual constituents, commercially available mixed formulations, or ready-to-use forms of LB broth or agar may also be used.

4.6.3 Inoculation and growth of bacterial cultures

Materials

Pre-sterile 50 mL plastic falcon tubes

Pre-sterile plastic pipettes (3 mL, with 0.5 mL graduations)

Sterile wooden sticks

Sterile LB broth and LB agar plates

Three days before the day of the experiment, the bacterial strain *Escherichia coli* DH5α was streaked onto a plate of LB agar and allowed to grow at room temperature for 48 hours. The bacterial strain was shipped in soft agar (0.6%) in plastic cryovials to the school. Bacterial cultures are put up from these plates.

The bacterial strain *E. coli* DH5α is considered non-pathogenic to humans. Classified in Risk Group 1 (Biosafety level (BSL) 1) and posing minimum risk to humans, this strain can be worked with on a laboratory bench top using an open flame and requires no additional precautions. It is important to note, that these guidelines apply only to BSL 1 organisms. For working with organisms that are not BSL 1, please refer to the Center for Disease Control (CDC) biosafety guidelines.

Procedure

Inoculation of bacterial cultures should be done near a flame using sterile technique. Using a pre-sterile plastic, disposable pipette (or automated pipette, if available), add 10 mL of LB broth into a 50 mL plastic Falcon tube or sterile glass tube. With a wooden stick pick a bacterial colony from the surface of the agar plate and gently suspend the colony into the LB broth. Loosely cap the plastic tube and incubate at room temperature for 24 hours.

4.6.4 Preparation of lawns of bacterial growth

Materials needed

Overnight bacterial cultures grown in LB broth

Pre-sterile plastic pipettes (3 mL, with 0.5 mL graduations)

LB agar plates (if stored at 4°C, allow to warm and dry at room temperature prior to use)

Pre-sterile L-cell spreaders

Procedure

Preparation of bacterial lawns should be done near a flame using sterile technique. Using a pre-sterile plastic pipette (3 mL, with 0.5 mL graduations), add 2 large drops (~100 μL) of the bacterial culture grown in LB broth onto the surface of a warm, dry LB agar plate. Using an L-cell spreader gently spread the drop of bacterial culture over the entire surface of the agar. It is advisable to hold the L spreader in the dominant hand and agar plate in the non-dominant hand. Rotating the plate gently, make sure to cover the entire agar surface well including the center and rim. Spread thoroughly, repeating strokes several times. After spreading is complete, allow the plates to dry for a few minutes.

4.6.5 Deposition of antimicrobial compounds

Materials needed

Bacterial lawns spread on the surface of LB agar

Sterile filter discs (7-mm diameter)

Sterile metal forceps

Antimicrobial test compounds

We will be testing three compounds – the natural extract eucalyptus oil (100%, *Eucalyptus globulus*) [201], and the chemical compounds ethanol (70%) and hydrogen peroxide (3%) [202]. Eucalyptus oil was procured from NOW® Solutions and ethanol and hydrogen peroxide were obtained from a local pharmacy in Trieste, Italy.

Procedure

Using a metal forceps place a filter disc (7-mm diameter) on the surface of the bacterial lawn. Using a plastic, disposable pipette, add a drop (~50 μL) of eucalyptus oil or ethanol or hydrogen peroxide on the filter disc, minimizing the amount of spillover around the disc as much as possible. As a control, deposit a sterile filter disc onto the lawn but do not apply any antimicrobial compound. Allow the antimicrobial compounds to dry and incubate plates at room temperature for 24-48 hours. Make sure to label each plate appropriately using a Sharpie pen. This technique is called the 'disc diffusion' assay [113] and is routinely used in clinical and research microbiology laboratories to study the antibiotic susceptibility of bacterial strains.

4.6.6 Evaluating the efficacies of the antimicrobial compounds

Materials needed

Experiment plates from previous work

Ruler

Procedure

Following incubation at room temperature for 24-48 hours, antimicrobial efficacy is observed as 'zones of inhibition' of the bacterial lawn around the filter discs (Figure 3.2). Using a ruler, measure the size of the zones of inhibition from the edge of the filter disc to the edge of the zone. We refer to this width of the inhibition zone as X. Alternatively, plates can be photographed and the zones of inhibition can be measures using an open-source, image analysis software (such as ImageJ). By measuring the size of the zone of inhibition, the efficacies of different antimicrobial compounds and the susceptibility of different bacterial strains can also be compared.

4.6.7 Using an analytical model to determine the physical characteristics of the active ingredient of an antimicrobial compound

To determine the physical properties of the active ingredient of a compound (I) exhibiting antimicrobial activity, our laboratory has developed a numerical model based on the disc-diffusion assay [147].

The assumptions of the model include –

1. The active ingredient of the antimicrobial compound is released at a concentration C_0 at the filter disc.
2. The active ingredient diffuses out of the disc with a constant diffusion coefficient D.
3. A threshold concentration of the active ingredient is required to inhibit bacterial cells.
4. The active ingredient no longer effects inhibition after a critical time T_c of incubation.

Assumption (4) corresponds an increase in the number of cells in the lawn that causes the per-cell concentration of the active ingredient to drop to sub-inhibitory levels.

Based on this model,

$$X^2 = 4DT_c \ln(C_0) + F(D, T_c, C_c) \qquad (1)$$

where C_0 is the concentration of the antimicrobial compound deposited on the filter disc, which we assume to be linearly proportional to the concentration of the active ingredient. F is a function independent of C_0. C_c corresponds to the lowest concentration of the active ingredient required to cause measurable inhibition. T_c is the critical time of incubation (also called pre-incubation time) after which the inhibition is no longer observed. At this time, the density of the bacterial lawn increases to a critical level (due to bacterial growth), resulting in

the concentration of the active ingredient falling below the critical threshold concentration required to effect inhibition. As seen in equation 1, the slope of X^2 (square of the width of inhibition) as a function of $\ln(C_0)$ gives the diffusion coefficient D, if critical time T_c is known. Further, using the calculated diffusion coefficient D, we can determine the molecular weight (MW). According to the Stokes-Einstein equation [204], the diffusion coefficient of a molecule is inversely proportional to its radius.

From the equations,

$$D = \frac{\kappa_B T}{6\pi\eta R} \qquad (2)$$

where is κ Boltzman constant, T is temperature, η is solvent viscosity and R is radius of the molecule,

and $MW = N\rho V = N\rho * \frac{4}{3}\pi R^3$ (3)

where N is Avogadro's number, ρ is density of the molecule, V is volume of the molecule, and R is radius of a spherical molecule, we get that $D \propto \frac{1}{MW^{1/3}}$

To first order, a molecule's volume and therefore its molecular weight is proportional to its radius, thus for the active ingredient of antimicrobial compound I and a known molecule A:

$$MW_I = MW_A(\frac{D_A}{D_I})^3 \qquad (4)$$

Owing to insufficient time, experiments to measure the slope of X^2 (square of the width of inhibition) as a function of $\ln(C_0)$ and pre-incubation time T_c are demonstrated in these video clips. To measure the slope of X^2 as a function of $\ln(C_0)$ decreasing concentrations of the antimicrobial compound are deposited on bacterial lawns and after overnight incubation, the width of inhibition (X) for each concentration is measured. Using linear regression, the slope of X^2 as a function of $\ln(C_0)$ is obtained. To measure pre-incubation time, a given concentration of the antimicrobial compound is deposited on the bacterial lawn after different time intervals of incubation. After overnight incubation, the width of inhibition (X) for each time point is measured. Using linear regression, the time after which no inhibition is observed (X = 0 mm) is determined as the critical time of pre-incubation.

4.6.8 Analysis of data to determine diffusion coefficient D and molecular weight (MW) of the active ingredient of compound I

To provide representative data sets for analysis, we performed the above experiments with hydrogen peroxide (compound I) and a known antibiotic tobramycin (MW = 467.5 Da).

Raw Data for compound I (hydrogen peroxide)

Increasing concentrations of compound I (hydrogen peroxide) and corresponding sizes of zones of inhibition (X) (Table 4.2).

Hint: Use this to obtain the slope of X^2 as a function of $\ln(C_0)$ as seen in equation (1).

Increasing time of pre-incubation and corresponding sizes of the zones of inhibition (X) for compound I (hydrogen peroxide) (Table 4.3).

Hint: Use this data to obtain the critical pre-incubation time T_c of the active ingredient of compound I as seen in equation (1).

Using the slope and value of T_c obtained above, calculate the diffusion coefficient D of the active ingredient of compound I.

Table 4.2 Increasing concentrations of compound I (hydrogen peroxide) and corresponding sizes of zones of inhibition (X)

Relative concentration	X **(mm)**
1	13
1	16.75
1	14.5
0.1	11.25
0.1	10.5
0.1	13.5
0.01	6
0.01	6
0.01	5.5
0.001	2
0.001	2
0.001	2

Table 4.3 Increasing time of pre-incubation and corresponding sizes of the zones of inhibition (X) for compound I (hydrogen peroxide)

Time (min)	X (mm)
0	18
0	20.25
0	20.25
45	15.5
45	16
45	16.25
90	11.6
90	13
90	15
135	11
135	10.75
135	11
210	10
210	10
210	10
300	6
300	6
300	6

Raw Data for known compound A

The known antibiotic tobramycin (MW = 467.5 Da) was used as the standard to calculate the molecular weight of the active ingredient of compound I.

Increasing concentrations of tobramycin and corresponding sizes of zones of inhibition (X) (Table 4.4).

Increasing time of pre-incubation (T_c) and corresponding sizes of the zones of inhibition (X) for tobramycin (Table 4.5).

Using the slope and value of T_c obtained above, calculate the diffusion coefficient D of tobramycin.

Table 4.4 Increasing concentrations of tobramycin and corresponding sizes of zones of inhibition (X)

Relative Concentration	X (mm)
1	15.5
1	14.5
1	14.3
0.1	11.25
0.1	10
0.1	10
0.01	9.25
0.01	8
0.01	8.5
0.001	4
0.001	4
0.001	4.25
0.0001	0
0.0001	0
0.0001	0
0.00001	0
0.00001	0
0.00001	0

Table 4.5 Increasing time of pre-incubation (T_c) and corresponding sizes of the zones of inhibition (X) for tobramycin

Time (min)	X (mm)
0	12.75
0	13.25
0	12
45	11.5
45	11
45	11.75
90	10
90	7.3
90	9.5
135	8
135	8.75
135	9
210	6.3
210	6
210	5.75

Using the value of the diffusion coefficients for compound I and tobramycin calculated above and the known molecular weight of tobramycin (MW 467.5 Da), obtain the molecular weight of the active ingredient of compound I.

Important to note: The values of D and T_c obtained above depend on the bacterial strain, media and incubation conditions. It is therefore essential that the experiments for the test antimicrobial compound and known molecular weight standard be done under identical conditions.

4.6.9 Solution to data analysis

For compound I

Slope of X^2 as a function of $\ln(C_0)$ for compound I (Figure 4.3).

Using linear regression, we get the slope of X^2 as a function of $\ln(C_0)$ (y = ax+ b).

Pre-incubation time T_c for compound I (Figure 4.3).

Using linear regression, the pre-incubation time (y-intercept) is determined as 301 ± 39 minutes.

From the above values we get the diffusion coefficient D of the compound I as 4.5 ± 0.8 X 10^{-6} cm^2/sec.

For Tobramycin

Slope of X^2 as a function of $\ln(C_0)$ for tobramycin (Figure 4.4).

Using linear regression, we get the slope of X^2 as a function of $\ln(C_0)$ (y = ax+ b).

Pre-incubation time T_c for tobramycin (Figure 4.4).

Using linear regression, the pre-incubation time (y-intercept) is determined as 260 ± 28 minutes.

From the above values we get the diffusion coefficient D of tobramycin as 2.9 ± 0.5 X 10^{-6} cm^2/sec.

Using $MW_I = MW_A(\frac{D_A}{D_I})^3$ and the known molecular weight of tobramycin as 467.5 Da, we get the molecular weight of the active ingredient of compound I as 128 ± 96 Da. This is consistent with the molecular weight of hydrogen peroxide which is 34 Da. Based on our module, we can conclude that the antimicrobial component is a small, low-molecular weight compound, approximately 32-224 Da in size.

4.6.10 Supplemental Videos

4.6.10.1 Preparation of broth media for bacterial growth

This video shows liquid LB media being prepared for bacterial growth. It was shown as part of the hands-on session since there were neither time nor facilities to prepare sterile media at the Hands-On School itself.

4.6.10.2 Preparation of solid media for bacterial growth

This video shows agar LB media being prepared for bacterial growth. It was shown as part of the hands-on session since there were neither time nor facilities to prepare sterile media at the Hands-On School itself.

4.6.10.3 Sterilization of tools

This video shows tools being sterilized. It was shown as part of the hands-on session since there were neither time nor facilities to sterilize tools at the Hands-on School itself.

4.6.10.4 Preparation of filter discs

This video shows filter discs being made and packaged for subsequent sterilization. It was shown as part of the hands-on session since there were neither time nor facilities to sterilize discs at the Hands-On School itself.

4.6.10.5 Preparation of bacterial strains for shipping

This video shows bacterial strains being prepared for shipping. This was not shown during the hands-on session but was available as a link through the handout.

4.6.10.6 Inoculating bacterial cultures

This video shows bacteria being inoculated for growth. It was shown as part of the hands-on session. Then the assistant instructor demonstrated inoculation in person, and then each participant inoculated bacteria.

4.6.10.7 Performing the disc diffusion assay

This video shows the disc diffusion assay being performed. It was shown as part of the hands-on session. It was shown as part of the hands-on session. Then the assistant instructor demonstrated the disc diffusion assay in person, and then each participant performed the assay.

4.6.10.8 Experiment to measure the slope of X^2 (square of the width of inhibition) as a function of $\ln(C_0)$

This video shows the experiment, based on the disc diffusion assay, which measures the relationship between the width of the zone of inhibition and the amount of inhibitory material deposited. First the instructor presented the analytical model, then this video shown during the hands-on session, and then

example data obtained from this experiment was made available to students for fitting to the model.

4.6.10.9 Experiment to measure pre-incubation time T_c

This video shows the experiment, based on the disc diffusion assay, which measures the critical pre-incubation time. First the instructor presented the analytical model, then this video was shown during the hands-on session, and then example data obtained from this experiment was made available to students for fitting to the model.

4.7 PARTICIPANT FEEDBACK

We did not conduct formal evaluations, but based on verbal feedback the participants found the module to be educational, scientifically challenging, engaging and interesting. As physical scientists, they had almost no prior familiarity with biological experiments, and none had ever performed the disc diffusion assay. They found the choice of the scientific problem, antibiotic resistance, a relevant, relatable issue and appreciated the ease of performing the disc diffusion assay, which helped sustain their interest and boost their confidence. As theoretical and quantitative scientists, almost all of them were familiar with the laws of diffusion and diffusion-based analytical models. However, several participants reported that they had never thought of applying these conventional physical concepts to a biological problem. Some participants also said that the module provoked them to think of biology as a quantitative discipline in contrast to standard school and undergraduate curricula, which often teach biology as a purely descriptive science.

Participant responses

“The session was very interesting. I have heard of antibiotic resistance and worked with analytical models, but never thought that I could merge the two by applying physics to study this problem” - Ph.D. candidate (Physics) from the Philippines

“This module was listed as my top choice as I have been offered a post-doc in a quantitative biology lab which works with yeast. This exercise has given me the confidence to work with biological organisms, and assured me that my scientific training has a place in biology” - Ph.D. (Mathematics) from Italy

“I appreciate the effort put in to make this module exciting and informative. I always thought of biology experiments as complicated and expensive, requiring extensive skill. I never thought I would perform a biological assay, much less one that was both time and cost-effective” - Ph.D. (Physics) and Government Scientist from Cameroon

“I am an advocate for open-source science in Mexico, and can see myself using this module as a teaching tool for school children in rural and peripheral parts of my country. However, given that I do have some basic biology experience, I would have liked to have actually performed the experiments to measure slope and critical time for the analytical model” - Ph.D. candidate and Synthetic Biologist from Mexic0

In one session, participants with no basic biology background had notable difficulty in understanding the science. This resulted in a substantial gap between their baseline knowledge and rudimentary concepts needed to understand this module. For example, one of the participants had never encountered the biological concept of a cell. While we did try to briefly address this lacuna in knowledge once we realized it, all the logical leaps that followed could not be explained in the limited time available. In subsequent implementations of this module, this could be overcome with a short, concise overview of basic biological concepts such as structure of a bacterial cell, bacterial growth and physiology, and cell death.

This was the first time this module was implemented as a science outreach tool. As a result, the logistics of executing the module in a resource-limited setting, such as shipping delays, a classroom and building not intended for biological work, and tailoring the program to suit the available budget, posed formidable challenges. Owing to this, we did not focus on conducting a systematic assessment of the impact of this module on the participants. In the future, we plan to incorporate an evaluation step into this module by implementing the use of pre- and post-session surveys (using brief questionnaires) to gain a quantitative estimate of the outcome of this module on participants' knowledge and attitudes about biophysical research. The questionnaire could be designed to measure not only understanding of the

specific material presented (*e.g.*, the problem of antibiotic resistance, potential modifications of the disc-diffusion assay, incorporating additional parameters into the analytical model) but also gauge changes in their perceptions of larger concepts such as application of quantitative techniques to biological data and use of interdisciplinary approaches to address scientific challenges.

4.8 DISCUSSION AND CONCLUSIONS

Taken together, the features of this hands-on module make it particularly suited for science outreach in resource-limited settings such as field areas, STEM camps, high-and middle-school programs, workshops, and laboratory training exercises. This is valuable not only to developing and emerging countries, but also to developed countries, where scarcity of science funding is constraining science education and outreach initiatives. Given the lack of structured training opportunities that bridge scientific fields, this module can provide valuable interdisciplinary research experience in these settings.

We thank the organizers of the Hands-on school (2014) held at Trieste, Italy. We are grateful to Anna Comel and Dr. Giannino Del Sal (Laboratorio Nazionale Consorzio Interuniversitario per le Biotecnologie and Department of Life Sciences, University of Trieste) for providing additional LB agar plates for our experiments. We thank Dr. Maria Liz Crespo (ICTP, Trieste) for her help with organization and procurement of chemicals.

Chapter 5: Overall Conclusions and Future Directions

5.1 POPULATION STRUCTURE IMPACTS THE GROWTH OF ANTIBIOTIC-RESISTANT MUTANTS

5.1.1 Overview of results

It has previously been shown using experimental techniques and mathematical models that spatial organization accelerates the development of antibiotic resistance in microbial populations [27, 28, 34]. However, the impact microbial population structure had not been explicitly addressed.

In Chapter 2, I began to investigate the impact of microbial population structure on the survival and growth of antibiotic-resistant mutants of *P. aeruginosa* [102]. In spatially-mixed systems, the survival of antibiotic-resistant mutants was seen to vary non-monotonically with increasing cell density, with impaired survival at high-cell densities. Further, the mutant colony frequency or the probability of antibiotic-resistant mutant survival decreased with increasing cell density. In spatially-structured systems, wild-type (WT) *P. aeruginosa* cells deposited on the filter disc produced inhibition of antibiotic-resistant mutant lawns in their vicinity, in the presence of aminoglycoside antibiotics. Using a diffusion-based analytical model, the inhibitory factor was determined to be a small, diffusible compound of low-molecular weight. A wide range of bacterial species including *S. aureus* and *E. coli* were found to produce inhibition. Production of

this IF was observed with growing cells, and in the presence of two different aminoglycoside antibiotics. However, the yeast strain *Saccharomyces* cerevisiae did not produce inhibition. On pH indicator agar containing bromthymol blue (BTB), deposition of bacterial strains resulted in a blue (alkaline) color change in the region of deposition. This alkaline change was observed for all bacterial strains that produced inhibition, and a correlation was observed between the width of the alkaline change and the width of inhibition. Deposition of *Saccharomyces cerevisiae* failed to produce this alkaline change, but instead produced a slightly acidic to no color change. All bacterial strains were grown overnight in Luria-Bertani medium, in which amino acids are the major source of carbon and nitrogen [153]. Breakdown of amino acids is known to produce alkaline by-products such as ammonia and amines [153]. The yeast strain *Saccharomyces cerevisiae* is incapable of using amino acids as the sole source of carbon, and hence was grown in Yeast-Peptone-Dextrose (YPD) medium, in which dextrose (a sugar) is the source of carbon [108]. Breakdown of sugars via fermentation produces acidic by-products. Exogenous alkaline compounds were seen to recapitulate this phenomenon of inhibition, notably ammonium hydroxide and sodium bicarbonate. Further, using an ion-selective electrode, we detected ammonia and or amine emission following deposition of *P. aeruginosa* cells on agar. This indicates that the IF is likely a native product of amino acid catabolism, likely ammonia or amines. These observations indicate that nutrient conditions can provide a switch to control inhibition. Using the bacterial strains *P.*

aeruginosa, *S. aureus*, and *E. coli* and the yeast strain *Saccharomyces cerevisiae*, this possibility was investigated. *P. aeruginosa*, *S. aureus*, and *E. coli* produced inhibition when grown in the presence of amino acids as the sole source of carbon, however, in the presence of amino acids and sugar carbon sources, *S. aureus*, and *E. coli* failed to produce inhibition. *P. aeruginosa* produced inhibition under both conditions, reflective of its inability to ferment sugars as a source of carbon. As expected, *Saccharomyces cerevisiae* grew poorly in the presence of amino acids alone, and also failed to produce inhibition under both conditions. Finally, it seems paradoxical that mutant cells are able to grow into high-density colonies on the plate without inhibiting themselves. To resolve this paradox, we examine the effect of spatial fluctuations in initial population density on the survival of resistant mutants. Guided by this model, we postulate that antibiotic-resistant mutants are able to grow into high-density colonies on antibiotic-containing agar because they are shielded from antibiotics by their WT neighbors.

My work opens the possibility that the impact of microbial population structure on antibiotic-resistant mutants could open the way for novel therapeutic approaches to tackle the rising threat of antibiotic resistance.

5.1.2 Future directions

There are several possible future studies arising from this work.

5.1.2.1 Population structure as a novel therapeutic approach

One approach towards further understanding the potential of these findings as a therapeutic strategy would be to artificially structure microbial communities using optical trapping [52]. Using this technique in a flow-cell system, we could create small-scale patterned microbial communities of varying cell density, spatial organization, and cell types. We could modulate the nutrient conditions available by changing the carbon sources, and the concentration of aminoglycoside in the system. This would further our understanding of the interplay of spatial structure and nutrient conditions on antibiotic-resistant mutant survival at much smaller spatial scales, which would more closely resemble microbial communities in nature, and also more closely resemble the biofilm phenotype.

This could pave the way for testing the impact of population structure using an *in vivo* infection model such as a murine acute or chronic wound infection. In this case, we could infect wounds with microbial populations that vary in composition, density, and metabolic capabilities. Following treatment with aminoglycosides and management of wound nutrient conditions, we could

assess the impact of population structure on the survival of antibiotic-resistant mutants in *vivo.*

Together, these insights will assess the feasibility of harnessing the therapeutic potential of population structure to target antibiotic-resistant mutants. This could lead to a new approach whereby we could engineer the population structure and nutrient availability at infection sites to enable bacteria inhibit the antibiotic-resistant mutants arising in the population. For example, for polymicrobial infections such as *P. aeruginosa* and *S. aureus* co-infections (as in chronic wounds), we could design a therapeutic approach that first eradicates *S. aureus*, which is capable of fermenting sugars and producing acidic by-products. This would prevent a major decrease in local pH at the infection site, and enable *P. aeruginosa* alkaline metabolic by-products to enhance the efficacy of aminoglycosides against antibiotic-resistant mutants. Another possible option in the case of post-surgical wound infections would be to irrigate the wound with a combined solution of antibiotic and an alkaline amino acid. This would permit infecting *P. aeruginosa* strain to utilize amino acids and produce alkaline by-products, which could enhance the efficacy of aminoglycosides. While these approaches hold promise, it is clear that more work needs to be done to fully understand the effects of local pH at wound infection sites. For example, increased pH early in treatment (>8.5) is associated with delayed wound healing, wounds that are too acidic are less likely to accept grafts [196].

5.1.2.2 Mutational resistance to aminoglycosides

While resistance to aminoglycoside antibiotics mediated by the production of aminoglycoside-modifying enzymes is a better understood mechanism, resistance conferred by single-nucleotide polymorphisms (SNPs) is less documented [85]. In this work, the spontaneously-generated antibiotic-resistant mutant sequenced had SNPs in EF-Tu, TrkH, and *phzD* [102]. We could further understand the mechanism of resistance by creating each of these individual mutations in a wild-type *P. aeruginosa* PA14 strain and testing the minimum inhibitory concentration to tobramycin for each of them. This would allow us to identify the mutation responsible for conferring resistance in these strains.

5.2 ASSESSMENT OF THE *IN VITRO* EFFICACY OF THE COMBINATION OF TOBRAMYCIN AND BICARBONATE AGAINST PLANKTONIC AND BIOFILM CELLS OF *P. AERUGINOSA*

5.2.1 Overview of results

My work in Chapter 2 showed that alkaline by-products of bacterial metabolism could enhance the efficacy of aminoglycoside antibiotics against antibiotic-resistant mutants of *P. aeruginosa.* The inhibitory factor mediating this effect is likely ammonia and/or amines, resulting from the catabolism of amino acids. Further, exogenous alkaline compounds such as sodium bicarbonate also produce this effect, indicating that the mechanism of inhibition is related to a pH change.

In Cystic Fibrosis (CF), a defect in the CFTR membrane protein leads to defective secretion of bicarbonate in airway epithelial cells. This results in decreased airway surface liquid (ASL) pH, which impairs function of innate antimicrobial factors. Restoration of ASL pH by aerosolization of sodium bicarbonate was seen to improve the activity of these factors [76]. In addition, aerosolized bicarbonate is being evaluated for its role in facilitating the unfolding and thinning of mucous, thereby increasing mucociliary clearance [77].

For *P. aeruginosa* infections, aminoglycosides, such as tobramycin, are the standard of care [104]. Long-term therapy and widespread usage has resulted in the development of resistance to this class of drugs. Further,

aminoglycosides cause severe toxic side effects [183]. Hence, developing treatment strategies to minimize the duration of treatment, therapeutic dosage, development of resistance while extending the lifetime of aminoglycoside usage is imperative.

In Chapter 3, I began to evaluate the effect of sodium bicarbonate in enhancing the activity of aminoglycosides. Using the standard microdilution checkerboard assay, I examined the effect of a combination of tobramycin (an aminoglycoside) and sodium bicarbonate on planktonic cells of *P. aeruginosa.* Briefly, I tested an array of different combinations of tobramycin and bicarbonate, in addition to their effects alone on the survival of planktonic *P. aeruginosa* cells. Isobologram analysis reveals that for planktonic cells of *P. aeruginosa*, the combination has a strong synergistic effect (ΣFIC index <0.5). This effect is seen for laboratory strains PAO1 and PA14, for four different spontaneously-generated antibiotic-resistant mutants and for clinical CF isolates (including mucoid, dwarf, and class phenotypes). Further analysis revealed that a synergistic effect was attained at a bicarbonate concentration as low as 5 mM (corresponding to a pH of 7.12 ± 0.07 in sterile Luria-Bertani medium). This synergy observed was also tested using time-kill assays. For all strains tested, time-kill analysis revealed a strong synergistic effect of the specific tobramycin-bicarbonate concentration tested. As expected with a synergistic combination, addition of bicarbonate was seen to reduce the concentration of tobramycin needed to eradicate planktonic

cells. It was also observed to significantly enhance the rate of killing of cells in comparison to inhibitory concentrations of tobramycin.

We next tested the effect of this synergy against biofilm cells of *P. aeruginosa.* Briefly, biofilms were grown on the bottom and sides of a microtiter dish for 24-hours. These pre-formed biofilms were then treated with different combinations of tobramycin and bicarbonate, in addition to each agent alone. After treatment, the biofilms were examined for metabolic activity using the XTT assay (in which a monotetrazolium salt is converted to the colored product formazan by metabolically-active cells). Based on our observations, the combination of tobramycin and bicarbonate was at best additive against biofilm cells of *P. aeruginosa*, and was antagonistic in most combinations.

To understand the mechanism of synergy of tobramycin and bicarbonate, we propose a model based on the entry of tobramycin into the bacterial cell. It is important to note that this model is speculative, and further work needs to be done to test it. Tobramycin is actively transported into the cell, and the process depends on the proton motive force (PMF) [87]. Based on this model, following its addition, bicarbonate (in the form of carbonic acid) traverses the outer membrane of the cell to reach the periplasmic space. In this intermembarne space, carbonic acid dissociates to release free bicarbonate and a hydrogen ion. The hydrogen ion joins the cloud of protons in the periplasmic space, which are pumped out during transport of electrons in the electron transport chain

(Complexes I-IV). The bicarbonate ion is transported across the inner membrane via an anion exchange transporter. In the cytosol, bicarbonate sequesters hydrogen ions to once again form carbonic acid. The combined effect is an increase in the pH in the periplasmic space and a decrease in the intracellular pH, which increases the inflow of hydrogen ions through ATP synthase (or complex V). This increases the proton motive force (PMF) and synthesis of ATP, both of which could thereby drive the entry of tobramycin into the cell. This model also explains the lack of synergy observed in biofilm cells, where the presence of extracellular polymer could prevent the diffusion of bicarbonate into the biofilm or regions of low pH (as known to exist in biofilms) [16] could neutralize bicarbonate before it reached cellular proximity.

Finally, we present a method for analyzing drug interactions using analytical dose-response surfaces, which examines drug combinations in greater detail than traditional methods [187]. Of its many advantages, this dose-response surface analysis allows us to more accurately estimate synergy regimes and make testable predictions of synergy combinations. Further, we analyze the difference of the measured response surface from that predicted by Loewe additivity [188], which provides a direct assessment of the degree of synergy and antagonism present.

Based on this work, another additional role for bicarbonate therapy in CF patients could be speculated, where it would augment the activity of tobramycin

therapy against planktonic *P. aeruginosa* infections. This approach would also hold potential in the management of non-CF infections such as acute burn and post-surgical wounds, sepsis, urinary tract infections, and meningitis [55]. Our results indicate that this approach may however not work if biofilms are already established, and further work is needed to understand and overcome this aspect.

5.2.2 Future directions

My work on the evaluation of tobramycin and bicarbonate has provided insights into the *in vitro* efficacy of this combination against planktonic and biofilm cells of *P. aeruginosa.* This work has implications in evaluating the efficacy of this combination as a therapeutic approach not only for early infections in CF patients but also for other acute *Pseudomonas* infections. There are several future studies to take this work forward into in possible therapeutic application.

5.2.2.1 Efficacy of the combination against planktonic cells in an vitro wound model

To estimate the potential of this combination *in vivo*, we could first test the effects of the combination of tobramycin and bicarbonate in medium containing serum. I did a few preliminary experiments by adding 25% serum to standard LB media, and observed that the synergistic effect did not persist. This could be due to the buffering effect of serum. To test this, I measured the pH of serum with different concentrations of bicarbonate and compared the values with those in LB

media with bicarbonate. Indeed, the corresponding pH in LB media with serum is lower than that in LB medium alone. In the future, we could adjust the concentration of bicarbonate in the LB + serum media to allow for a rise in pH, and test synergy with tobramycin at those concentrations. An even more-realistic *in vivo* scenario would be to test the effects of the combination in wound-like media. Our collaborators at the laboratory of Dr. Kendra Rumbaugh at Texas Tech Health Sciences Center, Lubbock Texas have developed in *in vitro* chronic biofilm wound infection model [193], incorporating bovine serum, laked horse blood, and Bolton broth. We could modify this using composition and model to simulate acute wound conditions to test the synergistic effect on planktonic cells. We could test for synergistic effects against planktonic cells using media containing a similar wound composition. To actually simulate an acute we could create artificial wounds suspended with planktonic cells containing blood, serum, and media. These wounds are then embedded into agar media in petri dishes. This would resemble an acute wound containing free-living cells surrounded by a wound bed. We could then treat these artificial ‘wounds’ with dressings of tobramycin, bicarbonate, and the combination and enumerate the colony forming units (CFUs). I did some preliminary work using this system (Figure 3.16), and while we observe a synergistic effect, we could test more combinations, and use different dressing materials.

5.2.2.2 Efficacy of the combination against acute infections in an vivo wound model

After *in vitro* testing in *in vivo*-like conditions, we could directly test the *in vivo* effects of the combination using a murine acute infection model [72]. Using an acute burn wound and sepsis model, we could treat mice with tobramycin, bicarbonate, and different combination at various time points following infection. CFUs measured from the wound site and from systemic organs such as the spleen, would provide an indication of the effect of the combination on local wound bacterial burden as well as dissemination to distant sites.

5.2.2.3 Testing the proposed model for the entry-based mechanism of synergy

We proposed a model to explain the mechanism of synergy based on bicarbonate increasing the PMF to drive the increased entry of tobramycin into the cell. This model is based on our observations of synergy and is supported by relevant literature. To directly test this model, we could use tobramycin conjugated with the fluorophore Texas Red. Tobramycin uptake by bacterial cells following addition of different concentration of bicarbonate could them be measured using FACS flow cytometer.

5.2.2.4 Testing the predictions of synergistic combinations from the dose-response surface analysis

Our analysis of tobramycin and bicarbonate interactions using the analytical dose-response surface method, allows us to identify synergistic combinations that were not directly tested in our assays for synergy. As a next step, we could test these predicted combinations for synergy. Identifying additional synergistic combinations would expand the potential of this combination as a therapeutic tool.

5.3 A LOW-COST, HANDS-ON MODULE TO PROVIDE INTERDISCIPLINARY RESEARCH EXPERIENCE

5.3.1 Overview of results

There is a paucity of structured training programs the bridge concepts across scientific fields. This lack is observed both in formal school and college curriculum, and science outreach initiatives. One possible way to overcome this is to design low-cost, educational modules that highlight the potential of interdisciplinary research. We had the opportunity to develop and conduct such a module for the Hands-On Research in Complex Systems School held at The Abdus Salam International Centre for Theoretical Physics (ICTP), Trieste, Italy, July 2014 [199]. For this we developed a low-cost module to characterize antimicrobial compounds using an interdisciplinary, biophysical approach. This module was a spin-off of the research project in Chapter 1. This module was conducted over a two-week period with three-hour laboratory session each day. Each session had a new set of 4-5 participants. Participants were mostly physical scientists or engineers with little or no biology expertise. The module was designed to have two components: a hands-on experimental component and analysis of data. The budget for the entire module for 14 days for 60 participants was $150.

The goal of our module was to test the antimicrobial efficacy of a range of compounds and apply the biological data to an analytical model to gain insights

into the physical characteristics of the active antimicrobial component. Participants tested three antimicrobial compounds ethanol (70%), hydrogen peroxide (30%), and eucalyptus oil for antimicrobial activity against *E. coli* DH5α using the disc-diffusion assay. They were then provided with biological data to apply to a diffusion-based analytical model to estimate the diffusion coefficient and molecular weight of the active antimicrobial component.

In our experience, the module was resource-efficient and reproducible, and engaged the interest of the participants. Additional resources such as budget and time will enable several future modifications of the module.

5.3.2 Future directions

5.3.2.1 Modifications of the module

As stated earlier, the entire budget for the hands-on session for 10 days for 60 participants was $150, which had to include consumables, equipment, and shipping costs. In addition, the hands-on school was conducted at the International Center for Theoretical Physics (ICTP), which did not have standard facilities to conduct biological experiments. For example, we had no access to an autoclave, incubator, or rotary shaker. However, if the facilities and resources are available, this basic experimental protocol could be advanced to achieve greater accuracy and resolution.

For junior biology researchers, the module can be expanded to study a wide-range of antimicrobial compounds, microbial competitive interactions, and prospecting for novel antibiotics. This includes testing well-known clinical antibiotics and a wide-range of biological extracts, and determining molecular weights. Using antibiotics, as test antimicrobial agents will further strengthen the association with antibiotic resistance. The module can also be adapted to a 'bioprospecting for antibiotics' exercise, used to compare efficacies of different local and indigenous medicinal extracts, and antibiotics form different commercial sources. This is particularly important in the context of developing countries, where antibiotics are often sold over-the-counter (OTC), resulting in a market of spurious antibiotics. We discussed with the participants' how the module could be adapted to compare antimicrobial efficacies of antibiotics from different commercial and distribution sources. In countries where local and indigenous compounds, such as eucalyptus oil, tea tree oil, or cinnamon bark oil, are used as medicinal remedies, an interesting exercise would be to use this module to test the antimicrobial efficacies of compounds obtained from different sources.

Additionally, the module can be adapted to test intra- and inter- species microbial competition by depositing one bacterial species or strain on the filter disc laid on a lawn of another bacterial species. The analytical model would provide additional insights into the active microbial product producing inhibition. The module could be extended to testing the effect of antimicrobial compounds

on mixed microbial communities, including both bacterial and fungal strains. If the requisite biosafety levels are met, these could be environmental communities such as in soil, water, and air, clinical specimens from nares or throat swabs, or mixed laboratory cultures.

The target audience for the outreach module we presented were scientists in physical and mathematical disciplines, mostly from the developing world and little to no experience with biology or with experiments in general. Thus, the biology presented in this module and the concept of using physical analysis to understand biology were largely new to them, but the modeling itself and fitting the model to data were more familiar concepts, quickly digested. For a different audience, with more biological background, this emphasis could be modified to focus on teaching physical concepts of diffusion and transport and to delve into least-squares linear fitting more deeply.

Subject to increased time and budget availability, technical modifications could also be included in the module. This could include the use of nonvolatile compounds and if available, an automated pipette could be used to deposit a defined volume of 10 μL on the filter disc, which would be soaked up by the filter disc avoiding any spillover. Alternatively, filter discs could be impregnated with a set amount of antimicrobial compound (diluted in a volatile solvent) and the solvent allowed to evaporate. The dry disc could then be placed on the plate using metal forceps. If available, bacterial cultures could be grown using an

incubator with well-controlled temperature and a rotary shaker. More hands-on experiments, including measurement of slope and critical time could be included.

5.3.2.2 The module as part of an interdisciplinary research curriculum

The Common Core is a set of academic standards in mathematics and language arts for grades K-12. In the USA, 43 states, the District of Columbia, four territories, and the Department of Defense Educational Activity have adopted the Common Core standards. The content of this module teaches concepts that are required in Common Core Mathematics standards for Algebra, Functions, and Modeling. The handout, along with additional reading, could be used to teach competencies required in the Language Arts standards for Literacy in Science & Technical Subjects.

Texas has not adopted the Common Core. Instead, it uses the Texas Essential Knowledge and Skills (TEKS) standards. The content of this module includes concepts required in the TEKS standards for Algebra I and II, Precalculus, Mathematical Models with Applications, Biology, Chemistry, and Physics.

Thus, the low cost and relative ease of performance of this module could make it suitable for adaption for use in high schools, either as a part of the normal instructional curriculum or as an outreach.

Additionally, the module could be expanded and subsequently included as a component of an undergraduate research curriculum or Freshman Research Initiative stream. It would provide hands-on experience in biology and application of biological data to an analytical model, as well as introduce concepts of antibiotic resistance, bioprospecting, biosafety, diffusion, and the relationship between diffusion coefficient and molecular weight.

5.4 FINAL DISCUSSION

With the rising trend of antibiotic resistance, the search for novel therapeutic approaches has gained significance. My work has determined that microbial population structure inhibits the survival and growth of antibiotic-resistant mutants of *P. aeruginosa*, in the presence of aminoglycoside antibiotics. This opens the possibility of designing treatment options that target or harness population structure to overcome antibiotic resistance. This effect was mediated by an alkaline product, which led me to test the effect of bicarbonate in conjunction with the antibiotic tobramycin against *P. aeruginosa*. This work determined that the combination of bicarbonate and tobramycin had a synergistic effect against planktonic *P. aeruginosa* cells. This lays the foundation for further studies to test the potential use of this combination against planktonic *P. aeruginosa* infections. Finally, my work has contributed a low-cost, hands-on, educational module to characterize antimicrobial compounds, which can be used to provide valuable interdisciplinary research experience.

Bibliography

1. Peters, B.M., et al., Polymicrobial interactions: impact on pathogenesis and human disease*. Clin Microbiol Rev*, 2012. **25**(1): p. 193-213.
2. Antonovics J, C.K., Schmidt J, The measurement of small-scale environmental heterogeneity using clonal transplants of Anthoxanthum odoratum and Danthonia spicata. *Oecologia.*, 1987. **71**: p. 601-607.
3. Bell, G., et al., The Spatial Structure of the Physical-Environment*. Oecologia*, 1993. **96**(1): p. 114-121.
4. Belgrano, A., et al., Spatial structure and ecological variation of meroplankton on the Belgian-Dutch coast of the North Sea*. Marine Ecology Progress Series*, 1995. **128**(1-3): p. 51-59.
5. Borcard, D., et al., Dissecting the spatial structure of ecological data at multiple scales*. Ecology*, 2004. **85**(7): p. 1826-1832.
6. Frenette, J.J., P. Massicotte, and J.F. Lapierre, Colorful Niches of Phytoplankton Shaped by the Spatial Connectivity in a Large River Ecosystem: A Riverscape Perspective*. Plos One*, 2012. **7**(4): e35891.
7. Ritz, K., et al., Spatial structure in soil chemical and microbiological properties in an upland grassland*. Fems Microbiology Ecology*, 2004. **49**(2): p. 191-205.
8. Meredith, L. (http://www.laurameredith.com/p=470). Accessed May 8, 2015.
9. Tolker-Nielsen, T. and S. Molin, Spatial organization of microbial biofilm communities*. Microbial Ecology*, 2000. **40**(2): p. 75-84.
10. Folkesson, A., et al., Adaptation of *Pseudomonas aeruginosa* to the cystic fibrosis airway: an evolutionary perspective*. Nat Rev Microbiol*, 2012. **10**(12): p. 841-51.
11. The Josephine Bay Paul Center (http://www.mbl.edu/). Accessed May 8, 2015.
12. Valm, A.M., et al., Systems-level analysis of microbial community organization through combinatorial labeling and spectral imaging*. Proc Natl Acad Sci U S A*, 2011. **108**(10): p. 4152-7.
13. Marsh, P.D., A. Moter, and D.A. Devine, Dental plaque biofilms: communities, conflict and control*. Periodontol 2000*, 2011. **55**(1): p. 16-35.
14. Davies, D.G., et al., The involvement of cell-to-cell signals in the development of a bacterial biofilm*. Science*, 1998. **280**(5361): p. 295-8.
15. Costerton, J.W., et al., Microbial biofilms*. Annu Rev Microbiol*, 1995. **49**: p. 711-45.
16. Wimpenny, J., W. Manz, and U. Szewzyk, Heterogeneity in biofilms*. FEMS Microbiol Rev*, 2000. **24**(5): p. 661-71.
17. Taylor, P.K., A.T. Yeung, and R.E. Hancock, Antibiotic resistance in *Pseudomonas aeruginosa* biofilms: towards the development of novel anti-biofilm therapies*. J Biotechnol*, 2014. **191**: p. 121-30.

18. Kryazhimskiy, S., G. Tkacik, and J.B. Plotkin, The dynamics of adaptation on correlated fitness landscapes. *Proc Natl Acad Sci U S A*, 2009. **106**(44): p. 18638-43.
19. HR, P., Sources, sinks and population dynamics. *Am Nat*, 1988. **132**: p. 652 – 661.
20. Holt, R.D. and M.S. Gaines, Analysis of Adaptation in Heterogeneous Landscapes - Implications for the Evolution of Fundamental Niches. *Evolutionary Ecology*, 1992. **6**(5): p. 433-447.
21. Perron, G.G., A. Gonzalez, and A. Buckling, Source-sink dynamics shape the evolution of antibiotic resistance and its pleiotropic fitness cost. *Proceedings of the Royal Society B-Biological Sciences*, 2007. **274**(1623): p. 2351-2356.
22. Kepler, T.B. and A.S. Perelson, Drug concentration heterogeneity facilitates the evolution of drug resistance. *Proceedings of the National Academy of Sciences of the United States of America*, 1998. **95**(20): p. 11514-11519.
23. Baquero, F. and M.C. Negri, Selective compartments for resistant microorganisms in antibiotic gradients. *Bioessays*, 1997. **19**(8): p. 731-736.
24. Nau, R., F. Sorgel, and H. Eiffert, Penetration of Drugs through the Blood-Cerebrospinal Fluid/Blood-Brain Barrier for Treatment of Central Nervous System Infections. *Clinical Microbiology Reviews*, 2010. **23**(4): p. 858-+.
25. Regamey, N., et al., Airway remodelling and its relationship to inflammation in cystic fibrosis. *Thorax*, 2011. **66**(7): p. 624-629.
26. Hoiby, N., et al., Antibiotic resistance of bacterial biofilms. *International Journal of Antimicrobial Agents*, 2010. **35**(4): p. 322-332.
27. Hermsen, R. and T. Hwa, Sources and sinks: a stochastic model of evolution in heterogeneous environments. *Phys Rev Lett*, 2010. **105**(24): p. 248104.
28. Greulich, P., B. Waclaw, and R.J. Allen, Mutational pathway determines whether drug gradients accelerate evolution of drug-resistant cells. *Phys Rev Lett*, 2012. **109**(8): p. 088101.
29. Hermsen, R., J.B. Deris, and T. Hwa, On the rapidity of antibiotic resistance evolution facilitated by a concentration gradient. *Proc Natl Acad Sci U S A*, 2012. **109**(27): p. 10775-80.
30. Muller, M., A. dela Pena, and H. Derendorf, Issues in pharmacokinetics and pharmacodynamics of anti-infective agents: distribution in tissue. *Antimicrob Agents Chemother*, 2004. **48**(5): p. 1441-53.
31. Wolf, L. and J.E. Barrick. Tracking winners and losers in *E. coli* evolution experiments. *Microbe Magazine,* 2012 (www.microbemagazine.org)
32. Palmer, A.C. and R. Kishony, Understanding, predicting and manipulating the genotypic evolution of antibiotic resistance. *Nat Rev Genet*, 2013. **14**(4): p. 243-8.

33. Wong, A., N. Rodrigue, and R. Kassen, Genomics of adaptation during experimental evolution of the opportunistic pathogen *Pseudomonas aeruginosa. PLoS Genet*, 2012. **8**(9): p. e1002928.
34. Zhang, Q., et al., Acceleration of emergence of bacterial antibiotic resistance in connected microenvironments. *Science*, 2011. **333**(6050): p. 1764-7.
35. Read, A.F. and L.H. Taylor, The ecology of genetically diverse infections. *Science*, 2001. **292**(5519): p. 1099-102.
36. Trosvik, P., et al., Characterizing mixed microbial population dynamics using time-series analysis. *ISME J*, 2008. **2**(7): p. 707-15.
37. Popat, R., S.A. Crusz, and S.P. Diggle, The social behaviours of bacterial pathogens. *Br Med Bull*, 2008. **87**: p. 63-75.
38. Ross-Gillespie, A., et al., Density dependence and cooperation: theory and a test with bacteria. *Evolution*, 2009. **63**(9): p. 2315-25.
39. Stephens, P.A. and W.J. Sutherland, Consequences of the Allee effect for behaviour, ecology and conservation. *Trends Ecol Evol*, 1999. **14**(10): p. 401-405.
40. Udekwu, K.I., et al., Functional relationship between bacterial cell density and the efficacy of antibiotics. *J Antimicrob Chemother*, 2009. **63**(4): p. 745-57.
41. Chiang, W.C., et al., Extracellular DNA shields against aminoglycosides in *Pseudomonas aeruginosa* biofilms. *Antimicrob Agents Chemother*, 2013. **57**(5): p. 2352-61.
42. Mah, T.F., et al., A genetic basis for *Pseudomonas aeruginosa* biofilm antibiotic resistance. *Nature*, 2003. **426**(6964): p. 306-10.
43. Diggle, S.P., et al., Cooperation and conflict in quorum-sensing bacterial populations. *Nature*, 2007. **450**(7168): p. 411-4.
44. Lemonnier, M., et al., The evolution of contact-dependent inhibition in non-growing populations of *Escherichia coli. Proc Biol Sci*, 2008. **275**(1630): p. 3-10.
45. Dunny, G.M., T.J. Brickman, and M. Dworkin, Multicellular behavior in bacteria: communication, cooperation, competition and cheating. *Bioessays*, 2008. **30**(4): p. 296-298.
46. Rosenberg, S.M., Life, Death, Differentiation, and the Multicellularity of Bacteria. *Plos Genetics*, 2009. **5**(3).
47. Kim, H.J., et al., Defined spatial structure stabilizes a synthetic multispecies bacterial community. *Proceedings of the National Academy of Sciences of the United States of America*, 2008. **105**(47): p. 18188-18193.
48. Basu, S., et al., A synthetic multicellular system for programmed pattern formation. *Nature*, 2005. **434**(7037): p. 1130-1134.

49. Nadell, C.D., K.R. Foster, and J.B. Xavier, Emergence of Spatial Structure in Cell Groups and the Evolution of Cooperation. *Plos Computational Biology*, 2010. **6**(3).
50. Lee, H.H., et al., Bacterial charity work leads to population-wide resistance. *Nature*, 2010. **467**(7311): p. 82-U113.
51. Connell, J.L., et al., 3D printing of microscopic bacterial communities. *Proceedings of the National Academy of Sciences of the United States of America*, 2013. **110**(46): p. 18380-18385.
52. Hutchison, J.B., et al., Single-Cell Control of Initial Spatial Structure in Biofilm Development Using Laser Trapping. *Langmuir*, 2014. **30**(15): p. 4522-4530.
53. Korgaonkar, A., et al., Community surveillance enhances *Pseudomonas aeruginosa* virulence during polymicrobial infection. *Proc Natl Acad Sci U S A*, 2013. **110**(3): p. 1059-64.
54. Korgaonkar, A.K. and M. Whiteley, *Pseudomonas aeruginosa* enhances production of an antimicrobial in response to N-acetylglucosamine and peptidoglycan. *J Bacteriol*, 2011. **193**(4): p. 909-17.
55. Bodey, G.P., et al., Infections caused by *Pseudomonas aeruginosa. Rev Infect Dis*, 1983. **5**(2): p. 279-313.
56. Quick, J., et al., Seeking the source of *Pseudomonas aeruginosa* infections in a recently opened hospital: an observational study using whole-genome sequencing. *BMJ Open*, 2014. **4**(11): p. e006278.
57. Lister, P.D., D.J. Wolter, and N.D. Hanson, Antibacterial-resistant *Pseudomonas aeruginosa*: clinical impact and complex regulation of chromosomally encoded resistance mechanisms. *Clin Microbiol Rev*, 2009. **22**(4): p. 582-610.
58. CDC Antibiotic Resistance Threat Report, 2013. (www.cdc.gov/drugresistance/threat-report-2013/). Accessed May 8, 2015.
59. Aloush, V., et al., Multidrug-resistant *Pseudomonas aeruginosa*: risk factors and clinical impact. *Antimicrob Agents Chemother*, 2006. **50**(1): p. 43-8.
60. CDC MMWR, 2009. (http://www.cdc.gov/mmwr/). Accessed May 8, 2015.
61. Hirsch, E.B. and V.H. Tam, Impact of multidrug-resistant *Pseudomonas aeruginosa* infection on patient outcomes. *Expert Rev Pharmacoecon Outcomes Res*, 2010. **10**(4): p. 441-51.
62. Sharma, G., et al., *Pseudomonas aeruginosa* biofilm: potential therapeutic targets. *Biologicals*, 2014. **42**(1): p. 1-7.
63. de Kievit, T.R., Quorum sensing in *Pseudomonas aeruginosa* biofilms. *Environ Microbiol*, 2009. **11**(2): p. 279-88.
64. Sutherland, I.W., The biofilm matrix--an immobilized but dynamic microbial environment. *Trends Microbiol*, 2001. **9**(5): p. 222-7.

65. Klausen, M., et al., Biofilm formation by *Pseudomonas aeruginosa* wild type, flagella and type IV pili mutants. *Mol Microbiol*, 2003. **48**(6): p. 1511-24.
66. Workentine, M. and M.G. Surette, Complex *Pseudomonas* population structure in cystic fibrosis airway infections. *Am J Respir Crit Care Med*, 2011. **183**(12): p. 1581-3.
67. Mowat, E., et al., *Pseudomonas aeruginosa* population diversity and turnover in cystic fibrosis chronic infections. *Am J Respir Crit Care Med*, 2011. **183**(12): p. 1674-9.
68. Stewart, P.S. and M.J. Franklin, Physiological heterogeneity in biofilms. *Nat Rev Microbiol*, 2008. **6**(3): p. 199-210.
69. LaBauve, A.E. and M.J. Wargo, Growth and laboratory maintenance of *Pseudomonas aeruginosa*. *Curr Protoc Microbiol*, 2012. **Chapter 6**: p. Unit 6E 1.
70. Stover, C.K., et al., Complete genome sequence of *Pseudomonas aeruginosa* PAO1, an opportunistic pathogen. *Nature*, 2000. **406**(6799): p. 959-64.
71. Liberati, N.T., et al., An ordered, nonredundant library of *Pseudomonas aeruginosa* strain PA14 transposon insertion mutants. *Proc Natl Acad Sci U S A*, 2006. **103**(8): p. 2833-8.
72. Turner, K.H., et al., Requirements for *Pseudomonas aeruginosa* acute burn and chronic surgical wound infection. *PLoS Genet*, 2014. **10**(7): p. e1004518.
73. Cystic Fibrosis Foundation (http://www.cff.org/). Accessed May 8, 2015.
74. Davidson, D.J. and D.J. Porteous, Genetics and pulmonary medicine. 1. The genetics of cystic fibrosis lung disease. *Thorax*, 1998. **53**(5): p. 389-97.
75. Quinton, P.M., Cystic fibrosis: impaired bicarbonate secretion and mucoviscidosis. *Lancet*, 2008. **372**(9636): p. 415-7.
76. Pezzulo, A.A., et al., Reduced airway surface pH impairs bacterial killing in the porcine cystic fibrosis lung. *Nature*, 2012. **487**(7405): p. 109-13.
77. Pier, G.B., The challenges and promises of new therapies for cystic fibrosis. *J Exp Med*, 2012. **209**(7): p. 1235-9.
78. Davies, J.C., *Pseudomonas aeruginosa* in cystic fibrosis: pathogenesis and persistence. *Paediatr Respir Rev*, 2002. **3**(2): p. 128-34.
79. Hentzer, M., et al., Alginate overproduction affects *Pseudomonas aeruginosa* biofilm structure and function. *J Bacteriol*, 2001. **183**(18): p. 5395-401.
80. Tang, A.C., et al., Current concepts: host-pathogen interactions in cystic fibrosis airways disease. *Eur Respir Rev*, 2014. **23**(133): p. 320-32.
81. Fazli, M., et al., Nonrandom distribution of *Pseudomonas aeruginosa* and *Staphylococcus aureus* in chronic wounds. *J Clin Microbiol*, 2009. **47**(12): p. 4084-9.

82. Furukawa, S., S.L. Kuchma, and G.A. O'Toole, Keeping their options open: acute versus persistent infections. *J Bacteriol*, 2006. **188**(4): p. 1211-7.
83. Lambert, P.A., Mechanisms of antibiotic resistance in *Pseudomonas aeruginosa*. *J R Soc Med*, 2002. **95(**Suppl 41): p. 22-6.
84. Kanj, S.S. and Z.A. Kanafani, Current concepts in antimicrobial therapy against resistant gram-negative organisms: extended-spectrum beta-lactamase-producing Enterobacteriaceae, carbapenem-resistant Enterobacteriaceae, and multidrug-resistant *Pseudomonas aeruginosa*. *Mayo Clin Proc*, 2011. **86**(3): p. 250-9.
85. Kotra, L.P., J. Haddad, and S. Mobashery, Aminoglycosides: perspectives on mechanisms of action and resistance and strategies to counter resistance. *Antimicrob Agents Chemother*, 2000. **44**(12): p. 3249-56.
86. Borovinskaya, M.A., et al., Structural basis for aminoglycoside inhibition of bacterial ribosome recycling. *Nat Struct Mol Biol*, 2007. **14**(8): p. 727-32.
87. Taber, H.W., et al., Bacterial uptake of aminoglycoside antibiotics. *Microbiol Rev*, 1987. **51**(4): p. 439-57.
88. Lewis, K., Riddle of biofilm resistance. *Antimicrob Agents Chemother*, 2001. **45**(4): p. 999-1007.
89. Lewis, K., Multidrug tolerance of biofilms and persister cells. *Curr Top Microbiol Immunol*, 2008. **322**: p. 107-31.
90. Williamson, K.S., et al., Heterogeneity in *Pseudomonas aeruginosa* biofilms includes expression of ribosome hibernation factors in the antibiotic-tolerant subpopulation and hypoxia-induced stress response in the metabolically active population. *J Bacteriol*, 2012. **194**(8): p. 2062-73.
91. Sherrard, L.J., M.M. Tunney, and J.S. Elborn, Antimicrobial resistance in the respiratory microbiota of people with cystic fibrosis. *Lancet*, 2014. **384**(9944): p. 703-13.
92. Bridging Disciplines in the Brain, B., and Clinical Sciences. In: Pellmar TC, Eisenberg L, editors. Institute of Medicine (US) Committee on Building Bridges in the Brain, Behavioral, and Clinical Sciences. Washington (DC): National Academies Press (US). 2000: p. 15-22.
93. Bridging Disciplines in the Brain, B., and Clinical Sciences. In: Pellmar TC, Eisenberg L, editors. Institute of Medicine (US) Committee on Building Bridges in the Brain, Behavioral, and Clinical Sciences. Washington (DC): National Academies Press (US). , 2000: p. 41-53.
94. Bridging Disciplines in the Brain, B., and Clinical Sciences. In: Pellmar TC, Eisenberg L, editors. Institute of Medicine (US) Committee on Building Bridges in the Brain, Behavioral, and Clinical Sciences. Washington (DC): National Academies Press (US). 2000: p. 99-107.
95. Martino, R.L., The importance of multidisciplinary teams in a large biomedical research program. *Proceedings of the 26th Annual*

International Conference of the Ieee Engineering in Medicine and Biology Society, Vols 1-7, 2004. **26**: p. 5188-5191.
96. J., G., The benefits of interdisciplinary research: our experience with pathogen bioinformatics. Science Career Magazine. 2003.
97. R Development Core Team (2008). R: A language and environment for statistical computing. R Foundation for Statistical Computing, V., Austria. ISBN 3-900051-07-0. .
98. Davey O, S.J., Nathwani D., Overview of strategies for overcoming the challenge of antimicrobial resistance*. Expert. Rev. Clin. Phamacol.* , 2010. **3**: p. 667-686.
99. Li, K., et al., Analyses of the microbial diversity across the human microbiome*. PLoS One*, 2012. **7**(6): p. e32118.
100. Delhaes, L., et al., The airway microbiota in cystic fibrosis: a complex fungal and bacterial community--implications for therapeutic management*. PLoS One*, 2012. **7**(4): p. e36313.
101. Eng, R.H., S.M. Smith, and C. Cherubin, Inoculum effect of new beta-lactam antibiotics on *Pseudomonas aeruginosa. Antimicrob Agents Chemother*, 1984. **26**(1): p. 42-7.
102. Kaushik, K.S., et al., The spatial profiles and metabolic capabilities of microbial populations impact the growth of antibiotic-resistant mutants of *P. aeruginosa. J Roy Soc Interface* 2015. **12**: 20150018.
103. Geller, D.E., et al., Pharmacokinetics and bioavailability of aerosolized tobramycin in cystic fibrosis*. Chest*, 2002. **122**(1): p. 219-26.
104. Gonzalez, L.S., 3rd and J.P. Spencer, Aminoglycosides: a practical review*. Am Fam Physician*, 1998. **58**(8): p. 1811-20.
105. Huse, H.K., et al., Parallel evolution in *Pseudomonas aeruginosa* over 39,000 generations in vivo*. mBio*, 2010. **1**(4): e00199-10.
106. Cui, L., et al., Contribution of a thickened cell wall and its glutamine nonamidated component to the vancomycin resistance expressed by *Staphylococcus aureus* Mu50*. Antimicrob Agents Chemother*, 2000. **44**(9): p. 2276-85.
107. Hibbing, M.E., et al., Bacterial competition: surviving and thriving in the microbial jungle*. Nat Rev Microbiol*, 2010. **8**(1): p. 15-25.
108. Treco, D.A. and F. Winston, Growth and manipulation of yeast*. Curr Protoc Mol Biol*, 2008. **Chapter 13**: p. Unit 13 2.
109. CLSI, Performance standards for antimicrobial susceptibility testing. M100-S20 CLSI, Wayne, PA.
110. Abramoff M.D., P.J. Magalhaes, and S. J. Ram, Image Processing with ImageJ. *Biophotonics International*, 2004. **11**: p. 36-42.
111. Wu X, G.Y., Wei G. , Theoretical equations for agar-diffusion bioassay. *Ind. Eng. Chem. Res* 1990. **29**(1731-4).

112. Pope, C.F., et al., A practical guide to measuring mutation rates in antibiotic resistance*. Antimicrob Agents Chemother*, 2008. **52**(4): p. 1209-14.
113. Kirby WMM, Y.G., Sundsted KS, Warren JH. Antibiotics. Annu. , Clinical usefulness of a single disc method for antibiotic sensitivity testing. *. Antibiotics. Annu.* , 1957. **1956-1957**: p. 892-7.
114. Hayes, C.S., S.K. Aoki, and D.A. Low, Bacterial contact-dependent delivery systems*. Annu Rev Genet*, 2010. **44**: p. 71-90.
115. Poole, S.J., et al., Identification of functional toxin/immunity genes linked to contact-dependent growth inhibition (CDI) and rearrangement hotspot (Rhs) systems*. PLoS Genet*, 2011. **7**(8): p. e1002217.
116. Sawant, A.A., et al., Proximity-dependent inhibition in *Escherichia coli* isolates from cattle*. Appl Environ Microbiol*, 2011. **77**(7): p. 2345-51.
117. Eberhart, L.J., et al., Characterization of a novel microcin that kills enterohemorrhagic *Escherichia coli* O157:H7 and O26*. Appl Environ Microbiol*, 2012. **78**(18): p. 6592-9.
118. Yeung, A.T., et al., Swarming of *Pseudomonas aeruginosa* is controlled by a broad spectrum of transcriptional regulators, including MetR*. J Bacteriol*, 2009. **191**(18): p. 5592-602.
119. Frisk, A., et al., Identification and functional characterization of flgM, a gene encoding the anti-sigma 28 factor in *Pseudomonas aeruginosa. J Bacteriol*, 2002. **184**(6): p. 1514-21.
120. Starnbach, M.N. and S. Lory, The fliA (rpoF) gene of *Pseudomonas aeruginosa* encodes an alternative sigma factor required for flagellin synthesis*. Mol Microbiol*, 1992. **6**(4): p. 459-69.
121. Comolli, J.C., et al., *Pseudomonas aeruginosa* gene products PilT and PilU are required for cytotoxicity in vitro and virulence in a mouse model of acute pneumonia*. Infect Immun*, 1999. **67**(7): p. 3625-30.
122. Rashid, M.H. and A. Kornberg, Inorganic polyphosphate is needed for swimming, swarming, and twitching motilities of *Pseudomonas aeruginosa. Proc Natl Acad Sci U S A*, 2000. **97**(9): p. 4885-90.
123. Murray, T.S. and B.I. Kazmierczak, *Pseudomonas aeruginosa* exhibits sliding motility in the absence of type IV pili and flagella*. J Bacteriol*, 2008. **190**(8): p. 2700-8.
124. Murray, T.S. and B.I. Kazmierczak, FlhF is required for swimming and swarming in *Pseudomonas aeruginosa. J Bacteriol*, 2006. **188**(19): p. 6995-7004.
125. Kohler, T., et al., Swarming of *Pseudomonas aeruginosa* is dependent on cell-to-cell signaling and requires flagella and pili*. J Bacteriol*, 2000. **182**(21): p. 5990-6.
126. Semmler, A.B., C.B. Whitchurch, and J.S. Mattick, A re-examination of twitching motility in *Pseudomonas aeruginosa. Microbiology*, 1999. **145 (10)**: p. 2863-73.

127. Hill HW, E.J., Report on Brooklyn water supply. . 1897: p. 164-169.
128. Jordan EO, I.E., Notes on bacterial water analysis, public health papers and reports. . *Amer. Pub. Health. Ass'n.*, 1899. 25564-9.
129. Breed RS, D.W., The number of colonies allowable on satisfactory agar plates. . 1916. **1**(321-331).
130. Smith, V.H., Effects of resource supplies on the structure and function of microbial communities*. Antonie Van Leeuwenhoek*, 2002. **81**(1-4): p. 99-106.
131. Brand YM, B.C., The pyocins of *Pseudomonas aeruginosa. Biochimie*, 2002. **84**: p. 499-510.
132. Matsui, H., et al., Regulation of pyocin genes in *Pseudomonas aeruginosa* by positive (prtN) and negative (prtR) regulatory genes*. J Bacteriol*, 1993. **175**(5): p. 1257-63.
133. Schauder, S. and B.L. Bassler, The languages of bacteria*. Genes Dev*, 2001. **15**(12): p. 1468-80.
134. Venturi, V., Regulation of quorum sensing in *Pseudomonas. FEMS Microbiol Rev*, 2006. **30**(2): p. 274-91.
135. Nelson, L.K., et al., *Pseudomonas aeruginosa* las and rhl quorum-sensing systems are important for infection and inflammation in a rat prostatitis model*. Microbiology*, 2009. **155**(Pt 8): p. 2612-9.
136. D'Autreaux, B. and M.B. Toledano, ROS as signalling molecules: mechanisms that generate specificity in ROS homeostasis*. Nat Rev Mol Cell Biol*, 2007. **8**(10): p. 813-24.
137. Brynildsen, M.P., et al., Potentiating antibacterial activity by predictably enhancing endogenous microbial ROS production*. Nat Biotechnol*, 2013. **31**(2): p. 160-5.
138. George, P., Reaction between catalase and hydrogen peroxide*. Nature*, 1947. **159**(4054): p. 41-3.
139. Lumppio, H.L., et al., Rubrerythrin and rubredoxin oxidoreductase in Desulfovibrio vulgaris: a novel oxidative stress protection system*. J Bacteriol*, 2001. **183**(1): p. 101-8.
140. Dietrich, L.E., et al., Redox-active antibiotics control gene expression and community behavior in divergent bacteria*. Science*, 2008. **321**(5893): p. 1203-6.
141. Wang, Y., S.E. Kern, and D.K. Newman, Endogenous phenazine antibiotics promote anaerobic survival of *Pseudomonas aeruginosa* via extracellular electron transfer*. J Bacteriol*, 2010. **192**(1): p. 365-9.
142. Recinos, D.A., et al., Redundant phenazine operons in *Pseudomonas aeruginosa* exhibit environment-dependent expression and differential roles in pathogenicity*. Proc Natl Acad Sci U S A*, 2012. **109**(47): p. 19420-5.

143. Price-Whelan, A., L.E. Dietrich, and D.K. Newman, Rethinking 'secondary' metabolism: physiological roles for phenazine antibiotics. *Nat Chem Biol*, 2006. **2**(2): p. 71-8.
144. Das, T. and M. Manefield, Pyocyanin promotes extracellular DNA release in *Pseudomonas aeruginosa. PLoS One*, 2012. **7**(10): p. e46718.
145. Das, T. and M. Manefield, Phenazine production enhances extracellular DNA release via hydrogen peroxide generation in *Pseudomonas aeruginosa. Commun Integr Biol*, 2013. **6**(3): p. e23570.
146. Goebel-Stengel M, S.A., Tache Y, Reeve JR, Jr. , The importance of using optimal plastic and glassware in studies involving peptides. *Anal. Biochem.*, 2011. **414**(38-46).
147. Cooper, K.E., Theory of antibiotic inhibition zones in agar media. *Nature*, 1955. **176**(4480): p. 510-1.
148. Finn, R.K., Theory of agar diffusion methods for bioassay. *Anal. Chem.*, 1959. **31**(975-977).
149. Linton, A.H., Influence of inoculum size on antibiotic assays by the agar diffusion technique with Klebsiella pneumoniae and streptomycin. *J Bacteriol*, 1958. **76**(1): p. 94-103.
150. Baldan, R., et al., Adaptation of *Pseudomonas aeruginosa* in Cystic Fibrosis airways influences virulence of *Staphylococcus aureus* in vitro and murine models of co-infection. *PLoS One*, 2014. **9**(3): p. e89614.
151. Kurz, C.L., et al., Virulence factors of the human opportunistic pathogen *Serratia marcescens* identified by in vivo screening. *EMBO J*, 2003. **22**(7): p. 1451-60.
152. Eberl, L. and B. Tummler, *Pseudomonas aeruginosa* and *Burkholderia cepacia* in cystic fibrosis: genome evolution, interactions and adaptation. *Int J Med Microbiol*, 2004. **294**(2-3): p. 123-31.
153. Sezonov, G., D. Joseleau-Petit, and R. D'Ari, *Escherichia coli* physiology in Luria-Bertani broth. *J Bacteriol*, 2007. **189**(23): p. 8746-9.
154. Quinn, R.A., et al., Biogeochemical forces shape the composition and physiology of polymicrobial communities in the cystic fibrosis lung. *MBio*, 2014. **5**(2): p. e00956-13.
155. Pronk, J.T., H. Yde Steensma, and J.P. Van Dijken, Pyruvate metabolism in *Saccharomyces cerevisiae. Yeast*, 1996. **12**(16): p. 1607-33.
156. Moriarty, T.F., J.S. Elborn, and M.M. Tunney, Effect of pH on the antimicrobial susceptibility of planktonic and biofilm-grown clinical *Pseudomonas aeruginosa* isolates. *Br J Biomed Sci*, 2007. **64**(3): p. 101-4.
157. Lebeaux, D., et al., pH-mediated potentiation of aminoglycosides kills bacterial persisters and eradicates in vivo biofilms. *J Infect Dis*, 2014. **210**(9): p. 1357-66.

158. Frainmow HS, G.J., Leviton IM, Dougherty TJ, Miller MH., Tobramycin uptake in *Escherichia coli* is driven by either electrical potential or ATP. *J. Bacteriol*, 1991. **173**: p. 2800-2808. .
159. Gale, E.F., The production of amines by bacteria: The production of putrescine from l(+)-arginine by *Bacterium coli* in symbiosis with *Streptococcus faecalis. Biochem J*, 1940. **34**(6): p. 853-7.
160. Palkova, Z., et al., Ammonia mediates communication between yeast colonies*. Nature*, 1997. **390**(6659): p. 532-6.
161. Weise, T., M. Kai, and B. Piechulla, Bacterial ammonia causes significant plant growth inhibition*. PLoS One*, 2013. **8**(5): p. e63538.
162. Kim, Y.C., et al., Effects of polyamines on contractility of guinea-pig gastric smooth muscle*. J Korean Med Sci*, 2007. **22**(1): p. 48-56.
163. Cepl, J., et al., Ammonia produced by bacterial colonies promotes growth of ampicillin-sensitive Serratia sp. by means of antibiotic inactivation*. FEMS Microbiol Lett*, 2014. **354**(2): p. 126-32.
164. Bernier, S.P., et al., Biogenic ammonia modifies antibiotic resistance at a distance in physically separated bacteria*. Mol Microbiol*, 2011. **81**(3): p. 705-16.
165. Letoffe, S., et al., Aerial exposure to the bacterial volatile compound trimethylamine modifies antibiotic resistance of physically separated bacteria by raising culture medium pH*. MBio*, 2014. **5**(1): p. e00944-13.
166. Damper, P.D. and W. Epstein, Role of the membrane potential in bacterial resistance to aminoglycoside antibiotics*. Antimicrob Agents Chemother*, 1981. **20**(6): p. 803-8.
167. Aleksandrov, A. and M. Field, Mechanism of activation of elongation factor Tu by ribosome: catalytic histidine activates GTP by protonation*. RNA*, 2013. **19**(9): p. 1218-25.
168. Scarano, G., et al., Relevance of histidine-84 in the elongation factor Tu GTPase activity and in poly(Phe) synthesis: its substitution by glutamine and alanine*. FEBS Lett*, 1995. **365**(2-3): p. 214-8.
169. Zeidler, W., et al., Site-directed mutagenesis of Thermus thermophilus elongation factor Tu. Replacement of His85, Asp81 and Arg300*. Eur J Biochem*, 1995. **229**(3): p. 596-604.
170. Dinman, J.D. and T.G. Kinzy, Translational misreading: mutations in translation elongation factor 1alpha differentially affect programmed ribosomal frameshifting and drug sensitivity*. RNA*, 1997. **3**(8): p. 870-81.
171. Lazar, V., et al., Bacterial evolution of antibiotic hypersensitivity*. Mol Syst Biol*, 2013. **9**: p. 700.
172. Johanson, U. and D. Hughes, Fusidic acid-resistant mutants define three regions in elongation factor G of Salmonella typhimurium*. Gene*, 1994. **143**(1): p. 55-9.

173. Schlosser, A., et al., TrkH and its homolog, TrkG, determine the specificity and kinetics of cation transport by the Trk system of *Escherichia coli. J Bacteriol*, 1995. **177**(7): p. 1908-10.
174. Gallagher, L.A., J. Shendure, and C. Manoil, Genome-scale identification of resistance functions in *Pseudomonas aeruginosa* using Tn-seq*. MBio*, 2011. **2**(1): p. e00315-10.
175. Castaneda-Garcia, A., T.T. Do, and J. Blazquez, The K+ uptake regulator TrkA controls membrane potential, pH homeostasis and multidrug susceptibility in Mycobacterium smegmatis*. J Antimicrob Chemother*, 2011. **66**(7): p. 1489-98.
176. Fraimow, H.S., et al., Tobramycin uptake in *Escherichia coli* is driven by either electrical potential or ATP*. J Bacteriol*, 1991. **173**(9): p. 2800-8.
177. Palmer, K.L., L.M. Aye, and M. Whiteley, Nutritional cues control *Pseudomonas aeruginosa* multicellular behavior in cystic fibrosis sputum*. J Bacteriol*, 2007. **189**(22): p. 8079-87.
178. Thomas, S.R., et al., Increased sputum amino acid concentrations and auxotrophy of *Pseudomonas aeruginosa* in severe cystic fibrosis lung disease*. Thorax*, 2000. **55**(9): p. 795-7.
179. Tate, S., et al., Airways in cystic fibrosis are acidified: detection by exhaled breath condensate*. Thorax*, 2002. **57**(11): p. 926-9.
180. Levy, S.B., Factors impacting the problem of antibiotic resistance. *J Antimicrob Chemother,* 2002. **49**: p. 25-30.
181. Serra, R., et al., Chronic wound infections: the role of *Pseudomonas aeruginosa* and *Staphylococcus aureus*. *Expert Rev Anti Infect Ther,* 2013. **13**(5): p. 605-613.
182. Ratjen, F., Brockhaus, F, and Angyalosi, G, Aminoglycoside therapy against *Pseudomonas aeruginosa* in cystic fibrosis: A review. *J Cystic Fibros,* 2009. **8**(6): p. 361-9.
183. Prayle, A., et al., Side effects of aminoglycosides on the kidney, ear and balance in cystic fibrosis. *Thorax,* 2010. **65**: p. 654-8.
184. Sheppard, D.N. and M.J. Welsh, Structure and function of the CFTR chloride channel. *Physiol Rev,* 1999. **79**(1 Suppl): p. S23-45.
185. Tang, L., Fatehi, M, and Lindsell, P, Mechanism of direct bicarbonate transport by the CFTR anion channel. *J Cystic Fibros,* 2009. **8**(2): p. 115-21.
186. Hanson, G.C., Sparkling water - bicarbonate for the cervix and cystic fibrosis. *J Physiol,* 2010. **588**(Pt 15): p. 2685.
187. Tallarida, R.J., An overview of drug combination analysis with isobolograms. *J Pharmacol Exp Ther,* 2006. **319**(1): p. 1-7.

188. Loewe, S., The problem of synergism and antagonism of combined drugs. *Arzneimittelforschung,* 1953. **319**(3): p. 285-90.
189. Hsieh, M., et al., Synergy assessed by checkerboard: a critical analysis. *Diagn Microbiol Infect Dis,* 1993. **16**: p. 343-9.
190. Hall, F., Middleton, R.F, and Westmacott, D, The fractional inhibitory concentration (FIC) index as a meausre of synergy. *J Antimicrob Chemother,* 1983. **11**(5): p. 427-33.
191. Sabaeifard, P., et al., Optimization of tetrazolium salt assay for *Pseudomonas aeruginosa* biofilm using microtiter plate method. *J Microbiol Methods,* 2014. **105**: p. 134-40.
192. O'Toole, G.A., Microtiter dish biofilm formation assay. *J Vis Exp,* 2011. **47**: p. 2437.
193. DeLeon, S., et al., Synergistic interactions of *Pseudomonas aeruginosa* and *Staphylococcus aureus* in an In vitro Wound model. *Infect Immun,* 2014. (Published ahead of print).
194. Meletiadis, J., et al., Defining fractional inhibitory concentration index cutoffs for additive interactions based on self-drug additive combinations, Monte Carlo simulations analysis, and *In Vitro-In Vivo* correlation data for antifungal drug combinations against *Aspergillus fumigatus*. *Antimicrob Agents Chemother,* 2010. **54** (2): p. 602-9.
195. Thomassen, M.J. and C.A. Demko, Serum bactericidal effect on *Pseudomonas aeruginosa* isolates from cystic fibrosis patients. *Infect Immun,* 1981. **33**(2): p. 512-8.
196. Watters, C., Yuan, T.T, and K.P. Rumbaugh, Benefecial and deleterious bacterial-host interactions in chronic wound pathophysiology. *Chronic Wound Care Management and Research,* 2015. **2**: p. 53-62.
197. Kaushik, K.S., et al., A low-cost, hands-on module to characterize antimicrobial compounds using an interdisciplinary, biophysical approach. *PLoS Biol,* 2014. **13**(1): e1002044.
198. Luzhetskyy, A., Pelzer, S., and A. Bechthold, The future of natural products as a source of new antibiotics. *Curr Opin Invest Drugs*, 2007. 8: p. 608-13.
199. Hands-On Research School in Complex Systems. (http://handsonresearch.org/). Accessed 2 September 2014.
200. Center for Disease Control and Prevention, Biological Risk Assessment. (http://www.cdc.gov/biosafety/publications/bmbl5/bmbl5_sect_ii.pdf). Accessed 2 September 2014.

201. Hendry, E.R., et al., Antimicrobial efficacy of eucalyptus oil and 1,8 – cineole alone and in combination with chlorhexidine digluconate against microorganisms grown in planktonic and biofilm cultures. *J Antimicrob Chemother*, 2009. **64**: p. 1219-25.
202. McDonnell, G. and A.D. Russell, Antiseptics and disinfectants: activity, action and resistance. *Clin Microbiol Rev*, 1999. **12**: p. 147-179.
203. Center for Disease Control and Prevention, Guidelines for disinfection and sterilization in healthcare facilities, 2008. (http://www.cdc.gov/hicpac/pdf/guidelines/Disinfection_Nov_2008.pdf). Accessed 5 September 2014.
204. Edward, J.T., Molecular volumes and the Stokes-Einstein equation. *J Chem Educ*, 1970. **47**: p. 261-70.

Vita

Karishma Surendra Kaushik was born June 30, 1981 in Mumbai (Bombay), India, the daughter of Surendra and Dr. Vineeta Kaushik. She completed her medical degree (M.B.B.S.) from Dr. D. Y. Patil Medical College (Maharashtra University of Health Sciences), Pune, India, followed by an internship at Sassoon General Hospital, Pune (1999-2005). She went on to complete her residency in Clinical Microbiology (M.D.) from the Armed Forces Medical College, Pune (2005–2008). She started her Ph.D. at the University of Texas at Austin in 2010 and began her dissertation research under Dr. Vernita Gordon in 2011.

Permanent address: karishmaskaushik@gmail.com

This dissertation was typed by the author.